

# **Engineering the Microstructure of Hydrogels to Achieve Enhanced Mechanical Properties**

By  
Tiffany Suekama  
Copyright 2014

Submitted to the graduate degree program in Chemical & Petroleum  
Engineering and the Graduate Faculty of the University of Kansas School of  
Engineering in partial fulfillment of the requirements for the degree of Doctor  
of Philosophy

Committee members

---

Dr. Stevin Gehrke,  
Committee Chair

---

Dr. Cory Berkland

---

Dr. Michael Detamore

---

Dr. Laird Forrest

---

Dr. Paulette Spencer

---

Date Defended

## Acceptance Page

The Dissertation Committee for Tiffany Suekama certifies that this is the approved version of the following dissertation:

### **Engineering the Microstructure of Hydrogels to Achieve Enhanced Mechanical Properties**

Committee members

---

Dr. Stevin Gehrke,  
Committee Chair

---

Dr. Cory Berkland

---

Dr. Michael Detamore

---

Dr. Laird Forrest

---

Dr. Paulette Spencer

---

Date Defended

## Abstract

Hydrogels are three-dimensional, cross-linked, polymeric networks that are typically soft materials that contain more than 90% water. Many technologies require hydrogels with improved mechanical properties (modulus, failure properties and toughness). Drawing inspiration from biological systems that are complex and highly ordered, yet constructed efficiently, this dissertation advances understanding of multi-component hydrogels. This work also develops correlating relationships of composition, water content, microstructure network properties and mechanical properties.

This dissertation investigates three multi-component hydrogel systems which fall into the category of interpenetrating network (IPN): two or more networks which are interlaced, independent of each other and each network is covalently cross-linked.

**(1) Semi-IPN hydrogels:** A subcategory of IPNs in which two or more networks are interlaced and independent of each other, but one is chemically cross-linked and one is an entangled polymer. A systematic study of the formulations of single-network (SN) and semi-IPNs of agarose and poly(ethylene glycol) diacrylate (PEGDA) showed that these gels typically exhibited an effect somewhat greater than the sum of the two component SNs, in moduli, fracture stress and toughness. The semi-IPNs of agarose/PEGDA also behaved as ideal elastomers. Imaging hydrated semi-IPNs of agarose/PEGDA using scanning electron microscopy (SEM) and atomic force microscopy (AFM) revealed that the semi-IPNs had pores sizes that are between the two SNs, 1-4  $\mu\text{m}$  pores. The pore size decreased as the PEGDA concentration was increased.

**(2) Double-network (DN) hydrogels:** A subcategory of IPNs in which two independent,

covalently cross-linked networks display the DN effect: substantial yielding and significant improvement in mechanical properties compared to the SNs, notably toughness and modulus. The most widely accepted view for the improvement of the mechanical properties in DN is that sacrificial covalent bonds breaking in the brittle first network dissipates strain energy while the ductile second network hold the gel together. This work explored the molecular mechanisms produced in DN such as the sacrificial covalent bonds breaking leading to irreversible network damage.

When this work began, the first synthesized DN, poly(2-acrylamido-2-methylpropanesulfonic acid) (PAMPS)/polyacrylamide (PAAm) was the only composition that produced the DN effect. This led to the question of the generality of the DN effect. Here, the generality of the DN effect was demonstrated by synthesizing the first biopolymer-based DN. This was accomplished by replacing the PAMPS network with a biopolymer, methacrylated chondroitin sulfate (MCS), which forms a brittle network similar to PAMPS but has a fundamentally different structure. The generality was further emphasized by replacing the second network PAAm with poly(*N,N*-dimethylacrylamide) (PDMAAm) to synthesize a DN of MCS/PDMAAm.

Detailed analysis of mechanical properties in tension and compression were completed to understand why DN are so tough. **In tension**, the MCS/PAAm DN formulations were manipulated by adjusting the concentration and cross-linking of the two networks to achieve mechanical properties (failure stress, failure strain, Young's modulus, and yielding behavior) that cover a broad range (more than five times in most cases). Increasing cross-linking in the first network by (1) increasing the MCS concentration from 13 to 20% in MCS/PAAm DN or (2) adding PEGDA as a cross-linker increases the modulus and failure stress, but decreases the

yielding region. Since the increased modulus in DN gels is believed to be the result of strain energy dissipation by fracturing of the first network, the primary effect of cross-linking appears to be the reduction of chain extensibility resulting in failure at lower strains. **In compression**, the mechanisms for toughening were believed to be different than tension. Although energy dissipation mechanisms from the fracture of the first network may increase the toughness of DN, based on this work the improved failure properties under compression are believed to be from the entanglement and rearrangement of the two networks.

**(3) IPN hydrogel with high density charge complexation** that are engineered with the non-covalent sacrificial bonds, which was hypothesized to improve toughness. IPNs of poly(N-vinyl formamide) (PNVF) and polyacrylamide (PAAm) were hypothesized to have intimate molecular mixing of the two networks (monomers are isomers of each other, and polymers have similar interaction with water) to help minimize molecular phase separation.

First, synthesis of a new hydrogel, SN PNVF, is significant because PNVF gels provide an alternative to commercially important PAAm and provide a simple route to poly(vinylamine) (PVAm), high density cationic network. Then creating an IPN from the high charge density of both of the hydrolyzed counterparts poly(acrylic acid) (PAAc) and poly(vinylamine) (PVAm) maximizes interactions between the two networks which improved charge complexation, as evidenced by deswelling of the IPNs at intermediate pHs. Furthermore, comparing the toughness and failure stress of the hydrolyzed IPN immediately after hydrolysis to the same IPN at intermediate pHs showed 15-fold increases in the complexed state.

In developing these multi-component hydrogels, a deeper understanding of the complexity of the interactions of the networks requires the visualization of the hydrogels in the hydrated state.

Common techniques such as AFM and SEM have limitations when imaging in the swollen state. Introductory work on applying a super resolution microscopy technique, direct stochastic optical reconstruction microscopy (dSTORM), allows for imaging hydrated materials.

The work in this dissertation is important for advancing basic science of hydrogels for potential applications in fields such as tissue engineering, drug delivery, and gel-based separation techniques. This work focused on identifying and correlating the mechanisms between the materials, formulations and network properties (water content, mechanical properties, structure) on tough multi-component hydrogels.

In order to educate and communicate to a broader audience, a summarized research statement in the form AND, BUT, THEREFORE is stated below:

Hydrogels are water-loving three-dimensional materials.

AND they can be manipulated to have unique properties.

BUT manipulating hydrogels requires understanding of the inner mechanisms in order to improve properties (toughness, fracture properties, moduli).

THEREFORE I am doing research to understand the molecular mechanisms of hydrogels.

## Acknowledgements

I want first want to acknowledge my committee members Drs. Stevin Gehrke, Cory Berkland, Michael Detamore, Paulette Spencer and Laird Forrest for their intellect, support and suggestions as well as challenging me though out my PhD journey. I also would like to acknowledge many of the professors inside and outside of the chemical engineering department who helped my academic career, particularly, Drs. Prajna Dhar, David Moore, Lisa Friis, Steve Case and Shenqiang Ren.

I would also like to acknowledge the funding sources I have received: National Science Foundation (NSF) Grant DMR 0805264, the NSF East Asia and Pacific Summer Institutes and Japan Society for the Promotion of Science (JSPS) under Grant 1108344, NSF Graduate Teaching Fellows in K-12 Education (GK-12) Program and Whitaker International Program.

Special thanks to my undergraduate academic and research advisor, Dr. Travis Bailey at Colorado State University, who introduced me to the idea of an advanced degree, research, good writing, excellent teaching and polymers. Also, I would like to thank Dr. Kyle Camarda who introduced and recruited me to KU.

To my academic father, Dr. Stevin Gehrke, I would like thank-you for your guidance and teaching. I am lucky to have had the opportunity for your endless knowledge to rub off on me (even if only briefly). I have enjoyed your passion, dedication, perfection and constant aim for good science. I want to thank-you for being an extremely patient and caring teacher. I also want to thank-you for encouraging me to do what I love by allowing me to include my passions for the medical field, food, education and traveling as a part of my PhD.

To my wonderful lab mates: Anahita Khanlari, Tricia Sprouse, Erik Van Kampen, Linda Steele and Ganesh Ingavle whom have pushed and encouraged me through out. I have enjoyed our

countless conversations and you have become my close friends. I would like to thank the previous lab members who have helped to pave the way Vara Aziz and Joe Lomakin. I would also like to acknowledge my lab mates from other labs who have helped teach me, who I have gotten the opportunity to work with and collaborate with, especially Lindsey Ott, Zahra Mohammadi, Emily Beck, Huili Guan, Chuda Chittasupho, Joshua Sestack and AJ Mellott.

To all of the undergraduates whom I have gotten the opportunity to work with thank-you for working with me and all of your assistance in the realm of hydrogels: Anisha Patel, Mehrdad Hosni, Anthony Livengood, Joe Scalet, Bradley Strathman, Deena Rennerfeldt, Justin Smith, Tayla Bickerton, Andrea Brown and Joshua Schroeder.

To the GK-12 fellows and the teachers who I have worked with thank-you for sharing your work with me: Sam Wyrick, Elizabeth Fincham, and Kate Parker.

I would like to express my gratitude to my three advisors abroad who welcomed me into their labs, guided my research and brought international collaboration to the University of Kansas. I would like to thank Professor Jian Ping Gong at the University of Hokkaido, Japan for sharing your knowledge, guiding my research which led to several publications and for being such an inspiration. I also would like to thank Drs. Angus Johnston and Georgina Such at University of Melbourne, Australia for sharing your expertise and passions (in and outside [cake and chocolate] of lab) but most of all for encouraging my new ideas to advance the field. I would like to extend my acknowledgement to Shinji Kondo, a student who I met in my travels in Japan, and his advisors Drs. Takamasa Sakai and Ung-il Chung at the University of Tokyo who work on the homogeneous structure of tetra-polyethylene glycol hydrogels and graciously collaborated with me.

To my friends who I have met while traveling, while at KU or prior to KU thank-you for



supporting me, helping me, loving me and all around being a joy to be around. I really appreciate you! In particular, thanks to Jackie Acres, Justin Smith, Daniel Kiefer, Arely Torres, Cate Wisdom, Brock and Mary Roughton, JR and Nikki Hacker, Haiyan Yin, Haiyin Liu, Nicole Moody, Seb Krigelski, Renee O'Connor, Ben Hibbs, Rasheed Rabata, Keyata La'chelle, Keli Sakamoto, Daphen Pino, Marina Orozco, Golda Dunn and Christa Wood.

Finally, I would like to acknowledge all of my family for being patient and so understanding in my long journey. I want to thank-you for simply loving me. It has given me courage and drive to accomplish everything I have desired.

I hope my journey has inspired my siblings to think big but most of all to go after their passions.

## Table of Contents

<b>Section: Preface</b>	<b>Page</b>
Acceptance Page.....	i
Abstract.....	ii
Acknowledgements .....	vi
Table of Contents .....	ix
List of Tables .....	xvii
List of Figures.....	xviii
Nomenclature .....	xxii

<b>Section: Introduction</b>	<b>Page</b>
<b>Chapter 1: Introduction .....</b>	<b>1</b>
Overall Goal.....	1
<i>Specific Aim 1: Correlate formulation in semi-interpenetrating (semi-IPN) hydrogels with mechanical properties</i> .....	2
<i>Specific Aim 2: Understanding double-networks (DN) using biopolymer hydrogel systems.....</i>	2
<i>Specific Aim 3: Interpenetrating networks (IPN) with high density charge complexation to improve toughness</i>	3
<i>Specific Aim 4: Microscopic understanding of hydrated hydrogel networks using direct stochastic optical reconstruction microscopy (dSTORM) .....</i>	4
<i>The progression of the dissertation chapters are as follows: .....</i>	4

<b>Section: Background</b>	<b>Page</b>
<b>Chapter 2: General Background, Terminology and Theory .....</b>	<b>10</b>
Abstract.....	10
Hydrogels:.....	11
<i>Multi-component Hydrogels .....</i>	12
<i>Interpenetrating Networks .....</i>	12
<i>Semi-Interpenetrating Networks .....</i>	13

<i>Double-Network Hydrogels</i> .....	13
Swelling and Mechanical Properties .....	14
<i>Equilibrium swelling degree</i> .....	14
<i>Mechanical properties</i> .....	15
Basic Theory .....	20
<i>Swelling and Physical Properties</i> .....	20

## Section: Research Chapters

Page

### **Chapter 3: Semi-Interpenetrating Hydrogels of Agarose and Poly(ethylene glycol diacrylate) (PEGDA) Display Additive Behavior in Mechanical Properties<sup>3</sup> .....**

Abstract .....	27
Introduction .....	28
Materials .....	29
Methods .....	30
<i>Synthesis of Single-Network (SN) PEGDA Hydrogel</i> .....	30
<i>Synthesis of Single-Network (SN) Agarose Hydrogel and Interpenetrating Network of Agarose/PEGDA</i> .....	31
<i>Swelling Properties:</i> .....	31
<i>Mechanical Analysis:</i> .....	32
<i>Imaging: SEM and AFM</i> .....	33
Results .....	34
<i>Equilibrium Swelling Degree</i> .....	34
<i>Mechanical Analysis</i> .....	35
<i>Imaging</i> .....	43
Discussion .....	52
Conclusions .....	55
<b>Chapter 4: Double-Network Strategy Improves Fracture Properties of Chondroitin Sulfate Networks<sup>4</sup> .....</b>	<b>56</b>
Abstract .....	56

Introduction.....	57
Materials .....	60
Methods .....	60
<i>Synthesis of Single-Network (SN) PAAm Hydrogel:</i> .....	60
<i>Synthesis of MCS and Ultrathin DN (UTDN) Hydrogels of MCS/PAAm:</i> .....	61
<i>Swelling Properties:</i> .....	62
<i>Mechanical Analysis:</i> .....	62
Results and Discussion .....	63
Conclusions.....	67
<b>Chapter 5: Tuning Mechanical Properties of Chondroitin Sulfate-Based Double-Network Hydrogels<sup>5</sup>.....</b>	<b>68</b>
Abstract.....	68
Introduction.....	69
Materials .....	71
Methods .....	72
<i>Synthesis of SN PAAm</i> .....	73
<i>Synthesis of SN of MCS, CP of MCS-PEGDA and DN of MCS-PEGDA/PAAm</i> .....	73
<i>Swelling Properties</i> .....	74
<i>Mechanical Analysis</i> .....	75
Results and Discussion .....	77
<i>Varying the First Network: Concentration of MCS</i> .....	79
<i>Varying the First Network: Copolymerization with MCS with PEGDA</i> .....	80
<i>Varying the Second Network: Concentration of AAm and BIS</i> .....	84
Conclusions.....	85
<b>Chapter 6: Unique Features Shown Under Compression when Using the Double-Network Strategy<sup>6</sup>.....</b>	<b>87</b>
Abstract.....	87
Introduction.....	88

Materials and Methods.....	90
<i>Materials:</i> .....	90
<i>Synthesis of SN PAAM:</i> .....	90
<i>Synthesis of SN of MCS, CP of MCS-PAAM and DN of MCS/PAAM:</i> .....	91
<i>Swelling Properties:</i> .....	91
<i>Mechanical Analysis:</i> .....	92
<i>Statistics</i> .....	92
Results and Discussion .....	93
<i>Does the DN of MCS/PAAM Outperform CP and SNs Under Compression?</i> .....	93
<i>Yielding Mechanism Under Compression</i> .....	95
<i>Non-Ideal Elastomer behavior</i> .....	96
<i>Repeated loading in DNs of MCS/PAAM to 15%, 25% and 45% Strain</i> .....	98
Conclusions.....	106
<b>Bridge to Chapter 7: Overview of Work on Chondroitin Sulfate-Based Hydrogels Using the Double-Network Strategy.....</b>	<b>108</b>
<b>Chapter 7: Overview of Work on Chondroitin Sulfate-Based Hydrogels.....</b>	<b>109</b>
<b>Using the Double-Network Strategy<sup>7</sup> .....</b>	<b>109</b>
Abstract.....	109
Introduction.....	110
Materials and Methods.....	110
<i>Synthesis of Single and Double Networks:</i> .....	111
<i>Swelling Properties:</i> .....	111
<i>Mechanical Analysis:</i> .....	111
Results and Discussion .....	112
Conclusions.....	116
<b>Chapter 8: Updating the Definition of Double-Network Hydrogels after a Decade of Development<sup>8</sup> .....</b>	<b>117</b>
Abstract.....	117

Introduction.....	118
<i>Hydrogels</i> .....	119
<i>What is an IPN?</i> .....	120
Double-Network Hydrogels.....	120
<i>Composition of DNs</i> .....	122
<i>Mechanical Properties of DNs</i> .....	122
<i>DN Hydrogels in the Literature</i> .....	124
Conclusions.....	127
<b>Chapter 9: Synthesis and Characterization of Poly(N-Vinyl Formamide) Hydrogels – a Potential Alternative to Polyacrylamide Hydrogels<sup>9</sup>.....</b>	<b>128</b>
Abstract.....	128
Introduction.....	129
Experimental.....	131
<i>Materials</i> .....	131
<i>Synthesis of PNVF and PAAm Hydrogels</i> .....	132
<i>Swelling Properties</i> .....	133
<i>Mechanical Analysis</i> .....	134
Results.....	134
<i>Equilibrium Swelling Degree</i> .....	136
<i>Mechanical Analysis</i> .....	139
<i>Theoretical Parameters</i> .....	145
Discussion.....	148
Conclusions.....	152
<b>Supplementary Information for Chapter 9: Synthesis and Characterization of Poly(N-Vinyl Formamide) Hydrogels – a Potential Alternative to Polyacrylamide Hydrogels .....</b>	<b>154</b>
<b>Chapter 10: High Charge Density Interpenetrating Hydrogels of Hydrolyzed Networks of Poly(N-Vinyl Formamide) and Polyacrylamide<sup>10</sup> .....</b>	<b>159</b>
Abstract.....	159
Introduction.....	160

Materials and Methods.....	161
<i>Materials</i> .....	161
<i>Synthesis of single-network hydrogels</i> .....	161
<i>Synthesis of IPN hydrogels</i> .....	162
<i>Hydrolysis of hydrogels</i> .....	163
<i>Swelling and mechanical tests</i> .....	164
<i>Equilibrium Swelling Degree and Mechanical Analysis</i> .....	164
Results.....	165
Conclusions.....	173
<b>Chapter 11: An Introduction to a New Technique for Visualizing Hydrogel Networks: dSTORM Microscopy<sup>11</sup>.....</b>	<b>174</b>
Abstract.....	174
Introduction.....	175
Materials and Methods.....	176
<i>Synthesis of heterogeneous network (PAAm) and samples of heterogeneous networks (tetra-PEG)</i> .....	176
<i>Imaging</i> .....	178
Results and Discussion.....	178
Conclusions and Future Directions.....	180
<b>Section: Conclusion and Recommendations for Future Work</b>	<b>Page</b>
<b>Chapter 12: Conclusion and Recommendations for Future Work.....</b>	<b>181</b>
<b>Recommendations for Future Work.....</b>	<b>185</b>
Continuation of Current Projects.....	186
<i>PNVF using commercially available cross-linker 1,3-Divinylimidazolidin-2-one BVU*</i> .....	186
<i>Conjugating small molecules or peptides to PNVF*</i> .....	189
Studying Fracturing Mechanisms in Hydrogels.....	189
<i>Macro-scale investigating of network structure through fracturing mechanisms</i> .....	189
<i>Investigating network structure and fracturing mechanisms using environmental SEM (ESEM)*</i> .....	190

Multi-component Hydrogels .....	191
<i>Graphene hydrogels as a method of improving strength*</i> .....	191
<i>Electrospinning mats for reinforced hydrogel matrices*</i> .....	192
<i>Methacrylated hyaluronic acid (mHA) nanogels in macrogel*</i> .....	195
Controlling Microstructure of Hydrogels through Controlled Radical Polymerizations .....	196
<i>Hydrogels with controlled microstructure using nitroxide-mediated polymerization (NMP)</i> .....	196

## Section: References Page

<b>References .....</b>	<b>198</b>
-------------------------	------------

## Section: Appendix Page

<b>Appendix for Chapter 2.....</b>	<b>207</b>
------------------------------------	------------

Conversion: X (%) .....	207
<i>Synthesis</i> .....	208
<i>The formulations:</i> .....	209
<i>Swelling</i> .....	210
<i>Mechanical Testing</i> .....	210
<i>Biopsy samples for cylindrical compression</i> .....	210
Imaging .....	213
<i>Scanning electron microscopy (SEM)</i> .....	213
<i>Atomic force microscopy (AFM)</i> .....	214
<i>Direct stochastic optical reconstruction microscopy (dSTORM)</i> . .....	214
How to use Excel DMATEMPLATE .....	216
<b>Appendix for Chapters 4, 5 and 6.....</b>	<b>219</b>
Synthesizing Ultrathin Film Hydrogels .....	219
<i>The formulation: (___ - ___ - ___) monomer concentration (M) -crosslinker concentration (mol%)-initiator concentration (mol%)</i> .....	219
<i>Polymerization of PAAm:</i> .....	220



<i>Synthesis Protocol for film DN gels MCS network:</i> .....	221
<i>Swelling Tests:</i> .....	222
<i>Swelling Protocol:</i> .....	222
<i>Gel Thickness</i> .....	223
<b>Appendix for Chapter 9.....</b>	<b>224</b>
Synthesis of NVEE .....	224
<i>Synthesis Protocol for NVEE:</i> .....	224
Purification of NVEE.....	226
<i>Purification Protocol for NVEE:</i> .....	226
<i>Purification assay of NVEE:</i> .....	227
Polymerization of PAAm.....	228
<i>Synthesis Protocol for PAAm:</i> .....	228
Polymerization of PNVF.....	230
<i>Synthesis Protocol for PNVF:</i> .....	230
<b>Appendix for Chapter 10.....</b>	<b>232</b>
Hydrolysis of PAAm and PNVF.....	232
<i>Hydrolysis Protocol for PAAm and PNVF:</i> .....	232
Titration of PAAm and PNVF .....	233
<i>Titration Protocol for PAAm and PNVF:</i> .....	233
<b>Appendix for Chapter 12.....</b>	<b>234</b>
PAAm Nanoparticles .....	234
PNVF Nanoparticles .....	235

## List of Tables

<b>Chapter 1</b>	<b>Page</b>
Table 1.1: Outline of hydrogels and experimental methods throughout this dissertation. ....	7
Table 3.1. Measured properties of agarose, PEGDA and semi-IPNs of Agarose/PEGDA gels swollen to equilibrium in water. ....	35
Table 3.2: Summary of SEM and AFM images .....	51
Table 4.1: Swelling and Mechanical Properties of Different Hydrogel Networks.....	65
Table 5.1. Effect of compositional changes in the first network of MCS-PEGDA on mechanical properties of double network gels. The second network composition is 25x0.04 PAAm. ....	78
Table 5.2. Effect of compositional changes in the second network of PAAm and BIS on mechanical properties of double network gels. First network composition is 15% MCS. ....	79
Table 6.1. Measured mechanical properties of SN MCS, SN PAAm and DN MCS/PAAm hydrogels swollen to equilibrium in water.....	98
Table 7.1. Swelling and mechanical properties under tension and compression of DN's of MCS/PAAm and SNs of MCS or PAAm. ....	114
Table 9.1: Measured properties of PNVF gels swollen to equilibrium in water. ....	138
Table 9.2: Measured properties of PAAm gels swollen to equilibrium in water. ....	139
Table 9.2: Calculated parameters for PNVF using the affine network model.....	146
Table 9.3: Calculated parameters for PNVF using the affine network model.....	147
Supplementary Table S-9.1: Calculated parameters for PNVF gels using phantom network model. ....	158
Supplementary Table S-9.2: Calculated parameters for PAAm gels using phantom network model. ....	158

## List of Figures

Chapter 1	Page
Figure 1.1: Progression of aims through the dissertation .....	2
Figure 1.2: Interconnections of properties and techniques used within dissertation .....	6
Figure 2.1: Schematic of research on hydrogels .....	10
Figure 2.2: Highly swollen hydrogel. ....	11
Figure 2.3: Typical stress-strain curves under uniaxial compression for ideal elastomeric hydrogel .....	17
Figure 2.4: Typical DN stress-strain curves under tension, non-ideal elastomeric hydrogel .....	18
Figure 2.5: 3 modes in tearing tests .....	19
Figure 2.6: Typical force-extension curve for tearing tests. ....	19
Figure 2.6: Swelling and elastic forces in balance in hydrophilic hydrogels swollen to equilibrium .....	21
Figure 3.1: Swelling decreases with total polymer concentration until plateauing around 3. ....	34
Figure 3.2a, 3.2b and 3.2c: Representative stress-strain and stress-strain function curves of semi-IPN of agarose/PEGDA, SN agarose and SN PEGDA .....	37
Figure 3.5: PEGDA is shown to be the dominant property in semi-IPNs .....	40
Figures 3.6a and 3.6b: Fracture strain of the hydrogels around 50% .....	41
Figures 3.7a and 3.7b: Increasing fracture stress with polymer volume fraction and PEGDA content .....	42
Figures 3.8a and 3.8b: .....	42
Figure 3.9a, 3.9b and 3.9c: Various sizes of pores found on different length scales in 2 wt. % agarose shown in SEM images. ....	44
Figure 3.10: AFM of 2 wt. % SN agarose shows pores $\sim 2-5\mu\text{m}$ . ....	45
Figure 3.11a and 3.11b: Large strut size in between pores in 5 wt. % agarose on both SEM and AFM .....	46
Figures 3.12a and 3.12b: Distinct pores in 10wt. % of agarose in SEM and AFM. ....	46
Figures 3.13a and 3.13b: Image of 10 wt.% SN PEGDA show ambiguous results .....	47
Figures 3.14a and 3.14b: Image of 10 wt.% SN PEGDA show ambiguous results .....	48
Figure 3.15a and 3.15b: Rough surfaces formed in SN PEGDA at 30 wt. % .....	48
Figures 3.16a and 3.16b: Semi-IPN of 5 wt. % agarose/10wt% PEGDA show a pore size in between both SNs .....	49
Both AFM and SEM images show $2-4\mu\text{m}$ pore size which is an intermediate size to the SN agarose and SN PEGDA. ....	49

Figures 3.17a and 3.17b Semi-IPNs of 5wt. % agarose/PEGDA show decrease in pore size with increase in PEGDA content from 10-20wt. %.....	50
Both AFM and SEM images show 1-2 $\mu$ m pore size which is an intermediate size to the SN agarose and SN PEGDA. ....	50
Figures 3.18a and 3.18b Rough surfaces formed in semi-IPNs of 5wt. % agarose/30 wt. % PEGDA .....	50
Figure 4.1: Schematic of single (SN) and double (DN) network gels.....	59
Figures 4.2a (top) and 4.2b (bottom): Stress-strain response under tension single (SN) and double (DN) network gels.....	64
Figure 5.1: Stress-strain curve for DN hydrogels.....	70
Figure 5.2: Double-network formulations with copolymers of MCS and PEGDA as the first network and PAAm as the second network.....	72
Figure 5.3: Schematic tuning of MCS-PEGDA/PAAm DN formulations by changing the first and second networks.....	76
Figure 5.4: Varying MCS concentrations in DN of MCS/24x0.04 PAAm.....	80
Figure 5.5: Further cross-linking of first network with PEGDA leads to increase in modulus and failure stress but decrease in yielding region.....	81
Figure 5.6: 20% MCS-PEGDA/25x0.04 PAAm DN formulations shows that the addition of PEGDA causes a decrease in failure properties.....	82
Figures 6.1a, 6.1b and 6.1c: Stress-strain curves of DN of MCS/PAAm, CP of MCS-PAAm, SN of MCS and SN of PAAm. ....	94
Figures 6.2a and 6.2b: Non-ideal elastic behavior is exhibited even at a low strain function.....	97
Figure 6.3: No permanent damage shown in 12 compressive loading cycles up to 15% strain...	99
Figure 6.4: No statically relevant trend for toughness of average loading curves up to 15% strain in repeating cycles 1-12 .....	100
Figure 6.5: No statically relevant trend for toughness of average loading curves up to 25% strain in repeating cycles 1-12 .....	102
Figure 6.6: Slight damage in material evident in repeated loading curves of certain formulations but no damage evident in other formulations .....	102
Figure 6.7: Decrease in toughness in average loading curves up to 45% strain in first few cycles but no further damage after cycle 7 (up to cycle 12) .....	103
Figures 6.8a, 6.8b, 6.8c and 6.8d: Change of shape in stress-strain curved for repeated loading cycles which leads to decrease in toughnesses but similar stresses.....	104
Figure 7.1: Schematic of DN hydrogel progression .....	108
Figure 7.2. Improved mechanical properties from DN strategy are shown in stress-strain responses under both tension (closed symbols) and compression (open symbols).....	113

Figure 8.1: Hierarchical classification chart of tough multi-component hydrogels. ....	118
Figure 8.2: Typical stress-strain curve of DN hydrogels in tension .....	124
Figure 8.3: Increase in the number of publications per year on hydrogels with “double network” in the title, from 2003 to 2012, through an online search in both “Web of Knowledge” and “Google Scholar” .....	125
Figure 9.1: Chemical structures .....	129
Figures 9.2a and 9.2b: Decrease in swelling degree, increase NVF or AAm monomer concentration .....	137
Figure 9.3: Swelling in various acetone concentration.....	138
Figure 9.4: Similarity in shape of stress-strain curves of PNVF and PAAm .....	140
Figure 9.5: Linearization of data in stress-strain function curves of PNVF and PAAm .....	140
Figures 9.6a and 9.6b: G of PAAm $\sim 2x$ PNVF but have similar trends.....	142
Figure 9.7: G follows scaling theory, PNVF is more hydrophilic .....	144
Figure 9.8: Correlation of fracture strain with polymer volume fraction .....	144
Figure 9.9: Failure stress not dependent on polymer volume fraction .....	145
Figure 9.10: Flory-Huggins parameter lower for PNVF, more hydrophilic.....	147
Supplementary Figure S-9.1: Normalized swelling degree as a function of acetone concentration .....	156
Supplementary Figures S-9.2a and S-9.2b: E $\sim 2x$ greater in PAAm than PNVF .....	156
Supplementary Figure S-9.3a and S-39.b: G falls on a single curve when plotted against the polymer volume fraction.....	157
Supplementary Figure S-9.4: Flory-Huggins parameter lower in PNVF, more hydrophilic in .	157
Figure 10.1: Schematic of formulations and the treatments. ....	162
Figures 10.2a and 10.2b: Decreased swelling degree at intermediate pHs indicate complexation .....	166
Figures 10.3a and 10.3b: Charge complexed IPNs show large improvements in failure stress (10.3a) and failure strain (10.3b) .....	167
Figure 10.4: Toughness improved at intermediate pHs.....	168
Figure 10.5: Failure strain decreases with increasing equilibrium swelling.....	169
Figures 10.8a and 10.8b: Failure strain increases with increasing polymer volume fraction at low polymer volume fraction.....	170
Figures 10.6a, 10.6b and 10.6c: Failure stress decreasing at high swelling degrees and no obveous trens at lower swelling .....	171
Figures 10.7a and 10.7b: Failure stress slightly increasing at small polymer volume fractions .	172
Figure 11.1: Schematic of the layered view of the prepared gel for imaging.....	178
Figure 11.2: Image of a PAAc hydrogels through dSTORM. ....	179

Figure 12.1: Progression of aims throughout the dissertation .....	181
Figure 12.2: Random copolymerization of monomers and crosslinkers is needed to yield good gels. .....	187
Figure 12.3: Structure of 1,3-Divinylimidazolidin-2-one (BVU) from BASF .....	188
Figure 12.4: Swelling data for PNVF hydrogels with BVU cross-linker .....	188
Figure 12.5: 5% Agarose hydrogel imaged using ESEM .....	191
Figure 12.6: Electrospun fibers of PVA shown in SEM .....	193
Figure 12.7: Scheme of electrospun fibers in networks .....	194
Figure 12.8: SEM of unique structures formed by electrospaying .....	195
Figure 12.9: Schematic of heterogeneous (left) and homogeneous (right) network structures ..	196
Appendix Figure A-2.1: Typical single-network and IPN hydrogel synthesis methods .....	209
Appendix Figure A-2.2: Typical hydrogel shapes .....	211
Appendix Figure A-2.3: Gel cutting device, SDAP-100N Dumbbell Co, Ltd .....	211
Appendix Figure A-2.4: Cut dogbone gels .....	212
Appendix Figures A-2.5a, A-2.5b and A-2.5c .....	213
Appendix Figure A-2.7: Nikon – N –Storm system for dSTORM imaging .....	215

## Nomenclature

### Symbols [units]\*

$A_0$  = undeformed cross-sectional area of the swollen polymer [ $\text{m}^2$ ]

$c$  = molar concentration of mobile ions in the solution inside the gel [ $\text{mol}/\text{m}^3$ ]

$C$  = mass fraction of crosslinker in the bulk

$c^*$  = molar concentration of mobile ions in the solution outside the gel [ $\text{mol}/\text{m}^3$ ]

$c_s$  = molar concentration of electrolyte in the gel originating in the external solution [ $\text{mol}/\text{m}^3$ ]

$c_s^*$  = molar concentration of electrolyte in the external solution [ $\text{mol}/\text{m}^3$ ]

$E$  = Elastic modulus [Pa]

EWC = equilibrium water content

$f$  = crosslinker functionality (4 for most common crosslinkers)

$F$  = applied force [N]

$G$  = Shear modulus [Pa]

$G, \Delta G$  = Gibbs free energy [J]

$i$  = fraction of monomeric units on the gel which are ionized

$L$  = sample length under stress [mm]

$L_0$  = undeformed sample length [mm]

$M_c$  = molecular weight between crosslinks [g/mol]

$P_{\text{ext}}$  = externally applied pressure [ $\text{g}/\text{cm}^2$ ]

$R$  = gas constant [J/(mol K)]

$T$  = absolute temperature [K]

$q$  = mass degree of swelling

$Q$  = volume degree of swelling

$\tilde{v}_1$  = solvent molar volume [mol/m<sup>3</sup>]

$\tilde{v}_m$  = molar volume of a monomeric unit [mol/m<sup>3</sup>]

$V_0$  = unswollen gel volume [m<sup>3</sup>]

$X$  = mass conversion

**Greek Symbols [units]\***

$\Pi$  = osmotic pressure [g/cm<sup>2</sup>]

$\phi_{2f}$  = polymer volume fraction at network formation

$\phi_2$  = polymer volume fraction

$\phi'_2$  = polymer volume fraction

$\varepsilon$  = strain

$\chi$  = Flory-Huggins solubility parameter

$\rho_x$  = effective crosslink density relative to the solid state [g/cm<sup>3</sup>]

$\rho_t$  = theoretical crosslink density [g/cm<sup>3</sup>]

$\rho_2$  = crosslink density of the polymer [g/cm<sup>3</sup>]



$\tau$  = engineering stress [Pa]

$\sigma$  = stress [Pa]

$\eta_c$  = efficiency of crosslinking

$\nu$  = Poisson's ratio

$\nu$  = number of ions into which a dissolved salt dissociated

$\nu_e$  = number of elastically effective polymer chains (those which are deformed by stress)

$\lambda$  = extension ratio

$\mu$  = chemical potential [J/mol]

$\mu_1$  = chemical potential in of swelling for water in the gel [J/mol]

$\mu_1^0$  = chemical potential of swelling for water in the bulk (outside the gel) [J/mol]

\* For calculations a conversion factor may be needed.

## Chapter 1: Introduction

This chapter provides an overview of the work completed in this dissertation. It begins with a discussion of the overall goal of this work followed by the four specific aims of this research. Lastly, this chapter provides a progression of the dissertation chapters.

### Overall Goal

The main objective of this dissertation was to advance the understanding of the molecular mechanisms of hydrogels to engineer the microstructure resulting in highly swollen networks with enhanced mechanical properties (modulus, failure properties and toughness). This work has been inspired by hierarchical nature of biological structures such as the extracellular matrix (ECM) which are highly ordered and complex structures. Mimicking these structures with synthetic hydrogels provides a new class of materials and the derived concepts may be applied to a variety of fields, in particular tissue engineering (TE). To better understand the molecular structure and mechanism of hydrogel networks, this work studies multi-component hydrogel systems. A specific type of multi-component hydrogels was studied: interpenetrating network (IPN), where two networks are independent of each other and each network is covalently cross-linked. Two subcategories of IPNs are (1) semi-IPN in which the two networks are still independent of each other but only one is chemically cross-linked and the other is an entangled polymer and (2) double-network (DN) in which the two independent, chemically cross-linked networks lead to superior mechanical properties, notably toughness and yielding. Thus, this work targets the overall goal by improving and advancing understanding of molecular network structures and interactions in order to control network performance of hydrogels of semi-IPNs, DNs and IPNs.



**Figure 1.1: Progression of aims through the dissertation**

***Specific Aim 1: Correlate formulation in semi-interpenetrating (semi-IPN) hydrogels with mechanical properties***

A systematic study of the formulations of semi-IPNs of agarose/PEGDA will expand the understanding these multi-component hydrogels. Our group and collaborators at the University of Kansas (KU) have been actively studying the mechanical properties, cell encapsulation, cell viability and bioactive signaling of various formulations of semi-IPN hydrogels of agarose and poly(ethylene glycol) diacrylate (PEGDA). This work aims to relate formulation and mechanical properties to the microstructure. Furthermore, this work intends to compare imaging techniques of hydrated hydrogels using scanning electron microscopy (SEM) and atomic force microscopy (AFM). The formulations were varied but the mechanical properties of the semi-IPNs of agarose/PEGDA were dominated by the PEGDA network and did not show significant improvement to either single-network.

***Specific Aim 2: Understanding double-networks (DN) using biopolymer hydrogel systems***

DN hydrogels were pioneered by Gong and Osada in 2003 and the DN of poly(2-acrylamido-2-methylpropanesulfonic acid) (PAMPS)/polyacrylamide (PAAm) gained a lot of attention for the high toughness and yielding. At the time, PAMPS/PAAm was the only formulation displaying these enhanced mechanical properties. Therefore, the goals of the aim are two-fold: (1) to determine the generality of the DN effect and (2) critique the mechanisms behind the improved toughness in DN; the current understanding of the superior toughness of DN hydrogels arises

from the first network breaking irreversibly providing sacrificial bonds and the second network holding the DN together.

The first goal to determine the generality of DN effect was tested by replacing the PAMPS network with a biopolymer, methacrylated chondroitin sulfate (MCS), which is sulfonated and forms a brittle network similar to PAMPS, but has a fundamentally different structure. Also, the ductile poly(*N*, *N*-dimethylacrylamide) (PDMAAm) was hypothesized to be able to replace PAAm; thus, testing the hypothesis that hydrogen bonding between PAMPS and PAAm improves the toughness. The second goal was tested from detailed analysis of mechanical properties in tension and compression to understand why DNs are so tough: Under tension, the DN formulations were varied to correlate with mechanical properties (failure stress, failure strain, Young's modulus, and yielding behavior). Under compression, energy dissipation mechanisms from the covalent bonds of first network breaking irreversibly were tested with repeated loading tests.

While the DN strategy created high strength, tough, bio-based networks, the sacrificial bonds which are hypothesized to improve toughness in DNs are from the covalent bonds of the first network breaking irreversibly. This is a limitation in many applications including tissue engineering; therefore, creating a hydrogel with similar mechanical properties but has non-covalent bonds which can break and reform was desired.

***Specific Aim 3: Interpenetrating networks (IPN) with high density charge complexation to improve toughness***

The intent of this aim was to create high density charge complexation between two networks which would provide non-covalent sacrificial bonds that can be broken and reformed, reversibly. The objective was to use two polymers which had limited phase separation and a high charge

density to achieve notable molecular level complexation. This was tested by synthesizing IPNs from polyacrylamide (PAAm) and poly(N-vinyl formamide) (PNVF). The monomers are chemically similar (isomers) and they produce neutral networks, but after hydrolysis PAAm and PNVF, networks produce similarly matching molar ratios of high charge density networks of polyacrylic acid (PAAc) and polyvinylamine (PVAm), respectively. First, the ability for the two networks to be synthesized without phase separation will be tested by synthesizing IPNs of PAAm/PNVF and PNVF/PAAm. Next, charge complexation will be examined by subjecting the hydrolyzed IPNs, PAAc/PVAm and PVAm/PAAc, to various pH baths, hypothesizing that there will be deswelling and enhanced mechanical properties (toughness, failure properties) at the collapsed state. This process creates high strength and tough hydrogels from charge complexation, but understanding the fundamentals of the network interactions in the hydrated state was desirable.

***Specific Aim 4: Microscopic understanding of hydrated hydrogel networks using direct stochastic optical reconstruction microscopy (dSTORM)***

Imaging on sub-diffraction levels is possible with super-resolution techniques such as dSTORM. Imaging on a nanoscale would allow for better understanding of the structure on the properties of hydrogels. dSTORM images a single-molecule, fluorophore, and can image down to ~20nm. The technique would allow for resolution of the polymeric networks. Furthermore, dSTORM has potential to be applicable for tracking individual molecules over time within a hydrogel matrix. dSTORM is most commonly applied to imaging biological structures; however, the goal of this work is to demonstrate the potential of dSTORM imaging of hydrogels.

***The progression of the dissertation chapters are as follows:***

A conceptual map illustrating the interconnections of the chapters and main concepts as they

pertain to the network properties and analysis techniques which were studied within the dissertation is shown in Figure 1.2. Figure 1.2 starts with the main idea and title of this dissertation (large black rectangular box in the middle): engineering the microstructure of hydrogels to achieve enhanced mechanical properties. This points to the major hydrogels studied in this dissertation (green, small rectangles), interpenetrating networks and the three types (semi- interpenetrating networks, double-networks and interpenetrating networks using charge complexation). The larger boxes show the chapters, red are reviews and blue are research chapters. They pertain to the hydrogel studied in the chapters and also their connection to the major techniques or properties (orange ellipses). Finally, the small purple boxes are the specific techniques used parameters measured or parameters calculated.

Table 1.1 shows the chapters which correspond with the type of hydrogel (single-network (SN), co-polymer (CP), interpenetrating network (IPN), semi-IPN, double-network (DN)) and the final polymeric material, as well as the experimental techniques used (mechanical analysis, synthesis method and imaging analysis)

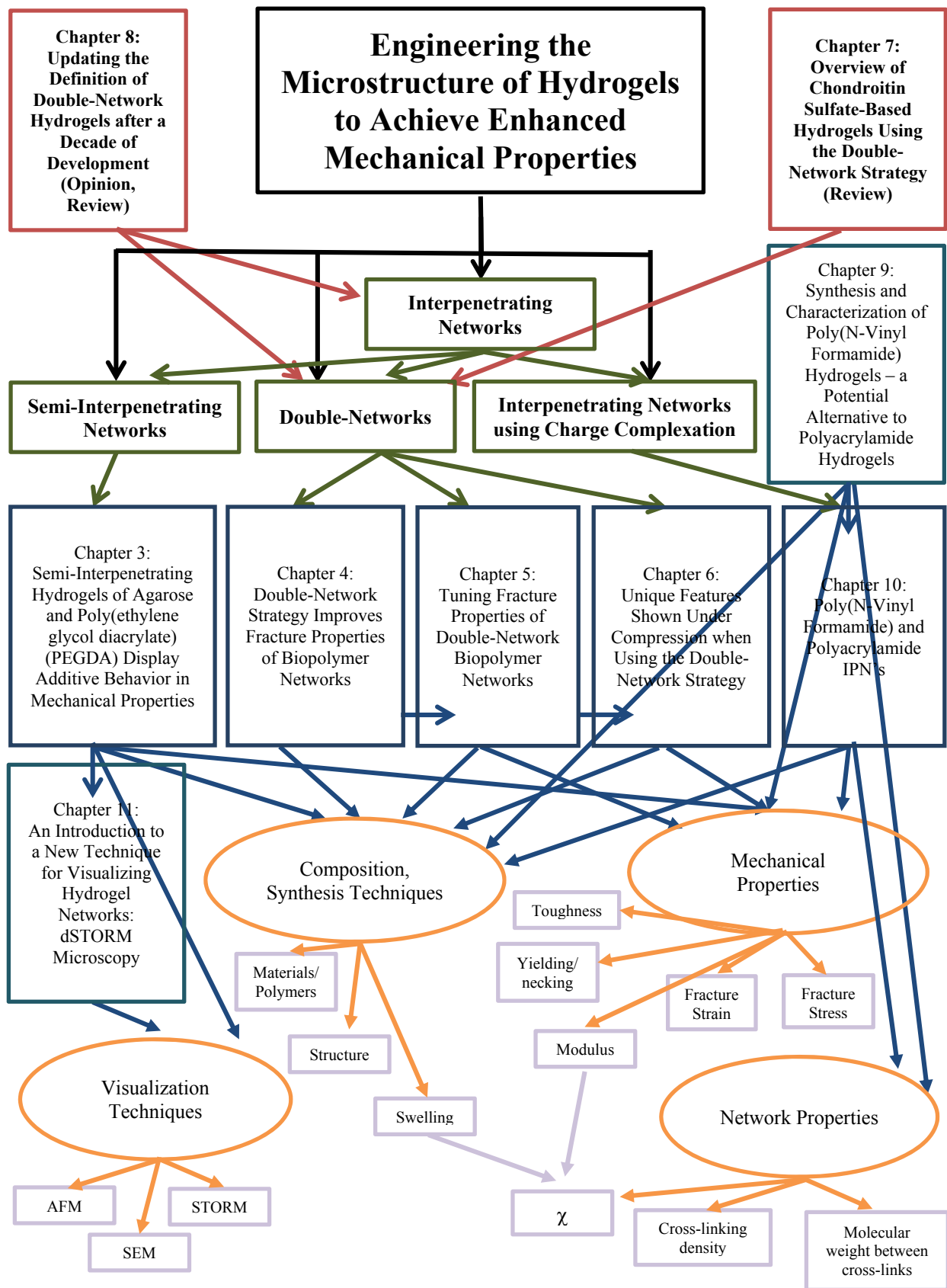


**Figure 1.2: Interconnections of properties and techniques used within dissertation**

**Table 1.1: Outline of hydrogels and experimental methods throughout this dissertation.**

Chapter	Type and Material (s)	Mechanical Analysis			Initiation Method	Imaging
		Compression	Tension	Tearing		
3	SN: PEGDA	X	-	-	UV	AFM & SEM
	SN: Agarose	X	-	-		
	Semi-IPN: Agarose/PEGDA	X	-	-		
4	SN:MCS	-	X	-	UV	-
	SN: PAAm	-	X	-		
	DN: MCS/PAAm	-	X	X		
	DN: MCS/PDMAAm	-	X	X		
5	DN: MCS/PAAm	-	X	X	UV	-
	DN: MCS-PEGDA/PAAm	-	X	X		
6	SN: MCS	X	-	-	UV	-
	SN: PAAm	X	-	-		
	CP: MCS-PAAm	X	-	-		
	DN: MCS/PAAm	X	-	-		
7	SN: MCS	X	X	-	UV	-
	SN: PAAm	X	X	-		
	DN: MCS/PAAm	X	X	-		
9	SN: PAAm	X	-	-	Redox	-
	SN: PNVF	X	-	-		
10	SN: PAAm	-	-	-	Thermal	-
	SN: PNVF	-	-	-	Thermal	
	IPN: PAAm/PNVF	-	-	-		
	IPN: PNVF/PAAm	-	-	-		
	SN: PAAc	-	-	-		
	SN: PVAm	-	-	-		
	IPN: PAAc/PVAm	-	-	-		
IPN: PVAm/PAAc	-	-	-			
11	SN: PAAc	-	-	-	-	dSTORM
	SN: tetra-PEG	-	-	-		

Chapter 2 familiarizes the reader with basic hydrogel concepts providing general background, terminology and theory that are used throughout the dissertation. The intent of Chapter 2 is to set the stage for the remaining experimental chapters (Chapters 3-11).

Chapter 3 addresses *Specific Aim 1* by advancing work on semi-IPNs of agarose/PEGDA by varying formulation to understand the structure-property relationships. PEGDA is the dominant network in the semi-IPNs. Further, semi-IPN of agarose/PEGDA show ideal elastomeric behavior. Although the semi-IPNs had modest improvements in mechanical properties (toughness and fracture stress), the desire to develop hydrogels with a 10 or 100 fold increase in modulus, failure properties and toughness led to the work on DNs.



Chapters 4-8 targets *Specific Aim 2* using a novel MCS/PAAm DN system. The goals of the aim are two-fold: (1) to determine the generality of the DN effect and (2) critique the hypothesis about the mechanisms behind the improved toughness in DNs. The current understanding of the superior toughness of DN hydrogels arises from energy dissipation from first network breaking irreversibly providing sacrificial bonds and the second network holding the DN together. Chapters 4-6 were the experimental work on DN gels. Chapter 4 develops biopolymer DN system of MCS/PAAm and MCS/PDMAAm, which demonstrates that DNs are not limited to the original PAMPS/PAAm and verifying the generality of the DN effect. By swapping the second network PAAm for PDMAAm, this confirms that the hydrogen bonding of the PAAm network is not key to producing tough and ductile DNs. Chapter 5 evaluates the formulations of DNs by changing the MCS-PEGDA/PAAm DNs to control the mechanical properties: failure stress, failure strain, Young's modulus, and yielding behavior over a broad range more than five times in most cases. Chapter 6 shows that DNs of MCS/PAAm produces superior properties under compression to both single-networks and co-polymers of both. The compression tests critique the energy dissipation mechanisms, from the sacrificial bonds in the first network, which produce superior properties in DNs. Chapter 7 is a summary of the work directly comparing tension and compression of MCS/PAAm DN gels. Chapter 8 wraps up the work on DN hydrogels by redefining the DN term so the term emphasizes the distinction between DN hydrogels and IPNs, (a distinction not always made) and better encompasses current understanding of DN hydrogels.

Chapter 9 and 10 focuses on *Specific Aim 3* which intends to create high charge density complexation networks from PAAm and PNVF. PAAm and PNVF are both neutral networks with similar chemical structures and after hydrolysis PAAm and PNVF networks produce similarly matching molar ratios of high charge density networks. Phase separation was hypothesized to be

minimal when creating an IPN of the two polymers enabling molecular-level mixing which will maximize interactions. Chapter 9 developed a novel hydrogel, PNVF, as an alternative to commercially important PAAm. PNVF also provides a simple route to PVAm, high charge density cationic network. From the swelling and mechanical tests, the PNVF can be formulated to be the same as PAAm but with the exact same formulation PNVF was slightly more hydrophilic than PAAm. Chapter 10 shows the synthesis of the interpenetrating network of PAAm/PNVF and PNVF/PAAm. Charge complexation was evident from a deswelling at intermediate pHs of PAAc/PVAm and PVAm/PAAc networks. In the complexed state the failure strain and the toughness were 15 times greater than right after hydrolysis (from  $\sim 1$  MPa to 15 MPa in failure stress and  $\sim 90$  kJ/m<sup>3</sup> to 1500 kJ/m<sup>3</sup> in toughness).

Chapter 11 investigates *Specific Aim 4*, which is an effort to overcome some of the limitations of SEM and AFM identified in Chapter 3. This work applies a super-resolution microscopy technique: direct stochastic optical reconstruction microscopy (dSTORM) to hydrogels. The network was fluorescently tagged and then imaged in the fully hydrated state.

Overall, this dissertation provides advances to understanding multi-component networks especially IPNs, by improving the understanding of the interactions which control properties such as modulus, fracture properties, toughness, and porosity. This is important for many applications such as tissue engineering, drug delivery and gel-based separation media and also for advancing the basic science of hydrogel and complex multi-component networks.

## Chapter 2: General Background, Terminology and Theory

### Abstract

This chapter is a general overview of hydrogels. The purpose is to orient a novice in the field to the background, terminology and theory. The thesis aims to engineer the microstructure of hydrogels to achieve enhanced mechanical properties. There are many ways to change the microstructure of hydrogels, but this work focuses on the synthesis techniques and the composition of the hydrogel to achieve optimal swelling, mechanical properties and network structures, as depicted in Figure 2.1.

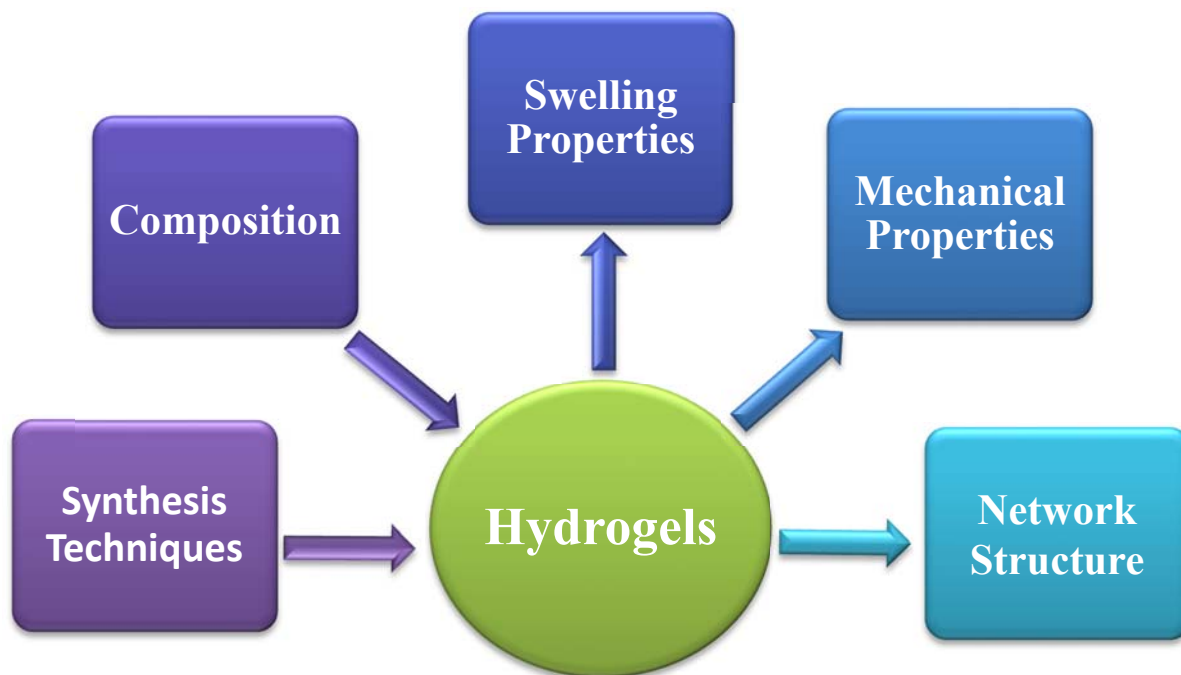


**Figure 2.1: Schematic of research on hydrogels**

By engineering hydrogels through the synthesis techniques and composition the swelling properties, mechanical properties, and the network structures are altered.

Chapter 2 begins with a description of hydrogels and the major categories of hydrogels explored in this dissertation: multi-component hydrogels, interpenetrating (IPN) hydrogels, semi-IPN hydrogels and double-network (DN) hydrogels. Next, the terminology and techniques to measuring the swelling and mechanical properties of hydrogels were explained. Then the swelling thermodynamics is described including rubber elastic models.

### **Hydrogels:**

A hydrogel is conventionally a network of a hydrophilic polymer that has a high water content.<sup>[45,138]</sup> Figure 2.2 shows a highly swollen hydrogel. Their ability to contain over 95% water content is a physical property that is desirable in many applications. In particular, hydrogels are being studied for use in many fields including pharmaceutical and biomedical, especially in tissue engineering (TE).<sup>[137]</sup> Hydrogels have already become widely used as contact lenses and superabsorbents (for example: diapers), and is seen in the food industry (for example: gum) and agriculture (for example: Watersorb).<sup>[137]</sup>

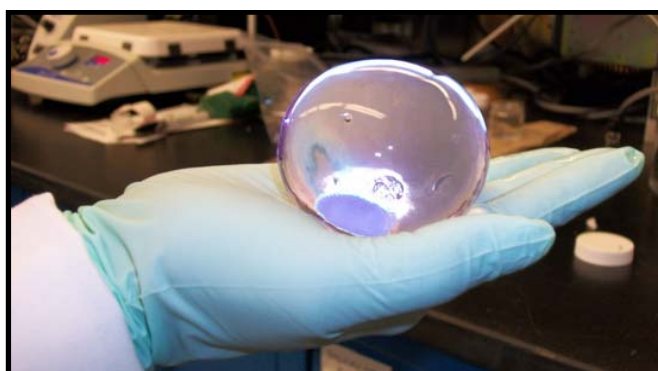


**Figure 2.2: Highly swollen hydrogel.**

### ***Multi-component Hydrogels***

Developing multi-component hydrogels has been an active area of research for many scientists because of improvements in mechanical properties that are attained (modulus, fracture stress, fracture strain, toughness and tearing energy) while maintaining high water content. Outlined in Chapter 8 are six major categories of multi-component hydrogels which have improved mechanical properties: copolymers (such as tetra-PEG), slide-ring (SR) or topological gel (TP), IPN (semi-IPN and DN), nanocomposite (NC), microgel-reinforced (MR) and mixtures of ionically and covalently cross-linked gels such as ionic-covalent entanglement (ICE) gels (shown in Chapter 8, Figure 8.1).

### ***Interpenetrating Networks***

IPN hydrogels are two independent chemically cross-linked networks in which the two networks remain interconnected because of physical entanglements.<sup>[85]</sup> Because of residual unreacted cross-linkers of the first network, slight covalent cross-linking between the first and second networks many occur; however they are still called IPNs because they show similar fracture mechanisms.<sup>[123]</sup> IPN hydrogels typically have physical properties that are an average of the single networks or are similar to one of the networks but not usually significantly greater than both single networks.<sup>[85]</sup> IPNs can be synthesized in a two-step sequential process in which the first network is created, soaked in the solution of the second network precursor which is subsequently polymerized.<sup>[118]</sup> IPNs can also be synthesized simultaneously if the reaction mechanisms of the two networks do not interfere with each other – a simultaneous IPN – for example, a free radical polymerization reaction and a condensation cross-linking reaction that occurs at the same time.<sup>[118]</sup>

### ***Semi-Interpenetrating Networks***

Semi-interpenetrating networks are a subcategory of IPNs. Semi-IPNs are synthesized in the same manner as IPNs as a two-step sequential process or simultaneously, as described above. Semi-IPNs also have similar physical properties to IPNs, thus they are typically just an average of the single networks or are similar to one of the networks but not significantly greater than both of the networks.<sup>[85]</sup> However the major difference between an IPN and a semi-IPNs is that semi-IPNs contain one network that is not chemically cross-linked

### ***Double-Network Hydrogels***

DNs comprise another subcategory of IPNs, synthesized by the same method but strategically produced so the two components lead to superior mechanical properties.<sup>[50,61,192]</sup> The composition and the resulting mechanical properties distinguish DN hydrogels substantially from other IPNs hydrogels. DNs have two independently chemically cross-linked networks in which the two networks remain interconnected because of physical entanglements, the same as an IPN (slight covalent cross-linking of first to second networks can occur<sup>[123]</sup>). But not all IPNs are DNs because DNs are constructed in such a way that provides superior mechanical properties and unique features in the stress-strain curves. The first network is highly cross-linked and brittle (typically a polyelectrolyte). The brittle nature is key to producing the high toughness from the fracturing of the first network which leads to high energy dissipation. The second network is in excess to the first and is highly concentrated, loosely cross-linked, ductile and neutral. The ductile nature of the second networks is what allows the DN to hold together at high extensions. Thus, the combination of brittle and ductile networks is one of the unique features of DN hydrogels. Thus, emphasizing that DNs include the unique mechanical properties which are achieved, and the synergistic internal

molecular structures thus lead to superior toughness and fracture properties, outlined below:

- (1) Synthesized as an IPN of a brittle (typically polyelectrolyte) first network and a ductile (typically neutral) second network where the:
  - a. Second network is in excess to the first network and
  - b. The first network is highly cross-linked, the second network is lightly cross-linked
- (2) Enhanced mechanical properties relative to either single network where
  - a. High toughness is achieved
  - b. Non-ideal elastic behavior is exhibited and
  - c. Yielding region is observed (under tension)

## **Swelling and Mechanical Properties**

This section goes through the major properties that were studied throughout the dissertation, first describing the equilibrium swelling and then describing the mechanical properties (modulus, failure properties, toughness, yielding properties, tearing energy) explored, as well as going over typical stress-strain curves seen in this work.

### ***Equilibrium swelling degree***

The equilibrium swelling degree is the most important property in a hydrogel and is described as the volume degree of swelling (Q) or mass degree of swelling (q), Equations (2.1) and (2.2). The equilibrium swelling degree can vary from 1.2 to over 1000<sup>[45]</sup>. The equilibrium water content (EWC) can vary from 20% to over 95%, Equation (2.3).<sup>[45]</sup>

$$Q = \frac{\text{volume of swollen hydrogel}}{\text{volume of dry polymer}} \quad (2.1)$$

$$q = \frac{\text{mass of swollen gel}}{\text{mass of dry polymer}} \quad (2.2)$$

$$\text{EWC} = \frac{\text{mass of water absorbed by gel}}{\text{mass of swollen gel}} 100 \% \quad (2.3)$$

The polymer volume fraction,  $\phi'_p$ , is the inverse of the volume degree of swelling:

$$\phi'_p = \frac{1}{Q} \quad (2.4)$$

### ***Mechanical properties***

The stress-strain curves provide information of the bulk mechanical properties of the hydrogels under either compression or tension. Figure 2.3 shows a typical stress-strain curve for the work in this dissertation under compression, which shows neo-Hookean behavior. Although the typical hydrogel behaves as neo-Hookean (ideal elastomers) in tension, DNs and do not display neo-Hookean behavior; therefore, Figure 2.4 shows a typical tensile test stress-strain curve for the work in this dissertation under tension. From the stress-strain curves the failure properties (fracture stress and fracture strain) are determined as the point at failure. The work to fracture, one measure of toughness, was calculated as the area under the stress-strain curve to the point of failure. If the hydrogels undergo yielding or necking then the yielding point (yielding stress, and yielding strain) was identified as the change in the slope.

The Young's modulus (E) is the slope of the initial linear portion of the stress-strain curve. The region at low strain % can be described by Equation (2.5)<sup>[154,179]</sup>, which is a simple linear fit that represents Hooke's law behavior. Strains up to 10% were typically used to calculate E.



$$\sigma = E\varepsilon = E(\lambda - 1) \quad (2.5)$$

The shear modulus (G) is the slope of the initial linear portion of the stress-strain function curve. When the stress is plotted vs. the strain function,  $(\lambda - \lambda^{-2})$ , linearity forms as in Figure 2.3. This shows that the material follows a neo-Hookean behavior<sup>[154]</sup>. Therefore, if the stress-strain functions are linear then G can be computed from Equation (2.6)<sup>[154]</sup>. Strains up to 70% (strain function of 10) were used in determining G. G is only valid if the hydrogels behaved as neo-Hookean.<sup>[154]</sup>

$$\sigma = \frac{F}{A_0} = G(\lambda - \lambda^{-2}) \quad (2.6)$$

$$\lambda = \frac{L}{L_0} \quad (2.7)$$

To evaluate if the data is consistent and the experimental techniques are dependable, Equation (2.8)<sup>[154]</sup> was used, which defines the relationship between E and G.

$$E = 2G(1 + \nu) \quad (2.8)$$

The Poisson's ratio,  $\nu$ , (ratio of transverse contraction strain to longitudinal strain) is  $\sim 0.5$  for ideal elastomers, thus the ratio of E/G is 3.<sup>[154]</sup> Some of the values may have a variance from 3. For swollen gels, this ratio is typically slightly greater than 3 under compression and less than 3 upon extension.<sup>[202]</sup> When measuring moduli it is found that E is very sensitive to slight defects in samples at small strains while G is not, and G uses much more of the stress-strain data, suggesting G is the more accurate parameter. Discrepancy can be due to experimental error such as nonparallel surfaces, surface irregularities, or sticking. Also, in the DN systems and some other multi-component hydrogels, the hydrogels do not behave as neo-Hookean materials. Therefore, Equation. (2.6) does not apply.

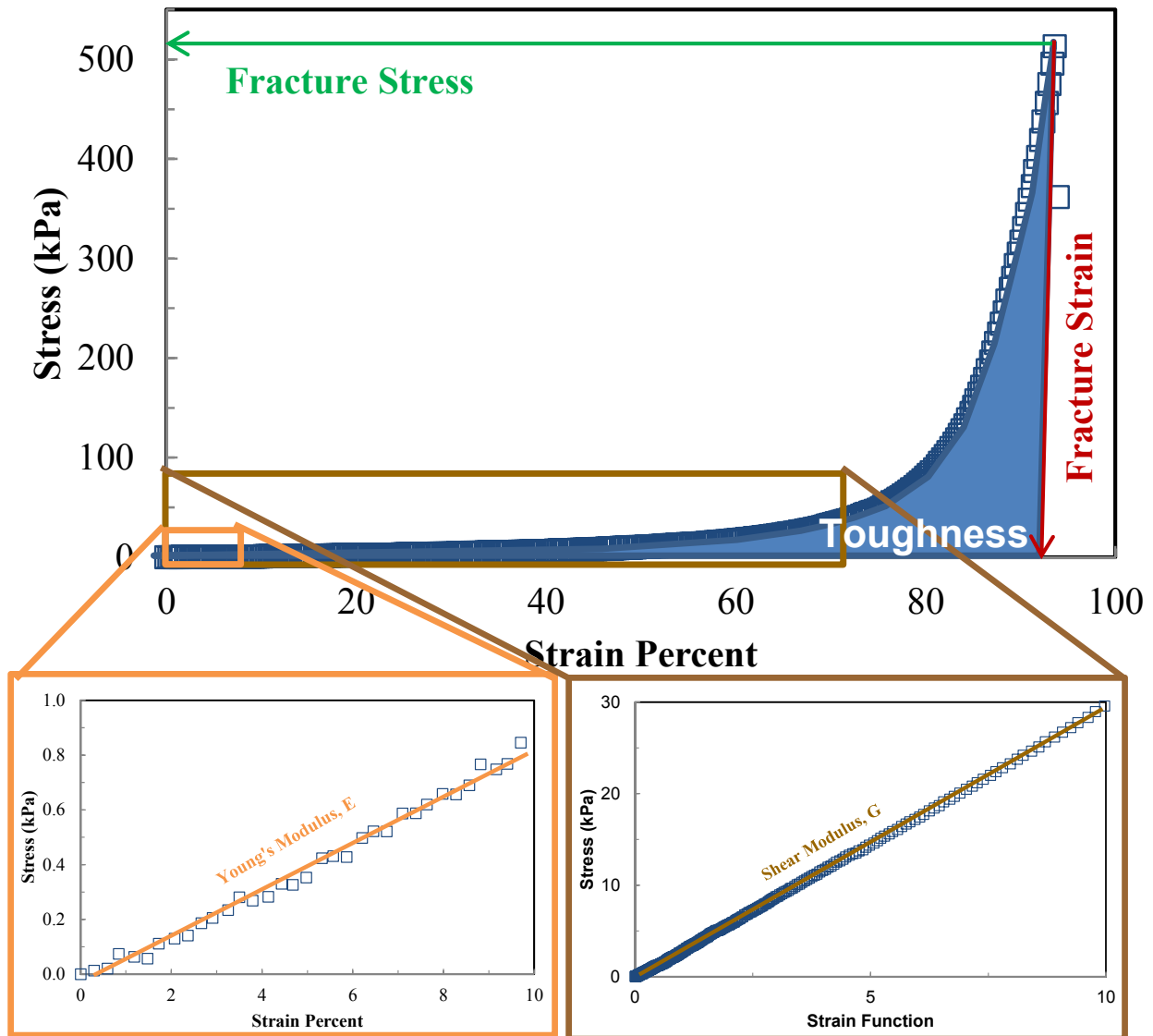


**Figure 2.3: Typical stress-strain curves under uniaxial compression for ideal elastomeric hydrogel**

From the stress-strain curves the mechanical properties were determined: failure properties (fracture stress and fracture strain), Young's Modulus (E), Shear Modulus (G) and toughness (work to fracture and area under the curve).

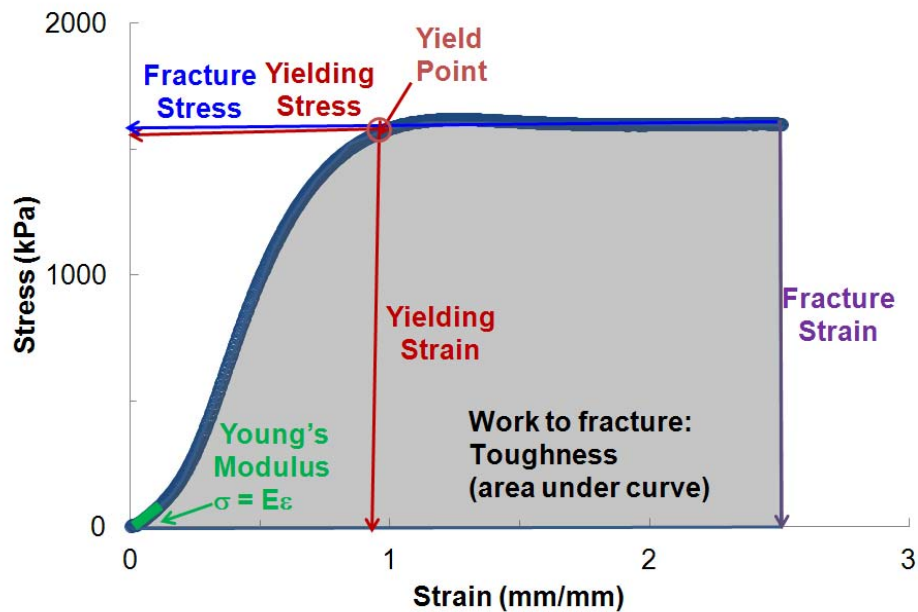


**Figure 2.4: Typical DN stress-strain curves under tension, non-ideal elastomeric hydrogel**

From the stress-strain curves the mechanical properties were determined: failure properties(fracture stress and fracture strain), Young’s Modulus (E), yielding properties (yielding stress, yielding strain and yield point), and toughness (work to fracture and area under the curve).

Tearing tests are not as common in hydrogels as compression or tension tests, but are important for analyzing another type of toughness, tearing energy. In tearing tests the fracture properties are independent of sample geometry.<sup>[54]</sup> The tearing tests were completed in mode III: out-of-plane shear, Figure 2.5.

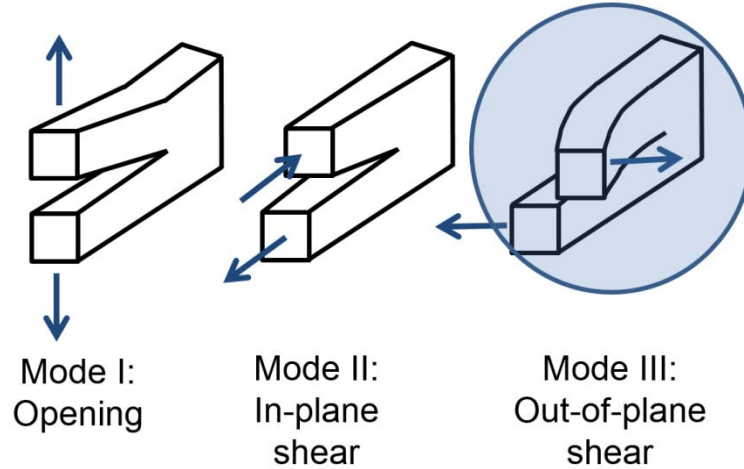


**Figure 2.5: 3 modes in tearing tests**

The tearing tests completed in this work were done in mode III, out-of-plane shear.

Figure 2.6 shows a typical force-extension curve from tearing tests on DN hydrogels.  $T$  represents the tearing energy, energy required from a unit area to create a newly fracture surface of the hydrogel, Equation 2.9.  $F_{avg}$  is the average force, or tearing resistance.  $W$  is the gel thickness. A typical force-extension curve is shown in Figure 2.5. The linear portion of the curve was averaged (minus the initial and final 5%) to determine the  $F_{avg}$ .

$$T = \frac{2F_{avg}}{w} \quad (2.9)$$

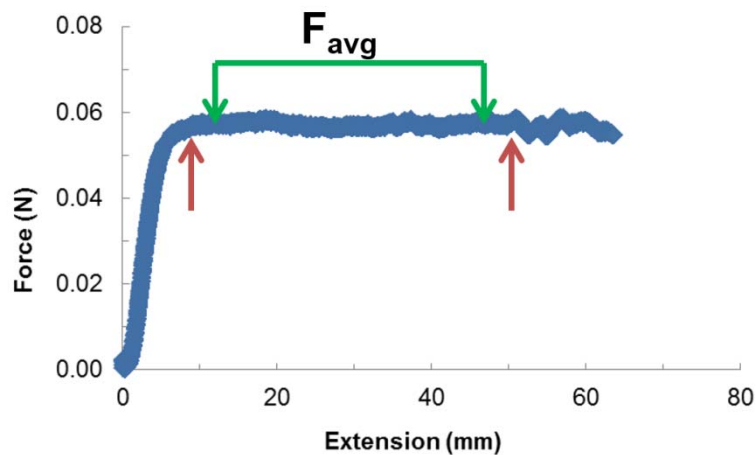


**Figure 2.6: Typical force-extension curve for tearing tests.**

The linear portion was averaged to determine the force which was then used to calculate tearing energy.

## Basic Theory

### *Swelling and Physical Properties*

In the 1940's, the basic theory to predict the swelling of a gel in equilibrium with a solvent was developed by Paul Flory and others, and is still in use today.<sup>[38]</sup> Flory used the fundamental thermodynamics to explain the swelling behavior of a gel; starting with the total Gibbs free energy written as the individual contributing terms (mixing of polymer and solvent, elastic response, concentration differences from ions in the gel and solution and electrostatic interactions, respectively)<sup>[67,152]</sup>:

$$\Delta G_{tot} = \Delta G_{mix} + \Delta G_{elas} + \Delta G_{ion} + \Delta G_{elec} \quad (2.10)$$

The chemical potential  $\mu_i$  is obtained by differentiating  $\Delta G$  at a constant P, T and  $n_{j \neq i}$ <sup>[67]</sup>,

$$\left( \frac{\partial \Delta G}{\partial n_i} \right)_{T,P,n_{j \neq i}} = \Delta \mu_i \quad (2.11)$$

From this, the relationship for the chemical potential for water in the gel develops. Species 1 is water and 2 is polymer (denoted as subscript in this section).

$$\mu_1 - \mu_1^0 = \Delta \mu_{mix} + \Delta \mu_{elas} + \Delta \mu_{ion} + \Delta \mu_{elec} \quad (2.12)$$

where  $\mu_1 - \mu_1^0$  is the difference between the chemical potential for the water in the gel and the reference chemical potential for the outside the gel, which in the case of this dissertation is water.

The osmotic pressure,  $\Pi$ , is related to the chemical potential by this relationship<sup>[178]</sup>:

$$\Pi = - \frac{\Delta \mu_1}{\tilde{v}_1} \quad (2.13)$$

where  $\tilde{v}_1$  is the solvent molar volume.

The swelling of a gel can be described using  $P_{ext}$  = externally applied pressure and the individual contributing terms (mixing of polymer and solvent, elastic response, osmotic pressure

of ions arising concentration differences from ions in the gel and solution and the electrostatic interactions of charges on polymer chains, respectively)<sup>[45]</sup>.

$$P_{\text{ext}} = \Pi_{\text{mix}} + \Pi_{\text{elas}} + \Pi_{\text{ion}} + \Pi_{\text{elec}} \quad (2.14)$$

During free swelling,  $P_{\text{ext}} = 0$ .<sup>[135]</sup> If there are no ionizable groups (neutral networks), there is no ion osmotic pressure generated  $\Pi_{\text{ion}} = 0$  and no electrostatic interactions  $\Pi_{\text{el}} = 0$ . The nonionic gel can then be described as:

$$0 = \Pi_{\text{mix}} + \Pi_{\text{elas}} \text{ or } \Pi_{\text{mix}} = -\Pi_{\text{elas}} \quad (2.15)$$

Physically, the swelling forces – hydrophilic polymer-water interactions, electrostatic and osmotic forces – of the water try to expand the network and are continuously countered by the entropic elastic restoring force from cross-linking junctions; this gives the gel its elasticity, Figure 2.6. When the two forces are balanced, the gel is in its swollen equilibrium<sup>[38]</sup>. The swollen gel, hydrogel, acts as an elastic solution.<sup>[38] [40] [135]</sup>

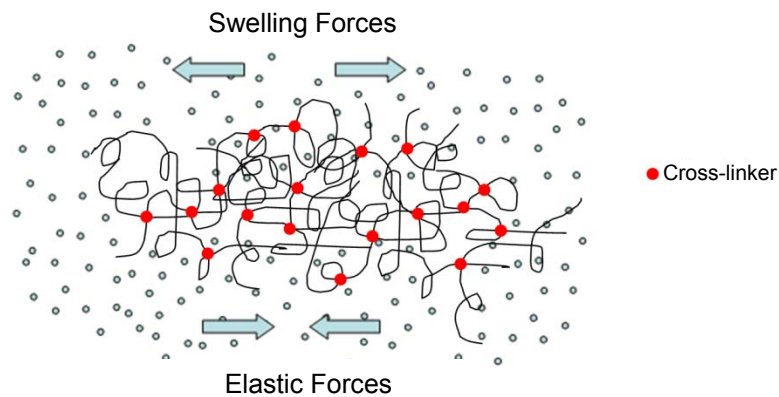


**Figure 2.6: Swelling and elastic forces in balance in hydrophilic hydrogels swollen to equilibrium**

When the gel is swelling in the solvent the two forces oppose each other. In equilibrium the forces are balanced.

The polymer solvent mixing term,  $\Pi_{\text{mix}}$ , is most commonly described using the Flory-Huggins solution theory.<sup>[38]</sup> The polymer-solvent interaction parameter,  $\chi$ , results from changes in the enthalpic interactions upon mixing the polymer and solvent (though empirically it is found to include non-ideal entropic contributions).

$\chi < \frac{1}{2}$  favors dissolution: polymer-solvent interaction dominate

$\chi > \frac{1}{2}$  disfavors dissolution: polymer-polymer or solvent-solvent interaction dominate

$\chi = \frac{1}{2}$  “theta state” no net interactions

Complete, systematic derivations can be seen by Flory<sup>[38] [40] [39]</sup> or Fried<sup>[41]</sup>.

$$\Pi_{\text{mix}} = -\left(\frac{RT}{\bar{v}_1}\right) [\ln(1 - \phi_2) + \phi_2 + \chi\phi_2^2] \quad (2.16)$$

where  $R$  is the ideal gas constant,  $T$  is the temperature,  $\phi_2$  is the polymer volume fraction in the gel.

The elastic term,  $\Pi_{\text{elas}}$ , was derived by Flory and Wall from the basic thermodynamics using the statistical rubber elasticity theory<sup>[38]</sup>. This theory is also known as the affine theory (later in this section the phantom model was also discussed). The derivations of this theory, given in Eq. 2.17 can be seen by Flory<sup>[38] [40] [39]</sup> or Treloar.<sup>[179]</sup>

$$\Pi_{\text{elas}} = -\frac{RTv_e}{V_0} \left( \frac{1}{2}\phi_2^{1/3} - \frac{1}{2}\phi_2 \right) = -RT\rho_x \left( \phi_2^{1/3} - \frac{1}{2}\phi_2 \right) \quad (2.17)$$

where  $v_e$  = number of elastically effective polymer chains (those which are deformed by stress),  $V_0$  = unswollen gel volume and  $\rho_x$  = effective crosslink density relative to the solid state.

For networks made in solution (such as is the case with many common hydrogels and those in this thesis) Equation (12) was derived by Peppas and Merrill.<sup>[135]</sup>

$$\Pi_{\text{elas}} = -RT\rho_x\phi_{2f} \left[ \left( \frac{\phi_2}{\phi_{2f}} \right)^{1/3} - \frac{1}{2} \left( \frac{\phi_2}{\phi_{2f}} \right) \right] \quad (2.18)$$

where  $\phi_{2f}$  = polymer volume fraction at network formation

By combining Equation (2.16) and (2.17) in (2.15), free swelling of a non-ionic polymer network in equilibrium with a solvent is given as:

$$0 = [\ln(1 - \phi_2) + \phi_2 + \chi\phi_2^2] + \tilde{v}_1\rho_x\phi_{2f} \left[ \left( \frac{\phi_2}{\phi_{2f}} \right)^{1/3} - \frac{1}{2} \left( \frac{\phi_2}{\phi_{2f}} \right) \right] \quad (2.19)$$

In this particular case, the ion term,  $\Pi_{\text{ion}}$ , was neglected; however, if the polymer network has ionizable groups (polyelectrolyte gels), the ion term would be described by the following Equations (2.20)<sup>[67]</sup> or (2.21)<sup>[45]</sup>. When the ions are present in solution and form an ideal solution, Equation (2.20)<sup>[67]</sup> is the limiting case. Equation (2.21)<sup>[45]</sup> is a way of calculating  $c^*$  in terms of the ions in the gel.

$$\Pi_{\text{ion}} = RT(c - c^*) \quad (2.20)$$

$$\Pi_{\text{ion}} = RT \left[ \left( \frac{i\phi_2}{\tilde{v}_m} \right) + (c_s - c_s^*) \right] \quad (2.21)$$

where  $c$  = molar concentration of mobile ions in the solution inside the gel,  $c^*$  = molar concentration of mobile ions in the solution outside the gel,  $c_s$  = molar concentration of electrolyte in the gel originating in the external solution and  $c_s^*$  = molar concentration of electrolyte in the external solution

By combining mechanical tests with synthesis properties the effective crosslink density,  $\rho_x$ , molecular weight between crosslinks,  $M_c$ , and the polymer-solvent interaction parameter,  $\chi$ , can be calculated. This is achieved using an elastic model for hydrogels. The most commonly used elastic model for hydrogels is the affine model, Equation (2.17).<sup>[34]</sup> In this model, the macroscopic deformations are the same at all length scales.<sup>[34]</sup> Also, the junctions are fixed in the network.<sup>[34]</sup> The affine model has been used in Equations (2.18), (2.19) and (2.23). The junctions in the hydrogel matrix do not necessarily stay fixed; they move around in an area such as in Brownian



motion<sup>[38]</sup>. James and Guth presented the phantom network theory<sup>[34]</sup> which takes into account the movement and matches typically matches swollen networks more accurately<sup>[45]</sup>. In the phantom theory the chain entanglements in which the chains can cross each other are neglected.<sup>[34]</sup> Similar to how a “ghost,” can move through walls. Equation (2.22) is the derived phantom model. The  $(1 - 2/f)$ , factor describes the effective crosslink density on the dry basis<sup>[34]</sup>. For typical cross-linkers, the junction functionality,  $f = 2$  therefore  $(1 - 2/f) = 0.5$ .

$$\rho_x = \frac{G}{(1-2/f)RT\phi_2(\phi_{2f}/\phi_2)^{2/3}} \quad (\text{phantom}) \quad (2.22)$$

$$\rho_x = \frac{G}{RT\phi_2(\phi_{2f}/\phi_2)^{2/3}} \quad (\text{affine}) \quad (2.23)$$

Where:  $f$  is junction functionality;  $R$  is the ideal gas constant;  $T$  is the temperature;  $\phi_2$  is the polymer volume fraction in the gel;  $\phi_{2f}$  is the polymer volume fraction at network formation;  $\rho_x$  is the effective cross-link density in the polymer network (moles per volume polymer).

If all of the cross-linkers created effective cross-links the crosslink density would be described by theoretical cross-link density,  $\rho_t$ , Equation (2.24)<sup>[45]</sup>.

$$\rho_t = \frac{cf}{2} \quad (2.24)$$

Where  $C$  is the cross-linker concentration.

Therefore the crosslink efficiency is just the ratio of the effective crosslink density over the theoretical crosslink density, Equation (2.25)

$$\eta_c = \frac{\rho_x}{\rho_t} \quad (2.25)$$

The molecular weight between cross-links,  $\rho_x$ , is related to the molecular weight between cross-links,  $M_c$  by  $\rho_2$ , the cross-link density on the dry basis.

$$\rho_x = \frac{\rho_2}{M_c} \quad (2.26)$$

By combining Equations (2.23) and (2.26) for the affine model or Equation (2.22) and (2.26)

for the phantom model,<sup>[45]</sup> the molecular weight between cross-links can be determined: Equations (2.27) and (2.28).

$$M_c = \frac{(1-2/f)RT\rho_2\phi_{2f}^{2/3}}{GQ^{1/3}} \quad (\text{Phantom}) \quad (2.27)$$

$$M_c = \frac{RT\rho_2\phi_{2f}^{2/3}}{GQ^{1/3}} \quad (\text{Affine}) \quad (2.28)$$

The Flory-Huggins solubility parameter can be calculated by rearranging Equation (2.19) with the previous experimental data<sup>[135]</sup>:

$$\chi = - \frac{[\ln(1-\phi_2) + \phi_2] + \tilde{v}_1\rho_x(\phi_{2f})^{\frac{2}{3}}(\phi_2)^{\frac{1}{3}}\left(1-\frac{2}{f}\right)}{\phi_2^2} \quad (\text{Phantom}) \quad (2.29)$$

$$\chi = - \frac{[\ln(1-\phi_2) + \phi_2] + \tilde{v}_1\rho_x\phi_{2f}\left[\left(\frac{\phi_2}{\phi_{2f}}\right)^{1/3} - \frac{1}{2}\left(\frac{\phi_2}{\phi_{2f}}\right)\right]}{\phi_2^2} \quad (\text{Affine}) \quad (2.30)$$

The biggest problem for using  $\chi$  for hydrogels interactions of the water with the polymer such as hydrogen bonding, polar interactions and water structuring.<sup>[46]</sup> Other difficulties with  $\chi$  are dependencies with many variables: temperature, concentration, molecular weight, etc.<sup>[45]</sup> Also, the methods for predicting  $\chi$  values are difficult for hydrogels because  $\chi$  was developed for linear polymers and although the theory is typically good for lightly cross-linked networks, disparities may occur.<sup>[46]</sup> Hydrogels are not completely homogeneous within the entire matrix<sup>[135]</sup>. Imagining only a few starting points of the growth of the polymer chains, the polymer will be more dense closer to these points and less dense the further away to these sites.

There are more advanced theories for predicting the mixing and elastic terms, though these theories can be complex and require parameters which are difficult to measure accurately for hydrogels<sup>[45]</sup> Researchers have used Sanchez and Lacombe polymer solution model for  $\Pi_{\text{mix}}$  and

have been able to reliably and precisely predict theoretical swelling properties for hydrogels, but the models need parameters that are hard to determine accurately using experimental techniques.<sup>[45]</sup> Furthermore, the elastic term assumes a Gaussian distribution of chain extensions, which is often true for nonionic networks, for polyelectrolytes, though non-Gaussian chain distributions need to be considered. Non-Gaussian models have been developed but they require additional parameters<sup>[135]</sup>.

## Chapter 3: Semi-Interpenetrating Hydrogels of Agarose and Poly(ethylene glycol diacrylate) (PEGDA) Display Additive Behavior in Mechanical Properties<sup>3</sup>

### Abstract

Researchers have greatly improved the mechanical properties (toughness, fracture properties, and modulus) of hydrogels and are approaching the reality of using hydrogels in tissue engineering applications which require a mechanically robust material to replace cartilage tissue. Polyethylene glycol (PEG) and agarose systems have been under investigation by many scientists and a systematic study of the formulations of semi-IPNs of agarose/PEGDA will expand the understanding these multi-component hydrogels. The potential of this semi-IPN system has not been fully explored and direct evidence of the network structure of semi-IPNs of agarose and PEGDA is still not available. Therefore, the objective was to systematically study formulations of single-network (SN) and semi-IPNs of agarose and PEGDA to determine a range of desirable properties, and then to image the hydrogels using atomic force microscopy (AFM) and scanning electron microscopy (SEM) to correlate these properties. The semi-IPNs typically exhibited a modest improvement in the mechanical properties (modulus, fracture stress, and toughness). The pore size of the semi-IPNs were an intermediate in size compared to the corresponding SNs. Overall, the compression tests revealed that the semi-IPNs behaved as ideal elastomers and had additive rather than synergistic mechanical properties.

---

<sup>3</sup>To be submitted as **Tiffany C. Suekama**, Ganesh Ingavle, David Moore, Joseph Lomakin, Micheal S. Detamore, Stevin H. Gehrke

## Introduction

Semi-interpenetrating network (semi-IPN)s are a subcategory of IPNs in which two networks are interlaced and independent of each other, but one is chemically cross-linked and one is an entangled polymer. Each network retains its properties but improved properties in comparison to the single networks can be achieved.<sup>[85]</sup>

Using the strategy of interpenetrating networks, our group has recently published semi-IPN hydrogels of agarose/poly(ethylene glycol) diacrylate (PEGDA).<sup>[28,73]</sup> Agarose and PEGDA are both widely used materials for biomedical applications such as TE. Agarose is a linear polysaccharide that can form gels at low concentrations, but it is too viscous to process at higher concentrations.<sup>[127,197]</sup> Thus, the total polymer content is limited and the gels fracture at low stresses and strains (low toughness).<sup>[30]</sup> However, agarose has large pores (micro-pores 0.2-8  $\mu\text{m}$ )<sup>[30,83,97]</sup> which decrease with concentration.<sup>[30,83,97]</sup> PEGDA can be photopolymerized into a gel over a broad range of concentrations but these gels do not have large pores for transport of large molecules such as proteins, and migration of cells. PEG-based gels are highly researched due to being neutral and biocompatible with tunable mechanical properties.<sup>[94,126]</sup> Plus, PEG-based gels can be functionalized to add cell signaling groups and controlled synthesis or degradation.<sup>[94,103,107,133,181,184,193]</sup> PEGDA was found to be nano-porous (with small angle x-ray scattering(SAXS) PEGDA had nanoscale ordered structure of 6 to 16 nm<sup>[188,189]</sup>).

Multi-component semi-IPNs hydrogels of agarose/PEGDA have been previously shown to have improvement in mechanical strength.<sup>[28,148,178]</sup> Semi-IPNs of agarose and PEGDA (MW 2000) led to improvements of 4 fold or greater in the mechanical properties such as shear modulus in comparison to either SN alone.<sup>[28,178]</sup> Also, fracture properties of semi-IPNs were greater than SN agarose.<sup>[28,178]</sup> When comparing various formulations increasing the PEGDA content was

determined to be a significant factor to increase the shear moduli and the increase in MW of PEGDA was critical in increasing the fracture properties.<sup>[178]</sup> Chondrocytes were successfully encapsulated in the semi-IPN networks, the cells were viable after one week and showed glycosaminoglycan synthesis.<sup>[28,178]</sup> Furthermore, bioactive signaling using aggrecan or chondroitin sulfate had improved the cell viability in six week studies.<sup>[73,74]</sup> Although a lot of work has been done on semi-IPNs of agarose and PEGDA hydrogels there is an unclear influence of the formulation of the hydrogels on the mechanical properties. The network structure impacts the transport of small molecules to diffuse or bioactive components to migrate. Also, to the best of our knowledge there is no direct evidence of the structure of semi-IPNs and the relationship of the structure to the mechanical properties. Therefore, the objective was to study a range of formulations of single-network and semi-IPNs of agarose and PEGDA to develop relationships between the mechanical properties, to determine the limit of the semi-IPN system, and to image the networks using atomic force microscopy (AFM) and scanning electron microscopy (SEM) to obtain a complete view of the structure-mechanics relationship.

## Materials

All of the reagents were used as received. A low gelling agarose, 2-Hydroxyethyl agarose (agarose; Type VII-A: gel point  $26\text{ }^{\circ}\text{C} \pm 2\text{ }^{\circ}\text{C}$ ) and poly(ethylene glycol) diacrylate (PEGDA; Average MW 700Da) were obtained from Sigma-Aldrich. The initiator 1-[4-(2-Hydroxyethoxy)-phenyl]-2-hydroxy-2-methyl-1-propane-1-one (Irgacure 2959) was donated by Ciba (Basel, Switzerland). Deionized ultra-filtered (DIUF) water from Fisher Scientific was used for all of the synthesis solutions.

## Methods

Important parameters when considering hydrogels for TE scaffolds as outlined by Hoffman include degradability, injectability, sterilizability, mechanical properties, pore structure and interconnectivity (e.g. open vs. closed pores), shape of construct, water content, chemical modifications and bioactive components.<sup>[66]</sup> TE hydrogel scaffolds can be designed with pores in the network<sup>[78,83,149]</sup> for enhanced transport of cells, proteins, drugs, oxygen and/or nutrients through the matrix, important for cellular survival and activity.<sup>[10,104]</sup> When considering the pores in the hydrogel network there are many factors to consider such as the average pore size (diameter if spherical)<sup>[107]</sup>, shape of the pores (most cases spherical)<sup>[107]</sup>, pore size distribution<sup>[7,78,153]</sup>, strut-wall thickness (polymeric network between pores)<sup>[107]</sup>, strut geometry<sup>[16]</sup>, and interconnectivity<sup>[80,107]</sup>. The mesh size or correlation length ( $\zeta$ ), the distance between two adjacent cross-links, is the parameter that commonly describes the size of a pore and is valid when considering a molecular level uniform mesh. *Therefore, this work classifies the hydrogels on the pore size (pore width): (1) macro-porous pores larger than 100  $\mu\text{m}$ ; (2) meso-porous, pore width 10–100  $\mu\text{m}$ ; (3) micro-porous, pore width 0.1–10  $\mu\text{m}$ ; (4) nano-porous, pores smaller than 0.1  $\mu\text{m}$ .*

### ***Synthesis of Single-Network (SN) PEGDA Hydrogel***

Synthesis methods were similar to previous procedures:<sup>[178]</sup> To prepare 11% (w/v) SN PEGDA hydrogel, PEGDA (12.36 g) and 0.03% (g/g) Irgacure 2959 (0.033 g) in DUIF water (100 mL) were mixed together in a glass vial. The solution was pipetted into a rectangular silicon rubber mold (~2 mm height) between two pre-cleaned microscope slides. The polymer solution was cross-linked by photopolymerization into a gel using a Spectrolinker (XL-1000, Spectronics Corp.) with a 312-nm light at ~10mW/cm<sup>2</sup> for 30 min (flipping after 15 min). The resulting gel was a SN PEGDA in the molded or as prepared state.

## ***Synthesis of Single-Network (SN) Agarose Hydrogel and Interpenetrating Network of Agarose/PEGDA***

Synthesizing a 2% (w/v) agarose hydrogel was as follows: agarose (0.08 g) and DUIF water (4 mL) are autoclaved until the agarose was fully dissolved. The solution was quickly pipetted into a rectangular silicon rubber mold (~2 mm height) between two pre-cleaned microscope slides. The molds were cooled at 4 °C for 24 hrs. For the synthesis of SN agarose gels in the molded state, no further action was taken. For semi-IPN of agarose/PEGDA the molded agarose hydrogel was allowed to swell to equilibrium in a PEGDA solution (as prepared in a single network) for 24 hrs. After swelling, the swollen gel was placed between two pre-cleaned microscope slides and was exposed to the Spectrolinker with a 312-nm light at ~10mW/cm<sup>2</sup> for 30 min (flipping after 15 min).

### ***Swelling Properties:***

Swelling procedures were similar to those previously reported.<sup>[166,178]</sup> Molded gel samples were swollen to equilibrium by submerging them in DUIF water at room temperature for 24 hrs. The water was changed every few hours to leach away unreacted chemicals. The excess water on the swollen gel was dabbed with a moist Kimwipe. The swollen gel was then weighed and then placed in a desiccator over CaSO<sub>4</sub> until it reached a constant weight. The dry weights were taken. The degree of swelling, Q (g/g), reported in the Results section are reported as the mass of the swollen gel over the mass of the desiccator dried gel.<sup>[45,135]</sup> Although this leads to a slight underestimate of the true gel swelling degree because of bound water in the desiccators dried gel.<sup>[45,135]</sup>



### ***Mechanical Analysis:***

Mechanical analysis and interpretation of the data to extract the mechanical properties were previously reported.<sup>[166,178]</sup> All of the cylindrical gels (~4mm diameter, ~2 mm height) were swollen to equilibrium and tested under unconfined, uniaxial compression using the RSA III dynamic mechanical analyzer (TA Instruments). Evaporation of water from the hydrogels can be visually observed within tens of minutes. Preliminary tests of strain rates between 0.1 mm/s to 0.0001 mm/s showed that a rates between 0.01 mm/s to 0.005 mm/s to be strain-rate independent with minimal evaporation effects. Therefore, at a rate of 0.05 mm/s was used for all compression tests. For precise accuracy, diameters of the samples were measured using a micrometer under a standard stereomicroscope (~10× magnification) and the heights were measured by the RSA III. Mineral oil was used to lubricate the plates so minimize adhesion and evaporation during testing.

Mechanical properties were found from the stress ( $\sigma$ )-strain ( $\epsilon$ ) data. The Young's modulus (E) was calculated as the slope of the linear portion of the stress-strain curve, the first 2-12% strain, due to artifacts in the mechanical testing from strains of 0-2%. If the hydrogels behave as ideal elastomers, the neo-Hookean model is valid, Equation 3.1.<sup>[179]</sup> Nearly all of the data will linearize when the stress is plotting against the strain function  $(\lambda-1/\lambda^2)$ .<sup>[179]</sup> Therefore, shear modulus (G) is found from the slope of the linear region of data typically up to the fracture point of the hydrogel (approx. 40-60%, strain function of 2-5). The fracture stress and fracture strain were found at the point that the gel ultimately failed resulting in an obvious drop in the stress.

$$\sigma = G(\lambda-1/\lambda^2) \text{ where } \lambda=L/L_0. \quad (3.1)$$

The toughness was determined as the area under the stress-strain curve up to failure (this measure of material toughness is also known as 'work to fracture').

### ***Imaging: SEM and AFM***

To properly visualize the networks of the hydrogels imaging was done by both scanning electron microscopy (SEM) and atomic force microscopy (AFM). SEM images on hydrogels typically have artifacts. Although AFM images can be difficult to interpret, AFM is desired over SEM because the images are taken in the hydrated state.

Ice crystals can lead to misleading network structures than found in the natural state of the hydrogel.<sup>[81]</sup> In order to properly vitrify the water from the sample and eliminate crystallization, the sample needs to be submerged in a substance with a high thermal conductivity (to transfer heat out of the gel quickly), a low freezing point, and a high boiling point and large heat capacity (so a vapor layer is not formed).<sup>[77]</sup> Thus, the fully swollen hydrogels were submerged into liquid ethane jacketed with liquid nitrogen (FEI Vitrobot; ~195 °C) for quick freezing. Some of the frozen samples were freeze-fractured then all of the frozen samples were placed in a lyophilizer (labconco) for ~2 days or until completely dry. The dry hydrogels were sputter coated with Au (10 mAmps for 2 min 200A thickness). Both the freeze-fractured and the unaltered samples were imaged using SEM (Leo 1550 field emission SEM).

To confirm the SEM images, AFM was performed on under tapping mode. on a vibration free table with a Veeco BioScope (Digital Instruments, Inc) with a Veeco Dimension XYZ head, Nanoscope 3D controller and Nanoscope software V613r1 To achieve good images the type of tip and properly mounting the samples was important. Veeco DNP1 tips were used for convectional topographic surface mapping. The sample was cut, taking care to provide a flat surface. To mount the sample a tiny dab on cyanoacrylate glue was placed on the bottom of the gel and then the gel was attached to a cell culture plate.<sup>[130]</sup> After a few minutes water was added to the plate so the gel could re-equilibrate. The cut samples were tested in the fully hydrated state, submerged in water.

## Results

### *Equilibrium Swelling Degree*

The equilibrium swelling degree is a defining property of a hydrogel because it affects all other properties and parameters. The swelling degrees for agarose, PEGDA and agarose/PEGDA semi-IPNs are given in Figure 3.1 and tabulated values are located in Table 3.1.

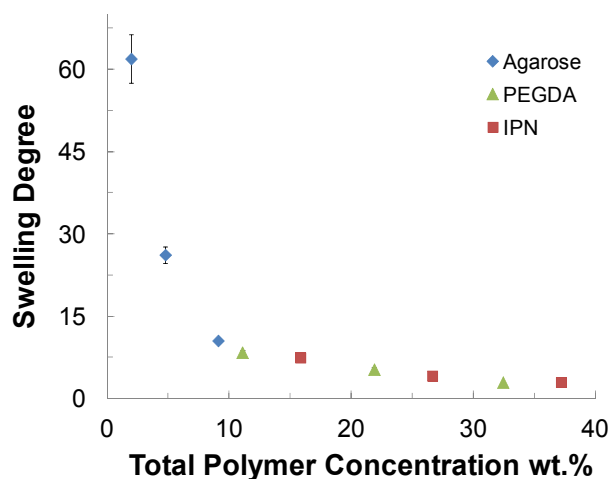


**Figure 3.1: Swelling decreases with total polymer concentration until plateauing around 3.**

The swelling degree decreases with increasing total polymer concentration (wt. %) Most error bars are smaller than symbols. Agarose (◆); PEGDA (▲); semi-IPN with 5% agarose and 10, 20 or 30% PEGDA (■).

The swelling degrees are plotted against the total polymer concentrations (wt. %). Agarose has high water content and low total polymer concentration (due to difficulties in processing from high viscosity). Overall, there is a sharp decrease in the swelling degree with increasing total polymer concentration until a total polymer concentration of ~10 (Q ~10). The swelling degrees continue to decrease with the total polymer concentration until ultimately plateauing around Q of ~3.

**Table 3.1. Measured properties of agarose, PEGDA and semi-IPNs of Agarose/PEGDA gels swollen to equilibrium in water.**

Agarose %	PEGDA %	Q (g/g)	E (kPa)	G (kPa)	E/G	Fracture Stress (kPa)	Fracture Strain (%)	Toughness (kJ/m <sup>3</sup> )
2	-	61.9±4.4	47.1±3.2	21.4±2.7	2.22±0.22	43.6±6.2	41.8±2.4	7.6±1.4
5	-	26.2±1.5	192±15	69.8±2.4	2.74±0.18	148.1±9.5	42.3±1.4	26.4±2.5
10	-	10.54±0.25	552±21	160.±5.2	3.451±0.038	461±33	47.9±2.0	88.6±9.8
-	10	8.40±0.40	126.2±7.1	76.6±5.7	1.66±0.15	320.±78	52.3±3.6	43.3±9.9
-	20	5.31±0.35	774±33	303±16	2.559±0.052	780.±91	44.0±1.7	117±16
-	30	2.965±0.013	3630±150	954±28	3.798±0.072	1860±320	38.6±3.5	304±73
5	10	7.45±0.21	388±22	127.6±8.1	3.04±0.12	520.±89	56.3±2.2	108±16
5	20	4.142±0.051	1214±72	415±12	2.927±0.096	1510±300	51.5±4.2	269±67
5	30	2.97±0.10	3289±349	869±66	3.77±0.11	2150±290	43.9±2.7	367±49
5	10	-	318±17*	146.5±6.2*	-	468±79*	-	70±10*
5	20	-	966±36*	373±16*	-	928±92*	-	143±17*
5	30	-	3820±150*	1024±28*	-	2000±320*	-	331±73*

(Mean ± Standard Deviation)

\*Hypothesized additive values

n= 3-5 for swelling tests

n=5-14 for mechanical tests

### ***Mechanical Analysis***

Compression tests were performed on hydrogels to determine the trends with the formulations of SN agarose, SN PEGDA and semi-IPNs of agarose/PEGDA. Mechanical analysis properties such as the E, G, fracture properties and toughness were determined from the stress-strain curves of these hydrogels and are tabulated in Table 3.1. The additive values of E, G, fracture stress and toughness are located in the bottom three rows of Table 3.1 and show if the properties

showed an additive, a greater than additive or a less than additive effect. The additive effect is further examined in greater detail in the discussion section.

Representative stress-strain curves of a typical agarose, PEGDA and agarose/PEGDA semi-IPN's are shown in Figure 3.2a. The hydrogels of SN agarose and SN PEGDA all fracture at around ~45% strain and the semi-IPN of agarose/PEGDA fracture at a slightly higher strain. The fracture stresses are much higher in the semi-IPN of agarose/PEGDA than either the SN of PEGDA or SN of agarose. As shown in Figure 3.2b, E is lowest in agarose compared to PEGDA or the semi-IPN of agarose/PEGDA. At higher concentrations of PEGDA, E of SN PEGDA and semi-IPN of agarose/PEGDA are similar (as described later in Figures 3.4b and 3.4d). When the strain data is plotted against the strain function all of the curves linearized ( $R^2 > 0.99$ ) demonstrating that they behave as ideal elastomers, Figure 3.2c. G is the slope of the stress-strain function ( $\lambda - 1/\lambda^2$ ) curves. Similar to E, G is greater in SN PEGDA and semi-IPN of agarose/PEGDA than SN agarose (as described later in Figures 3.4a and 3.4c).

Fracture strain, fracture stress, toughness, E and G are correlated with polymer volume fraction,  $\phi_2$  ( $\phi_2 = 1/Q$ ) and PEGDA content in Figures 3.3–3.8. Plotting against both  $\phi_2$  and PEGDA content removes biases produced from not having 100% conversion in polymerization. Plotting mechanical properties against  $\phi_2$  includes the dependence of the water content.

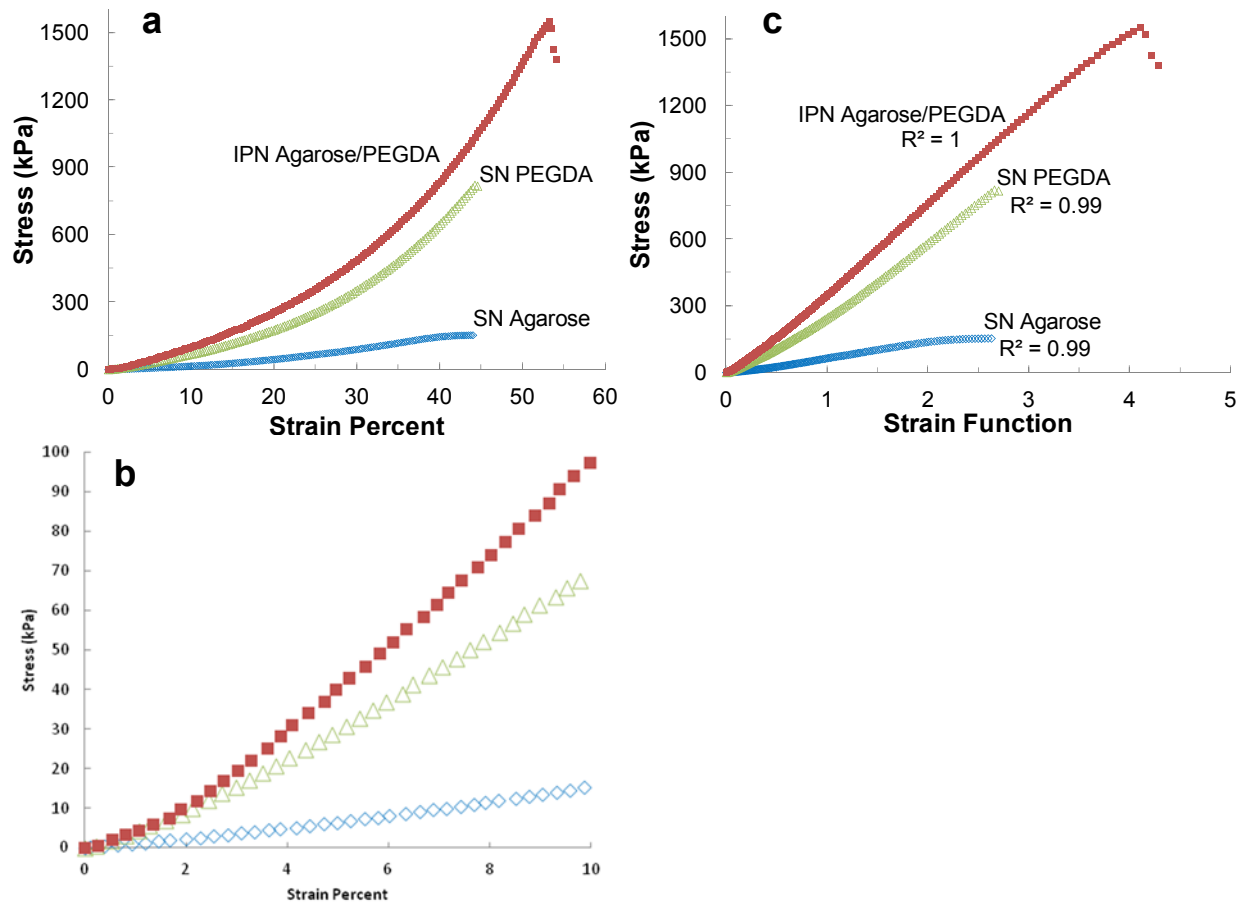


**Figure 3.2a, 3.2b and 3.2c: Representative stress-strain and stress-strain function curves of semi-IPN of agarose/PEGDA, SN agarose and SN PEGDA .**

Fracture strain % of semi-IPN agarose/PEGDA, SN PEGDA and SN agarose are all around 45% but the fracture stress are greatest in the semi-IPN (3.2a). Semi-IPN agarose/PEGDA, SN PEGDA and SN agarose behave as ideal elastomers with linear initial strains (3.2b) and the data linearizes when plotted against the strain function (3.2c). Agarose (◆); PEGDA (▲); semi-IPN with 5% agarose and 10, 20 or 30% PEGDA (■).

Comparing the moduli E and G of SN agarose, SN PEGDA and semi-IPN of agarose/PEGDA shows an overall trend that within each gel type the moduli increases with increasing polymer volume fraction or PEGDA content (for agarose and semi-IPNs), Figures 3.4a, 3.4b, 3.4c and 3.4d. Figures 3.4a and 3.4c display that moduli (E or G) of SN PEGDA and semi-IPN fall on nearly the same line when plotted against the polymer volume fraction. When the concentration of PEGDA is increased (30 wt. %) the SN PEGDA has a higher modulus than the

semi-IPN, Figures 3.4a and 3.4c. However, by plotting the moduli (E and G) against the PEGDA content, the semi-IPN of agarose/PEGDA has a slightly higher modulus, Figures 3.4b and 3.4d. The E/G ratio is around 3 for swollen gels which behave as ideal elastic solids but the ratio varies: slightly greater than 3 under compression and less than 3 upon extension.<sup>[202]</sup> The E/G ratio is close to 3 or slightly greater than 3 in only a few cases. The discrepancies could be due to slight sample defects in cutting the gels. However, most of the E/G ratios are increasing with increasing concentrations, Figure 3.3.

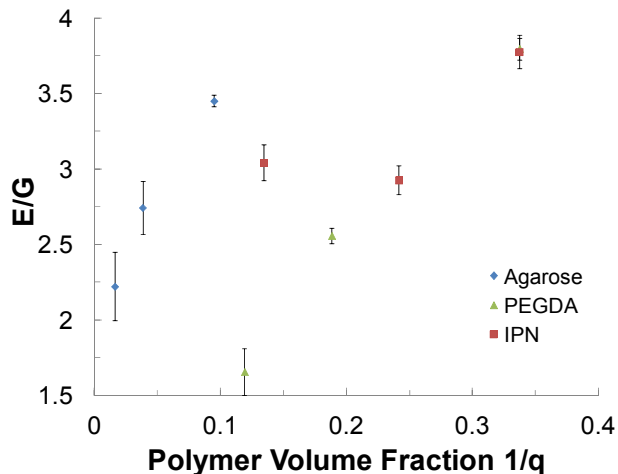
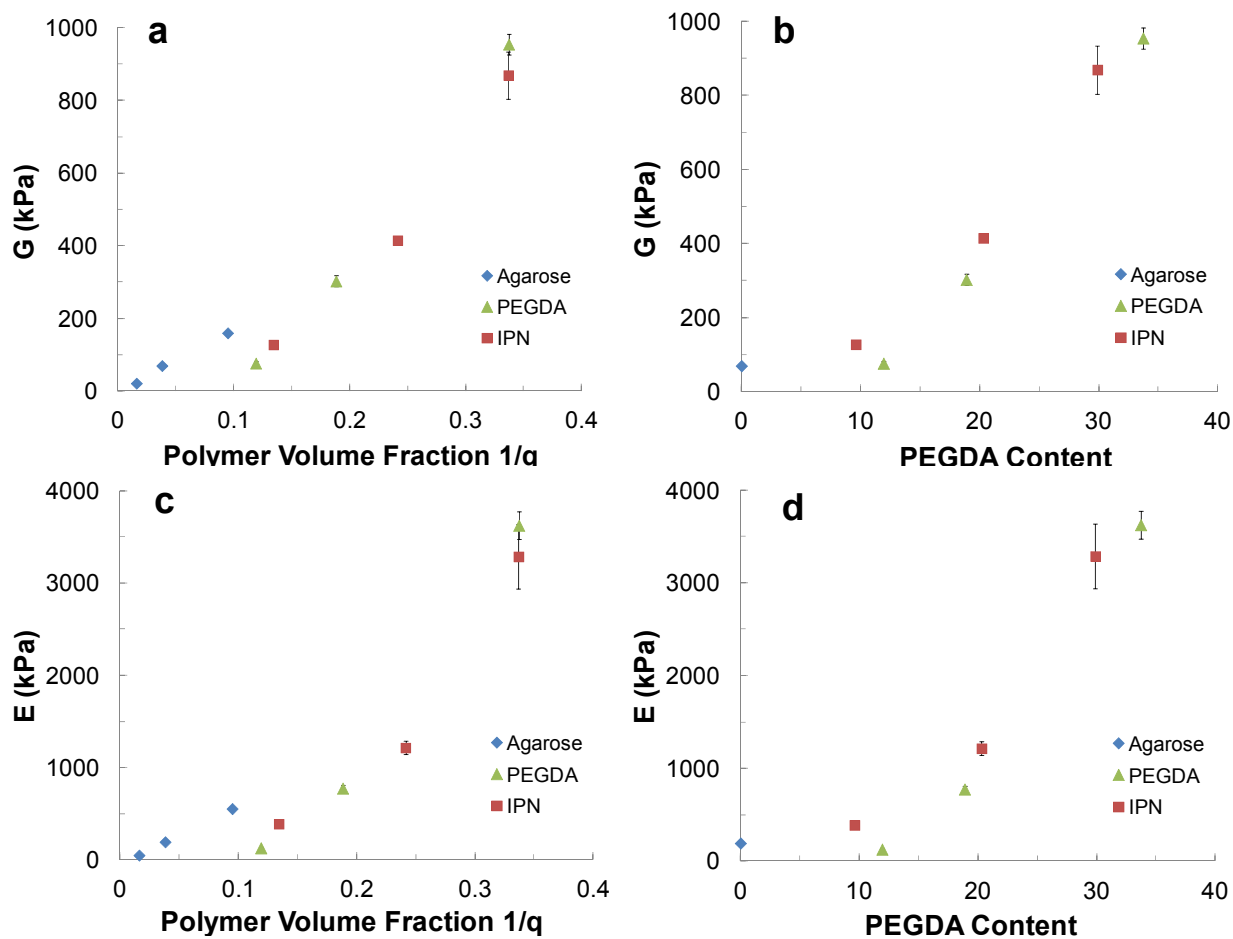


**Figure 3.3: E/G ratio typically increases with volume fraction**

SN PEGDA point behind the agarose at E/G ~3.8. Agarose (◆); PEGDA (▲); semi-IPN with 5% agarose and 10, 20 or 30% PEGDA (■).



Figures 3.4a, 3.4b, 3.4c and 3.4d: Moduli, E and G increase as polymer volume fraction and PEGDA content increase.

On investigation of the trends of moduli on the hydrogels, the shear modulus of SN PEGDA and semi-IPN of agarose/PEGDA nearly fall on a line (3.4a, 3.4c). However, at higher concentrations the SN PEGDA has both a higher E and G when plotted vs. volume fraction (3.4a, 3.4c). Though when plotting vs. the PEGDA content the semi-IPN of agarose/PEGDA has a higher moduli than SN PEGDA (3.4b, 3.4d). Most error bars are smaller than symbols. Agarose (◆); PEGDA (▲); semi-IPN with 5% agarose and 10, 20 or 30% PEGDA (■).

When the shear modulus is plotted on a log-log plot against the polymer volume fraction each type of gel (agarose, PEGDA and the semi-IPN) falls onto a single line and fits the function  $G \propto \phi^n$ , as shown in Figure 3.5. The exponents for the SN PEGDA,  $2.40 \pm 0.29$ , and semi-IPN,



2.08±0.055, are consistent with predictions of scaling theory for the modulus of a nonionic gel, which the modulus is proportional to the volume fraction raised to an exponent that for a good solvent:  $G \propto \phi_2^{9/4}$  and values of exponents between 2-2.5 are commonly reported.<sup>[21,22,31]</sup> Agarose is a rod-like polymer and has a fractal dimension close to 1.<sup>[57]</sup> The scaling theory model which links the dependence of modulus to the polymer volume fraction reduces to  $G \sim \phi_2^2$  for rigid cross-links and  $G \sim \phi_2^{3/2}$  for flexible cross-links.<sup>[128]</sup> The slope for the agarose is 1.13±0.13 which indicates flexible cross-links junctions.

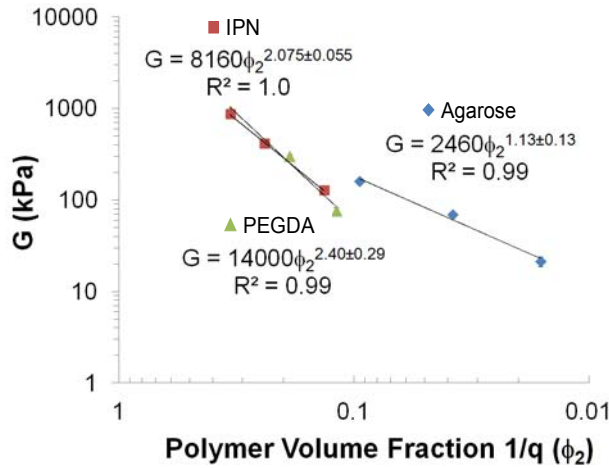
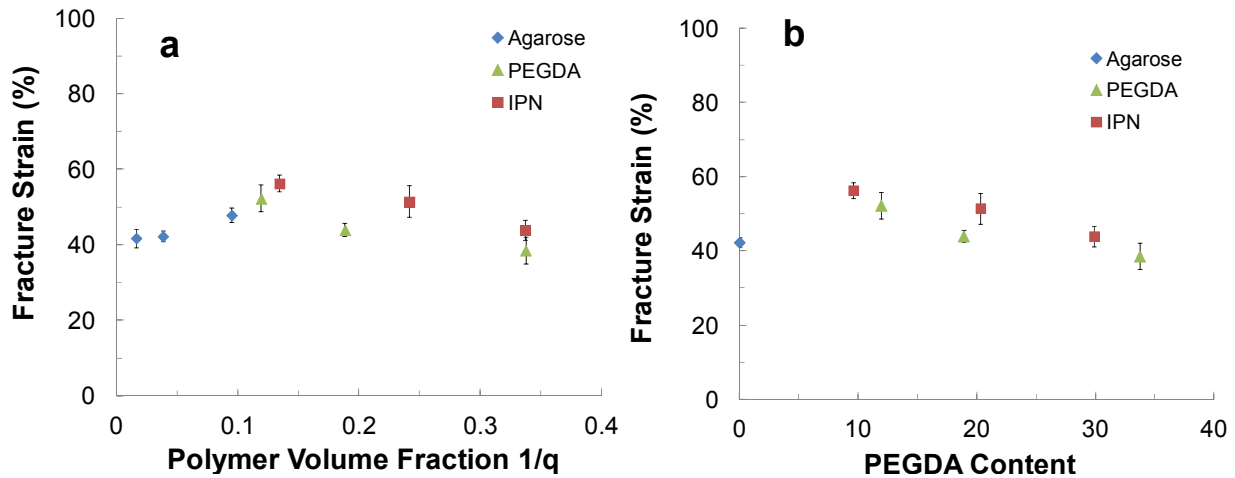


**Figure 3.5: PEGDA is shown to be the dominant property in semi-IPNs**

Both the shear moduli of the semi-IPN of agarose/PEGDA and SN PEGDA fall onto a single line on a log-log plot against polymer volume fraction and increases as the polymer volume fraction increases. The slopes are consistent with predictions of scaling theory that for a good solvent:  $G \propto \phi_2^{9/4}$ . Most error bars are smaller than symbols. Agarose (◆); PEGDA (▲); semi-IPN with 5% agarose and 10, 20 or 30% PEGDA (■).

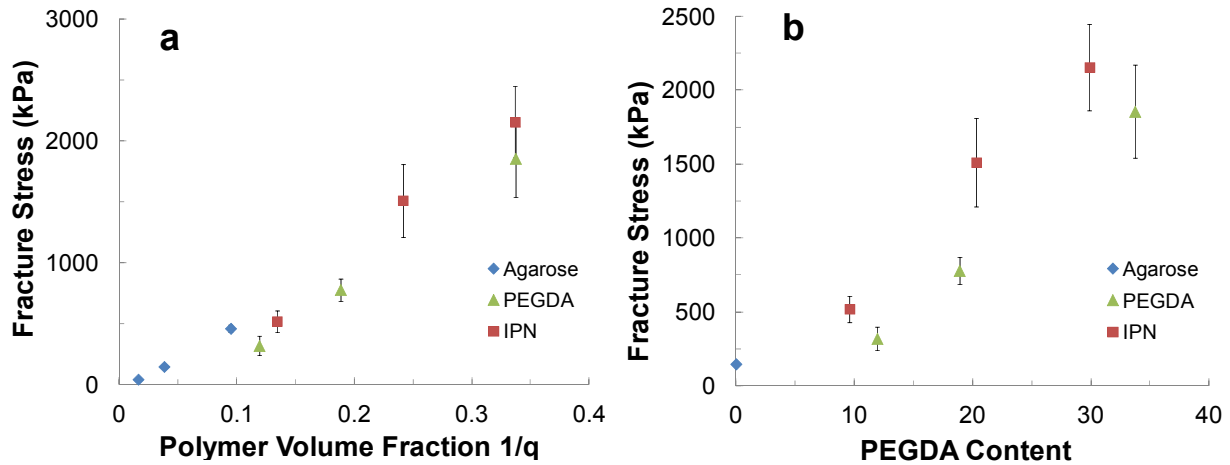
The fracture strains of the gels all are between 40-60% strain, but those for the semi-IPNs are slightly larger than the SN PEGDA gels, represented in Figures 3.6a and 3.6b. Furthermore, the fracture strain of SN agarose increases with polymer volume fraction. The fracture strain for

SN PEGDA and semi-IPN was shown to decrease with increasing polymer volume fraction or PEGDA content. On the other hand the fracture stresses show an obvious increase as the polymer volume increases, Figure 3.7a. The fracture stress appears linear with polymer volume fraction, Figure 3.7a. The trend that the fracture stresses of the semi-IPN hydrogel is higher than the SN PEGDA hydrogel becomes apparent when the fracture stress is plotted against the PEGDA content, Figure 3.7b. The toughness is also increasing as the polymer volume fraction or PEGDA content increases Toughness of the semi-IPN is better than the SN PEGDA, Figures 3.8a and 3.8b.

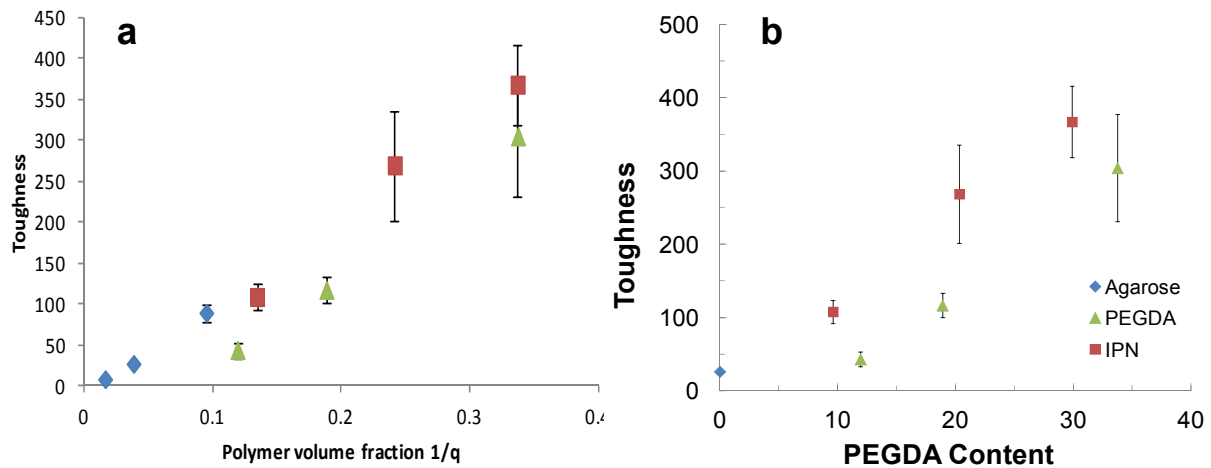


**Figures 3.6a and 3.6b: Fracture strain of the hydrogels around 50%**

All of the gels fracture ~40-55% regardless of formulation or type of gels; however the semi-IPN's have a fracture strain slightly better than the similar in polymer volume fraction PEGDA. Most error bars are smaller than symbols. Agarose (◆); PEGDA (▲); semi-IPN with 5% agarose and 10, 20 or 30% PEGDA (■).



**Figures 3.7a and 3.7b: Increasing fracture stress with polymer volume fraction and PEGDA content**  
 The fracture stress is increasing as the polymer volume fraction increases. The semi-IPN's have a fracture stress better than the similar in polymer volume fraction PEGDA. Some error bars are smaller than symbols. Agarose (◆); PEGDA (▲); semi-IPN with 5% agarose and 10, 20 or 30% PEGDA (■).



**Figures 3.8a and 3.8b:**  
 The toughness is increasing as the polymer volume fraction increases. The semi-IPN's have toughness better than the similar in polymer volume fraction PEGDA. Some error bars are smaller than symbols. Agarose (◆); PEGDA (▲); semi-IPN with 5% agarose and 10, 20 or 30% PEGDA (■).

## *Imaging*

Imaging under both SEM and AFM were completed for all of the formulations of gels. For all of the SEM images displayed in this work, the AFM images confirmed the SEM images were not a result of artifacts. Many researchers have used SEM as a technique to image network structures of hydrogels and although SEM provides a visually clear picture, the structure of hydrogels is hard to capture on using SEM due to artifacts which are hard to avoid. A few common artifacts are ice crystals that arise from not freezing quick enough, collapse of the structure upon drying, damage to the structure from sputtering, or damage to the energy from the electron beam.<sup>[81]</sup> Careful preparation is needed to achieve proper images. Therefore, this work couples SEM with atomic force microscopy (AFM) images. AFM can resolve nanometer scale resolution and can be seen in the natural state of materials (imaging in fluid) with no sample preparations (coatings, staining, or freezing).<sup>[6,48,79,89]</sup> However, imaging hydrogels have many difficulties. Hydrogels are typically soft materials and the cantilever tips often get caught in the gels causing “smearing” of the image.<sup>[206]</sup> Plus, long scanning rates are needed for imaging in fluid (even over an hour for one image). In general, the AFM images are typically not very clear and hard to interpret. This study used a combination of techniques to validate the results.

Agarose gels known to have micron-sized, phased separated, regions within the network and the polymer strands form bundles all which affects the structure.<sup>[97,143]</sup> The agarose gels are micro-porous and also have pores on many different length scales, as shown in Figure 3.9. SEM images of 2 wt. % agarose on a length scale of 10  $\mu\text{m}$  show 15-20  $\mu\text{m}$  pores (Figure 3.9a). At higher magnification focusing on the strut of the pore shows smaller and smaller pores. At a 2  $\mu\text{m}$  length scale 2-5  $\mu\text{m}$  pores are shown and at 0.2  $\mu\text{m}$  ~0.2-0.005  $\mu\text{m}$  pores are shown (Figures 3.9b and 3.9c respectively). The AFM image of 2 wt. % agarose show pores ~2-5 $\mu\text{m}$ , in Figure 3.10. The

AFM image indicates a large strut size show multiple different sizes of pores. The agarose samples are soft and the “smearing” effect from the tip catching the material can be seen in the AFM image.

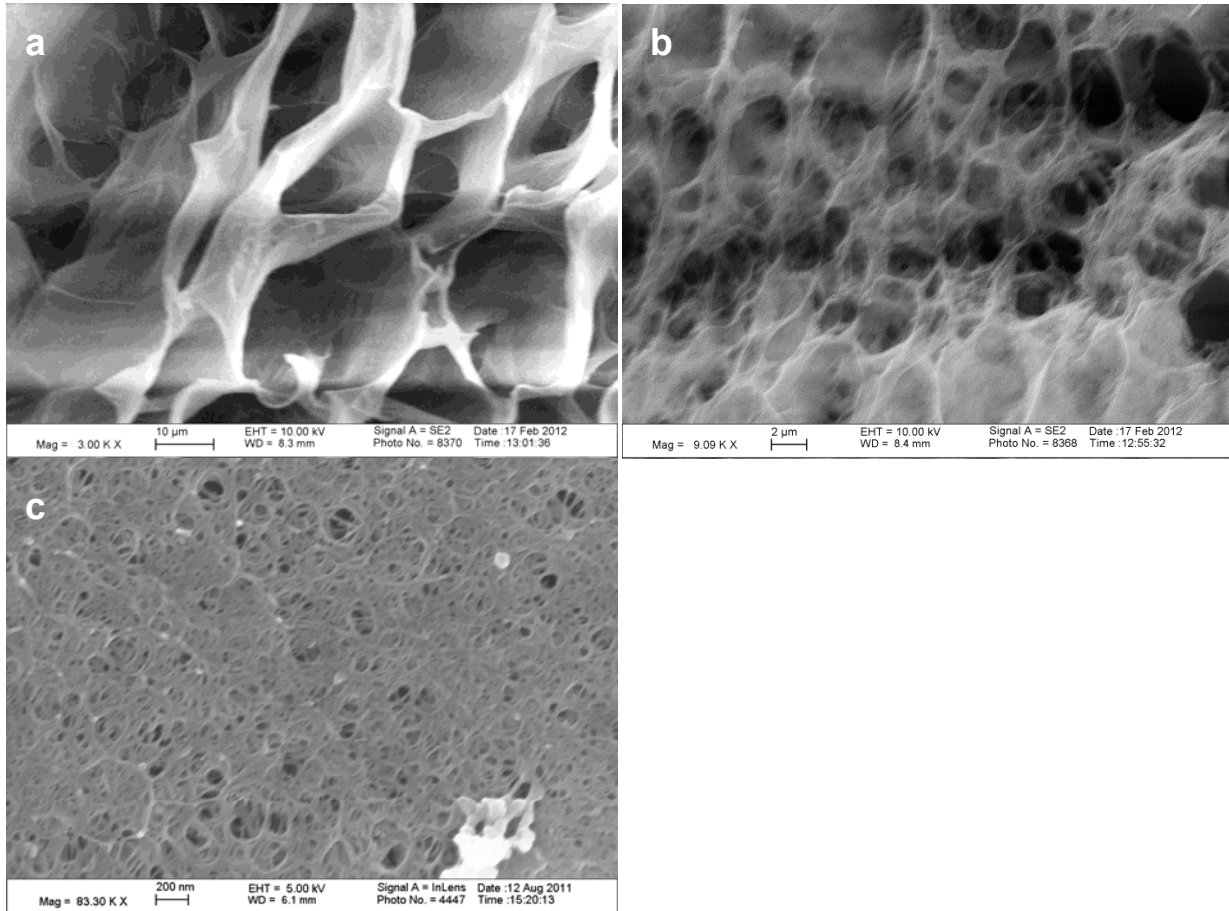


**Figure 3.9a, 3.9b and 3.9c: Various sizes of pores found on different length scales in 2 wt. % agarose shown in SEM images.**

Agarose 2 wt. % show various pore sizes at length scales of (3.9a) 10  $\mu$ m, (3.9b) 2  $\mu$ m and (3.9c) 0.2  $\mu$ m. These images are zoom in on the strut between the pore to discover smaller and smaller pores. (3.9a) 15-20  $\mu$ m pores are visible at 10  $\mu$ m, (3.9b) 2-5  $\mu$ m pores are shown at 2  $\mu$ m and (3.9c) ~0.2-0.005  $\mu$ m pores at 0.2  $\mu$ m.

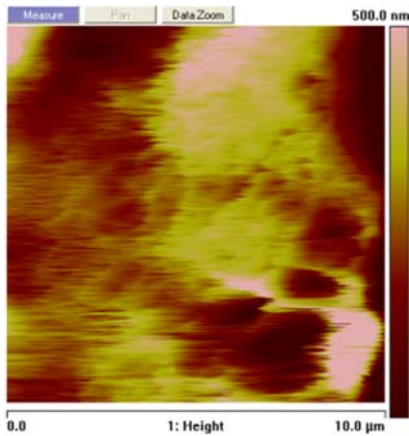


**Figure 3.10: AFM of 2 wt. % SN agarose shows pores  $\sim$ 2-5 $\mu$ m.**

SEM images of 2 wt. % SN Agarose display various pore sizes of 2-5  $\mu$ m. The shape and dimension of the pores are consistent with the SEM images at 2  $\mu$ m length scale (Figure 3.9b).

In addition to the decrease in pore size the overall look of the pore changes. At 10  $\mu$ m length scale (Figure 3.9a) the pores appear thin and have a variety of shapes but most are oblong. At 2  $\mu$ m length scale (Figure 3.9b) the network almost gives the impression of being a spider web or cotton candy. Interestingly, at 2  $\mu$ m length scale (Figure 3.9c) the pores are tighter, rounder and not as much void space (pore volume is decreased) as in the previous two length scales.

As the agarose concentration is increased the pore size decreases. In 5 wt. % agarose on the length scale of 10  $\mu$ m a broad distribution of pores that are  $\sim$ 3-8  $\mu$ m are seen (Figures 3.11a and 3.11b). In 10 wt. % agarose on the length scale 10  $\mu$ m scale distinct pores  $\sim$ 1.5-3  $\mu$ m are shown (Figure 3.12a). Comparing the visual appearance of the network as the concentration of agarose is increased is the strut size has increased in 5 wt. % agarose (Figure 3.11a) in comparison to 2 wt. % agarose (Figure 3.12a) the strut still appears thin. However the at 10 wt. % agarose (Figure 3.12a) distinct and round pores are present. Taken as a whole the changes in appearances by increasing agarose content is reminiscent of the changes of appearances by decreasing the length scale studied in only 2wt. % agarose gel.

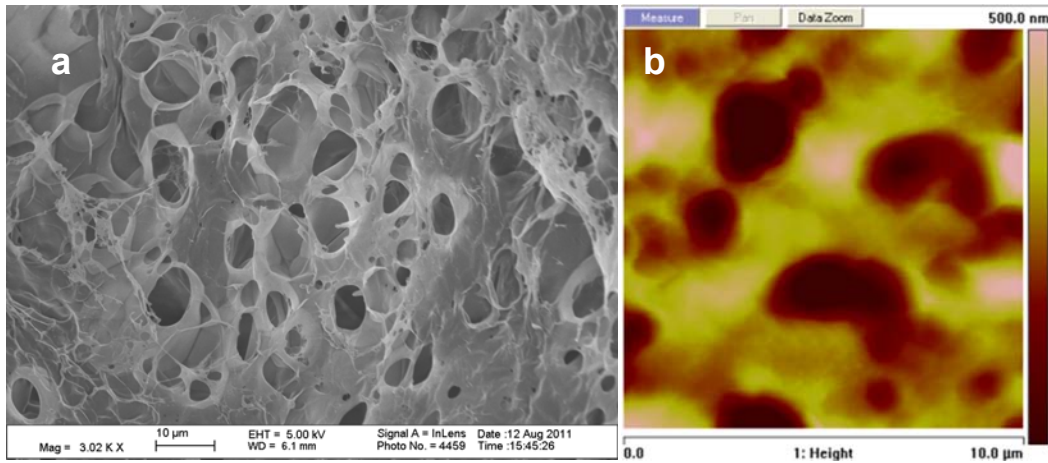
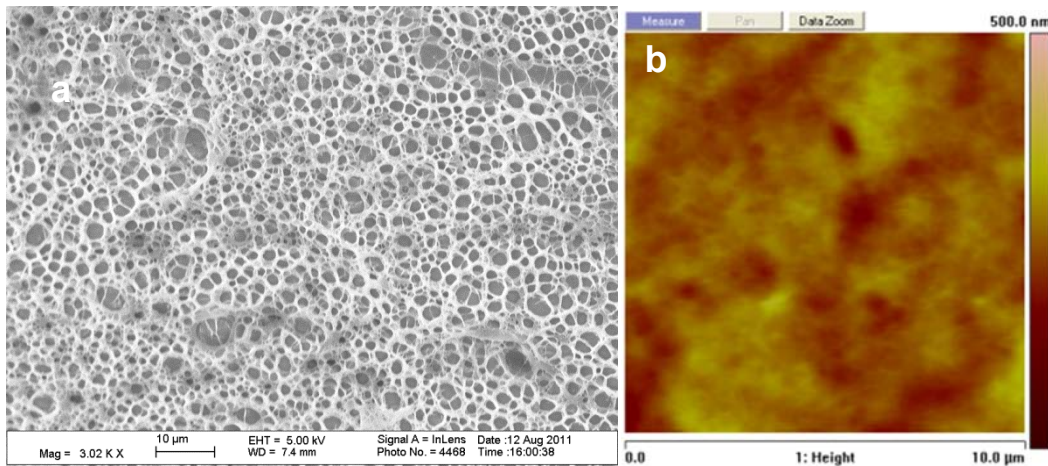
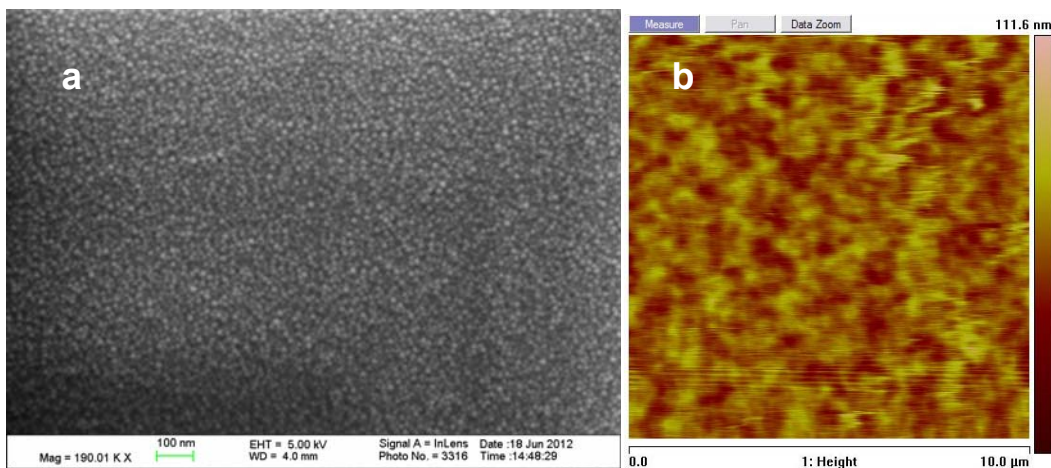


**Figure 3.11a and 3.11b: Large strut size in between pores in 5 wt. % agarose on both SEM and AFM**  
 In 5 wt. % agarose network there are broad distributions of pores that are ~3-8μm. The pores are shown in both SEM (3.11a) and AFM (3.11b)



**Figures 3.12a and 3.12b: Distinct pores in 10wt. % of agarose in SEM and AFM.**  
 10 wt. % agarose network shows ~1.5-3μm distinct pores in both SEM and AFM images.

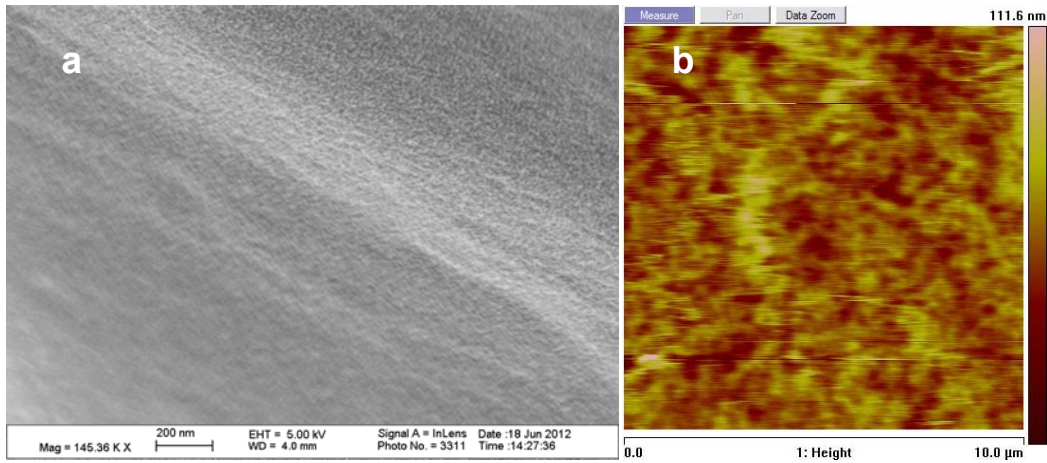
The SEM and AFM images of SN hydrogels with 10 and 20 wt% PEGDA do not agree. The SEM show the PEGDA is non-porous on the length scale between 0.2  $\mu\text{m}$  to 10  $\mu\text{m}$ , Figures 3.13a and 3.14a. In fact, the images show the gold particles (20 nm thickness). The AFM images of 10 and 20 wt% PEGDA are hard to interpret because the scale bar is so small but show small pores. Figure 3.13b is the AFM image of 10 wt. % SN PEGDA and it shows  $\sim 1 \mu\text{m}$  pores. Figure 3.14b is the AFM of 20 wt. % SN PEGDA and the pores have decreased to smaller than 1  $\mu\text{m}$ . By increasing to 30wt. % SN PEGDA the SEM and AFM images both show no pores but the surface appears to be rough, Figures 3.15a and 3.15b. The trend that as the concentration of PEGDA increases the pore size decreases is consistent with the trends in agarose. However, this is speculative due to the images of the two techniques not agreeing.



**Figures 3.13a and 3.13b: Image of 10 wt.% SN PEGDA show ambiguous results**

Figures 3.13a and 3.13b SEM and AFM are inconsistent with each other. SEM (3.13a) shows no pores but the pores may have collapsed from drying. On the SEM images the bumps are the gold particles (20 nm thickness) from sputter coating. AFM (3.13b) show small  $\sim 1 \mu\text{m}$  pores but due to the size of the pores the images are difficult to interpret.





**Figures 3.14a and 3.14b: Image of 10 wt.% SN PEGDA show ambiguous results**

Figures 3.14a and 3.14b SEM and AFM images show similar inconsistencies and Figures 3.13a and 3.13b. SEM (3.14a) shows no pores but the pores may have collapsed from drying. On the SEM images the bumps are the gold particles (20 nm thickness) from sputter coating. AFM (3.14b) show small  $<1\mu\text{m}$  pores but due to the size of the pores the images are difficult to interpret.

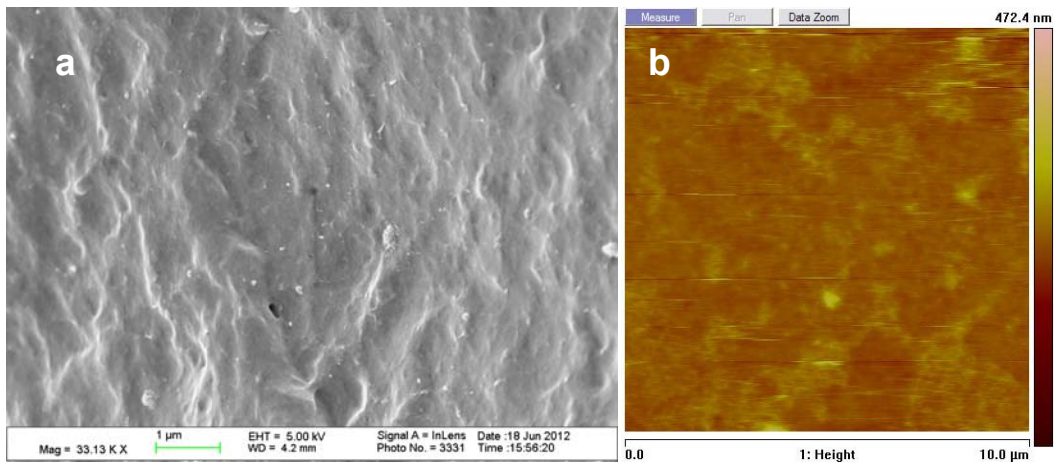
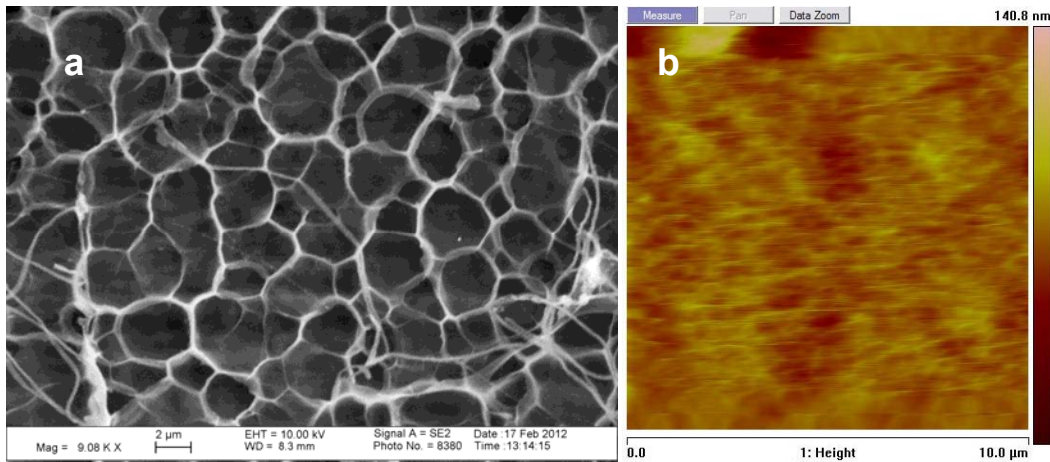


**Figure 3.15a and 3.15b: Rough surfaces formed in SN PEGDA at 30 wt. %**

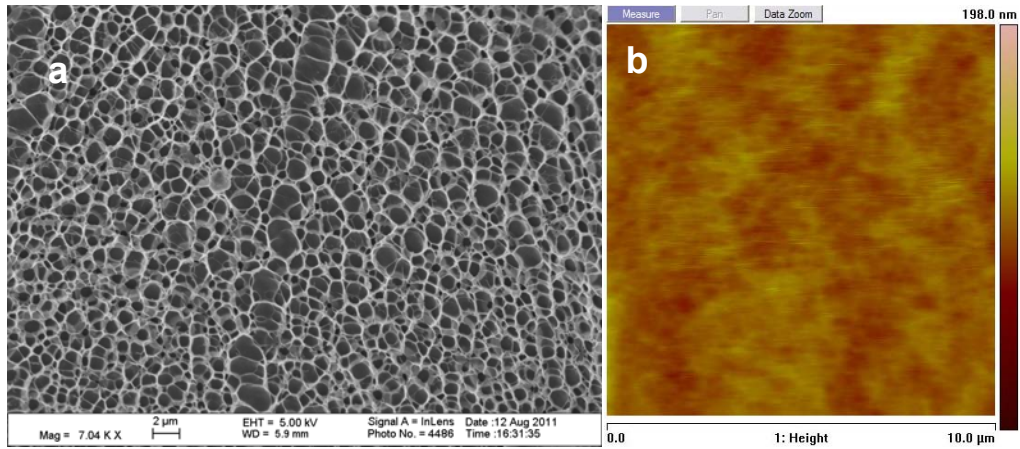
As the concentration of PEGDA increases to 30 wt. %, these rough regions are formed. These can be seen both in SEM and AFM.

The semi-IPNs of 5 wt. % agarose and 10, 20 or 30 wt. % PEGDA were imaged using AFM and SEM to determine the network structure. In the semi-IPNs of agarose with lower concentrations of PEGDA, micro-pores are shown, Figures 3.16a, 3.16b, 3.17a and 3.17b. The semi-IPN of 5 wt. % agarose and 10 wt. % PEGDA has 2-4  $\mu\text{m}$  pores shown in both SEM and AFM, Figures 3.16a and 3.16b. As the PEGDA concentration is increased to 20 wt. % the pore size decreases to 1-2  $\mu\text{m}$  Figures 3.17a and 3.17b. When the PEGDA concentration was increased to 30 wt. % the imaging showed the network to be non-porous Figures 3.18a and 3.18b. In addition, similar rough regions to pure 30 wt. % were shown, Figures 3.15a and 3.15b. Visually the pores of 5 wt. % agarose/10 wt. % PEGDA are distinct and have a relatively thin strut size and large pore volume. An increase in the PEGDA concentration to 20 wt. % (in a semi-IPN with 5 wt. % agarose) results in more pores which are smaller in size but appear to have relative strut size and a large pore volume.



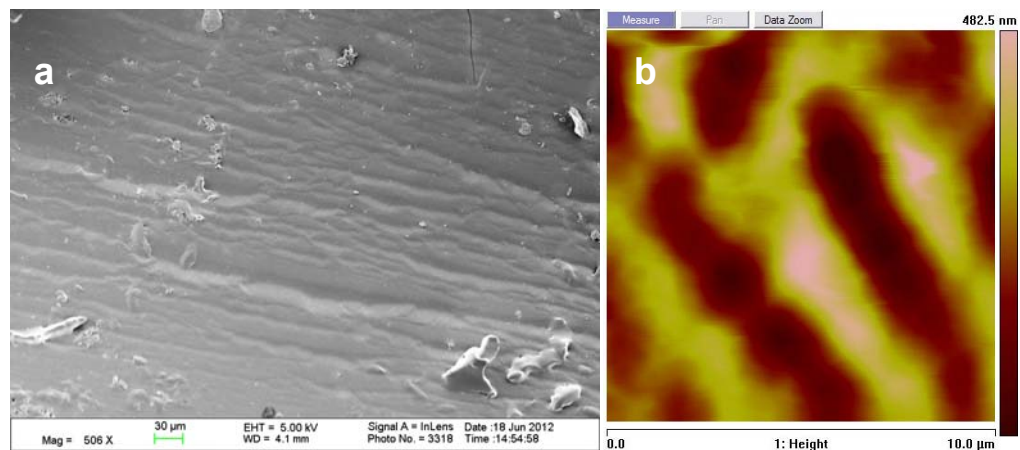
**Figures 3.16a and 3.16b: Semi-IPN of 5 wt. % agarose/10wt% PEGDA show a pore size in between both SNs**

Both AFM and SEM images show 2-4 $\mu\text{m}$  pore size which is an intermediate size to the SN agarose and SN PEGDA.



**Figures 3.17a and 3.17b** Semi-IPNs of 5wt. % agarose/PEGDA show decrease in pore size with increase in PEGDA content from 10-20wt. %

Both AFM and SEM images show 1-2 $\mu$ m pore size which is an intermediate size to the SN agarose and SN PEGDA.



**Figures 3.18a and 3.18b** Rough surfaces formed in semi-IPNs of 5wt. % agarose/30 wt. % PEGDA

As the concentration of PEGDA in semi-IPNs increases to 30 wt. %, these rough regions are formed. These are evident in both in SEM and AFM. This is also similar to SN PEGDA at 30wt. %.

**Table 3.2: Summary of SEM and AFM images**

Type of Gel	%	SEM	AFM	Comments
Agarose	2%	Clear SEM 10 $\mu\text{m}$ to 2 $\mu\text{m}$ to 0.2 $\mu\text{m}$ series show ~0.003-20 $\mu\text{m}$ pores 15-20 $\mu\text{m}$ pores are visible at 10 $\mu\text{m}$ length scale, 2-5 $\mu\text{m}$ pores are shown at 2 $\mu\text{m}$ length scale and ~0.2-0.005 $\mu\text{m}$ pores at 0.2 $\mu\text{m}$ length scale	Very good AFM but agarose is soft so "smearing" effect from the tip catching the material  ~2-5 $\mu\text{m}$ pores	SEM and AFM coupled shows large micro-porous material with smaller pores in the struts of the larger pores. 20 $\mu\text{m}$ -0.003 $\mu\text{m}$ which are very distinct
	5%	Very good SEM ~3-8 $\mu\text{m}$ pores at 10 $\mu\text{m}$ length scale	Excellent AFM ~3-5 $\mu\text{m}$ pores very distinct	SEM and AFM both show ~3-5 $\mu\text{m}$ pores with large strut size
	10%	Excellent SEM ~1.5-3 $\mu\text{m}$ distinct pores at 10 $\mu\text{m}$ length scale	AFM not as clear but shows ~1.5-3 $\mu\text{m}$ pores	SEM and AFM both show ~1.5-3 $\mu\text{m}$ distinct pores
PEGDA	10%	Clear SEM No pores	AFM hard to interpret but indicates ~1 $\mu\text{m}$ pores	SEM and AFM are inconsistent. SEM shows no pores but can from collapse from drying. AFM show small pores but is difficult to interpret.
	20%	Clear SEM No pores	AFM hard to interpret but indicates small < 1 $\mu\text{m}$ pores	SEM and AFM are inconsistent. SEM shows no pores but can from collapse from drying. AFM show small pores but is difficult to interpret.
	30%	Clear SEM No pores but rough surface	No pores but rough surface	SEM and AFM both show no pores but rough surface
5% Agarose and ___ PEGDA	10%	Excellent SEM 2-4 $\mu\text{m}$ pores	AFM hard to interpret but indicates 2-4 $\mu\text{m}$ pores	SEM and AFM are consistent but AFM is hard to interpret
	20%	Excellent SEM 1-2 $\mu\text{m}$ pores	AFM hard to interpret but indicates 1-2 $\mu\text{m}$ pores	SEM and AFM are consistent but AFM is hard to interpret
	30%	Clear SEM No pores but rough surface	No pores but rough surface	SEM and AFM both show no pores but rough surface
Imaging Technique Summary	--	Clear images but artifacts from sample preparation are hard to avoid -Misleading structures from ice crystals -Collapse of structure from drying or imaging	Imaging hydrated with minimal sample preparation but images can be ambiguous and hard to interpret -Hard to image soft materials -Long scanning rates	Overall, there are cons to imaging hydrogels using both SEM and AFM. The consistent images were SN agarose and semi-IPNs of 5% agarose/10 or 20% PEGDA show micro-pores. Also SN 30% PEGDA and semi-IPN with 5% agarose/30% PEGDA showed no pores and a rough surface.

Table 3.2 summarizes the SEM and AFM images. The SN agarose gels reveal large pores and the SEM and AFM images were consistent with each other. On the other hand the SN PEGDA AFM and SEM images do not agree with each other at 10 wt. % and 20 wt. % PEGDA. The SEM images showed no pores and the AFM images indicated small  $\sim 1\mu\text{m}$  or smaller pores. Because imaging with SEM has requires meticulous sample preparation to get representative images and often leads to artifacts, AFM images provide a more accurate view of the hydrogels.

## Discussion

Most SN hydrogels behave as ideal elastomers and this was the case for the SN of agarose and SN of PEGDA formulations in this work. Although, IPNs do not always follow ideal elastomeric behaviour, the semi-IPNs of 5 wt. % agarose/ 10, 20 or 30 wt. % PEGDA all behaved as ideal elastomers. When  $G$  is plotted against the polymer volume fraction, Figure C, the SN PEGDA and the semi-IPN of agarose/PEGDA have a similar scaling law exponent. This indicates that the semi-IPN of agarose/PEGDA is dominated by the PEGDA and there seems to be little influence of agarose. When comparing the moduli ( $G$  and  $E$ ), fracture stress, and toughness nearly all of the properties showed an effect that was greater than additive but not close to the magnitude shown by the double-networks.<sup>[51]</sup> The tabulated additive values are in Table 3.1. Thus, the average value for a 5 wt.% SN agarose is added to either 10, 20 or 30 wt.% SN PEGDA and compared to the average value for the corresponding semi-IPN (for properties:  $E, G$ , fracture stress, toughness). In three cases the semi-IPNs were better than the additive effect but still within the standard deviation of the average: for the fracture stresses of 5 wt.% agarose/10 wt.% PEGDA and 5 wt.% agarose/30 wt.% PEGDA, and the toughness of 5 wt.% agarose/30 wt.% PEGDA. Further, for

three properties the effect is less than additive. The shear modulus of 5 wt. % agarose/10 wt.% PEGDA is close to additive by shows a less than additive effect. Both of the E and G of 5 wt.% agarose/30 wt.% PEGDA show a less than additive effect. Because there was not a large (10-100 fold increase) in any of the mechanical properties, the two networks in the semi-IPN are acting separately from each other, thus displaying more of an additive effect and not a synergistic effect. Overall the semi-IPN networks behave similar to one of the networks, an effect which is additive or a bit better than additive but not synergistic.

From the semi-IPNs of 5 wt. % agarose and 10, 20 and 30 wt. % PEGDA, pores of 2-4  $\mu\text{m}$  were introduced in networks with a fracture stress of  $\sim 500$  kPa and a fracture strain of 56%. By increasing the concentration of PEGDA to 20 wt. % the semi-IPN network led to an increase in the fracture stress  $\sim 1500$  kPa but the pore size decreased and had a similar fracture strain of 52%. The network fracture stress is increased by  $\sim 3$  times and could be due to smaller pores providing more support to the overall network but ultimately the short chains, low MW, causes failure near 50%.<sup>[178]</sup> The semi-IPNs of agarose and PEGDA produces pore sizes that are in between the two SNs. The decrease in the pores size as more PEGDA is added, Figures 3.16a, 3.16b, 3.17a, 3.17b 3.18a and 3.18b, is speculated from the PEGDA filling in the agarose pores. Also, agarose has structural rearrangement in different solvents due disruptions to intrastrand bonding and this may be a factor when soaking in PEGDA solutions.<sup>[95]</sup>

Even if the pore size is not directly affecting the mechanical properties of this hydrogel system, having a meso- or macro-porous material is useful for many applications including drug delivery and tissue engineering. Decreasing agarose concentration of agarose, increases the pore size in the network; thus to create hydrogels with meso- or macro-pores, the agarose concentration can be decreased a trend established in this work and by Dillon et. al. who studied the impact of

porosity of various low concentrations of agarose.<sup>[30]</sup> Pernodet also imaged using AFM to show pores in the agarose networks.<sup>[142]</sup> With the conclusion that at higher concentration of agarose led to smaller pore distribution, increase in number of pores and smaller pores (2% agarose ~400nm, 5% agarose ~200nm on AFM).<sup>[143]</sup> The pore sizes imaged by Pernodet were an order of magnitude smaller than the size of the pores found in this work.<sup>[143]</sup> This could be because pore size of agarose was dependent on the scale that was imaged and agarose had many dimensions of pores at various length scales. Also, the type of agarose and the temperature and gelation time impact the structure of the network and Pernodet only allowed for 30 min.<sup>[143,206]</sup>

Hypothesizing that decreasing the first network agarose concentration, the concentration of the second network of PEGDA can be further increased past 30 wt. % in a semi-IPN, creating better mechanical properties, since it was determined that the PEGDA concentration was the most influential property in changing the mechanical properties<sup>[178]</sup>. However, 30 wt. % PEGDA may be the extent of creating an improved properties if phase separation is an issue. Comparing with the images, the semi-IPN of 5 wt.% agarose/30 wt.% PEGDA did not have pores and were reminiscent of SN 30% PEGDA because both had rough surfaces in the network. These rough surfaces regions are potentially phase separation at higher concentrations. Studies at higher concentrations of PEGDA may provide more information to the rough surfaces and the mechanical tests will be helpful in determining if the mechanical toughness plateaus at 30 wt. %.

Furthermore, this work showed some disagreement between the SEM and AFM images. Invasive techniques of preparing the sample are not preferred, but necessary in SEM, due to dehydrating the samples. Generally SEM provided a clear picture of the network parameters but in the case of SN PEGDA it was speculated that the pores collapsed and showed inconsistent images to the corresponding AFM. Better imaging techniques for hydrogels are warranted.

## Conclusions

Unlike the synergistic effect observed in double-network (DN) systems, the semi-IPNs of agarose/PEGDA act as two independent networks, thus the improvements of semi-IPNs were not as significant as the ones displayed in DNs. Even though orders of magnitude improvement in mechanical properties were not seen in this semi-IPN the semi-IPNs and their SN counterparts behaved as ideal elastomers as shown under compression. The ideal elastic behavior shown suggests the gels can endure unlimited number of mechanical cycles. This rubber elasticity of the semi-IPNs is especially important for tissue engineering constructs. The gels also display a dependence on the polymer volume fraction. The semi-IPN and the SN PEGDA fall on the same plot, thus show have a similar scaling exponent. This emphasizes that PEGDA is the dominant network in the semi-IPNs. The fracture strain is only slightly larger in the semi-IPN than than the SN PEGDA at a similar polymer volume fraction. The SEM and AFM images showed large micro-porous agarose networks and micro-porous semi-IPNs of 5 wt% agarose / 10 or 20% PEGDA. This work shows the capacity of semi-IPNs of agarose/PEGDA in terms of both the mechanical properties and the pore size. The conclusion from this work is that semi-IPNs exhibit an additive versus synergistic effect.



## Chapter 4: Double-Network Strategy Improves Fracture Properties of Chondroitin Sulfate Networks<sup>4</sup>

### Abstract

A tough and ductile, ultrathin film, double-network (DN), biopolymer-based hydrogel displaying the yielding phenomenon was synthesized from methacrylated chondroitin sulfate (MCS) and polyacrylamide (PAAm). The DN of MCS/PAAm exhibited a failure stress more than 20 times greater than the single-network (SN) of either MCS or PAAm and exhibited yielding stresses over 1500 kPa. In addition, the stress-strain behavior with a yielding region was also seen in a hydrogel of MCS and poly(*N, N*-dimethyl acrylamide (PDMAAm). By replacing PAAm with PDMAAm, interactions known to toughen the network are removed. This demonstration supports that the brittle/ductile combination is key to the DN effect over specific interactions between the networks. The MCS/PAAm and MCS/PDMAAm DN hydrogels had comparable mechanical properties to the standard DN hydrogels of poly(2-acrylamido-2-methylpropanesulfonic acid) (PAMPS)/PAAm. In addition, these tough and ductile, biopolymer-based, double-network hydrogels demonstrated a substantial yielding region

---

<sup>4</sup> Published as **Tiffany C. Suekama**, Jian Hu, Takayuki Kurokawa, Jian Ping Gong, Stevin H. Gehrke, “Double-Network Strategy Improves Fracture Properties of Chondroitin Sulfate Networks” ACS Macro Letters, **2013**, 2, 137-140.

## Introduction

In general, materials undergo either a yielding phenomenon or a brittle failure, and the strength of the material is determined by which process occurs first.<sup>[17]</sup> Many materials display yielding, however, synthetic, chemically cross-linked hydrogels always have a brittle fracture with the exception of double-network (DN) hydrogels of poly(2-acrylamido-2-methylpropanesulfonic acid) (PAMPS)/polyacrylamide (PAAm), which also have extraordinary fracture stresses.<sup>[17,50,61,68,84,101,119,207]</sup> Anisotropic gels such as poly(2,2'-disulfonyl-4,4'-benzidine terephthalamide) (PBDT)/PAAm DN hydrogels have also shown yielding.<sup>[204]</sup> Recently, Sun *et al.* created multi-component gels of ionically cross-linked alginate and covalently cross-linked PAAm.<sup>[172]</sup> These alginate/PAAm hydrogels displayed high extensibility, 20 times their initial length, and a yielding region but the fracture strength was only ~160 kPa.<sup>[172]</sup> Synthesizing tough and ductile biopolymer-based hydrogels that demonstrate the generality of yielding could lead to materials resistant to catastrophic failures, especially important in areas such as tissue engineering.<sup>[11,76]</sup> The goal of this work is to create a tough biopolymer-based DN hydrogel system with a yielding region using PAMPS/PAAm DN as a model and to test the hypothesis that the double-network effect is due to the combination of the brittle/ductile networks. We first replaced PAMPS with MCS, thus exchanging a sulfonated synthetic polymer with a sulfonated biopolymer synthesized by cross-linking a linear polymer, and then replaced PAAm with poly(*N, N*-dimethyl acrylamide) (PDMAAm) to eliminate the two protons of the amide group. This research shows that a biopolymer-based DN hydrogel can be designed to have high toughness and a distinct yielding region.

DN hydrogels are formed from a highly covalently cross-linked, brittle and stiff, polyelectrolyte first network with a lightly covalently cross-linked, soft and ductile, neutral

polymer second network.<sup>[50,61,192]</sup> The second network has a molar concentration 20-30 times greater than the first network.<sup>[50,61,192]</sup> DN hydrogels have significantly improved toughness in comparison to either single-network (SN) alone. The improved toughness is believed to be due to the fracturing of the first network, which dissipates the strain energy, while the ductile second network holds the bulk hydrogel together and supports high strains.<sup>[51,61]</sup> Ultrathin film DN hydrogels (~100  $\mu\text{m}$  thick) are comparable to bulk, solution-cast DN gels in mechanical properties such as toughness, yielding and necking. Thus they have a toughening mechanism similar to the toughening mechanism found in bulk, solution-cast DN gels. However ultrathin DN hydrogels have experimental advantages of allowing for observation of the tearing mechanism, requiring less material, and equilibrating more rapidly with solutions.<sup>[101,102]</sup>

Previously reported DN hydrogels made from PAMPS/PAAm have three characteristic regions: preyielding, yielding and hardening, and display a clear yield point (transition between preyielding and yielding regions).<sup>[50,61,101]</sup> The preyielding region is a region in which the brittle network starts absorbing the strain energy by fracturing, allowing the gel to sustain higher stresses.<sup>[50,61,101]</sup> The yield point in these gels is typically around 700 kPa for both bulk, solution-cast DN gels and film DN gels, and is nearly independent of the elongation velocity.<sup>[50,61]</sup> After the yielding point, the yielding zone forms, which develops as the PAMPS network breaks down entirely across a cross-section and allowing elongation of the PAAm chains.<sup>[50,61,101]</sup> Elongation occurs at a constant nominal stress as the yielding zone grows until the PAMPs network is fully fractured over the entire length of the specimen. The yielding region typically starts at 2-3 mm/mm and ends at 8-10 mm/mm in bulk, solution-cast DN hydrogels, where in film DN hydrogels the yielding region starts at 2 mm/mm and ends around 5 mm/mm.<sup>[50,61,101]</sup> In the hardening region the PAAm coils become highly extended and behave according to non-Gaussian chain statistics.<sup>[50,61,101]</sup> This

region can extend to 14 mm/mm.<sup>[50,61,101]</sup> While the DN principle is believed to be general, and many gel systems have been designed based on this concept which have improved fracture properties,<sup>[61]</sup> no research has demonstrated the full range of phenomena, other than with PAMPS/PAAm, much less a biopolymer-based system. Thus this work was motivated by a desire to create a biopolymer-based system that shows a yielding region, demonstrates the generality of the brittle/ductile combination hypothesis and reveals that the phenomena observed are not due unique structures or interactions in the PAMPS/PAAm system.

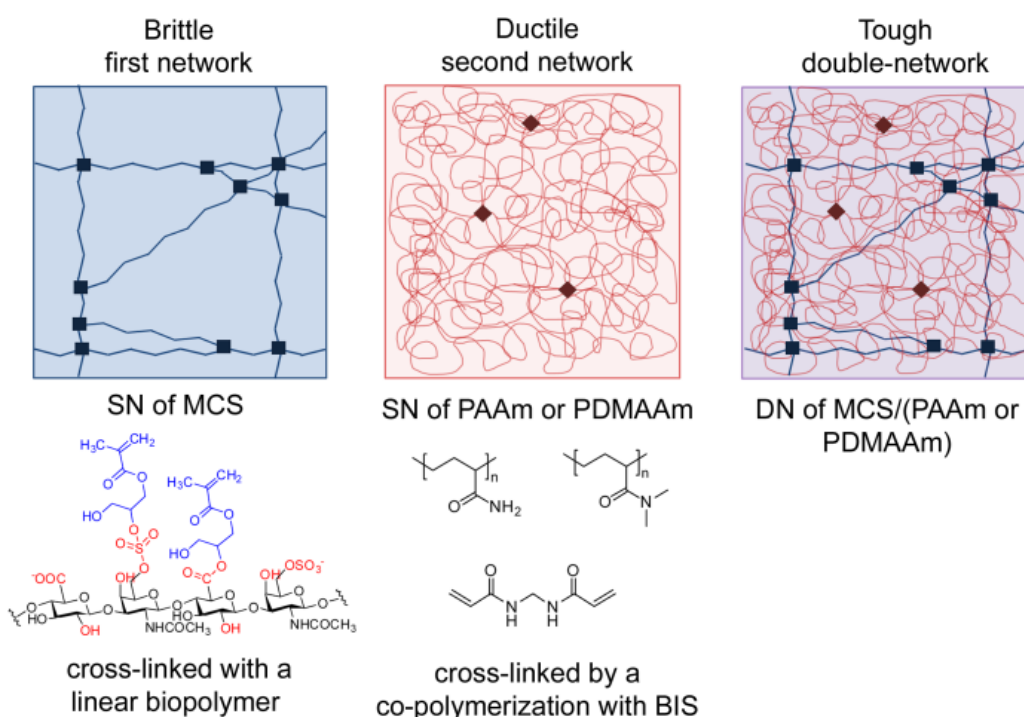


**Figure 4.1: Schematic of single (SN) and double (DN) network gels**

The first network is a highly cross-linked linear biopolymer of methacrylated chondroitin sulfate (MCS). The second network is polyacrylamide (PAAm) or poly(N,N-dimethyl acrylamide) (PDMAAm) cross-linked by a co-polymerization with N,N'-methylenebisacrylamide (BIS). Using the double-network strategy a tough and ductile DN biopolymer was synthesized.

We chose the biopolymer, chondroitin sulfate (CS) as the first component of the ultrathin film DN hydrogels because CS is a major component of cartilage that provides strength and allows for absorption of large amounts of water.<sup>[99,115]</sup> To create these hydrogels, methacrylated

chondroitin sulfate (MCS) was formed by modifying the CS with methacrylate groups; upon photoinitiation, the cross-linked linear polymer was reacted to form a cross-linked gel.<sup>[100]</sup> The second network was formed using a co-polymerization of PAAm or PDMAAm with the cross-linker N,N'-methylenebisacrylamide (BIS). AAm or DMAAm has a molar concentration 40-50 times greater than MCS disaccharide groups. A schematic of the single networks and the double network is shown in Figure 4.1.

## Materials

Methacrylated chondroitin sulfate (MCS) was synthesized using a previously reported procedure<sup>[73]</sup> adapted from Li *et al.*<sup>[100]</sup> with chondroitin sulfate A sodium salt (CS; Sigma-Aldrich: type A 70%, balanced with Type C, from bovine trachea) used as received; and glycidyl methacrylate (GMA; Sigma-Aldrich: 97%) used as received. The methacrylation of MCS was determined by NMR to be 34.5% after 15 days of reaction.<sup>[86]</sup> Acrylamide (AAm; Junsei Chemical Co., Ltd.) was recrystallized in chloroform; N,N-dimethyl acrylamide (DMAAm) (Kojin Co., Ltd., Tokyo, Japan) was used as received; the cross-linker, N,N'-methylenebisacrylamide (BIS; Tokyo Kasei Co., Ltd.) was recrystallized in ethanol; and the UV initiator, 2-methyl-1-propanone (Irgacure 2959; Ciba Specialty Chemicals Corp.) was used as received. Milli-Q (18.2 MΩ cm) water was used in all synthesis solutions.

## Methods

### ***Synthesis of Single-Network (SN) PAAm Hydrogel:***

A traditional gel electrophoresis notation, T x C, was used to describe the gel compositions

for PAAm<sup>[18,132]</sup>. T represents the total mass of monomer and cross-linker over the volume of solution (w/w) as a percentage. C represents the ratio of the mass of cross-linker by the total mass of monomer and cross-linker (w/w) as a percentage. An example of a 25 x 0.0446 (T x C) PAAm gel was synthesized by dissolving AAm (24.99 g) and BIS (0.01 g) in 100 mL of water. This polymerization used 0.02% (w/w) Irgacure 2959 to initiate the polymerization. The solution was degassed and placed, under argon atmosphere, in a mold consisting of two glass plates and a 100  $\mu\text{m}$  silicon spacer. The polymer solution was cross-linked into a gel with 365-nm light at  $\sim 10\text{mW}/\text{cm}^2$  for 30 min.

#### ***Synthesis of MCS and Ultrathin DN (UTDN) Hydrogels of MCS/PAAm:***

The MCS/PAAm UTDN hydrogels were prepared in a multistep process similar to Gong *et al.*<sup>[68,101,207]</sup>. First, the MCS hydrogel was prepared by mixing MCS (3.53 g) and Irgacure 2959 (0.0047 g) in 20 mL of water to create a formulation of 15% (w/w) MCS with 0.02% (w/w) Irgacure 2959. After degassing the viscous solution it was placed, under an argon atmosphere, in a mold consisting of two glass plates and a 100  $\mu\text{m}$  silicon spacer. The polymer solution was cross-linked into a gel with 365-nm light at  $\sim 10\text{mW}/\text{cm}^2$  for 30 min. The MCS hydrogel was taken out of the mold and allowed to swell to equilibrium in a PAAm solution (as prepared in a single network) for 1 hour. After swelling, the swollen gel was placed, under an argon atmosphere, between two glass plates and was exposed to 365-nm light at  $\sim 10\text{mW}/\text{cm}^2$  for 30 min. All solutions contained 0.1 M sodium chloride (NaCl) to help handle the brittle nature of the MCS hydrogels. All of the hydrogels were made with 0.02% (w/w) Irgacure 2959.

### ***Swelling Properties:***

Molded gel samples were submerged in milli-Q water at room temperature for 24 h, and the water was changed every few hours to leach away any sol fraction. The excess water on the swollen gels was dabbed with a moist Kimwipe. The swollen gel was then weighed and placed in a pre-weighed vial of sea sand (Wako Pure Chemical Industries, Ltd.; 20-35 mesh). The vial with the swollen gel was shaken until the sea sand covered the gel. The sea sand helped to draw out the residual water. Bound water in PAAm is released over temperatures of 20 to 220 °C<sup>[182]</sup>, and Tutas *et al.* show there is a 10% weight loss at 110 °C<sup>[180]</sup>. Therefore, the vials with the gels and the sea sand were placed into a vacuum oven at 120 °C until it reached a constant weight. The dry weights were taken. The degrees of swelling in the results section are reported as the mass of the swollen gel over the mass of the dried gel<sup>[45,135]</sup>.

### ***Mechanical Analysis:***

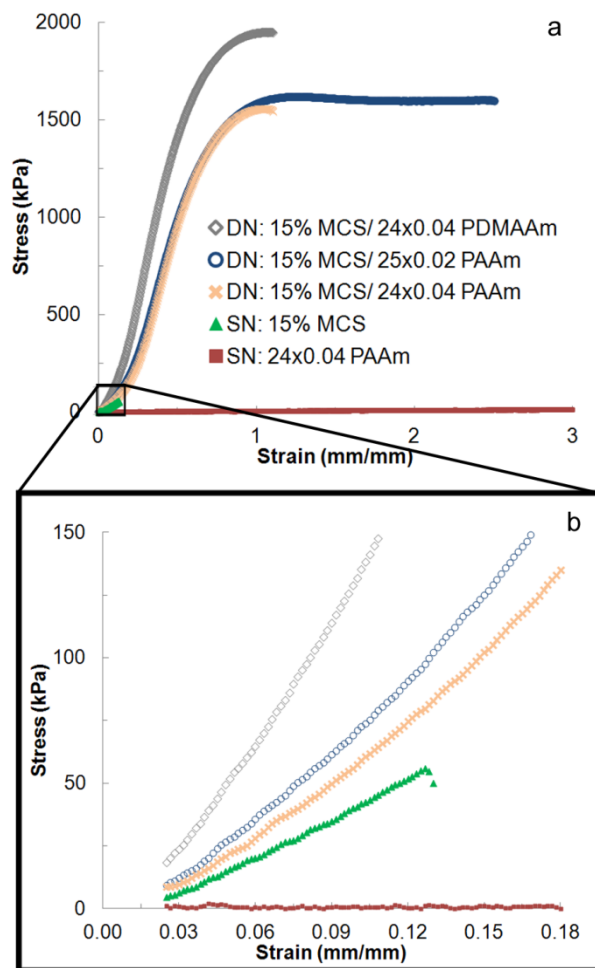
The fully swollen gels were cut into a dumbbell shape (standardized JIS-K6251-7; length 35mm, width 2 mm, gauge length 12 mm) for tension and a trouser shape (standardized JIS-K6252 ½; length 50mm, width 7.5 mm, initial notch 20mm) for tearing by a gel cutting machine (SDAP-100N Dumbbell Co, Ltd). All gel thicknesses were measured using a phase contrast optical microscope (Olympus CKX41). Tension and tearing tests were both performed using a Tensilon machine (RTC-1150A, Orientic Co), and all of the gels were lubricated with mineral oil to minimize evaporation of water from the gel during testing. Tension tests were performed at a constant velocity of 100 mm/min. From the stress ( $\sigma$ ) –strain ( $\epsilon$ ) data, Young's modulus (E), yield point ( $\sigma_c$ ,  $\epsilon_c$ ) fracture stress and fracture strain were determined. To calculate E, the slope of the initial data of a strain of 5-15% was used. Fracture stress and fracture strain were found at the point

that the gel began to split, identified in the data as a sharp drop in stress. The strain energy at fracture was calculated as the area under the stress-strain curve. Tearing was performed in Mode III<sup>[147]</sup>, pulling one arm at a constant velocity of 100 mm/min while the other arm remained stationary. From the force (F)-extension data, the tearing energy (T, work required to tear a unit area) is calculated by taking two times the average F during steady-state tear and then dividing by the thickness of the sample ( $T=2F_{\text{avg}}/w$ )<sup>[53,123]</sup>.

## Results and Discussion

The stress-strain behavior of a DN of MCS/PAAm to a SN of MCS and a SN of PAAm is compared in Figures 4.2a and 4.2b. Figure 4.2a, shows dramatic differences between the DN and the SN. The specific values for the swelling and mechanical properties for SN MCS, SN PAAm and select formulations of DN hydrogels are listed in Table 4.1. The failure stress of the DN MCS/PAAm was 16 times that of a SN of PAAm and 40 times that of a SN of MCS. The failure strain of the DN of MCS/PAAm, ~100-250%, was somewhat a mixture of the SN of MCS, ~10%, and the SN of PAAm, ~1000%. Figure 4.2b shows the initial stress-strain of the networks. The Young's modulus (E), from the initial data of a strain of 5-15%, is 100 times higher for the MCS/PAAm DN than it is for the SN of PAAm. E is also slightly higher in the DN of MCS/PAAm than the SN of MCS but can be attributed to the swelling of the DN is much less than the SN which normally increases the modulus. Besides that, the tearing energy was ~100 times greater in the DN of MCS/PAAm than the SN of PAAm. Due to the extremely brittle nature of the SN of MCS, the tearing could not be performed. Largely, the DN of MCS/PAAm showed superior properties to SN of MCS or SN of PAAm.





**Figures 4.2a (top) and 4.2b (bottom): Stress-strain response under tension single (SN) and double (DN) network gels.**

All of the curves have been truncated after failure. Figure 2a shows that combining brittle MCS with ductile PAAm into a double-network increases fracture stress over thirty times and introduces a yielding region. Failure of the SN of PAAm was 10.6 mm/mm and failure stress of 83 kPa. Replacing PAAm for PDMAAm shows the generality of the DN and yielding effect. Figure 2b shows the stiffness of the DN were slightly better than SN of MCS and significantly greater than the SN of PAAm. The data before a strain of  $\sim 0.03$  mm/mm is not recorded due to equipment inaccuracies at the low strain.

**Table 4.1: Swelling and Mechanical Properties of Different Hydrogel Networks**

MCS Formulation wt%	PAAm Formulation TxC	Swelling Q (g/g)	Young's Modulus E (kPa)	Toughness (kJ/m <sup>3</sup> )	Yielding Point Stress (kPa)	Failure Stress (kPa)	Failure Strain (mm/mm)	Tearing Energy T (J/m <sup>2</sup> )
15	-	34.1±4.3	487±50	1.89±1.59	N/A	40.1±22	0.10±0.04	*
-	24x0.04	26.5±0.1	7.83±0.3	349±92	N/A	96.7±19	10.8±1.2	67.7
15	24x0.04	7.0±0.3	748±103	709±467	1680±165	1670±150	1.09±0.08	695
15	25x0.02	6.9±0.2	1040 ±62	2940±528	1610±22	1600±12	2.27±0.34	585
15	25x0.04 (PDMAAm)	7.1±0.2	1700±125	1160±176	1930±47	1930±47	1.00±0.08	185

\* Too brittle to be measured (Mean ± Standard Deviation)

Further, the observed trend for the MCS/PAAm DN shows that two of the three characteristic regions can be achieved, open circles in Figure 4.2a. Similarly to previous literature, we attribute the modulus of the preyielding region is dominated by the densely cross-linked polyelectrolyte MCS network.<sup>[101,123]</sup> The initial part of the preyielding region or toe region of the curve is approximately elastic. The DN is shown to have a “J-shaped” curve that is not commonly seen in hydrogels, but is often observed in biomaterials, such as cartilage; which occurs upon realignment of the chains to the same orientation as the direction of extension.<sup>[17,186]</sup> In synthetic DN hydrogels this may indicate a different mechanism of toughening from the fracturing mechanism that is observed at higher strains. At the yielding point, the MCS/PAAm DN hydrogels were observed to have a stress of 1500 – 2400 kPa, nearly double that of the reported PAMPS/PAAm DN hydrogels; however, the strain (~100%) is only half that of the PAMPS/PAAm DN hydrogels.<sup>[101]</sup> The MCS/PAAm DN hydrogels also exhibited a yielding region where we believe the MCS network is fully fractured across a cross-section and the hydrogels undergo elongation of the PAAm coils.<sup>[61,101]</sup> The similar behavior of MCS/PAAm and PAMPS/PAAm suggests that a similar mechanism is occurring even though the first network of MCS/PAAm is a cross-linked, linear

biopolymer with a quite different microstructure than PAMPS. Even though the hardening region was not observed in the MCS/PAAm system we believe that with modifications of the formulations a longer yielding region, potentially stretching to a strain of 4-7 mm/mm, and a hardening region, that increases the fracture stress dramatically, can be achieved. The early failure of the MCS/PAAm could be attributed to the large yield stress created from a highly cross-linked MCS network which may not allow for high strain at such a high stress without prematurely breaking. Therefore, to reach the hardening region, the fracture stress of the PAAm network needs to exceed the yield stress of the MCS/PAAm DN, which can be obtained by increasing the concentration of PAAm or decreasing the cross-linking density of MCS. Nevertheless, this is the first demonstration of a biopolymer-based network that shows a substantial yielding region which leads to a ductile rather than brittle failure.

We then investigated changing the second network to *N,N*-dimethyl acrylamide (DMAAm) to test the hypothesis that hydrogen bonding between networks is responsible for the gel toughness. The CONH<sub>2</sub> group on acrylamide has a high hydrogen bonding capability and its interactions with the first network could significantly increase toughness, as has been seen in other systems.<sup>[42,64]</sup> Furthermore, DMAAm is potentially useful for biomedical applications since it is less toxic than AAm.<sup>[27,42]</sup> A typical MCS/PDMAAm DN stress-strain curve is shown as open diamonds in Figure 4.1. MCS/PDMMAm has a similar stress-strain curve to MCS/PAAm thus has comparable mechanical properties, Figure 4.2a. The DN of MCS/PDMAAm also has similar swelling (~7 g/g) to the DN of MCS/PAAm. Further, DN of MCS/PDMAAm exhibits a fairly high toughness of 1160 kJ/m<sup>3</sup>. This supports our hypothesis that the specific interaction between PAMPS/PAAm or MCS/PAAm is not essential to the toughening mechanism, but rather the brittle/ductile network combination.

## Conclusions

This is the first demonstration of a tough and ductile biopolymer-based hydrogel with a distinct yielding phenomenon. The MCS/PAAm DN hydrogels show two of the three characteristic regions: preyielding and yielding regions, with significantly improved mechanical properties. Besides that, this work supports the hypothesis that the brittle/ductile combination of networks is key to obtaining the DN effect, over specific interactions or particular microstructures of the networks. Replacement of PAAm with PDMAAm removes specific interactions (known to toughen networks) without significantly altering the stress-strain curves of MCS/PDMAAm, supporting the idea that the brittle-ductile combination is crucial relative to non-covalent interactions between the networks. MCS/PAAm and MCS/PDMAAm DN hydrogels are comparable to our previous work on tough double-network gels of PAMPS/PAAm and have proved to provide excellent toughness and strength with the use of biopolymers.

## Chapter 5: Tuning Mechanical Properties of Chondroitin Sulfate-Based Double-Network Hydrogels<sup>5</sup>

### Abstract

High strength double-network (DN) biopolymer-based hydrogels were created using copolymers of methacrylated chondroitin sulfate (MCS) and poly(ethylene glycol) diacrylate (PEGDA) as the first network and polyacrylamide (PAAm) as the second network. The concentration and cross-linking of the networks were adjusted to control the mechanical properties including the failure stress, failure strain, Young's modulus, and yielding behavior. First, we increased the cross-linking of the first network both by increasing the MCS concentration from 13 to 20 wt% and by copolymerizing MCS with 2 to 6 wt% PEGDA. The additional cross-linking increased the Young's modulus as much as five times, reaching 3.3 MPa, and the failure stress up as much as four times, reaching 2.9 MPa. However, this also reduced failure strain from a high of 2.9 mm/mm to a low of 0.12 mm/mm and diminished the yielding region. Changes in the concentrations of acrylamide or its cross-linking with N,N'-methylenebisacrylamide (BIS) in the second network had a lesser effect on the DN properties. We hypothesized that to obtain a yielding region which results in high toughness, we need to alter the cross-linking of the first network such that the yield stress of the MCS-PEGDA/PAAm DN does not exceed the failure stress of PAAm network. Because of the wide range of mechanical properties achieved in these DNs with limited changes in the swelling degrees, unlike conventional single-network gels, the DN approach allows attainment of a much greater range of mechanical behavior than is possible with single networks.

---

<sup>5</sup> Published as **Tiffany C. Suekama**, Jian Hu, Takayuki Kurokawa, Jian Ping Gong, Stevin H. Gehrke, "Tuning Fracture Properties of Biopolymer Networks", *Macromolecular Symposia*, Special Issue: Polymer Gels: Formation, Structure, Properties and Applications, **2013**, 329 (1), 9-18 (invited)

## Introduction

Although the high water content and three dimensional structure of hydrogels makes them great candidates for use as tissue engineering scaffolds and other applications, the high water content dilutes the load-bearing polymer component, making them inherently low in strength and toughness.<sup>[45]</sup> Thus there is an ongoing need to improve their mechanical properties.

We have shown that it is possible to create hydrogels with high strength and toughness by employing the double-network (DN) strategy. We have previously created DN hydrogels of poly(2-acrylamido-2-methylpropanesulfonic acid) (PAMPS)/polyacrylamide (PAAm), where we have seen significantly improved toughness to either single network alone.<sup>[17,50,61,68,84,101,119,207]</sup> The strategy of DN hydrogels is to combine a brittle, stiff and highly cross-linked polyelectrolyte first network with a ductile, soft and lightly cross-linked neutral second network, where the molar concentration of the second network is in excess relative to the first.<sup>[50,61,101,167]</sup> DN hydrogels have stress-strain behavior that is unlike other hydrogels, as illustrated in Figure 5.1. As shown in the figure, the DN of PAMPS/PAAm can have three characteristic regions: pre-yielding, yielding and hardening. The superior toughness of the DN hydrogels is attributed to the micro-fracturing of the brittle network, which allows for dissipation of strain energy (yielding region), while the ductile second network holds the hydrogel together despite the micro-fracturing.<sup>[50,61,101,167]</sup> At the transition between the pre-yielding and yielding regions there is a clear yield point in which the brittle first network has fractured across an entire cross-section, leading to necking with elongation of the second network.<sup>[50,61,101,167]</sup> In the hardening region, the coils of the second network are highly extended, and thus behave according to non-Gaussian chain statistics with stress rising rapidly with strain.<sup>[50,61,101]</sup>

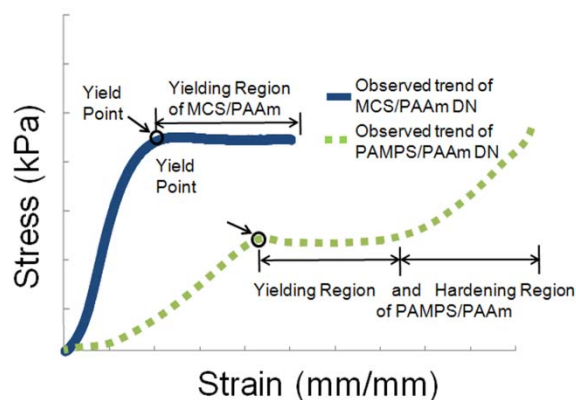


**Figure 5.1: Stress-strain curve for DN hydrogels.**

PAMPS/PAAm may display three distinct regions: pre-yielding, yielding and hardening. MCS/PAAm DN studied in this work can show the first two regions, notably yielding, an unusual phenomenon in hydrogels.

More recently, we have created tough and ductile, ultrathin film DN with methacrylated chondroitin sulfate (MCS), a linear biopolymer, as the first network and polyacrylamide (PAAm) as the second network.<sup>[167]</sup> Furthermore, we demonstrated the generality of the DN effect by replacing the PAAm with poly(*N*, *N*-dimethyl acrylamide) (PDMAAm).<sup>[167]</sup> The molar concentration of AAm or DMAAm was 40-50 times greater than that of the MCS disaccharide groups, emphasizing the importance of the second network being in excess to the first network.<sup>[50,61,101,167]</sup> Both MCS/PAAm and MCS/PDMAAm DN hydrogels showed stress-strain curves similar to the archetypal PAMPS/PAAm DN hydrogels, displaying two of the three distinct regions, pre-yielding and yielding, as illustrated in Figure 5.1.<sup>[167]</sup> The third region, strain-hardening region, was not observed in the MCS/PAAm DN, hypothesized to be due the high yielding stresses obtained, which are of the same magnitude as the failure stress of PAMPS/PAAm DN.<sup>[101]</sup> Moreover, all of the DN had superior strength and toughness to their SN (single network) components.<sup>[167]</sup> Being able to create a biobased hydrogel that is tough and ductile was significant; however, we wanted to demonstrate further control the mechanical properties of these DN.

Being able to control the mechanical properties such as modulus, failure stress, failure strain and yielding region would be important when constructing materials to meet a variety of design specifications for different applications. Therefore, the goals of this work are to determine the structural compositions of the first and second networks that lead to high failure stress and failure strain with a high Young's modulus, and to better understand the yielding phenomenon in these hydrogels. Specifically, we are tuning the mechanical properties of MCS/PAAm DNs by varying the MCS content, copolymerizing MCS with poly(ethylene glycol) diacrylate (PEGDA) to increase its modulus, and changing the concentration of acrylamide (AAm) and N,N'-methylenebisacrylamide (BIS) in the second network.

## Materials

Using the previously reported procedure<sup>[73]</sup> adapted from Li *et al.*,<sup>[100]</sup> methacrylated chondroitin sulfate (MCS) was synthesized with chondroitin sulfate A sodium salt (CS; Sigma-Aldrich: type A 70%, balanced with Type C, from bovine trachea) and glycidyl methacrylate (GMA; Sigma-Aldrich: 97%). Both CS and GMA were used as received. The methacrylation of MCS was determined by NMR to be 35% after 15 days of reaction.<sup>[152]</sup> Acrylamide (AAm; Junsei Chemical Co., Ltd.) was recrystallized in chloroform. Poly(ethylene glycol) diacrylates with  $M_n$  of 700 or 2000 (PEGDA 700 or PEGDA 2000; Sigma-Aldrich) were used as received. The AAm cross-linker, N,N'-methylene bisacrylamide (BIS; Tokyo Kasei Co., Ltd.) was recrystallized in ethanol. UV initiator, 2-methyl-1-propanone (Irgacure 2959; Ciba Specialty Chemicals Corp.) was used as received. Milli-Q (18.2 M $\Omega$  cm) water was used in all synthesis solutions.



<u>First Network</u>			<u>Second Network</u>	
%MCS (w/w)%	- %PEGDA (w/w)%	# (Avg $M_n$ )	$T_{AAm}$ (w/v)%	$\times C_{BIS}$ PAAm (w/w)%
13 %	0 %	700	30	$\times$ 0.04
15 %	2 %	2000	25	$\times$ 0.09
20 %	6 %		25	$\times$ 0.02
			24	$\times$ 0.04
			20	$\times$ 0.04

**Figure 5.2: Double-network formulations with copolymers of MCS and PEGDA as the first network and PAAm as the second network.**

Linear biopolymer, MCS is represented as (w/w)%, PEGDA with an average  $M_n$  of 700 or 2000 is represented as (w/w)% and the PAAm network is represented in a gel electrophoresis notation of T (w/v)%  $\times$  C (w/w)%. Listed are the formulations presented in this work.

## Methods

All of the hydrogels were synthesized in an ultrathin film (~100  $\mu\text{m}$  thick) form. Ultrathin film hydrogels have the benefits of requiring less material, allowing observation of tearing mechanisms and rapid equilibration.<sup>[101,102,167]</sup> In our previous work, we found no significant differences in the mechanical properties and toughening mechanisms between bulk, solution-cast and ultrathin film hydrogels.<sup>[101,102,167]</sup>

The notation used for DN formulations with copolymers of MCS and PEGDA as the first network and PAAm as the second network are illustrated in Figure 5.2. The first network is made of MCS, which is a functionalized linear biopolymer, or copolymers of MCS and PEGDA, where the PEGDA is used to increase the cross-link efficiency of the MCS network.<sup>[152]</sup> MCS is represented as a weight percent solution (w/w)%, independently of PEGDA content. PEGDA is

also represented as a weight percent solution (w/w)%, independently of MCS content. The PEGDA used had with an average  $M_n$  of either 700 or 2000. The second network in this study, PAAm, was represented in traditional gel electrophoresis notation,  $T \times C$ .<sup>[18,132]</sup>  $T$  is the total mass of monomer and cross-linker per unit volume of solvent (w/v), expressed as a percentage.  $C$  is the ratio of the mass of cross-linker by the total mass of monomer and cross-linker (w/w), expressed as a percentage.

### ***Synthesis of SN PAAm***

SN PAAm hydrogels were prepared in a single step process. For example, a 25x0.04 ( $T \times C$ ) PAAm gel was synthesized by dissolving AAm (24.99 g) and BIS (0.011 g) in 100 mL of water. This polymerization used 0.02% (w/w) Irgacure 2959 as a photo initiator. The solution was degassed and placed under argon atmosphere in a mold consisting of two glass plates separated by a 100  $\mu\text{m}$  silicon rubber spacer. The solution was cross-linked into a gel with 365-nm light at  $\sim 10\text{mW}/\text{cm}^2$  for 30 min.

### ***Synthesis of SN of MCS, CP of MCS-PEGDA and DN of MCS-PEGDA/PAAm***

MCS-PEGDA/PAAm hydrogels were prepared in a multistep process as described in our previous publications.<sup>[68,101,167,207]</sup> As example, a MCS-PEGDA 2000/PAAm DN hydrogel with a first network of 15% (w/w) MCS-2% (w/w) PEGDA 2000, and a second network of 25x0.04 PAAm was carried out as follows: the first network of MCS-PEGDA 2000 was prepared by first mixing MCS (3.53 g), PEGDA 2000 (0.408g) and Irgacure 2959 (0.0047 g) in 20 mL of water. The viscous solution was degassed in a vacuum oven for 20 min and then placed under argon atmosphere where it was inserted into a mold consisting of two glass plates and a 100  $\mu\text{m}$  silicon

rubber spacer. The polymer solution with 0.02% (w/w) Irgacure 2959 was exposed to 365-nm light at  $\sim 10\text{mW}/\text{cm}^2$  for 30 min that cross-linked it into a gel. To prepare the DN, the MCS-PEGDA 2000 hydrogel was taken out of the mold and allowed to swell to equilibrium in an AAm solution (as prepared for a single network) for 1 hour. Then the swollen gel was placed under argon atmosphere between two glass plates and was exposed to 365-nm light at  $\sim 10\text{mW}/\text{cm}^2$  for 30 min. All synthesis solutions included 0.1 M sodium chloride which deswells MCS gel to reduce its brittleness enough to handle without tearing.

### ***Swelling Properties***

The procedure to measure the swelling properties of the gels was taken from our previous papers.<sup>[166,167]</sup> Molded gel samples were submerged in Milli-Q water at room temperature for 24 hrs, and the water was changed every few hrs to leach away any sol fraction. The excess water on the swollen gels was dabbed away with a moist Kimwipe. The swollen gel was then weighed and placed in a pre-weighed vial of sea sand (Wako Pure Chemical Industries, Ltd.; 20-35 mesh). The vial with the swollen gel was shaken until the sea sand covered the gel. The sea sand helped draw out water. It has been shown that bound water in PAAm is released over temperatures of 20 to 220 °C<sup>[182]</sup> and Tutas *et al.* shows that there is 10% weight loss at 110 °C<sup>[180]</sup>. Therefore, the vials with the gels and the sea sand were placed into a vacuum oven at 120 °C until it reached a constant weight. The dry weights were taken. The degrees of swelling in the results section are reported as the mass of the swollen gel (polymer and water) over the mass of the dried gel (polymer).<sup>[45]</sup>

## ***Mechanical Analysis***

Mechanical test methods applied to the different gels were similar to our previously published work.<sup>[167]</sup> The fully swollen gels were cut by a gel cutting machine (SDAP-100N Dumbbell Co, Ltd) into a dumbbell shape (standardized JIS-K6251-7; length 35 mm, width 2 mm, gauge length 12 mm) for tension and a trouser shape (standardized JIS-K6252 ½; length 50mm, width 7.5 mm, initial notch 20mm) for tearing. To get precise thicknesses, all gel thicknesses were measured using a phase contrast optical microscope (Olympus CKX41) and the average gel thickness was taken for each gel formulation. The gels were then tested in tension and tearing using a Tensilon machine (RTC-1150A, Orientec Co) at a constant velocity of 100 mm/min. All of the gels were coated with a thin layer of mineral oil to minimize evaporation of water from the gel during testing.

After the gels were tested under tension, from the stress ( $\sigma$ ) – strain ( $\epsilon$ ) data the Young's modulus (E), yield point ( $\sigma_c$ ,  $\epsilon_c$ ), toughness (work to fracture), failure stress and failure strain were determined. To calculate E, the slope of the initial data from a strain of 5-15% was used. Conventional single-network hydrogels behave as ideal elastomers, and therefore can be analyzed using the neo-Hookean model, but DNs generally display non-ideal elastic behavior. Consequently, the shear modulus, G, cannot be calculated for DN gels under tension.<sup>[179]</sup> The toughness (work to fracture) was calculated as the area under the stress-strain curve up to failure. Failure stress and failure strain were found at the point that the gel began to split, identified in the data as a sharp drop in stress. Tearing was performed in Mode III<sup>[147]</sup>, pulling one arm at a constant velocity of 100 mm/min while the other arm remained stationary.<sup>[146]</sup> From the force (F)-extension data, tearing energy (T, work required to tear a unit area) is calculated as twice the average force during steady-state tear divided by the thickness of the sample ( $T=2F_{avg}/W$ ).<sup>[53,146]</sup>

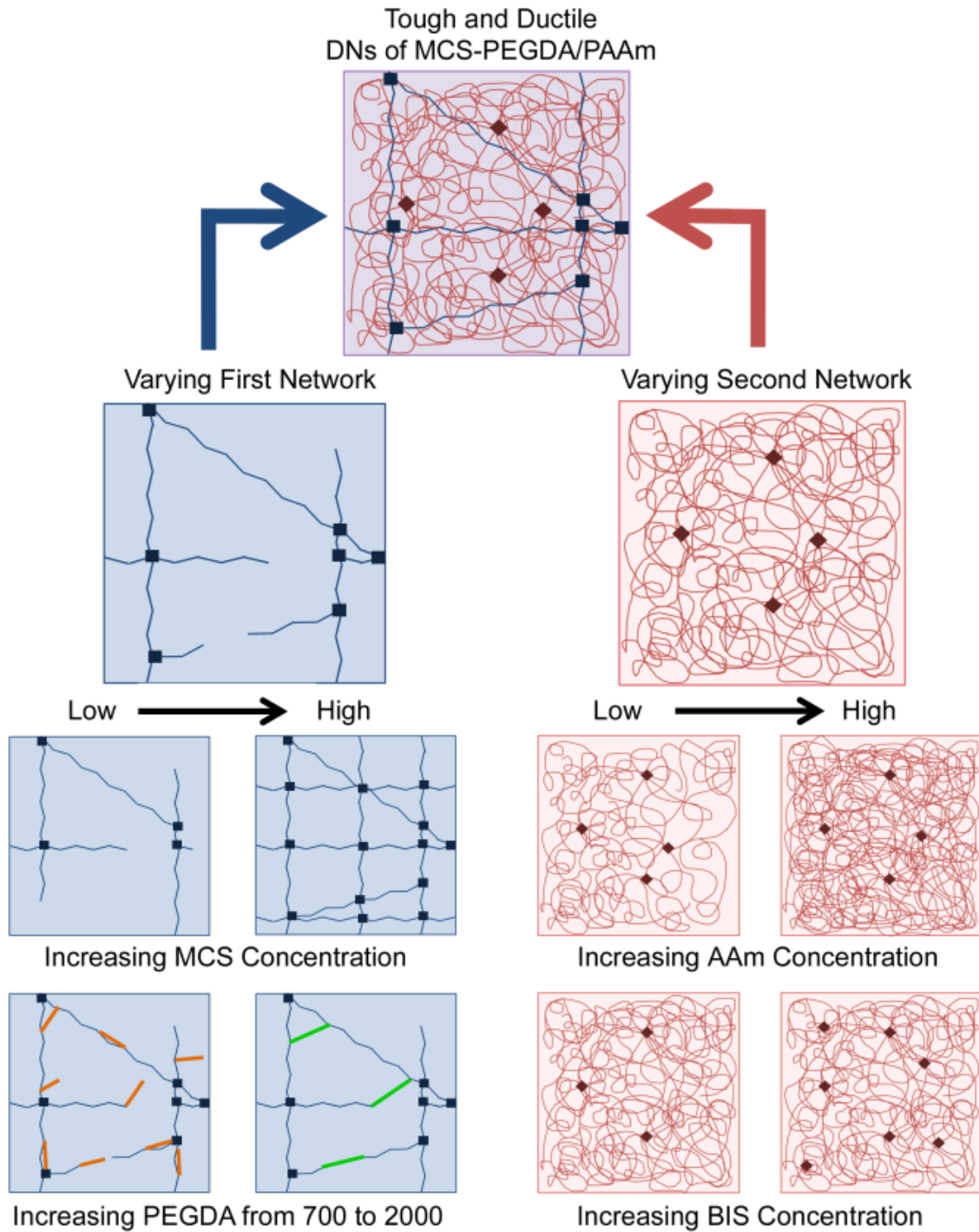


**Figure 5.3: Schematic tuning of MCS-PEGDA/PAAm DN formulations by changing the first and second networks.**

In the first network, different concentrations of MCS were investigated and additional cross-linking was added by copolymerization of MCS with PEGDA. In the second network, AAm and BIS concentrations were varied.

## Results and Discussion

We tuned the failure properties of tough and ductile, biopolymer-based MCS/PAAm DN hydrogels by varying the formulations, as illustrated in Figure 5.3, to obtain a wide variety of physical properties. First, we varied the MCS concentration in the first network. MCS has methacrylate groups that can polymerize and thus cross-link the polymer into a gel. We have found that using a greater concentration of MCS in the first network leads to a stiffer DN hydrogel by increasing the cross-link density. We also copolymerized the MCS with smaller amounts of PEGDA, which we have determined will increase the cross-link density of the MCS gels by improving the cross-linking efficiency.<sup>[152]</sup> Furthermore, we changed the second network by adjusting the AAm and BIS concentrations, which our prior work with PAMPS as a first network suggested would allow for increased elongation of the DN. The swelling and mechanical properties for varying the first network and keeping the second network constant with 25x0.04 PAAm are given in Table 5.1.

Similarly, the swelling and mechanical properties for varying the second network and keeping the first network constant with 15% MCS are given in Table 5.2. All of the swelling degrees range from 5-11 (g/g), generally clustering around 6-7 (g/g) as shown in Tables 5.1 and 5.2. The Young's modulus, toughness, yield point stress, failure properties, and tearing energy for the various DN hydrogels formulations are tabulated in Tables 5.1 and 5.2. The analysis of this data in subsequent sections focuses on the Young's modulus, yielding and failure properties as these are the key properties. For these gels, the toughness (work to fracture) in these materials is generally determined largely by the failure strain. Complex trends are seen with the tearing energy and more research will be needed to further interpret these. In general, the tearing energy is around 500-700 J/m<sup>3</sup>, but much higher and lower values are observed. For the data in these tables, there

was high reproducibility among samples from a single batch, but lesser reproducibility from batch-to-batch especially in the failure stress. The gel samples are sensitive to precise synthesis conditions, since the single network is highly brittle thus it is difficult to avoid introducing microscopic defects during the preparation of the hydrogels.

**Table 5.1. Effect of compositional changes in the first network of MCS-PEGDA on mechanical properties of double network gels. The second network composition is 25x0.04 PAAm.**

MCS wt%	PEGDA <sup>†</sup> wt%	Swelling Q (g/g)	Young's Modulus E (kPa)	Toughness (kJ/m <sup>3</sup> )	Yield Point Stress (kPa)	Failure Stress (kPa)	Failure Strain (mm/mm)	Tearing Energy T (J/m <sup>2</sup> )
13	-	9.9 ±1.5	670 ±40	1720 ±340	659 ±130	724 ±120	2.91 ±0.81	500 ±100
13	2 (700)	11.1 ±2.4	970 ±80	1490 ±50	1470 ±20	1270 ±540	1.52 ±0.06	1530 ±10
13	2 (2000)	6.0 ±0.1	1240 ±140	760 ±230	∅	2080 ±60	0.81 ±0.12	560 ±20
*15	-	*7.0 ±0.3	*750 ±100	*710 ±470	*1680 ±170	*1670 ±150	*1.09 ±0.08	*695
15	2 (700)	6.1 ±0.6	1610 ±240	300 ±80	∅	1850 ±390	0.48 ±0.04	615 ±6
15	6 (700)	5.5 ±0.2	1710 ±120	100 ±10	∅	680 ±90	0.33 ±0.01	‡
15	2 (2000)	6.8 ±0.0	1010 ±160	2480 ±580	1670 ±10	1700 ±30	1.90 ±0.33	730 ±80
15	6 (2000)	8.7 ±0.9	1610 ±170	1420 ±390	#	2600 ±170	1.02 ±0.15	600 ±100
20	-	6.0 ±0.5	2870 ±180	830 ±210	∅	2940 ±240	0.62 ±0.08	710 ±60
20	2 (700)	7.6 ±1.3	2980 ±70	130 ±20	∅	1060 ±50	0.29 ±0.02	600 ±400
20	6 (700)	4.5 ±0.0	2900 ±1300	30 ±20	∅	370 ±230	0.12 ±0.05	42 ±3
20	2 (2000)	5.5 ±0.4	2980 ±340	430 ±160	∅	2390 ±480	0.45 ±0.06	1120 ±130
20	6 (2000)	5.0 ±0.1	3300 ±210	230 ±30	∅	1750 ±130	0.35 ±0.02	200 ±50

\* Values taken from Suekama et. al<sup>[167]</sup> with the second network composition of 24x0.04

∅ No distinct yielding region

# Slight yielding near failure point

‡ Too brittle to measure

†(M<sub>n</sub> = 700 or 2000 as noted)

(Mean ± standard deviation)

**Table 5.2. Effect of compositional changes in the second network of PAAm and BIS on mechanical properties of double network gels. First network composition is 15% MCS.**

PAAm TxC	Swelling Q (g/g)	Young's Modulus E (kPa)	Toughness (kJ/m <sup>3</sup> )	Yield Point Stress (kPa)	Failure Stress (kPa)	Failure Strain (mm/mm)	Tearing Energy T (J/m <sup>2</sup> )
30x0.04	7.4 ±1.3	1280 ±180	2460 ±960	1300 ±100	1390 ±130	2.03 ±0.56	1010 ±190
20x0.04	8.6 ±0.5	1390 ±250	1710 ±330	#	2130 ±30	1.25 ±0.18	610 ±50
25x0.09	7.3 ±0.4	1430 ±270	4070 ±1860	1530 ±120	1730 ±160	2.88 ±1.04	630 ±10
*24x0.04	*7.0 ±0.3	*750 ±100	*710 ±470	*1680 ±170	*1670 ±150	*1.09 ±0.08	*695
*25x0.02	*6.9 ±0.2	*1040 ±62	*2940 ±530	*1610 ±20	*1600 ±12	*2.27 ±0.34	*585

\* Values taken from Suekama et. al<sup>[167]</sup>

# Slight yielding near failure point  
(Mean ± standard deviation)

### ***Varying the First Network: Concentration of MCS***

We first examined the effects of modifying the first network, either by varying the concentration of MCS or by copolymerization of the MCS with PEGDA, while keeping the second network constant at 25x0.04 PAAm. In our previously published work, the MCS concentration was fixed at 15%.<sup>[167]</sup> Here we examined the effect of both reducing and increasing the MCS concentration relative to 15%, as shown in Figure 5.4. We observe that increasing the MCS concentration above 15% nearly doubles the modulus and failure stress, but at the expense of the failure strain, which decreases by a similar factor as the yielding region is suppressed. In contrast, reducing the concentration to 13% reduces failure stress and modulus but leads to an extended yielding region and thus a higher failure strain. Increasing the MCS concentration is expected to improve the cross-link efficiency of the reaction, increasing the modulus but perhaps causing early failure by limiting chain extensibility.



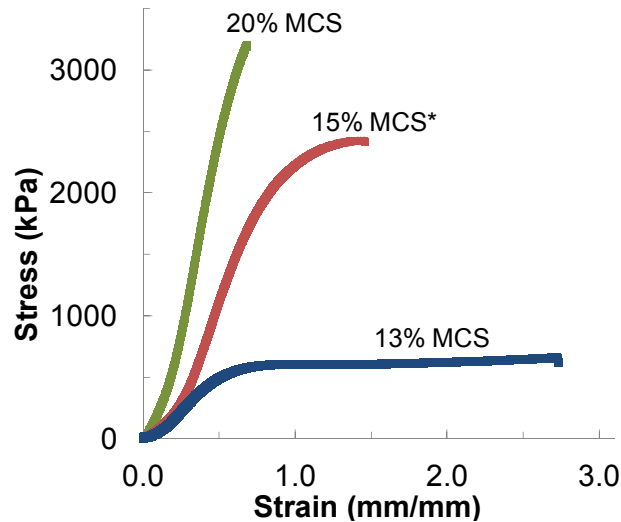


**Figure 5.4: Varying MCS concentrations in DN of MCS/24x0.04 PAAm.**

Increasing MCS concentration leads to larger modulus and higher failure stress, but decreases the yielding region. \*15% MCS/25x0.04 PAAm data from Suekama et. al<sup>[167]</sup>.

#### ***Varying the First Network: Copolymerization with MCS with PEGDA***

To test the hypothesis that the effects seen in Figure 5.4 are the result of increased cross-linking of the first network rather than being the direct result of the polymer concentration itself, we kept the MCS concentration constant but copolymerized it with PEGDA, which leads to a more efficiently cross-linked network with a higher modulus.<sup>[152]</sup> Stress-strain curves of 13% MCS-PEGDA/25x0.04 PAAm with 0% PEGDA, 2% PEGDA700 and 2% PEGDA2000 are shown in Figure 5.5. The addition of the 2% PEGDA700 led to an increase in the Young's modulus and the effect was greater with PEGDA2000, as we have observed in the single network MCS-PEGDA gels. However, these changes were accompanied by a shortened yielding region. Also, the failure stress between no PEGDA and PEGDA2000 is increased almost two-fold although the failure strain decreased 3.5 times. Regardless, the failure properties are still much greater than seen for SN MCS gels. We have shown with that PEGDA is an effective cross-linker of MCS even at low concentrations, with the effectiveness increasing with molecular weight. This is likely due to a

greater degree of intermolecular cross-linking relative to intramolecular cross-linking as the PEGDA spacer length is increased. Increased cross-linking would cause an increased modulus before yielding.<sup>[152]</sup> The trends of the stress-strain curves in Figure 5.5 are consistent with those of Figure 4 and are also consistent with the hypothesis that increasing cross-linking increases modulus and failure stress at the expense of failure strain. Furthermore, it appears that if the failure stress rises above the apparent yield stress of the PAAm network – about 1500 kPa based on our previous work with PAMPS/PAAm DN<sup>s</sup><sup>[167]</sup> – therefore, the gel fails before yielding.

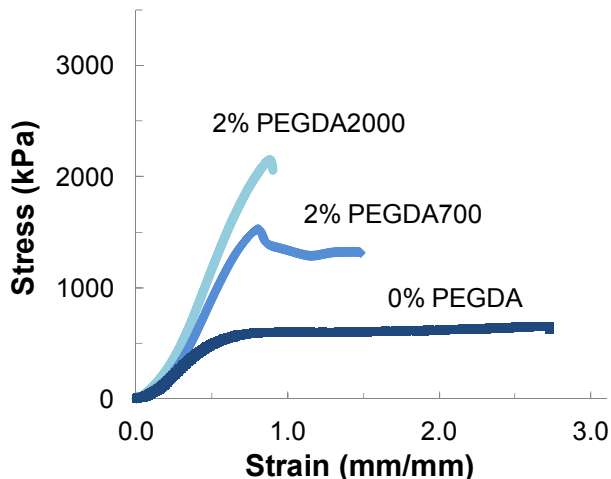


**Figure 5.5: Further cross-linking of first network with PEGDA leads to increase in modulus and failure stress but decrease in yielding region**

Adding PEGDA to the first network of 13%MCS-PEGDA/25x0.04PAAm DN formulations lead to an increase in modulus and failure stress, due to increased cross-linking efficiency, but a decrease yielding region. The trends are amplified with increased PEGDA molecular weight, likely due to increased intermolecular cross-linking with the higher molecular weights. The trends match those of Figure 4, where cross-linking was increased by increased polymer concentration.

We further increased the MCS concentration to 20%, anticipating that at this concentration we move the MCS toward the upper end of the semi-dilute entangled regime or the concentrated regime where its cross-linking efficiency would be greater due to greater chain entanglement. We

then synthesized 20% MCS-PEGDA/25x0.04 PAAm with 0, 2 and 6% PEGDA700. The shape of stress-strain curves and influence of the PEGDA is quite different at 20% MCS relative to 13%, as shown by a comparison between Figures 5.5 and 5.6. In Figure 5.6, for all cases, increasing concentrations of MCS to 20% and PEGDA up to 6% eliminated the yielding plateau, and the only significant effect of the PEGDA is a reduction the fracture strain with a negligible dependence upon PEGDA molecular weight. For PEGDA700, increasing PEGDA leads to a steady decrease, almost eight times, in the failure stress (from 2940 to 1060 to 370 kPa) and more than five times in failure strain (from 0.62 to 0.29 to 0.12 mm/mm), with statistically irrelevant changes in the modulus. For PEGDA2000, a similar but less substantial behavior in the stress-strain curves is observed: there is a steady decrease in the failure stress (from 2940 to 2390 to 1750 kPa) and in the failure strain (from 0.62 to 0.45 to 0.35 mm/mm) but also with statistically irrelevant changes in the modulus.

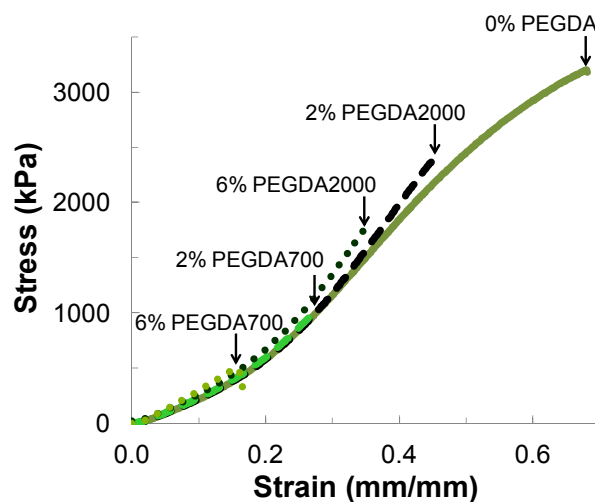


**Figure 5.6: 20% MCS-PEGDA/25x0.04 PAAm DN formulations shows that the addition of PEGDA causes a decrease in failure properties**

Varying PEGDA in 20% MCS-PEGDA/25x0.04 PAAm DN formulations shows that the addition of PEGDA causes a decrease in failure properties with minimal changes in the modulus and the overall shape of the stress-strain curve.

We believe that the explanation of the different trends observed in Figures 5.5 and 5.6 lies in consideration of the nature of the changes in the network structure as a function of polymer concentration, due to the different levels of MCS chain entanglement at 13% and 20%. 13% is near the lower limit of concentration at which MCS can be self-cross-linked into a gel. This suggests that at 13 wt% the MCS is in the semi-dilute unentangled state. In this regime, it could be expected that even though a macroscopic gel forms, the network may not be uniformly well-cross-linked with significant dangling ends and other network imperfections which are not elastically effective and thus do not contribute to the modulus (as sketched in Figure 5.3). Hence, these portions of the network would not be capable of transmitting stress or absorbing strain energy by fracturing as required to behave according to the DN mechanism. Therefore, more efficient cross-linking of 13 wt% MCS by PEGDA would reduce the level of elastically ineffective structures in the network, and increase both modulus and fracture stress.

In contrast, 20% MCS forms a strong SN gel, which suggests that at this concentration the MCS is in the semidilute entangled region or concentrated region; consequently the MCS is efficiently cross-linked and the level of elastically ineffective structures is lower. Hence, increasing cross-linking of 20% MCS with PEGDA increases the cross-link density of the network without significantly reducing the elastically ineffective structures, in contrast with the effects at 13%. For ideal elastic networks, increased cross-link density would result in increased modulus. However, modulus of DN gels is dominated by dissipation of strain energy by fracturing of the first network, therefore a direct relationship between modulus and cross-link density of the first network is not anticipated. Rather, dissipation of strain energy may be more directly linked to the polymer concentration (swelling degree) which is not significantly different for these DN. Consequently it appears that the primary effect of increased cross-linking of the first network is to

reduce the extensibility of the network before failure. A significant difference in inter- vs. intramolecular cross-linking at this MCS concentration is not anticipated for PEGDA700 and PEGDA 2000, and thus the molar concentration of acrylate groups would be the primary determinant of cross-link density. Hence the properties of 6 wt% PEGDA 2000 are comparable to PEGDA700, with 2 wt% PEGDA 2000 having the least influence and 6 wt% PEGDA 700 having the most.

### ***Varying the Second Network: Concentration of AAm and BIS***

Finally, we investigated the effect of changing the AAm and BIS concentrations in the second network while keeping the first network constant with 15% MCS. An example of the stress-strain response of a 15% MCS/PAAm DN gel is shown in Figure 5.4; Table 5.1 summarizes the results for other AAm/BIS combinations. Except for the T=20 PAAm gel which does not show a distinct yielding region, all of the formulations have the same general shape of the 15% curve in Figure 4. In DNs the BIS was held constant, C=0.04, and AAm concentration were created in a range of 20-30 wt%. All of the DNs broke relatively early, ~1.3 mm/mm with only a slight yielding near the breaking point, except the highest AAm concentration of T=30, which failed at 2 mm/mm. Increasing the PAAm concentration in the second network allows for the failure stress of PAAm network to exceed the yield stress of the MCS /PAAm DN producing high toughness and a yielding region. Further, in the DNs the AAm was held constant, T=25, and the BIS was varied from C=0.02-0.09, all producing lightly cross-linked second networks. To attain yielding, a narrow range of cross-linker concentration is needed, but the system is not sensitive to the amount of cross-linker in this small range. The DN strategy works as long as the second network is lightly cross-linked. These results support the hypothesis that the DN effect requires a concentrated yet lightly cross-linked second network.

## Conclusions

This work shows how to manipulate the MCS-PEGDA/PAAm DN formulations to vary failure stress, failure strain, Young's modulus and yielding behavior over a very broad range, more than five times in most cases. These variations occur largely independently of swelling degree, unlike conventional SN gels, whose properties generally correlate with swelling degree. Increasing cross-linking in the first network by (1) increasing the MCS concentration from 13 to 20% in MCS/PAAm DNs or (2) adding PEGDA as a cross-linker led to a higher modulus and higher failure stress, but decreased the yielding region. For the MCS used, 13% is the lower limit of concentration at which gelation occurs. Addition of PEGDA to 13% MCS appears to reduce the level of elastically ineffective structures in the network. Furthermore, both modulus and fracture stresses of the DN increase, with a greater effect seen as  $M_n$  was increased from 700 to 2000, likely due to the increasing levels of intermolecular cross-linking with higher molecular weight. At 20% MCS, the gel appears to be in the entangled semidilute or concentrated regime and the addition of PEGDA increases cross-linking (which reduces failure properties) without significantly reducing elastically ineffective structures (no change in modulus). Since the increased modulus in DN gels is believed to be the result of strain energy dissipation by fracturing of the first network, the primary effect of cross-linking appears to be the reduction of chain extensibility and thus failure at lower strains. Changing the AAm and BIS concentrations in the second network allowed for further elongation at high AAm concentration and minimal BIS concentrations, emphasizing the DN effect. These effects appear to be generally consistent with previously described mechanisms leading to the DN effect as observed in PAMPS/PAAm system.

Our demonstrated ability to adjust a full suite of mechanical properties of a gel class (MCS-PEGDA/PAAm DNs) over a broad range independently of the water content is significant

implications for many applications, including tissue engineering scaffolds. We also note that the double network structure of these gels is reminiscent of many biological structures, such as the mammalian extracellular matrix, where collagen fibers are embedded in a matrix of glycosaminoglycans, including CS. Since the MCS-PAAm results are broadly consistent with the well-established PAMPS/PAAm system, the results support the generality of the concept and suggest that other such systems using biopolymers may be designed.

## Chapter 6: Unique Features Shown Under Compression when Using the Double-Network Strategy<sup>6</sup>

### Abstract

This work investigates the molecular mechanisms of the sacrificial bonds through the exploration of (1) the compressive stress-strain curve of a DN hydrogel and (2) the ability of a DN hydrogel to endure continual compressive loading to the failure strain of the first network, 15%, and then two larger strains, 25% and 45%. The DN hydrogels of methacrylated chondroitin sulfate (MCS) and polyacrylamide (PAAm) have superior properties, under compression, to either single network or co-polymer of the two networks. The DNs display non-ideality even at low strains (unlike co-polymers or single-networks). The unusual shape of the stress-strain curves of DNs was believed to be caused by the complex but synergistic interactions of the two networks. Under compression there was no obvious yielding phenomenon but DNs show an inflection in the stress strain curves at 35-40% strain indicating microfracturing. The repeated loading cycles up to 15% strain revealed no permanent damage. In the repeated loading cycles, up to a strain of 45%, slight damage was shown between the first few cycles and no further damage was shown in cycles 7-12. Also, there was an improved stress in comparison to the initial cycle in some formulations. Overall, the MCS/PAAm hydrogels show superior properties under compression but the toughening mechanisms are hypothesized to be different from tension.

---

<sup>6</sup> To be submitted as **Tiffany C. Suekama**, Deena Rennerfeldt, Anahita Khanlari, Anthony Livengood, Stevin H. Gehrke,



## Introduction

Following Jian Ping Gong, Yoshihito Osada and their coworkers, many researchers have developed a number of double-network (DN) systems but the most notable is still the original from their group: poly(2-acrylamido-2-methylpropanesulfonic acid) (PAMPS)/polyacrylamide (PAAm) which has exceptionally high toughness and excellent fracture stresses.<sup>[17,50,61,68,84,101,119,207]</sup> DN hydrogels are formed from a combination of two networks. The first is a highly cross-linked, brittle and typically polyelectrolyte network and the second is a lightly cross-linked, ductile, and typically neutral network.<sup>[50,61,192]</sup> The second network concentration is significantly greater than the first network.<sup>[50,61,167,192]</sup> DN hydrogels have three characteristic regions under tension – preyielding, yielding and hardening – and display a clear yield point (transition between preyielding and yielding regions).<sup>[50,61,101,167]</sup> In the preyielding region fracturing of the first network starts which allows for high stresses to be achieved. At the yield point the first network fractures across an entire cross-section. In the yielding region, the first network continues to fracture as the yielding zone grows at a constant stress. The hardening region achieved from the extension of the coils of the second network approaches full extension in which it behaves according to non-Gaussian chain statistics.<sup>[50,61,101]</sup> Overall, the exceptional mechanical properties are believed to be a result of fracturing of the brittle first network which dissipates strain energy while the second network holds the system together.<sup>[51,61]</sup> The current understanding for the toughening mechanism of DN hydrogels under compression is believed to be the same as tension, however, the mechanism has not been extensively studied.

Due to the interesting properties achieved from DN of PAMPS/PAAm, researchers have investigated the mechanisms for toughening and failure. Webber *et al.* showed a significant hysteresis in the first loading cycle which increases at higher strains and only slight hysteresis in

the second cycle with stress-strain curves behaving elastically.<sup>[190]</sup> Further, the DN gels showed considerable strain hardening, nonlinear elastic behavior, in the second loading curve.<sup>[190]</sup> However, Webber *et al.* did not display yielding in their samples.<sup>[190]</sup>

To our knowledge, yielding under compression is unusual, especially for hydrogels; though, Hao and Weiss showed a inflection region which they described as yielding under compression, at ~15% and 280 kPa, in hydrogels of N,N-dimethylacrylamide (DMA) and 2-(N-ethylperfluorooctane sulfonamido) ethyl acrylate (FOSA).<sup>[59,60]</sup> We hypothesize that if the mechanisms for toughening and failure – energy dissipation through fracturing the first network while the second network holds the hydrogel together – shown under tension would be the same as under compression we should be able to achieve preyielding, yielding and potentially hardening, under compression. Specifically, we anticipated to see an indication of energy dissipation from the first network breaking in the preyielding zone that would lead to increased toughness along with an indication of yielding from the stress-strain curves.

Although, extensive research on DNs have been performed under tension the mechanisms for toughening are not as understood in compression. Our group has recently created and tested, under tension, tough and ductile hydrogels with a substantial yielding region demonstrating the DN effect in a bio-polymer based systems of methacrylated chondroitin sulfate (MCS)/polyacrylamide (PAAm) and MCS/poly(*N, N*-dimethyl acrylamide (PDMAAm)).<sup>[167]</sup> We want to show similar improvement, under compression, in DN hydrogels of MCS/PAAm over CP of MCS-PAAm, SN of MCS and SN of PAAm. DN hydrogels would be an excellent replacement for bio-tissues such as cartilage due to the high water content along with notable toughness and fracture properties but the irreversible toughening mechanism shown in tension is a drawback for applications of tissue engineering. Learning more about the microfracturing and energy dissipation

mechanisms under compression will help us to design constructs to avoid failure. Therefore this work aims to understand if mechanisms for improvement in failure properties, modulus and toughness which are occurring in DNs of MCS/PAAm under compression.

## Materials and Methods

### ***Materials:***

For MCS synthesis, the methacrylated chondroitin sulfate was synthesized using a previously reported procedure<sup>[73]</sup> adapted from Li *et al.*<sup>[100]</sup> with chondroitin sulfate A sodium salt (CS; Sigma-Aldrich: type A 70%, balanced with Type C, from bovine trachea); and glycidyl methacrylate (GMA; Sigma-Aldrich: 97%). The methacrylation of MCS was determined by NMR to be 34.5% after 15 days of reaction.<sup>[152]</sup> For synthesis of PAAm, the reagents comprised of the monomer, acrylamide (AAm; Sigma-Aldrich: 99+ %); the cross-linker, N,N'-methylenebisacrylamide (BIS; Sigma-Aldrich: 99+ %); and the UV initiator 2-methyl-1-propanone (Irgacure 2959; Ciba Specialty Chemicals Corp.) All of the reagents were used as received and deionized ultra-filtered (DIUF) water (Fisher Scientific) was used for all of the synthesis solutions.

### ***Synthesis of SN PAAm:***

A traditional gel electrophoresis notation, T x C, was used to describe the gel compositions for PAAm.<sup>[18,132]</sup> T represents the total mass of monomer and cross-linker over the volume of solution (w/v) as a percentage. C represents the ratio of the mass of cross-linker by the total mass of monomer and cross-linker (w/w) as a percentage. An example of a 25 x 0.0446 (T x C) PAAm gel was synthesized by dissolving AAm (24.99 g) and BIS (0.01 g) in 100 mL of water. This

polymerization used 0.02% (w/w) Irgacure 2959 to initiate the polymerization. The solution was placed in a mold consisting of two glass plates and a 2 mm silicon spacer. The solution was cross-linked into a gel with 365-nm light at  $\sim 10\text{mW/cm}^2$  for 30 min (flipping after 15 min).

***Synthesis of SN of MCS, CP of MCS-PAAm and DN of MCS/PAAm:***

The MCS/PAAm hydrogels were prepared in a multistep process similar to Gong *et al.*<sup>[68,101,207]</sup>. First, a SN MCS hydrogel was prepared by mixing MCS (17.65 g) and Irgacure 2959 (0.036 g) in 20 mL of water to create a formulation of 15% (w/w) MCS with 0.03% (w/w) Irgacure 2959. The viscous solution was sonicated for 40 min and then vortexed to remove bubbles before pipetting it in a mold consisting of two glass plates and a 2 mm silicon spacer. The polymer solution was cross-linked into a gel with 365-nm light at  $\sim 10\text{mW/cm}^2$  for 30 min (flipping after 15 min). The MCS hydrogel was taken out of the mold. To make a DN of MCS/PAAm the SN of MCS was allowed to swell to equilibrium in an AAm solution (as prepared in a single network) for 24 hours. After swelling, the swollen gel was placed between two glass plates and was exposed to 365-nm light at  $\sim 10\text{mW/cm}^2$  for 30 min (flipping after 15 min). A CP of MCS-PAAm was made by mixing the solutions of both SNs of MCS and PAAm. From the above examples it would create a CP of 15% MCS - 25x0.04 PAAm.

***Swelling Properties:***

The degree of swelling was measured for all of the gels. Molded gel samples were submerged in DUIF water at room temperature for 24 h, and the water was changed every few hours to leach away any sol fraction. The excess water on the swollen gels was dabbed with a moist Kimwipe. The swollen gel was weighed and put in a dessicator for 24 hours to dry. The dry weights were

taken. The degrees of swelling in the results section are reported as the mass of the swollen gel over the mass of the dried gel<sup>[45,135]</sup>.

### ***Mechanical Analysis:***

Mechanical tests were performed under unconfined uniaxial compression by the RSA III dynamic mechanical analyzer (DMA; TA Instruments). The fully swollen gels were cut into cylindrical disks. The sample diameters were measured under a standard stereomicroscope using a micrometer and the sample thicknesses were measured using the DMA. All of the gels were lightly lubricated with mineral oil to minimize gel adhesion to the plates and evaporation of water during testing. Compression tests were performed at a constant velocity of 0.05mm/s, which was tested to be strain-rate independent. For repeated loading experiments the gels were rehydrated in water and then re-measured before performing consecutive runs. Only runs 1, 2, 3, 7, and 12 are shown for simplicity. From the stress ( $\sigma$ )–strain ( $\epsilon$ ) data, Young’s modulus (E), toughness, failure stress and failure strain were determined. To calculate E, the slope of the initial data of a strain up to 10% was used. Failure stress and failure strain were found at the point that the gel began to split, identified in the data as a sharp drop in stress. The strain energy at failure, toughness, was calculated as the area under the stress-strain curve.

### ***Statistics***

To test for statistical differences between the repeated loading cycles a one-way analysis of variance (ANOVA) then a Tukey’s Honestly Significant Difference (HSD) *post hoc* test, was performed with SPSS 20.0 (IBM; Armonk, NY).

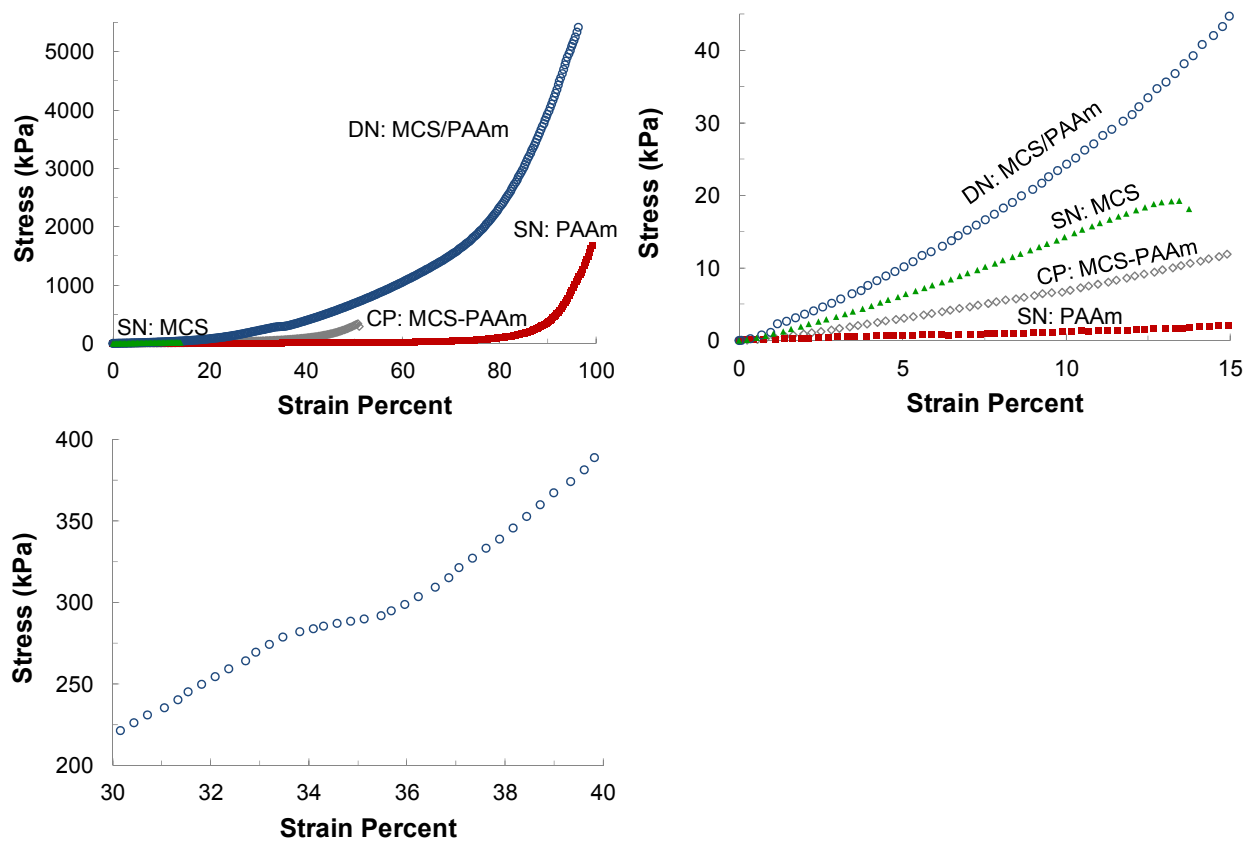
## Results and Discussion

DNs are excellent candidates for tissue replacement such as cartilage, but further research is needed to determine the (1) toughening and failure mechanisms of DNs under compression and (2) if the irreversible nature of DNs shown in tension is also occurring under compression. First we determined if DNs of MCS/PAAm performed better than CP of MCS-PAAm, SN of MCS and SN of PAAm under compression. We investigated the behavior of stress-strain curves of DNs under compression to see the features achieved. In particular, we wanted to know if we could see the same yielding mechanism and/or the distinct regions as we saw under tension. Further, we conducted repeated loading cycles to 15%, 25%, and 45% strain to determine if the DN gels undergo permanent damage under repeated loading. The SN of MCS fails just before 15% strain and if the second network does not impede fracturing of the DN of MCS/PAAm, we should see an indication of the MCS network breaking in the stress-strain curves. We also studied two higher strains, 25% and 45%, in the DN of MCS/PAAm to show the changes in the mechanical mechanisms at higher strains.

### *Does the DN of MCS/PAAm Outperform CP and SNs Under Compression?*

Pronounced improvement in the stress-strain curves of DN hydrogels are shown when comparing DN of MCS/PAAm, CP of MCS/PAAm, SN of MCS and SN of PAAm, Figures 6.1a and 6.1b. SN of MCS shows high modulus but fractures early. SN PAAm compresses to nearly 100% strain before fracturing, but is soft. CP of MCS-PAAm has failure properties, modulus and toughness in between its SN counterparts. DN of MCS/PAAm displays an improvement in failure stresses and toughness in comparison to both SNs and CP of the two polymers, similar to the tension data (Figure 6.1a).<sup>13</sup> The failure stress was 4 times greater than a SN of PAAm and over

300 times greater than a SN of MCS. The toughness of a DN was 10 times greater than SN of PAAm and 100 times greater than SN of MCS. The modulus of the DN is superior to the SN of PAAm and similar to SN of MCS, reinforcing the idea that the dominating effect to the modulus of the DN is the ridged MCS network (Figure 6.1b). Further, the DN at a strain of 12.2% (failure strain of SN MCS) has statistically higher average stress,  $24.3 \pm 6.5$  (kPa) than SN MCS, but not a statistically higher toughness,  $1.26 \pm 0.34$  kJ/m<sup>3</sup>. This is due to the unique shape of the stress-strain curve the DN.



**Figures 6.1a, 6.1b and 6.1c: Stress-strain curves of DN of MCS/PAAm, CP of MCS-PAAm, SN of MCS and SN of PAAm.**

Figure 6.1a: A clear picture of the superior properties achieved in the DN of MCS/PAAm than either SN alone or a CP of MCS-PAAm that leads to properties in-between the SNs. Figure 6.1b: When comparing the initial linear stress-strain curves the DN of MCS/PAAm shows a similar modulus to the SN of MCS and an increased modulus to the CP of MCS-PAAm or SN of PAAm. Figure 6.1c: Dip in stress-strain curve of DN of MCS/PAAm typically seen between 35-40% strain and also seen from 10-20% and 55+%.

### ***Yielding Mechanism Under Compression***

Our current understanding of DN hydrogels is that the improved properties result from energy dissipation from the first network fracturing while the second network holds the gel together. We have already shown that these improved properties exist in compression, but the mechanism for improvement is still in question. The yielding mechanism is shown in DN's when tested in tension but, to our knowledge, yielding under compression is not a commonly found observation in materials.

Close examination of the stress-strain curve of the DN of MCS/PAAm shows several sections with a constant stress with an increasing strain (Figure 6.1c) which suggests a yielding mechanism. These regions of constant stress appear in all of the DN hydrogels tested. The inflection in the stress-strain curves of DN's of MCS/PAAm are typically seen at strains between 35-40% (stress of 270 kPa) but can also be seen from 10-20% (stress ~ 50 kPa) and 55+% (stress ~700 kPa and above). Hao and Weiss show a similar inflection region, at ~15% and 280 kPa, in hydrogels of N,N-dimethylacrylamide (DMA) and 2-(N-ethylperfluorooctane sulfonamido) ethyl acrylate (FOSA) [59,60] The inflection in the DN occurs at a critical strain indicative of the point where the first network becomes fractured. The inflection in the stress-strain curves only lasts a few strain % and the inflections commonly occur again at higher strains. If this inflection is indicative of the yielding phenomenon and the mechanism of failure is the same under compression as it is under tension we would anticipate the first network being fractured across the entire cross-section and that further fracturing continues the yielding zone continues to grow. Because these samples are cylindrically shaped, it is likely that fracturing would occur at weakest parts, the edge versus right down the center. Therefore, this is shown on the stress-strain curves as the inflection which is not very long and can happen several times. However, Lomakin *et al.*

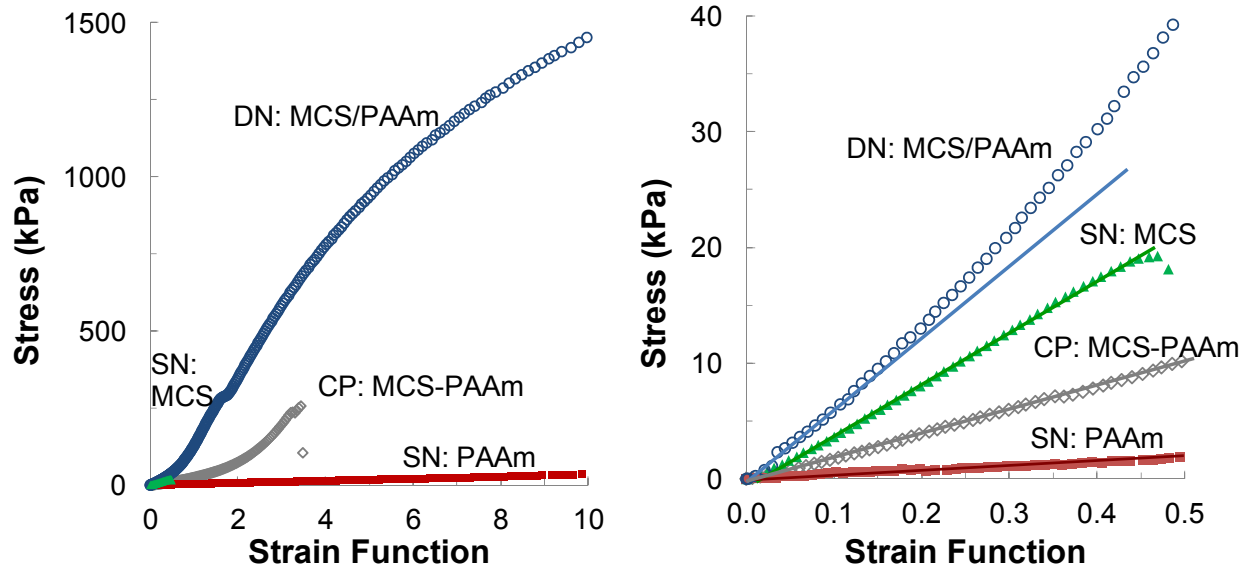


showed changes in modulus in beetle elytron associated with piecewise tearing,<sup>[106]</sup> thus we hypothesize that this change in slope in DN gels under compression is due to microfracturing of the network.

To further study the mechanisms of toughening and if permanent deformation occurs at these inflection points we did compressive loading cycles to 25% and 45%, above and below where the inflection is commonly seen. We did not see these inflection points in SN of MCS, SN of PAAm or CP of MCS-PAAm.

### ***Non-Ideal Elastomer behavior***

Since SN hydrogels commonly behave as ideal elastomers we have previously analyzed SN hydrogels with the neo-Hookean model:  $\sigma = G(\lambda - 1/\lambda^2)$ , where  $\lambda = L/L_0$ .<sup>[166,179]</sup> The shear modulus,  $G$ , was calculated up to a strain function,  $(\lambda - 1/\lambda^2)$ , of 10 (~69%). However, as shown in Figure 6.2a and 6.2b the DN of MCS/PAAm deviates significantly from linearity at large strain functions (up to 10) and even at small strain functions there is a deviation in the DN. On the other hand, all of the SNs are linear until their breaking point or strain function of 10, whichever comes first. Even the CP of MCS-PAAm remains linear at small strain functions, Figure 6.2b, but then deviates from linearity at larger strain functions, Figure 6.2a. The non-linearity means that these DN hydrogels do not behave as ideal elastomers even at low strains, which provides a clue for understanding the mechanisms of the DN behavior by implying the networks are interacting in a synergistic fashion.



**Figures 6.2a and 6.2b: Non-ideal elastic behavior is exhibited even at a low strain function**

Non-ideality shown in DN of MCS/PAAm over a strain function of ten (Figure 6.2a) and also in the initial portion of the curve (less than a strain function of 0.5) while the other stress-strain function curves of CP of MCS-PAAm, SN of MCS and SN of PAAm are linear in the initial strain function. The SNs are linear up to their breaking point or strain function of 10, whichever comes first.

The modulus of a DN should not be used as a concrete comparison between the hydrogels because of the non-linear stress-strain curves, especially in shear modulus and since the stress-strain curves are complex the individual curves should be taken into account. However, the modulus provides a rough idea that stiffness of DN is similar to SN of MCS and around 6 times greater than a SN of PAAm displayed in Table 6.1. The DN compresses to nearly 100% and thus has much higher failure stresses than CP of MCS/PAAm and SN of MCS and PAAm. Toughness, the area under the curve, takes into account the shape of the curve and allows for comparison of stress-strain curves thus this work analyzes the toughness of DN. Moreover, the earlier strain hardening causes the DN to have a toughness that is more than 10 times greater than the SN of PAAm, typically 1000 times greater than the SN of MCS and 30 times greater than the CP of MCS-PAAm (Table 6.1).

**Table 6.1. Measured mechanical properties of SN MCS, SN PAAm and DN MCS/PAAm hydrogels swollen to equilibrium in water**

MCS wt%	PAAm TxC	Swelling Q (g/g)	Young's Modulus E (kPa)	Failure Stress (kPa)	Failure Strain (%)	Toughness (kJ/m <sup>3</sup> )	Toughness (kJ/m <sup>3</sup> ) to 15% Strain	Toughness (kJ/m <sup>3</sup> ) to 25% Strain	Toughness (kJ/m <sup>3</sup> ) to 45% Strain
15	-	35.7±0.2	136±14	15.4±3.8	12.2±1.7	1.0±0.3	-	-	-
-	15x0.5	21.6±1.4	17.2±0.3	1130±110	95.8±0.9	81.9±4.4	-	-	-
-	25x0.04	43.6±0.2	3.4±0.1	82.2±3.9	94.8±0.6	9.6±1.1	-	-	-
-	25x0.5	13.7±0.5	36.4±1.4	736±330	90.6±5.2	90.1±32.9	-	-	-
15*	15x0.5*	25.5±0.3	71.2±2.4	297±57	50.2±0.8	27.8±3.4	-	-	-
15*	25x0.5*	38.4±1.1	139±11	283±56	41.5±2.6	27.5±6.3	-	-	-
15	15x0.04	12.4±0.3	131±16	4610±740	97.4±0.9	873±124	1.49±0.18	6.12±0.53	48.9±4.3
15	15x0.5	11.9±0.4	183±49	5070±550	95.4±1.1	1000±210	2.27±0.42	9.14±1.73	69.0±4.6
15	25x0.04	8.8±0.4	154±32	6570±34	99.8±0.8	1000±3.0	1.71±0.37	7.48±0.74	53.0±1.1
15	25x0.5	7.7±0.1	215±16	6340±790	96.2±1.9	1150±149	2.54±0.22	9.49±0.84	65.3±4.4

(Mean ± Standard Deviation)

\*Co-polymer

### ***Repeated loading in DNs of MCS/PAAm to 15%, 25% and 45% Strain***

In order to help determine the mechanism of strengthening and failure under compression, repeated loading was performed for 12 cycles to strains of 15%, 25% and 45% in DN of 15% MCS and varying formulations of PAAm (15x0.04, 25x0.04, 15x0.5, 25x0.5). Our previously published work investigated DNs of MCS/PAAm under tension and found that a concentration of 15% MCS and 25x0.04 PAAm produced yielding.<sup>[167,168]</sup> Our previous work also showed that by decreasing the PAAm concentration the yielding phenomenon was almost eliminated while obtaining high failure stresses.<sup>[168]</sup> Thus, various formulations of AAm concentrations were tested to show the mechanism of the yielding under compression through repeated loading cycles. Because a material

with a high strength was wanted for applications such as tissue engineering, the cross-linker concentration of the second network was significantly increased to produce a more rigid network. In our previous study only a narrow range of cross-linker concentrations in the second network (0.02-0.09) was considered and the research found this would not significantly impact the properties of the hydrogels. Through this work the effects of further increasing the cross-linking in the second network were investigating. Overall, this work aims to determining the mechanism of toughening, increase toughness and strength and also eliminate permanent damage and early failure in DN hydrogels of MCS/PAAm.

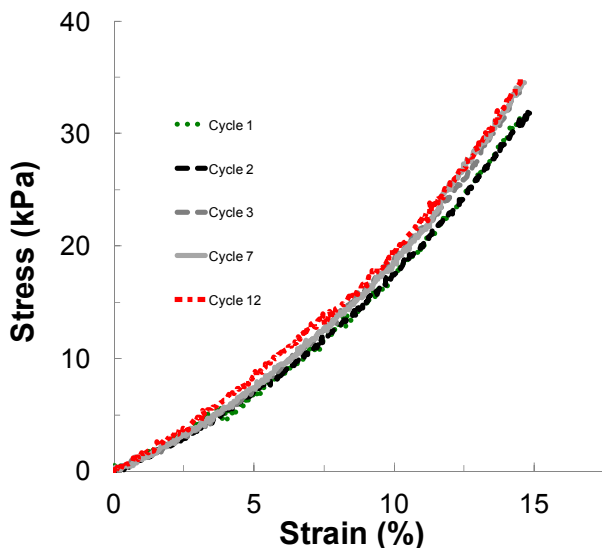


**Figure 6.3: No permanent damage shown in 12 compressive loading cycles up to 15% strain**

All DN hydrogels of MCS/PAAm in this study do not show permanent damage under repeated loading up to a 15% strain after 12 compression cycles. Shown are stress-strain curves of a representative sample. Also, only cycles 1, 2, 3, 7, and 12 are shown.

The cylindrical disks were compressed to a strain of 15%. As shown in Figure 6.3, none of the DNs showed permanent change in the material due to loading up to a strain of 15% in 12 cycles. Because the SN of MCS fails at about 12% strain, we hypothesized that the DNs would remain ideal elastomers up to 12%. However, there are no signs of breaking up to 15% strain.

Further, up to a strain of 15% and while keeping the first network constant, the cross-linker in the second network plays a more significant role to the toughness than the monomer concentration in the second network. Therefore the toughness of DNs of 15x0.5 and 25x0.5 are higher than the 15x0.04 and 25x0.04 formulations, Figure 6.4. This indicates that the initial strength is greater with a slightly higher cross-linked network.

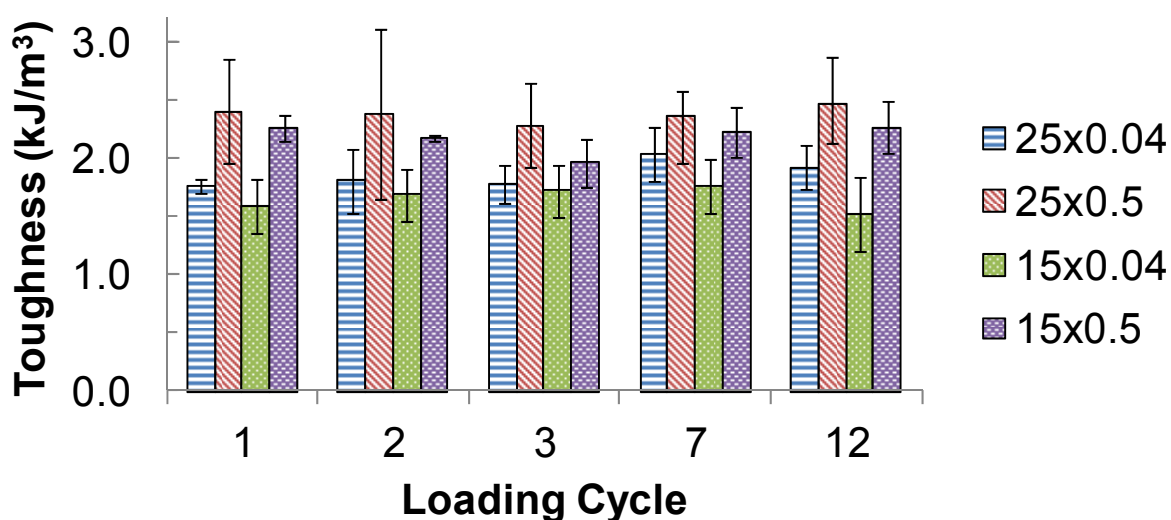


**Figure 6.4: No statically relevant trend for toughness of average loading curves up to 15% strain in repeating cycles 1-12**

No statically relevant trend between cycles 1-12 for average loading curves to 15% strain for various second network concentrations of 15% MCS/PAAm. Though, higher cross-linking in the second network produced tougher networks to 15%.

At 25% strain the complexity of DN hydrogels becomes evident; the trend for the cross-linker in the second network to play a more significant role in the toughness and permanent damage to the network continues at 25% strain. First, in every formulation there is no statistical difference between average toughness from cycle 1 to any other cycle, Figure 6.5. After investigating the stress-strain curves from network concentrations of 15x0.5 and 25x0.5 there was not any changes

in the repeated loading cycles 1-12 at 25% strain. On the other hand, further investigation of the individual stress-strain curves from network concentrations of 15x0.04 and 25x0.04 shows there is slight damage to the hydrogels within the first few cycles but does not persist beyond cycle 7. Although this damage does not impact the toughness to a statically relevant amount when averaged, the trend persists in every individual stress-strain curve. A representative stress-strain curve of a DN with a lower concentration of cross-linker in the second network (25x0.04) clearly displays the irreversible permanent damage that occurs in the first few cycles, but no further damage occurs after cycle 7, Figure 6.6. This slight damage in the hydrogels on the lower cross-linking concentrations of the second network of PAAm (25x0.04 and 15x0.04) indicates (1) the first network of MCS does not continue to break down beyond cycle 7 and (2) the second network of PAAm allows for the DN to hold together past strains of SN of MCS alone. Potentially, the higher cross-linking allows for a tighter PAAm network that distributes the stress more evenly. The toughness of all of the formulations are similar in the first cycle, but at further cycles, 7-12, the toughness of DNs of 15x0.5 and 25x0.5 are higher than the 15x0.04 and 25x0.04, a reflection of both a higher modulus and fracture strain. The 25x0.04 formulation of PAAm resulted in the lowest toughness possibly because of more entanglement with the longer PAAm chains and uneven stress distribution that causes increase stress on the MCS network, leading to the fracture of the MCS. Overall, permanent damage can be prevented by adjusting cross-linking in the second network.

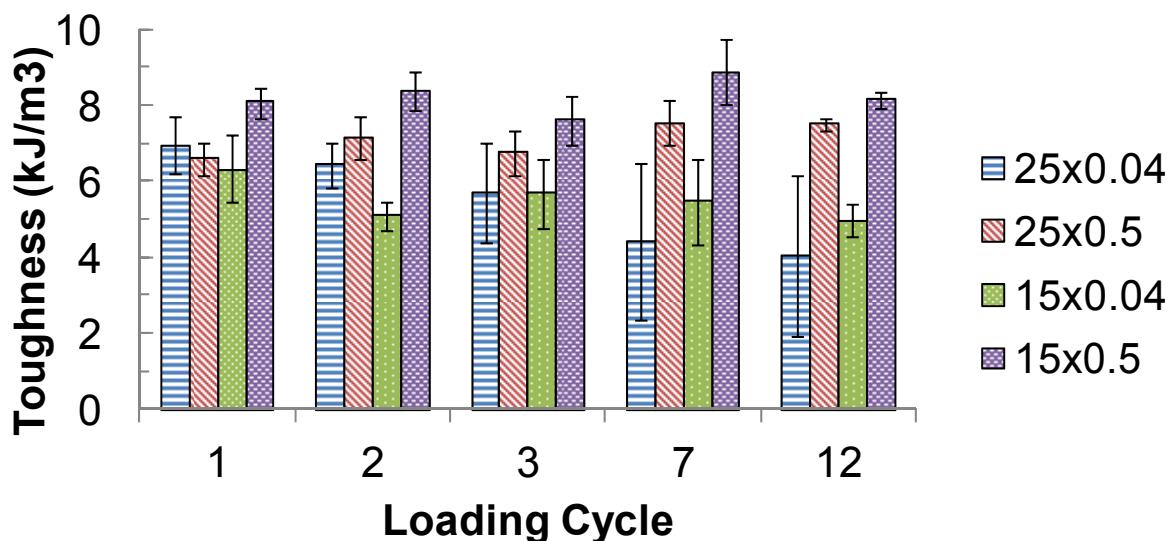


**Figure 6.5: No statically relevant trend for toughness of average loading curves up to 25% strain in repeating cycles 1-12**

No statically relevant trend between cycles 1-12 for average loading curves to 25% strain for various second network concentrations of 15% MCS/PAAm.

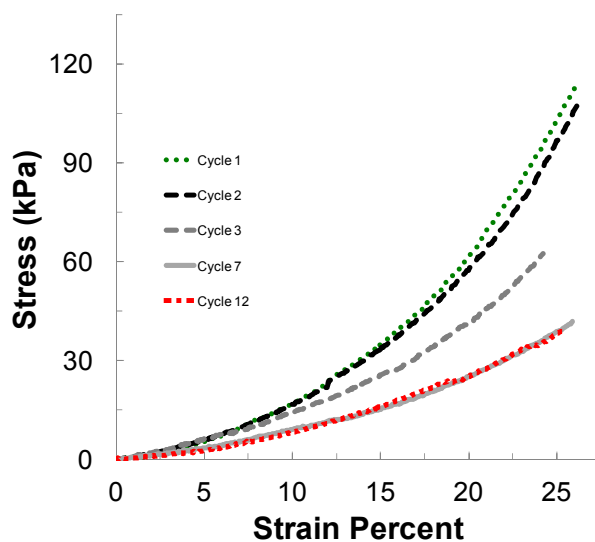


**Figure 6.6: Slight damage in material evident in repeated loading curves of certain formulations but no damage evident in other formulations**

Representative loading curves in DNs of 15% MCS/PAAm that shows the slight damage in the material in concentrations of lower cross-linking in the second network (25x0.04 and 15x0.04) despite the AAm concentration. Conversely, DNs of 15% MCS/PAAm with higher cross-linking concentrations in the second network (25x0.5 and 15x0.5) show no permanent damage, thus, allowing elimination of damage to the material in cycles from 0-25% strain by increasing cross-linking concentration.

Up to a strain of 45%, the compressive loading curves show permanent damage to the networks by cycle 7 but no further damage after the 7<sup>th</sup> cycle; evident when comparing the first cycle to the remaining cycles, there is no statistical difference from cycle 2 and typically cycle 3, but always a statistical difference from cycles 7-12, as shown in Figure 6.7. The toughness at 45% strain through repeated loading cycles 1-12 of DN of 15x0.5 and 25x0.5 are typically higher than the 15x0.04 and always higher than the 25x0.04 formulation. The toughness of the 25x0.04 formulation is the lowest. As before, the overall stiffness and stress of the material can be tuned by the second network composition.

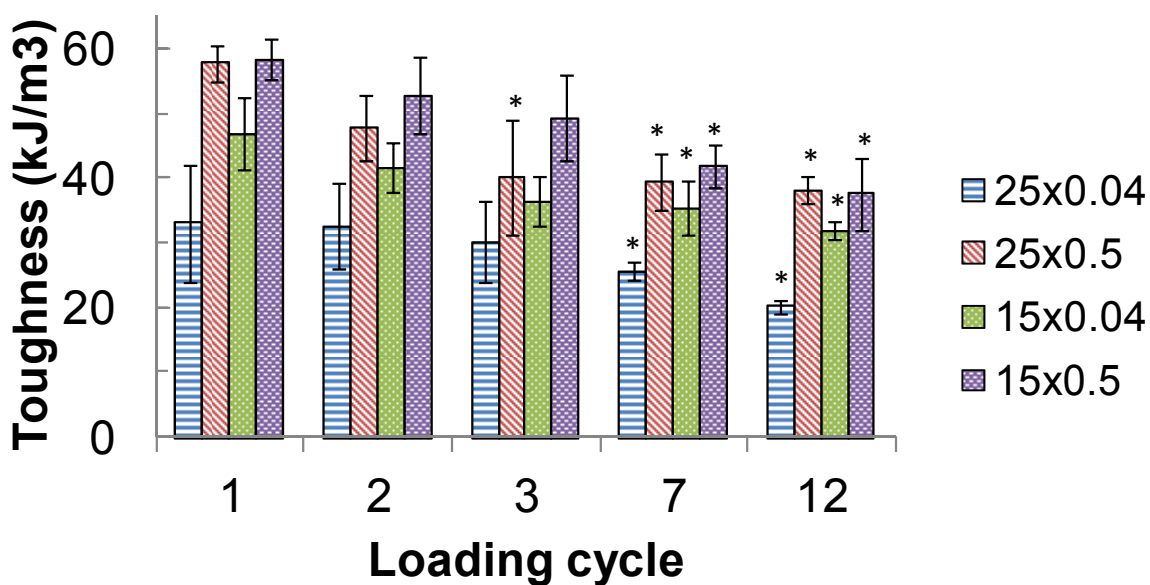
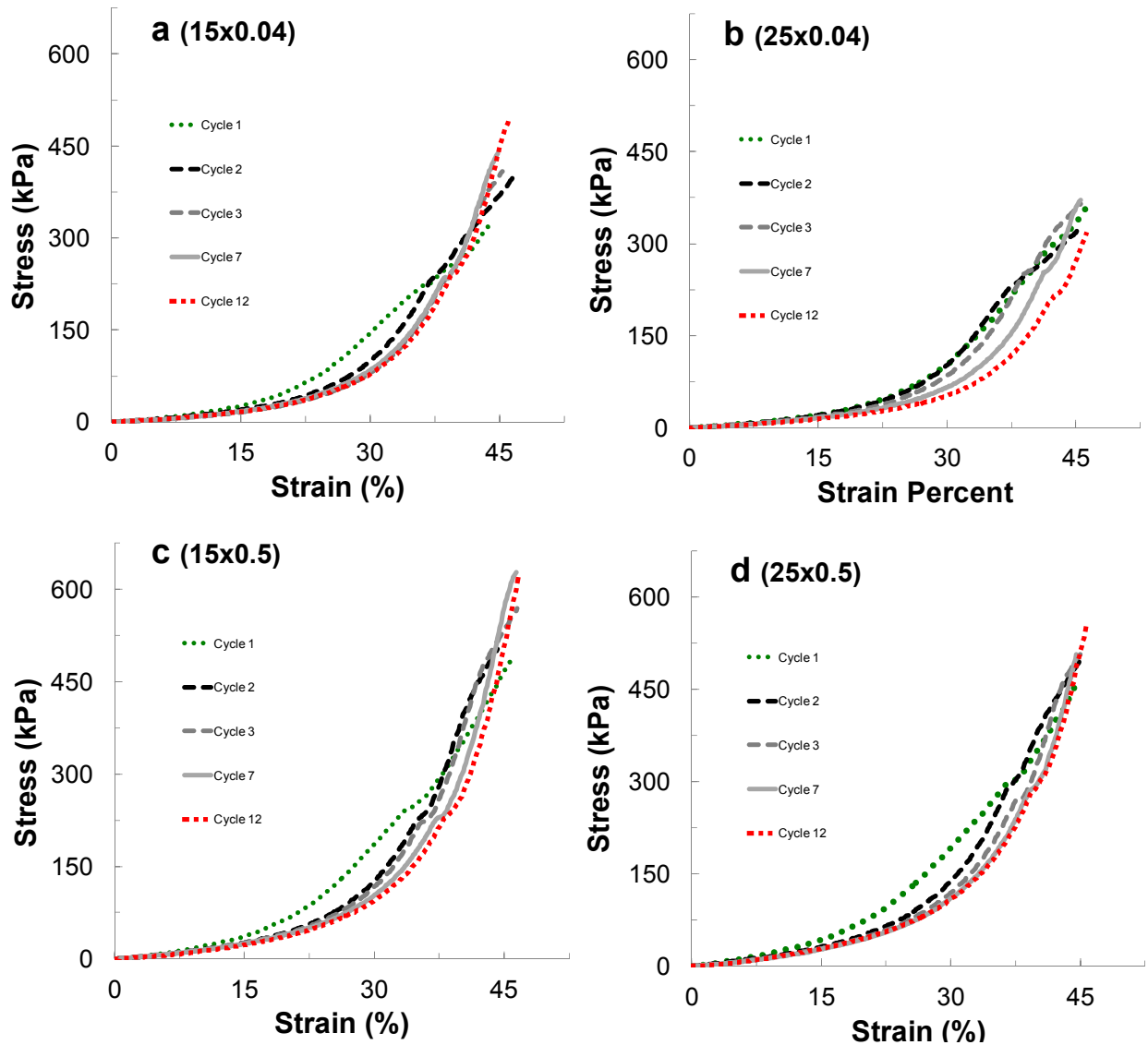


**Figure 6.7: Decrease in toughness in average loading curves up to 45% strain in first few cycles but no further damage after cycle 7 (up to cycle 12)**

Loading cycles up to a strain of 45% for DN of 15% MCS/PAAm for various second network concentrations.





**Figures 6.8a, 6.8b, 6.8c and 6.8d: Change of shape in stress-strain curved for repeated loading cycles which leads to decrease in toughneses but similar stresses.**

Representative loading curves of DN of 15% MCS/PAAm to 45% strain for various second network concentrations 6.8a: top left (15x0.04), 6.8b: top right (25x0.04), 6.8c: bottom left (15x0.5) and 6.8d: bottom right (25x0.5). All of the formulations show cycle 1 or cycles 1 and 2 are significant difference from cycles 3-12. Higher AAm and lower cross-linking concentrations leads to a decrease in stress at 45% strain.

Taking a closer look at the different loading curves up to a strain of 45% at various second network concentrations showed that decreasing the second network AAm concentration and increasing BIS concentration led to an increase of stress at 45%. Therefore the PAAm (15x0.5),

Figure 6.8c, displayed the largest stresses at 45% strain while PAAm (24x0.04) displayed the lowest stresses at 45% strain. At 45% strain the first cycle or first and second cycle had a significantly different shape to the stress-strain curves compared to cycles 3-12, Figures 6.8a-d. Although the toughness decreases from the first cycle to cycles 7-12, the stress at 45% becomes higher in the subsequent cycles.

Finally, comparing the trends of the DNs at complete failure of different PAAm formulations shows that the toughness is highest in the 25x0.5 formulation and lowest in the 15x0.04 formulation, Table 6.1. The failure stress is highest in the 25x0.04 formulation Table 6.1. This is accurate with the previously established idea that the second network needs to be highly concentrated but lightly cross-linked to create the high strength and toughness. The formulation 25x0.04 has the greatest damage in the material due to loading up to a strain of 25% and 45% and energy dissipation leads to ultimately high toughness. On the other hand, for tissue engineering applications, compressing the materials to nearly 100% strain is not common. For applications when the sample needs to be under multiple cycles without damaging the sample, it is best to have low high cross-linking concentrations for the PAAm network to elongate and essentially hold the MCS network together. Thus, consideration should be taken to determine the strain for the specific application and then optimize the concentrations.

When re-equilibrating with water the samples recovered to the original height and diameter. This indicates no noticeable physical damage to the network, though the changes in the loading cycles indicate a permanent damage in the overall DN hydrogel. Perhaps the PAAm network remains unchanged while the MCS network breaks down or maybe the microfracturing is not substantial to cause changes in swelling.

To date the most accepted explanation of the increased toughness in DNs is from the energy

dissipation of the breaking of the covalent bonds in the first network while the second network essentially holds the hydrogel together. The DNs display a yielding phenomenon under tension and the exact mechanism under compression has not been intensively explored. There was not large damage to the DNs under repeating loading cycles, especially after the first few cycles. There is no doubt that there is some permanent damage occurring from the breaking of covalent bonds but we hypothesize that a different mechanism for enhanced toughening under compression in DNs systems. Described as a molecular mechanism of synergistic physical entanglements of the two networks, we speculate that the second network systematically wraps around the first network providing “ties” and additional strengthening to the DNs.

## Conclusions

This work highlights the superior properties achievable under compression in MCS/PAAm DN hydrogels, producing toughness and fracture properties which are greater than copolymers of the MCS and PAAm or either SN, thus, emphasizing the importance of the synergy which occurs using the DN strategy. Also, unique features were shown in the DNs including non-ideality even at low strains (unlike CP or SN). Further the mechanism for toughness under compression was investigated by doing repeating loading. To investigate if the mechanism of strengthening and failure under compression are the same as tension, repeated loading was performed for 12 cycles to strains of 15%, 25% and 45% in DN of 15% MCS. The hypothesis was that the DNs would remain ideal elastomers up to 12% because the SN of MCS fails at about 12% strain. DN formulations showed no signs of permanent damage under repeated loading up to a 15% strain after 12 compression cycles. At 25% and 45% strain large deformations which continued through all 12 cycles was expected. Though, there were slight changes in either cycle 1 or cycles 1 and 2,

from there typically was no further damage cycles 7-12. In many cases there was an improvement in the stress in comparison to the initial cycle. Additionally, higher AAm and lower cross-linking concentrations leads to a decrease in stress at 45% strain. Given the improved toughness, no catastrophic damage from the network fracturing and in some cases even improvement in properties with loading cycles DN hydrogels a different mechanism under compression than tension was hypothesized. In which, DN hydrogels would be a useful replacement for load bearing tissues.

## Bridge to Chapter 7: Overview of Work on Chondroitin Sulfate-Based Hydrogels Using the Double-Network Strategy

The previous three chapters demonstrated the success in creating a double-network from other components besides the PAMPS/PAAm pioneered by Gong and Osada. Further, DNs were developed from a biopolymer. The exploration of double-network hydrogels under both tension and compression advanced the current understanding of the molecular mechanisms. This chapter gives an overview of the work and ties the chapters together to compare the tension and compression effects. Lastly, Chapter 7 gives advice about understanding DN hydrogels. This is shown in a schematic, Figure 7.1.

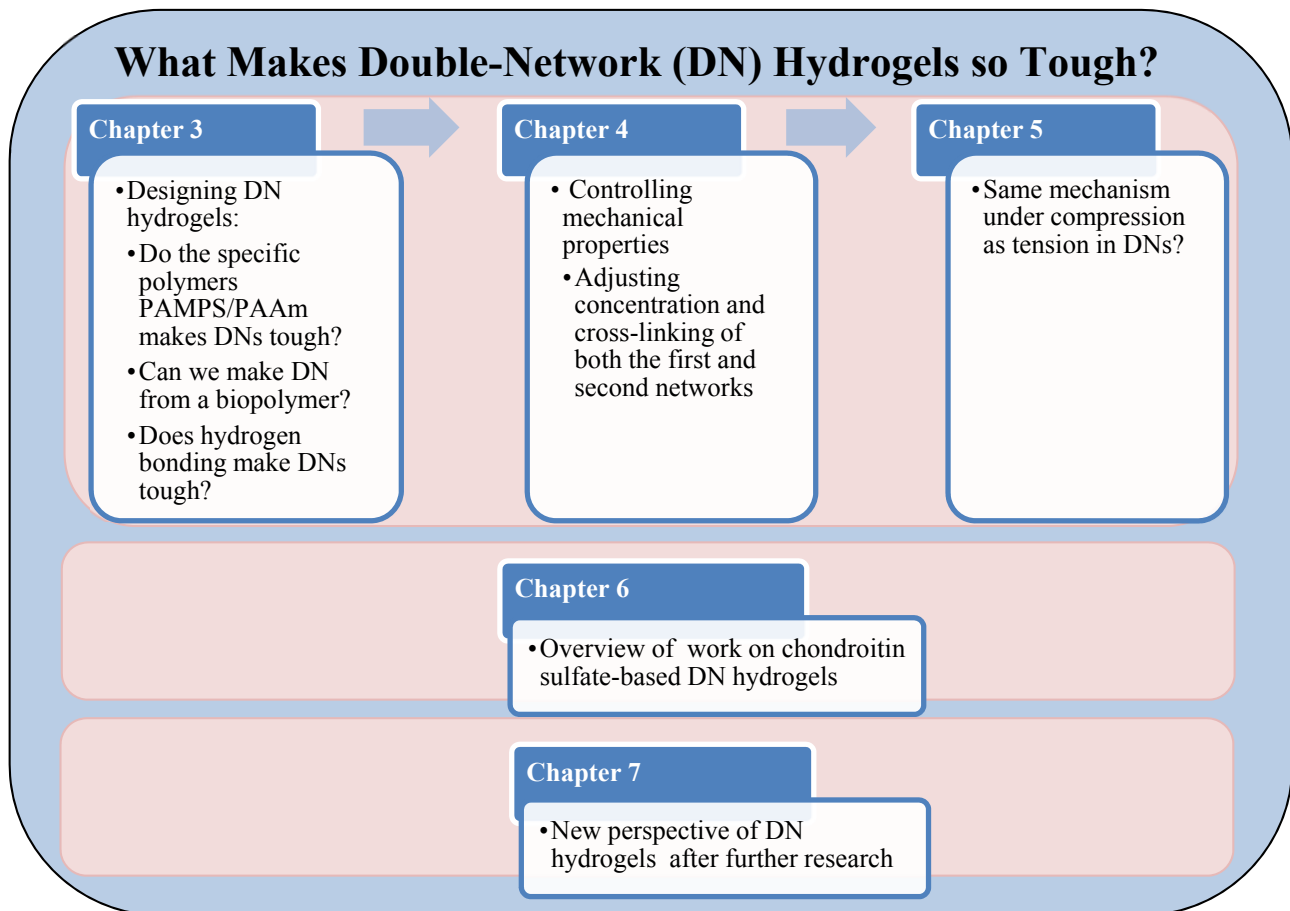


Figure 7.1: Schematic of DN hydrogel progression

## Chapter 7: Overview of Work on Chondroitin Sulfate-Based Hydrogels

### Using the Double-Network Strategy<sup>7</sup>

#### Abstract

The double-network (DN) hydrogel concept developed by J.P. Gong and Y. Osada builds upon interpenetrating networks by combining brittle and ductile components to have significantly enhanced fracture properties. The generality of the DN effect was tested by creating biopolymer-based hydrogels of methacrylated chondroitin sulfate (MCS) and polyacrylamide (PAAm) and extended upon creating DNs of MCS and poly(N,N dimethyl acrylamide) (PDMAAm), verifying that DNs were not limited to the original combination of poly(2-acrylamido-2-methylpropanesulfonic acid) (PAMPS)/polyacrylamide (PAAm). Further, the mechanical properties were varied by changing the monomer concentrations, cross-linker concentrations and the addition of cross-linking groups through copolymerizations of MCS and poly(ethylene glycol) diacrylate (PEGDA). Overall, this work demonstrates that a broad range of mechanical properties achievable through DN effect under tension and compression, generally independent of the swelling degree, which is fundamentally different behavior than possible with single networks.

---

<sup>7</sup>Adapted from: **Tiffany C. Suekama**, Anahita Khanlari, Stevin H. Gehrke, “Tuning Mechanical Properties of Chondroitin Sulfate-Based Hydrogels Using the Double-Network Strategy” MRS conference proceedings, **2013**.

## Introduction

Hydrogels are excellent materials for the tissue engineering field due to the high water content which is similar to biological tissues. However, hydrogels typically are mechanically weak materials, but by using the double-network (DN) strategy researchers have improved toughness and fracture properties in hydrogels. In fact, the mechanical properties of DN hydrogels are similar to soft load-bearing biotissues and rubbers.<sup>[50]</sup> DN hydrogels are tough and ductile networks produced from a highly cross-linked (typically polyelectrolyte) first network with a lightly cross-linked (typically neutral) second network. DN's are recognized from their improved properties relative to either single network alone. The enhanced mechanical properties are linked to the internal microfracturing that results in strain energy dissipation. Furthermore, DN hydrogels can have 3 characteristic regions (preyielding, yielding and hardening) with a clear yielding point (transition between preyielding and yielding) that is particularly unusual behavior for hydrogels.

Recently, we have demonstrated the utility of the DN concept to a DN gel based on the biopolymer, chondroitin sulfate (CS). CS is a glycosaminoglycan which is a significant structural component of aggrecan.<sup>[99,115]</sup> CS is modified by adding methacrylate groups allowing for the biopolymer to form a hydrogel upon photopolymerization. These MCS networks have been used in different matrices for tissue engineering.<sup>[73,100,152,167]</sup>

## Materials and Methods

Here the experimental methods are outlined. Further details of materials can be found in our recently published papers.<sup>[167,168]</sup> The methacrylation of MCS used in this report was determined by NMR to be 34.5% after 15 days of reaction.<sup>[152]</sup>

### ***Synthesis of Single and Double Networks:***

Monomer (or polymer), cross-linker (if applicable) and photo initiator were dissolved in DI water. The solution was placed in a mold consisting of two glass plates and a 2 mm silicon spacer. The solution was cross-linked into a gel with 365-nm light at  $\sim 10\text{mW}/\text{cm}^2$  for a set time.

The DN hydrogels were prepared in a multistep process.<sup>[68,101,207]</sup> The SN hydrogel was synthesized and taken out of the mold. The single network (SN) swelled to equilibrium, for 24 hours, in a solution of the second network (solution as prepared above). The swollen gel was placed between two glass plates and was exposed to 365-nm light at  $\sim 10\text{mW}/\text{cm}^2$  for a set time (typically 30 min). Specific synthesis details can be found in previously reported papers.<sup>[167,168]</sup>

### ***Swelling Properties:***

The equilibrium degree of swelling was measured for all of the gels. Molded gel samples were submerged in distilled water at room temperature for 24 hours. The excess water was removed. The swollen gel was weighed and put in a dessicator for 24 hours to dry. The dry weights were taken. The degrees of swelling in the results section are reported as the mass of the swollen gel over the mass of the dried gel.<sup>[45,135]</sup>

### ***Mechanical Analysis:***

Mechanical test methods applied and further details are in our previously published work.<sup>[167,168,171]</sup> Mechanical tests under tension were performed using a Tensilon machine (RTC-1150A, Orientec Co) at a constant velocity of 100 mm/min and under unconfined uniaxial compression by the RSA III dynamic mechanical analyzer (DMA; TA Instruments, New Castle,



DE). Compression tests were performed at a constant velocity of 0.05mm/s, which was tested to be strain-rate independent.

From the stress ( $\sigma$ ) – strain ( $\epsilon$ ) data, toughness, failure stress and failure strain were determined. Failure stress and failure strain were found at the point that the gel began to split, identified in the data as a sharp drop in stress. The strain energy at failure, toughness, was calculated as the area under the stress-strain curve.

## Results and Discussion

DN hydrogels have gained much attention over the past 10 years for their notable toughness and fracture properties. A number of different network combinations have been reported but none display the same range of behaviors as poly(2-acrylamido-2-methyl propanesulfonic acid) (PAMPS)/polyacrylamide (PAAm)<sup>[17,50,61,68,84,101,119,207]</sup>. Therefore, to test the generality of this concept, we synthesized a DN hydrogel with MCS as the first network and PAAm as the second network. CS and AMPS are both sulfonated, but MCS has a significantly different structure from PAMPS, enabling a test of the importance of gel microstructure in DNs.

We successfully synthesized a DN of MCS/PAAm, to our knowledge the first biopolymer-based hydrogel with improved toughness relative to either single network and also displaying a yielding region.<sup>[167]</sup> Figure 7.2, compares typical stress-strain curves of DN hydrogels of 15% MCS/ 24x0.04 PAAm to SNs of 15% MCS and of ~24x0.04 PAAm. The SNs display ideal elastomeric behavior but the DNs do not.<sup>[168]</sup> A DN of MCS/PAAm tested in tension can reach failure stresses >17 times greater than either MCS or PAAm gels.

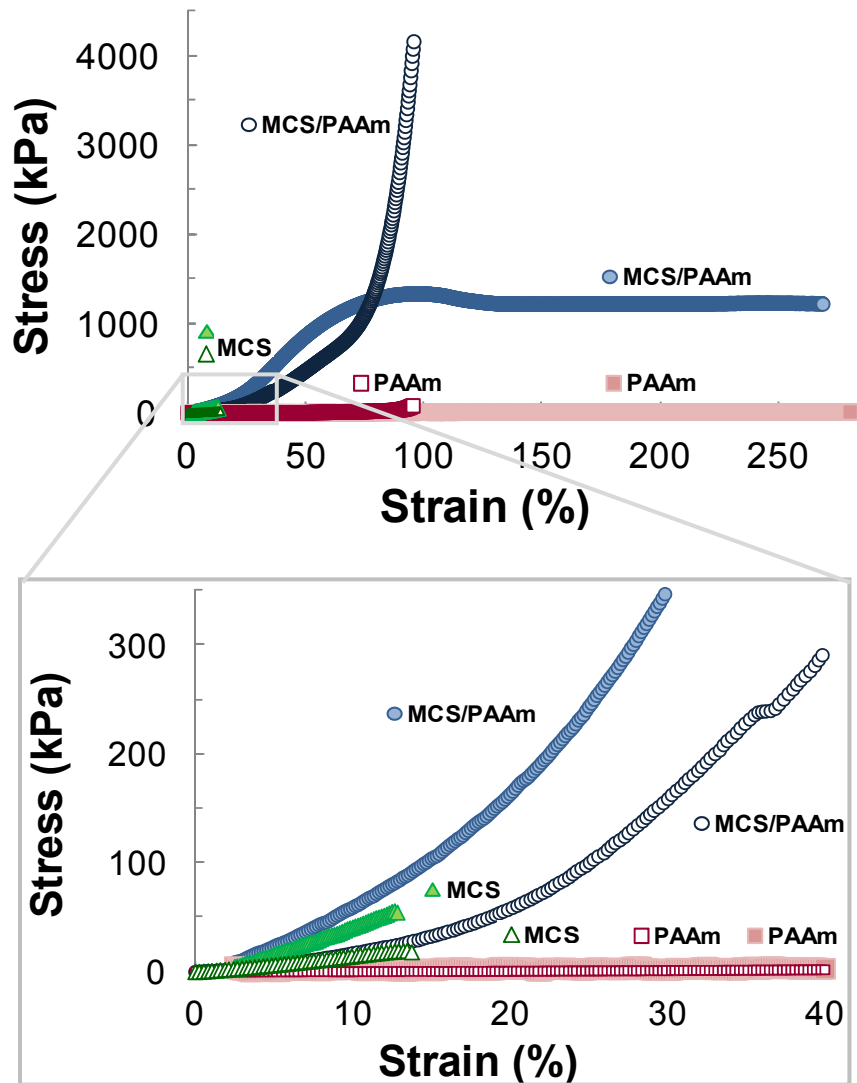


**Figure 7.2. Improved mechanical properties from DN strategy are shown in stress–strain responses under both tension (closed symbols) and compression (open symbols).**

**Top:** Combining brittle MCS with ductile PAAm into a double network increases failure stress over 17 times and introduces a yielding region in tension. In compression the failure stress of the DN is over 40 times greater than either SN. Failure of the SN of PAAm under tension is  $1,080 \pm 120$  % and failure stress of  $96.7 \pm 19$  kPa.<sup>[167]</sup> **Bottom:** Stiffness of the DN was slightly better than SN of MCS and significantly greater than the SN of PAAm. The curves have been truncated after failure. DN of MCS/PAAm under compression was truncated at 95%. The tension data before a strain of 2.5% is not recorded due to equipment inaccuracies at the low strain. All of the specific values and formulations are located in Table 7.1.

**Table 7.1. Swelling and mechanical properties under tension and compression of DN's of MCS/PAAm and SNs of MCS or PAAm.**

	MCS wt%	PAAm TxC	Swelling (g/g)	Q	Failure Stress (kPa)	Failure Strain (%)	Toughness (kJ/m <sup>3</sup> )
#Tension	15	--	34.1 ± 4.3		40. ± 22	9.8 ± 4.0	2.0 ± 1.6
	--	24 x 0.04	26.54 ± 0.16		83 ± 27	1160 ± 950	349 ± 92
	15	24 x 0.04	6.92 ± 0.18		1670 ± 150	108.6 ± 8.2	710 ± 470
*Compression	15	--	35.72 ± 0.19		15.4 ± 3.8	12.2 ± 1.7	1.06 ± 0.43
	--	25 x 0.04	43.62 ± 0.24		82.2 ± 3.9	94.82 ± 0.59	9.6 ± 1.1
	15	24 x 0.04	8.85 ± 0.45		6570. ± 34	99.81 ± 0.82	1003.9 ± 3.0

Tensile values taken from Suekama *et. al.* [167]  
 Compression values taken from Suekama *et. al.* [171]  
 (Means ± standard deviation) n ≥ 3

The DN of MCS/PAAm is double the toughness of either SN. Also, MCS/PAAm DN gels displayed distinct yielding, not previously observed in biopolymer hydrogels, with a yield stress over 1500 kPa. Specific values on the swelling and mechanical properties of DN and SN gels are included in Table 7.1.

Since most load-bearing materials endure compressive rather than tension we studied the effects of DN's of MCS/PAAm under compression. As shown in Figure 1, DN hydrogels behave similarly in compression as tension. DN's display failure stresses 40 times greater than either SN. Furthermore, the DN hydrogels show higher toughness' than the SNs. Although the improved mechanical properties provide the proper attributes for tissue engineering applications, the increase in properties results from the energy dissipation of the first network breaking while the second network holds the construct together. Therefore, studying if enhanced mechanical properties can

be maintained without fracturing the network is necessary and studying the effects of repeated loading to the DNs.

We successfully swapped out PAMPS for MCS and still achieved the DN effect as shown in Figure 7.2. However, to rule out that specific interactions between the networks such as hydrogen bonding facilitates strength, we swapped the second network PAAm for poly(N,N dimethyl acrylamide) (PDMAAm). Similar mechanical behavior was observed with a hydrogel of MCS/PDMAAm.<sup>[167]</sup> Replacing PAAm for PDMAAm shows the generality of the DN and yielding effect. Also PDMAAm has less toxicity problems and has been used as biomaterials.<sup>[1,61]</sup>

We have shown that we can significantly increase the cross-linking efficiency of a single network of MCS by copolymerization MCS with low levels of poly(ethylene glycol) diacrylate (PEGDA).<sup>[152]</sup> Thus we are able to change the modulus of the network with minor changes in the MCS chemical composition. Therefore, we created DN's aiming to improved network properties. We synthesized copolymers of MCS and PEGDA as the first network and PAAm as the second network and showed by adjusting the compositions we were able to modify the MCS-PEGDA/PAAm DN formulations to vary failure stress, failure strain, Young's modulus and yielding behavior over a very broad range.<sup>[168]</sup> It is significant that these changes in mechanical properties occur with minimal changes in the swelling degrees of the DNs.

The ratios of the first and second networks in DN hydrogels required to achieve optimal properties were explored by increasing the cross-link density of the MCS network both by increasing MCS concentration and by copolymerizing MCS with PEGDA.<sup>[168]</sup> These changes increases Young's modulus by five times and the failure stress by four times, though increased cross-linking reduced the failure strain up to a factor of five while diminishing the yielding region.<sup>[168]</sup> These results suggest that increases the cross-linking in the first network can stiffen the

network to the point that its yield stress exceeds the failure stress of PAAm network, hence diminishing or eliminating the yielding region that results in high toughness.<sup>[168]</sup> This work demonstrates the feasible range of mechanical properties in DNs.

## Conclusions

DN hydrogels are versatile, tough and strong materials with the potential of being altered with biocompatible networks for use in tissue engineering applications. We were able to create biopolymer-based hydrogels of MCS/PAAm and MCS/PDMAAm with improved mechanical properties to either SN alone, notably, increases in failure stress and toughness. Further, we were able to adjust the failure properties, toughness, and the yielding phenomenon by changing network concentrations as well as further cross-linking with PEGDA. Finally, the DN effect persists under compression. Thus we have confirmed the DN formula can be applied to biopolymer gels.

## Chapter 8: Updating the Definition of Double-Network Hydrogels after a Decade of Development<sup>8</sup>

### Abstract

Since the first publication on double-network (DN) hydrogels appeared in 2003, scientists have been inspired to advance work on multi-component gels with enhanced mechanical properties. Many researchers have used the synthesis conditions to define DNs which led to interchanging all IPNs with DNs or calling any tough multi-component hydrogel a DN. Because of the increased understanding of the mechanisms occurring and the unique mechanical properties that are achieved in DN gels, we are proposing to think of DN's in terms of both the composition and the enhanced mechanical properties of high toughness and yielding.

---

<sup>8</sup>To be submitted as **Tiffany C. Suekama**, Anahita Khanlari, Stevin H. Gehrke,

## Introduction

2013 marked the 10-year anniversary of the first published description of double-network (DN) hydrogels led by Dr. Yoshihito Osada and Dr. Jian Ping Gong.<sup>[51]</sup> These DNs displayed extremely high mechanical strength and over the subsequent decade researchers have exhibited a considerable amount of interest investigating the mechanisms which make these DNs so tough. DN's have also been used as a model for creating other multi-hydrogels which possess excellent mechanical performance. In fact, the term “double-network” has been used as a ‘buzz word’ to describe any multi-component gel of notable mechanical properties. Creating multi-component hydrogels has led to improvements in the gels modulus, fracture stress, fracture strain, toughness and tearing energy while keeping high water content. Six major categories of multi-component hydrogels result in exceptional mechanical properties: copolymers (such as tetra-PEG), slide-ring (SR) or topological gel (TP), IPN (semi-IPN and DN), nanocomposite (NC), microgel-reinforced (MR) and mixtures of ionically and covalently cross-linked gels such as ionic-covalent entanglement (ICE) gels (shown in Figure 8.1). This article focuses on IPNs and specifically the one subclass of IPNs: DNs.

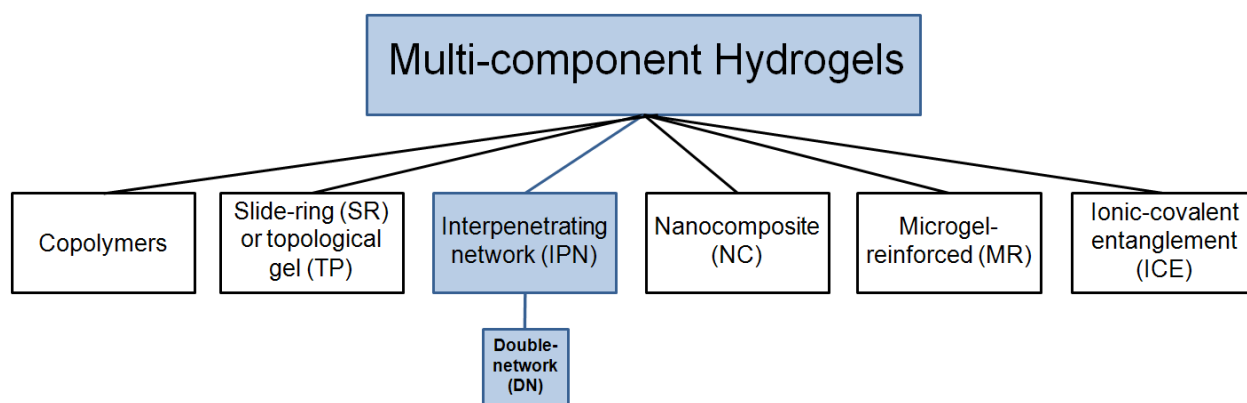


**Figure 8.1: Hierarchical classification chart of tough multi-component hydrogels.**

Since many new concepts for using multi-components to make improved gels have arisen, we describe the differences of DNs from other multi-component hydrogels to keep the term effective and current. The DN term has commonly been used to describe any mechanically tough gel, which does not distinguish the unique synthesis methods or the type of enhanced mechanical properties achieved by a DN hydrogel. We hope to get rid of confusion by clearly describing how DN gels distinctly differ from other multi-component hydrogels, including traditional interpenetrating network (IPN) hydrogels. Traditional IPNs have the same synthesis process to DNs but differs in mechanical mechanisms. DNs have improved toughness and a necking phenomenon that makes them clearly different from IPNs. To date, the most accepted view for the improved mechanical properties in DNs is from the internal mechanism in which the sacrificial covalent bonds break in the brittle first network providing energy dissipation and the ductile second network holds the gel together. This article focuses on explaining the DN phenomenon to emphasize the significance of the mechanical properties produced from the synthesis methods. This increased understanding stems from the past decade of research and clearly distinguishes this important class of gels from related hydrogels

### ***Hydrogels***

Hydrogels are conventionally a single-network (SN) of a cross-linked hydrophilic polymer that has a high water content (typically greater than 90 wt. %) which makes them soft, brittle and weak.<sup>[45]</sup> Typically, SN hydrogels fail at stresses below several hundred kPa and at strains well under 100%.<sup>[49]</sup> Hydrogels have generated a lot of interest (due to their high water content) by many industries, especially tissue engineering, thus, stressing the need for improving the mechanical properties.



### ***What is an IPN?***

IPN hydrogels are two independent chemically cross-linked networks in which the two networks remain interconnected because of physical entanglements.<sup>[85]</sup> Because of residual unreacted cross-linkers of the first network, slight covalent cross-linking between the first and second networks may occur; however we still call them IPNs because they show similar fracture mechanisms.<sup>[123]</sup> IPN hydrogels typically have physical properties that are an average of the SNs, are similar to one of the SNs or an additive value of both SNs but not usually significantly greater than both SNs.<sup>[85]</sup> IPNs can be synthesized in a two-step sequential process in which the first network is created, soaked in the solution of the second network and then polymerized a second time.<sup>[118]</sup> IPNs can also be synthesized simultaneously if the reaction mechanisms of the two networks do not interfere with each other – a simultaneous IPN – for example, a free radical polymerization reaction and a condensation cross-linking reaction that occurs at the same time.<sup>[118]</sup>

### **Double-Network Hydrogels**

DNs comprise a subcategory of IPNs, synthesized by the same method but strategically produced so the two components lead to superior mechanical properties.<sup>[50,61,192]</sup> The composition and the resulting mechanical properties distinguish DN hydrogels substantially from other IPN hydrogels. We are updating the definition because composition alone (the original definition) is not adequate to distinguish DN hydrogels, but both composition and the mechanism achieved are key.

The original definition of a DN gel focused on the composition as outlined:<sup>[51]</sup>

- (1) Synthesized as an IPN of a brittle (typically polyelectrolyte) first network and a ductile (typically neutral) second network where the:
  - a. Second network is in excess to the first network and
  - b. The first network is highly cross-linked, the second network is lightly cross-linked

The synthesis method is an important aspect of DN hydrogels but the behavior achieved from synthesis methods is what sets DN hydrogels apart from other hydrogels. The unique stress-strain curve that produces the distinctively high toughness is atypical for both conventional hydrogels and common IPNs. With the increased research on DN gels we better understand the key features of a DN gel include the composition and mechanical properties as well as the mechanism that produces improved toughness. Thus, we emphasize that DN hydrogels include the unique mechanical properties achieved, and the internal molecular structures are synergistic thus lead to superior toughness and fracture properties, outlined below:

- (3) Synthesized as an IPN of a brittle (typically polyelectrolyte) first network and a ductile (typically neutral) second network where the:
  - a. Second network is in excess to the first network and
  - b. The first network is highly cross-linked, the second network is lightly cross-linked
- (4) Enhanced mechanical properties relative to either single network where
  - a. High toughness is achieved
  - b. Non-ideal elastic behavior is exhibited and
  - c. Yielding region is observed (under tension)

### ***Composition of DNs***

DNs have two independently chemically cross-linked networks in which the two networks remain interconnected because of physical entanglements, the same as an IPN (slight covalent cross-linking of first to second networks can occur<sup>[123]</sup>) but, not all IPNs are DNs because DNs have a synergistic effect which leads to superior mechanical properties compared to either SN. The first network is highly cross-linked and brittle (typically polyelectrolyte). The brittle nature is key to producing the high toughness from the fracturing of the first network which results in high energy dissipation. The second network is in excess to the first and is highly concentrated, loosely cross-linked, ductile and neutral. The ductile nature of the second networks is what allows the DN to hold together at high extensibilities. Thus, the combination of brittle and ductile networks is one of the unique features of DN hydrogels.

### ***Mechanical Properties of DNs***

One of the ways of distinguishing a DN from a conventional IPN is in the stress-strain curve. DNs behave as non-ideal elastomers, and have negligible residual strain and hysteresis after large deformations (Mullin effect). Also, in tension DN hydrogels commonly have three distinct regions in the stress-strain curves: preyielding, yielding and hardening in addition to a clear yielding point (transition between preyielding and yielding), as shown in Figure 8.2. However, DN hydrogels may only display the preyielding and yielding regions with the yield point. In contrast, conventional IPN hydrogels can have a fairly linear initial stress-strain curve that could lead to strain hardening at high stresses and behave as ideal elastomers at small strains.

Under tension, the first region or the preyielding region of DNs are composed of two sections: the initial section in which does not produce permanent damage to either network and the following section in which permanent damage to the first networks leads to energy

dissipation.<sup>[190]</sup> The modulus of DNs are mainly sustained by the densely cross-linked first network. Under repeated cycles in the initial strain of DN hydrogels, permanent damage to the networks does not occur.<sup>[190]</sup> However, non-ideal elastomer behavior still persists. Also, a slight “J-shaped” curve is observed in the initial strain; this phenomenon is also commonly seen in biological materials such as cartilage but is not commonly seen in hydrogels.<sup>[17,186]</sup> This “J-shaped” curve in cartilage occurs from the alignment of the fibers and in DN hydrogel, we hypothesize the shape is due to molecular organizational changes with strain.<sup>[169]</sup> In the second section of the preyielding region, the most accepted understanding of the toughening mechanism is from the brittle network breaking down at a strain after the ultimate failure of a SN of the same material and composition of the first network. The breaking down causes energy dissipation and leads to high stress. A transition exists between the preyielding region and the yielding region, the yielding point, where the first network breaks across an entire cross section. The second distinct region found in DNs under tension is the yielding region where the first network continues to break down and the second network elongates and necking is observed. The yielding region is represented on the stress-strain curve as increasing strain as the stress remains fairly constant. The third region, the hardening region, is where the strain exceeds a critical yielding stress and the second network further elongations under external loading. Thus, the coils of the second network are highly extended and they behave according to non-Gaussian chain statistics.

In addition, hysteresis is shown in the loading-unloading stress-strain curves after large deformations (Mullins effect) in these DN hydrogels.<sup>[190]</sup> This irreversible damage in the network should lead to crack coalescence and ultimately failure but the DNs are constructed so the second network holds the entire construct together.<sup>[190]</sup> Overall, the combination of the brittle first network and the ductile second network is the main reason for improved toughness.

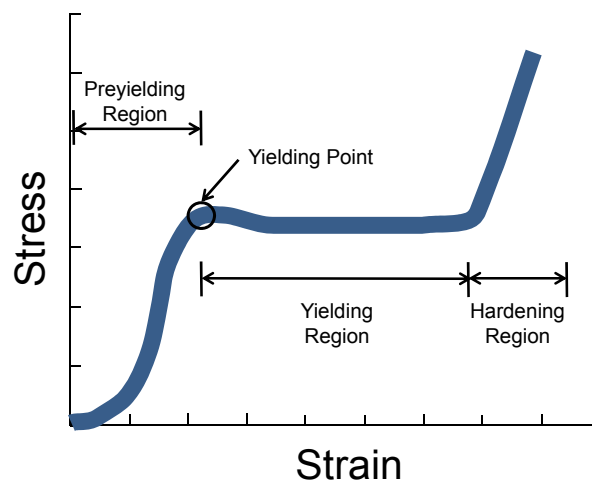


**Figure 8.2: Typical stress-strain curve of DN hydrogels in tension**

Illustration of the unique stress-strain curve of a DN hydrogels, in tension, which shows the three characteristic regions: preyielding, yielding and hardening. Also a clear yielding point can be observed. DN do not necessarily show the hardening region.

### *DN Hydrogels in the Literature*

Since 2003 the number of publications on double-network hydrogels has continued to increase each year. To date, we can identify five clear examples that fully fit our criteria of DN hydrogels. (1) poly(2-acrylamido-2-methylpropanesulfonic acid) (PAMPS)/polyacrylamide (PAAm)<sup>[51]</sup>, (2) methacrylated chondroitin sulfate (MCS)/PAAm<sup>[167]</sup> and (3) MCS/ poly(*N*, *N*-dimethyl acrylamide) (PDMAAm)<sup>[167]</sup>, (4) PAMPS/poly(*N*-(carboxymethyl)-*N*,*N*-dimethyl-2-(methacryloyloxy) ethanaminium, inner salt) (PCDME)<sup>[205]</sup>, and (5) poly(*N*-vinyl pyrrolidinone) (PNVP)/ polyacrylic acid (PAAc)<sup>[196]</sup>. Through an online search from 2003 to 2012 in both “Web of Knowledge” and “Google Scholar”, we have found 104 papers on hydrogels with “double network” in the title and a steady increase yearly. We have categorized the publications as DNs (composition and improved mechanical properties), IPNs or multi-component hydrogels. We found that 70% of the publications are DNs, but 25% are IPNs and 5% are multi-component hydrogels of various types illustrated in Figure 8.1. The interest in DN hydrogels keeps increasing each year.

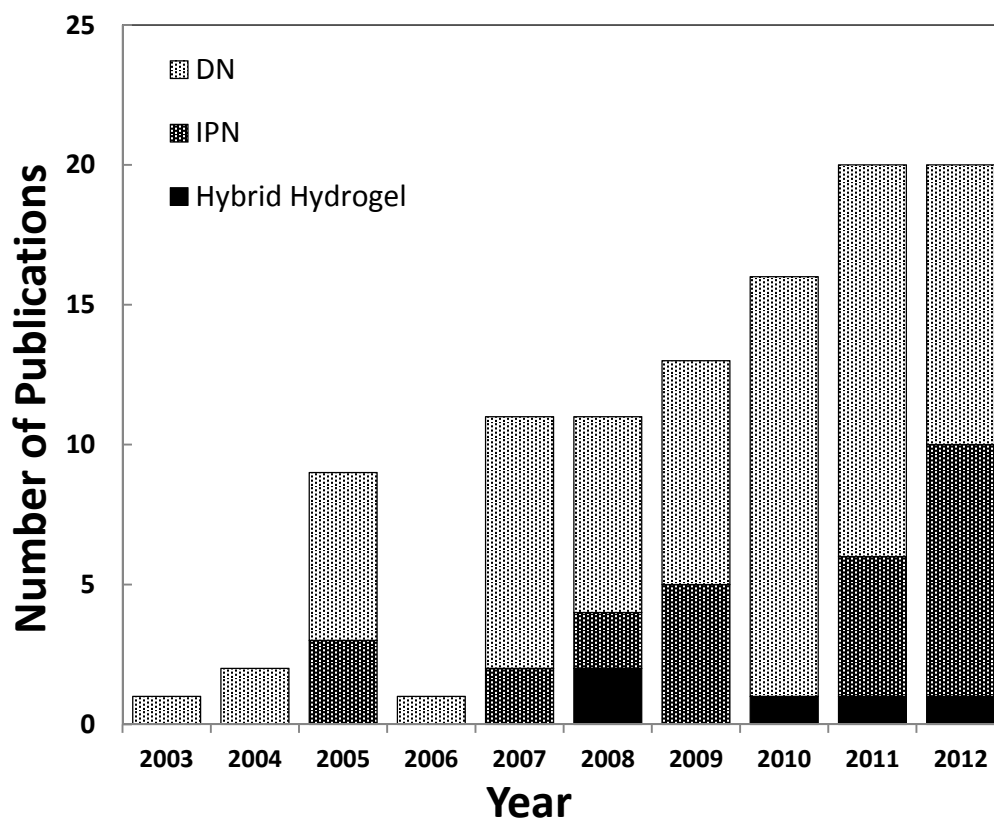


**Figure 8.3: Increase in the number of publications per year on hydrogels with “double network” in the title, from 2003 to 2012, through an online search in both “Web of Knowledge” and “Google Scholar”.**

These publications are categorized as DNs (composition and improved mechanical properties), IPNs or multi-component hydrogels.

In September 2013, more than 20 publications on hydrogels with “double network” in the title are already published. Because of the growing usage the term DN, there is an importance understand the underlying mechanisms of DNs.

The definition for DNs is continually changing and there are many new concepts for hydrogels that do not neatly fit into the category of DNs. Therefore, we have called these hydrogels “DN inspired” or “utilizing the DN concept”. More specifically we use these terms if researchers were (1) aiming to create DNs but only end up creating IPNs or other multi-component hydrogels,

(2) synthesize hydrogels using a brittle/ductile combination and it does not lead to these enhanced mechanical properties, or (3) achieve superior mechanical properties through other methods or combinations besides the using brittle/ductile network combination. Furthermore, if the tension data does not show clear yielding, or if we only have compression or tabulated data (with no observations of the Mullins effect) it is impossible to determine if the hydrogels are in fact DN hydrogels. For example, gellan gum (GM)/gelatin<sup>[160]</sup> does not include tension data and bacterial cellulose (BC)/PAAm<sup>[58]</sup> stress-strain curves indicates a potential yielding phenomenon but is not completely evident. These examples may be DN hydrogels but it is currently indeterminate. A few other DN “inspired” hydrogels include poly(ethylene glycol) diacrylate (PEGDA)/PAAc<sup>2,[116,117]</sup>, agarose/PEGDA<sup>[28,73]</sup>, and jellyfish/PAAm<sup>[187]</sup>. Slightly different processing of the networks can produce the DN effect as in Agar/PAAm (semi-DN)<sup>[19]</sup>, PAMPS/PAAm void-DN hydrogels<sup>[122]</sup>, microgel-reinforced (MR) hydrogels<sup>[68-70]</sup> and the molecular stent DN (st-DN)<sup>[124]</sup>. Liquid crystalline gels of poly(2,2'-disulfonyl-4,4'-benzidine terephthalamide) (PBDT)/PAAm<sup>[195,204]</sup>, layered BC/PAAm hydrogels<sup>[125]</sup> and anisotropic hydrogels of a polymerizable surfactant (dodecyl glyceryl itaconate:DGI) that forms bilayers in the PAAm matrix<sup>[62]</sup>, have also shown enhanced mechanical properties such as yielding but have internal structures which are directional. Combinations of ionically and covalently cross-linked hydrogels have become of interest due to the recoverable nature and high toughness of these systems such as alginate/PAAm<sup>[172]</sup> and kappa-carrageenan(k-CG)/ epoxy-amine (EA)<sup>[164]</sup>. In all, DNs have and continue to inspire many researchers to achieve improved mechanical properties through careful consideration of synthesis conditions.

## Conclusions

The first double-network hydrogel was introduced in 2003. The high toughness and unique mechanical behavior inspired research on DN hydrogels by numerous scientists in the past decade and the interest on DN hydrogels continues to grow. More recently, DN hydrogels have drawn a lot of attention and excitement because DN hydrogels are similar to both solvent-free elastomers and biological tissues for use in many applications, but especially as scaffolds in tissue engineering, a rapidly expanding field itself.<sup>[51]</sup> With the expansion of research on DN hydrogels over the past 10 years, understanding what makes DN hydrogels unique to other multi-component hydrogels using the knowledge gained makes the DN hydrogels specific and functional for others. DN hydrogels account both the strategic composition of brittle/ductile combination as well as the unique mechanical toughness and yielding phenomenon that arises from the composition. We hope we have clearly distinguished DN hydrogels from conventional IPNs and other multi-component hydrogels, and ultimately described DN hydrogels based on the newest research. Further, we hope the next decade inspires as much or more research as the past decade.



## Chapter 9: Synthesis and Characterization of Poly(N-Vinyl Formamide)

### Hydrogels – a Potential Alternative to Polyacrylamide Hydrogels<sup>9</sup>

#### Abstract

The synthesis and characterization of solution-cast, molded gels of N-vinyl formamide (NVF) has not been previously reported even though NVF is an isomer of acrylamide (AAm) and polyacrylamide (PAAm) hydrogels have many commercial applications. Aqueous NVF solutions were cross-linked into gels using a novel cross-linker, 2-(N-vinylformamido)ethylether, and the thermally-activated initiator VA-044. For a given formulation, PNVF gels swell up to twice that of PAAm gels cross-linked with N,N'-methylenebisacrylamide. From swelling and compression measurements, PNVF gels were found to be more hydrophilic than PAAm gels. Flory-Huggins solubility parameters were  $\chi=0.38\phi_2+0.48$  for PNVF and  $\chi=0.31\phi_2+0.49$  for PAAm, where  $\phi_2$  is the polymer volume fraction. The shear moduli for PNVF and PAAm scale with  $\phi_2^{2.0}$  and  $\phi_2^{2.5}$  respectively, consistent with good solvent behavior, also suggesting PNVF is more hydrophilic than PAAm. Similarity of mechanical properties for both gels as a function of  $\phi_2$  suggests that network structures of PNVF and PAAm gels are similar. Fracture strains of both gels declined with  $\phi_2$  by the same linear function while fracture stresses were about 500 kPa regardless of formulation. Since NVF is a liquid monomer, less toxic than AAm and can be hydrolyzed to a cationic form, PNVF gels could become technologically significant.

---

<sup>9</sup>Adapted from: **Tiffany C. Suekama**, Vara Aziz, Zahra Mohammadi, Cory J. Berkland, Stevin H. Gehrke, "Synthesis and Characterization of Poly(N-Vinyl Formamide) Hydrogels" *Journal of Polymer Science Part A: Polymer Science*, **2013**, 51 (2), 435-445.

## Introduction

This is the first report of the synthesis of solution-cast, molded hydrogels based on the water soluble monomer N-vinyl formamide (NVF), to the best of our knowledge. It demonstrates that the physical properties of poly(N-vinyl formamide) (PNVF) gels are quite similar to the technologically important hydrogel polyacrylamide (PAAm). Polyacrylamide (PAAm) hydrogels are used in electrophoresis<sup>[131]</sup>, chromatography<sup>[131]</sup>, cosmetics<sup>[9,131]</sup>, biomedical implants<sup>[20]</sup>, superabsorbent products<sup>[31]</sup> and soil conditioners<sup>[37]</sup> among numerous other applications. PNVF gels are also chemically related to poly(N-vinyl pyrrolidone) (PNVP) gels, another important biomedical hydrogel, widely used in contact lenses<sup>6</sup>, drug delivery systems and wound dressings.

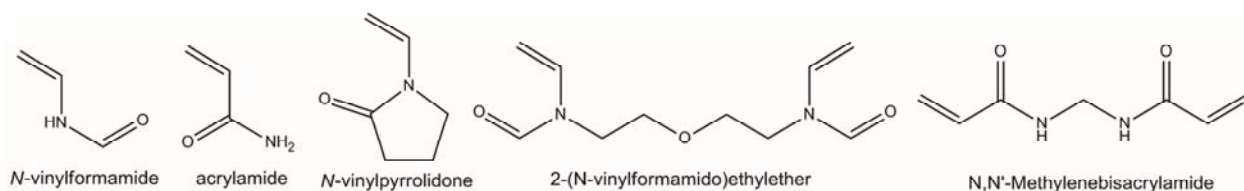


**Figure 9.1: Chemical structures**

Chemical structures of monomers (N-vinylformamide, acrylamide, and N-vinylpyrrolidone) and cross-linkers (2-(N-vinylformamido) ethyl ether and N,N'-methylenebisacrylamide).

NVF is an isomer of the acrylamide (AAm) monomer, as shown in Figure 9.1, but has been reported to be much less toxic than AAm.<sup>[144,145]</sup> Figure 9.1 also demonstrates the structural similarity of NVF to another commercially important monomer, N-vinyl pyrrolidone (NVP). NVF monomer has been produced on the commercial scale by several major chemical companies in the US, Europe and Japan, though the market is still developing.<sup>[145]</sup> These investments have been made due to the potential of NVF to be used as an alternative to other water-soluble monomers because of its low toxicity<sup>[93]</sup>, high reactivity<sup>[93,199]</sup> and ease in processing, as it is liquid at room temperature.<sup>[111]</sup>

PNVF is readily produced by conventional free radical polymerization methods.<sup>[144,145,163]</sup> PNVF and its hydrolysis product polyvinylamine (PVAm) have been evaluated for use in areas such as the papermaking, water treatment, radcure and oil recovery.<sup>[144]</sup> PVAm is of significant technological interest because it is a high charge density cationic polymer. However, PVAm cannot be produced directly from monomer since vinylamine is not stable in its free state, and thus polyvinylamine (PVAm) must be synthesized through indirect methods, typically hydrolysis of polymers such as PNVF, poly(N-vinylcarbamate) or poly(N-vinylacetamide).<sup>[4,55,144]</sup> PNVF is a good precursor polymer for PVAm as the hydrolysis reaction proceeds quickly under mild hydrolysis conditions.<sup>[145]</sup>

Cross-linked PNVF and PVAm networks have been produced as microgels<sup>[134,198]</sup>, nanogels<sup>[199]</sup>, and used in cross-linked coatings<sup>[144]</sup>, adhesives<sup>[144]</sup> and resins<sup>[144]</sup>. Pelton and co-workers have created thermally responsive microgels using poly(N-isopropylacrylamide) and PNVF.<sup>[198,199]</sup> Our group has previously synthesized PNVF nanogels<sup>[157-159]</sup> (~100 nm in diameter) for biomedical and drug delivery applications.<sup>[113,158]</sup> Using the cross-linker, 2-Bis[2,2'-di(N-vinylformamido)-ethoxy]propane<sup>[158]</sup> controlled degradation of the nanogels can be achieved, while stable magnetic PVAm nanoparticles<sup>[113]</sup> were made using the cross-linker, 2-(N-vinylformamido) ethyl ether (NVEE). Thaiboonrod *et al.* have made core-shell microgels of NVF and glycidyl methacrylate for similar applications.<sup>[177]</sup> Research teams at Air Products and Chemicals investigated the use of PNVF for coatings, adhesives and resins through a variety of mechanisms.<sup>[144]</sup> Akashi *et al.* studied copolymer gels of NVF with N-vinylisobutyramide and in a range of 0-40 mol% NVF.<sup>[203]</sup> The Akashi group has also produced a polyion complex, an interpenetrating polymer network (IPN) of poly(N-vinylacetamide) (PNVA)-*co*-PNVF-*co*-PVAm/poly(acrylic acid) (PAAc)<sup>[2]</sup> and a PNVA-*co*-PNVF hydrogel with a modified surface for

drug delivery<sup>[175]</sup>.

It is somewhat surprising that despite the established commercial importance of solution-cast molded PAAm and PNVP gels, synthesis of analogous PNVF hydrogels has not been reported, particularly since the potential technological utility of PNVF hydrogels is clearly evident, whether as an alternative to PAAm gels or as a precursor to functionalizable, high charge density cationic PVAm gels. Our work here suggests this may have been due to the lack of a readily available, effective cross-linker for NVF. The cross-linkers used in our work, NVEE and N,N'-methylenebisacrylamide (BIS) for PNVF and PAAm respectively, are shown in Figure 9.1. Development of many of the applications under current investigation using PNVF microgels and copolymers can advance more quickly with a better understanding of the cross-linking of NVF and the properties of the resulting gels. Therefore, in this work we have synthesized and characterized swelling behavior and mechanical performance (shear modulus and fracture properties) of the PNVF gels of various monomer and cross-linker concentrations and correlated these properties with theory. PAAm gels were used as a baseline for comparison of PNVF gels because of the availability of previously published data to establish accuracy of the methodology and the potential substitution of NVF for AAm in technological applications.

## Experimental

### *Materials*

For PNVF synthesis, the N-vinylformamide (NVF; Sigma-Aldrich: 98%) monomer was purified by distillation under vacuum at 80°C and stored at -10°C prior to polymerization. A novel cross-linker, 2-(N-vinylformamido) ethyl ether (NVEE; liquid of density of 1.3 g/mL), was synthesized and characterized by our previously reported procedure.<sup>[87,157,158]</sup> The initiator, 2,2'-

Azobis[2-(2-imidazolin-2-yl)propane]dihydrochloride (VA-044; Wako Pure Chemical Industries, Ltd) was used as received. Deionized, ultra-filtered (DIUF) water (Fisher Scientific) was used for all of the synthesis solutions.

For the synthesis of PAAm, all of the reagents were electrophoresis grade and were used as received. Reagents included the monomer, acrylamide (AAm; Sigma-Aldrich: 99+ %); the cross-linker, N,N'-methylenebisacrylamide (BIS; Sigma-Aldrich: 99+ %); the accelerator, N,N,N',N'-tetramethylethylenediamine (TEMED; Fisher Scientific: ~99%); and the initiator, ammonium persulfate (APS; Fisher Scientific:  $\geq 98\%$ ).

### ***Synthesis of PNVF and PAAm Hydrogels***

The conventional gel formulation notation,  $T \times C$ , was used to describe the gel composition.<sup>[17,132]</sup>  $T$  represents the total mass of monomer and cross-linker over the volume of water in which it was dissolved (w/v) as a percentage:

$$T = \frac{\text{total mass (monomer + cross-linker) (g)}}{\text{volume of water (ml)}} \times 100 \quad (9.1)$$

$C$  represents the ratio of the mass of cross-linker by the total mass of monomer and cross-linker (w/w) as a percentage:

$$C = \frac{\text{mass of cross-linker}}{\text{mass of monomer + cross-linker}} \times 100 \quad (9.2)$$

However, to directly compare formulations using cross-linkers with different molecular weights, a mole fraction is used in place of  $C$  and is defined here as  $C^*$ :

$$C^* = \frac{\text{moles of cross-linker}}{\text{moles of monomer + cross-linker}} \times 100 \quad (9.3)$$

An example of a  $15 \times 1.41$  ( $T \times C^*$ ) PNVF synthesis is as follows: NVF (0.566 mL), NVEE (0.021 mL) and thermal initiator VA-044 (0.15% w/v) were added to 4 mL of DIUF water in a 5

mL glass vial. The solution was mixed and then bubbled with nitrogen for 15 min to displace dissolved oxygen, then quickly capped. The free radical polymerization was carried out at 50°C for 24 h. After the reaction was complete, the hydrogel was cut into cylindrical disks (~4 mm diameter and ~2 mm height) and the mass of the sample, removed from the mold, was measured.

A similar procedure was used for the PAAm gel. For example, a 15 x 1.41 (T x C\*) PAAm gel was synthesized by dissolving AAm (0.582 g) and BIS (0.018 g) in 4 mL of DIUF water. This polymerization used the redox couple of APS (0.018% w/v) and TEMED (0.009% w/v), to initiate the polymerization. The solution was mixed and then bubbled with nitrogen, and the polymerization was carried out at room temperature for 24 h. The PAAm hydrogels were then prepared as noted for the PNVF gels.

### ***Swelling Properties***

Molded gel samples were submerged in DIUF water at room temperature for 24 h, and the water was changed every few hours to leach away any sol fraction. The excess water on the swollen gels was dabbed away with a Kimwipe. The swollen gel was then weighed and then placed in a desiccator over CaSO<sub>4</sub> until it reached a constant weight. It has been shown that bound water in PAAm is released over temperatures of 20 to 220 °C<sup>[182]</sup> and Tutas *et al.* reported that there is 10% weight loss at 110 °C.<sup>[180]</sup> The residual water content after desiccation was measured using a Pyris 1 Thermogravimetric Analyzer (TGA) (Perkin Elmer). The temperature was raised quickly from 20°C to 200°C and then held constant for over an hour until the mass was constant. For the gel samples tested, there was an additional 4-10% water loss over the desiccator drying. As this difference is not substantially greater than the limits of experimental reproducibility, and because the use of TGA to find the dry mass for every sample is not practical nor standard for most

published gel characterization studies, the degrees of swelling,  $Q$  (g/g), reported in the Results section are reported as the mass of the swollen gel over the mass of the desiccator-dried gel, although this leads to a slight underestimate of the true gel swelling degree.<sup>[45,135]</sup>

### ***Mechanical Analysis***

Mechanical properties were determined by testing the swollen gels under unconfined, uniaxial compression by the RSA III dynamic mechanical analyzer (TA Instruments). Compression was performed at a rate of 0.05 mm/s, which was determined to be a rate where stress-strain curves were strain-rate independent. The sample diameter was measured using calipers, and the height was measured by the RSA III. The plates were lubricated with mineral oil to minimize both gel adhesion to the plate and evaporation of water from the gel during testing. From the stress ( $\sigma$ )-strain ( $\epsilon$ ) data for each gel, the Young's modulus ( $E$ ), shear modulus ( $G$ ), fracture stress and fracture strain were extracted. To calculate  $E$ , the slope of the initial data up to a strain of 10% was used. Hydrogels typically behave as ideal elastomers and can be analyzed according to the neo-Hookean model:<sup>[179]</sup>

$$\sigma = G(\lambda - 1/\lambda^2) \text{ where } \lambda = L/L_0. \quad (9.4)$$

To calculate  $G$ , the slope of the data up to a strain function ( $\lambda - 1/\lambda^2$ ) value of 10 (equivalent to a strain of 69%) was used. Fracture stress and fracture strain were found at the point that the gel began to split, identified in the data as a sharp drop in stress.

## **Results**

Equilibrium swelling tests and mechanical analysis were completed on the gels to obtain swelling degree, moduli and fracture properties. Using the classic phantom (James and Guth) and

affine (Wall and Flory) models for rubber elasticity, the cross-link density,  $\rho_x$ , and the molecular weight between cross-links,  $M_c$ , were calculated from this data.<sup>[33,38,179]</sup> The theoretical development of these models is quite similar; the key difference between the two models is that in the affine model the cross-link junctions are locked into an elastic continuum while in the phantom model the junctions are unconstrained and thus may fluctuate over distances on the order of the chain dimensions.<sup>[33,38,179]</sup> Intermolecular interactions are not considered in either model. Mathematically, the only difference in the models is that the phantom model introduces a parameter for cross-link functionality,  $f$ . The cross-linkers in this work ideally yield tetrafunctional cross-links (four chains radiate from the cross-link junction) and therefore the only difference in the models is that the cross-link densities predicted by the phantom model are predicted to be twice the value of the affine model. The relationships between the shear modulus and the cross-link density for the two models are given as:

$$G = \begin{cases} \rho_x RT \phi_2^{1/3} \phi_{2f}^{2/3} & \text{(affine)} \\ \left(1 - \frac{2}{f}\right) \rho_x RT \phi_2^{1/3} \phi_{2f}^{2/3} & \text{(phantom)} \end{cases} \quad (9.5) \quad (9.6)$$

Where:  $f$  is junction functionality;  $R$  is the ideal gas constant;  $T$  is the temperature;  $\phi_2$  is the polymer volume fraction in the gel;  $\phi_{2f}$  is the polymer volume fraction at network formation;  $\rho_x$  is the effective cross-link density in the polymer network (moles per volume polymer).

Finally, the Flory-Huggins solubility parameter ( $\chi$ ) was found using both the standard Flory-Rehner theory of gel swelling, which uses the affine model for the elastic term, and a variation that uses the phantom model. The Flory-Rehner theory for the swelling at equilibrium of a polymer network in a solvent combines the Flory-Huggins model for polymer solubility with the affine model to yield Equation 9.7, where  $V_l$  is the molar volume of the solvent.<sup>[33,38,179]</sup> Its analog using



the phantom model to describe the elastic deformation of the network is given as Equation 9.8.

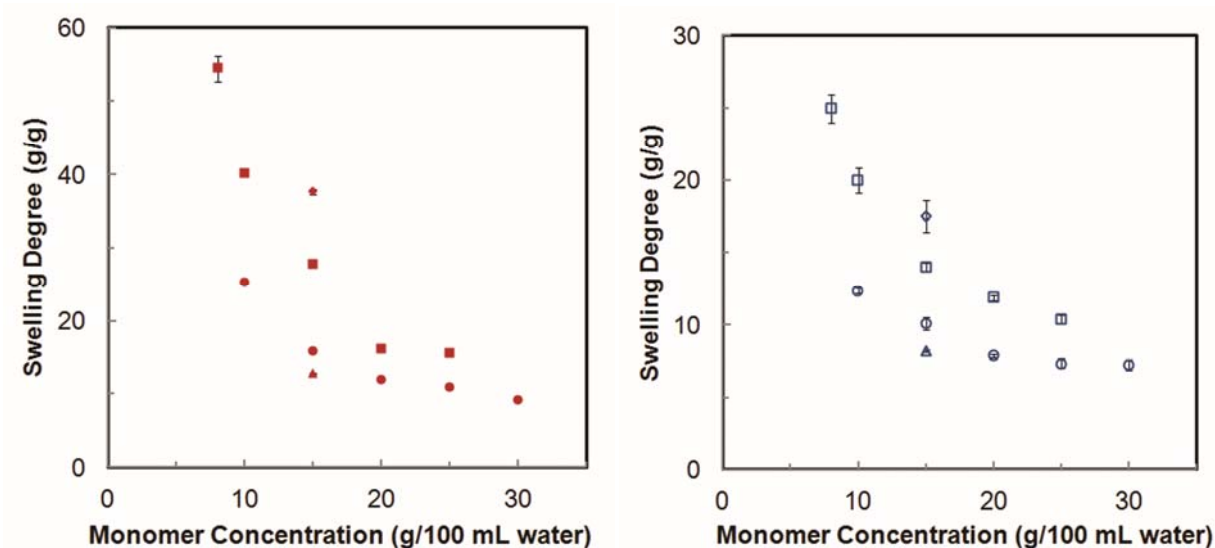
$$0 = \begin{cases} \ln(1 - \phi_2) + \phi_x + \chi\phi_2^2 + V_1\rho_x\phi_{2f} \left[ \left( \frac{\phi_2}{\phi_{2f}} \right)^{1/3} - \frac{1}{2} \left( \frac{\phi_2}{\phi_{2f}} \right) \right] & \text{(affine)} & (9.7) \\ \ln(1 - \phi_2) + \phi_2 + \chi\phi_2^2 + V_1 \left( 1 - \frac{2}{f} \right) \rho_x \phi_2^{1/3} \phi_{2f}^{2/3} & \text{(phantom)} & (9.8) \end{cases}$$

Since the polymer volume fraction is the inverse of the swelling degree,  $Q$  (g/g), (assuming a gel density of 1 g/cm<sup>3</sup>, a reasonable approximation) and the cross-link density is found from the shear modulus, these equations can be used to solve for the Flory-Huggins solubility parameter  $\chi$ . Although the Flory-Rehner theory is the most widely used gel swelling theory<sup>[40]</sup>, the phantom model has been reported to more closely predict the network properties of highly swollen networks since the chains are dilute, which decreases the correlation of a chain's deformation with others.<sup>[33]</sup> More advanced elasticity models such as constrained junction theory predict behavior intermediate between the limits of these models, tending toward the affine limit under compression and phantom limit under tension and high swelling.<sup>[32,33,39]</sup> Previous work on polyacrylamide gels where data was fitted to the constrained junction model yielded parameters that indicated lesser deviation from the affine limits than may have been expected for such gels based on swelling degree.<sup>[13]</sup> Thus we have chosen to report the parameters determined using standard Flory-Rehner theory; however, the equivalent values from the phantom network theory are provided in the supplementary information document for comparison. Choice of elastic model did not impact any conclusions of this work.

### ***Equilibrium Swelling Degree***

The swelling degrees in water of different PNVF and PAAm gel formulations are given in Figure 9.2a and 9.2b, and in acetone-water solutions in Figure 9.3. Detailed swelling data are listed on Tables 9.1 and 9.2 for PNVF and PAAm, respectively. As monomer concentration or cross-

linker concentration were increased, the degree of swelling decreased for both the PNVF and the PAAm gels, as shown in Figure 9.2a and Figure 9.2b respectively. The monomer concentration affects the degree of swelling most at lower concentrations with decreasing influence above 20 g/100 mL water. Such trends have been well-established for polyacrylamide gels.<sup>[12,191]</sup> Similar trends were observed for both gels, though the swelling degree of the PNVF gels is twice that of PAAm gels at low monomer concentrations. However, the degree of swelling is only slightly higher in PNVF than in PAAm at higher monomer concentrations. Figure 9.3 shows the swelling degree as a function of the acetone-water compositions. There is a sharp downward transition that occurs between 50-60% acetone in PNVF while in PAAm the transition occurs at lower concentrations of 30-40% acetone, which is consistent with the prior reports of the deswelling of PAAm at around 40% acetone.<sup>[72]</sup>



**Figures 9.2a and 9.2b: Decrease in swelling degree, increase NVF or AAm monomer concentration**

The swelling degree of PNVF shown in Figure 9.2a (closed symbols) and PAAm shown in Figure 9.2b (open symbols) decreases as either monomer or cross-linker concentration at synthesis increases. Similar trends are observed for both gels, though PNVF swells more than PAAm at a given formulation (hence the scale for swelling in 9.2a is drawn as twice that in 9.2b). Most error bars are smaller than symbols. Cross-linker concentration, C\*: (◆) 0.23; (■) 0.46; (●) 1.41; (▲) 2.35.

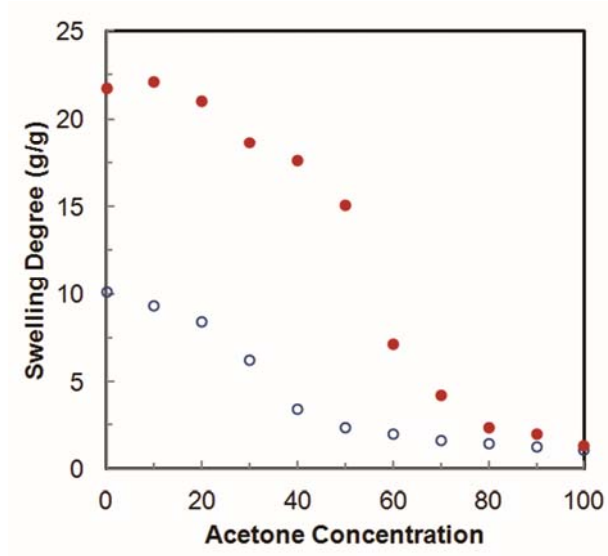


**Figure 9.3: Swelling in various acetone concentration**

Swelling of PNVF and PAAm in acetone-water solutions for GA higher concentration of acetone is required to induce deswelling of PNVF than PAAm. Formulation for both is 15 x 1.41 (T x C\*).

**Table 9.1: Measured properties of PNVF gels swollen to equilibrium in water.**

T (g/mL)	C (g/g)	C* (mol/ mol)	Q (g/g)	E (kPa)	G (kPa)	E/G	Fracture		
							Stress (kPa)	Fracture Strain (%)	Toughness (kJ/m <sup>3</sup> )
8.0	1.37	0.46	54.47 ± 1.75	3.5 ± 1.3	1.11 ± 0.33	3.12 ± 0.22	483 ± 339	98.2±2.0	28.3±6.8
10.0	1.37	0.46	40.13 ± 0.08	6.5 ± 1.2	2.35 ± 0.26	2.77 ± 0.15	662 ± 214	93.1±0.3	42.7±8.9
10.0	4.08	1.41	25.25 ± 0.28	15.6 ± 4.3	6.09 ± 1.68	2.57 ± 0.04	604 ± 294	88.8±2.8	56.5±22
15.0	0.69	0.23	37.61 ± 0.39	6.7 ± 0.3	2.74 ± 0.22	2.46 ± 0.17	841 ± 177	96.0±2.4	67.2±16
15.0	1.37	0.46	27.74 ± 0.26	17.3 ± 3.4	6.91 ± 1.32	2.51 ± 1.37	1139 ± 197	95.3±2.1	111±9.3
15.0	4.08	1.41	15.79 ± 0.18	30.6 ± 4.8	14.67 ± 0.63	2.08 ± 0.59	596 ± 283	86.3±3.8	80.7±24
15.0	6.75	2.37	12.76 ± 0.10	30.8 ± 7.3	20.88 ± 0.35	1.47 ± 0.35	303 ± 97	74.3±4.8	46.5±13
20.0	1.37	0.46	16.11 ± 0.04	35.8 ± 5.2	13.27 ± 1.11	2.70 ± 1.83	913 ± 290	90.7±3.0	109±38
20.0	4.08	1.41	11.95 ± 0.12	52.5 ± 18.4	25.09 ± 3.85	2.09 ± 0.38	530 ± 132	79.2±6.4	83.7±30
25.0	1.37	0.46	15.49 ± 0.28	34.8 ± 5.3	13.53 ± 0.98	2.57 ± 0.21	761 ± 277	89.2±2.2	94.7±23
25.0	4.08	1.41	10.82 ± 0.21	90.7 ± 19.1	32.00 ± 3.94	2.83 ± 0.53	371 ± 199	69.9±5.1	62.7±22
30.0	4.08	1.41	9.19 ± 0.15	83.2 ± 18.1	48.95 ± 4.45	1.70 ± 0.24	561 ± 148	70.6±4.2	90.3±22

**Table 9.2: Measured properties of PAAm gels swollen to equilibrium in water.**

T (g/mL)	C (g/g)	C* (mol/ mol)	Q (g/g)	E (kPa)	G (kPa)	E/G	Fracture	Fracture	Toughness (kJ/m <sup>3</sup> )
							Stress (kPa)	Strain (%)	
8.0	1.0	0.46	24.97 ± 0.96	9.75 ± 1.35	2.98 ± 0.24	3.27 ± 0.30	753 ± 212	96.5 ± 2.7	58.5±15
10.0	1.0	0.46	19.97 ± 0.90	14.10 ± 2.38	4.85 ± 0.15	2.91 ± 0.41	547 ± 299	92.2 ± 7.0	54.4±27
10.0	3.0	1.41	12.36 ± 0.17	34.86 ± 4.11	12.48 ± 1.50	2.79 ± 0.05	176 ± 72	71.9 ± 7.0	27.6±9.3
15.0	0.5	0.23	17.49 ± 0.20	17.76 ± 2.43	6.86 ± 1.08	2.59 ± 0.22	1238 ± 106	99.1 ± 1.2	120±6.8
15.0	1.0	0.46	14.01 ± 0.29	32.20 ± 3.56	10.12 ± 1.51	3.18 ± 0.27	269 ± 150	80.7 ± 7.3	43.3±19
15.0	3.0	1.41	10.12 ± 0.44	55.91 ± 11.23	28.62 ± 1.41	1.95 ± 0.16	463 ± 179	73.4 ± 5.9	67.4±21
15.0	5.0	2.37	8.20 ± 0.06	110.87 ± 2.08	43.16 ± 2.86	2.57 ± 0.22	549 ± 334	67.4 ± 11.9	79.1±43
20.0	1.0	0.46	11.89 ± 0.18	31.22 ± 10.65	12.91 ± 1.58	2.42 ± 1.08	297 ± 221	78.8 ± 7.5	22.4±10
20.0	3.0	1.41	7.90 ± 0.10	111.09 ± 15.20	45.25 ± 2.99	2.45 ± 0.20	534 ± 569	63.8 ± 13.5	63.9±66
25.0	1.0	0.46	10.39 ± 0.27	49.76 ± 14.01	19.83 ± 2.14	2.51 ± 0.90	404 ± 245	76.5 ± 6.4	36.4±17
25.0	3.0	1.41	7.36 ± 0.34	161.65 ± 12.79	65.57 ± 0.81	2.47 ± 0.16	633 ± 123	68.0 ± 3.1	93.6±23
30.0	3.0	1.41	7.27 ± 0.36	105.46 ± 73.79	66.66 ± 11.66	1.58 ± 0.77	553 ± 355	64.6 ± 6.8	74.9±20

### *Mechanical Analysis*

Compression tests were performed on both gels to characterize the mechanical properties and network structure of the gels. Representative stress vs. strain and stress vs. strain-function curves for both PAAm and PNVF are shown in Figure 9.4 and Figure 9.5, respectively. The parameters obtained from these tests are summarized in Tables 9.1 and 9.2 for PNVF and PAAm respectively.

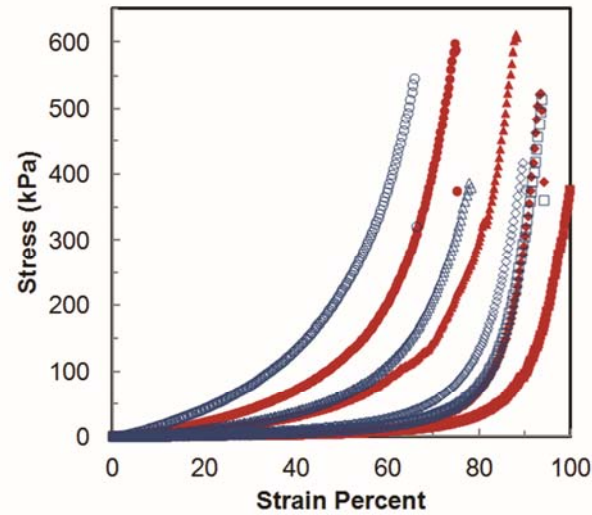


**Figure 9.4: Similarity in shape of stress-strain curves of PNVF and PAAM**

Representative stress versus strain curves for PNVF (closed symbols) and PAAM (open symbols) shows that the shape of the PNVF curves are similar to the PAAM curves except shifted to higher strains. All of the curves have been truncated after failure. Formulation in  $T \times C^*$ : (■)  $8 \times 0.46$ ; (◆)  $10 \times 0.46$ ; (▲)  $25 \times 0.46$ ; (●)  $25 \times 1.41$ .

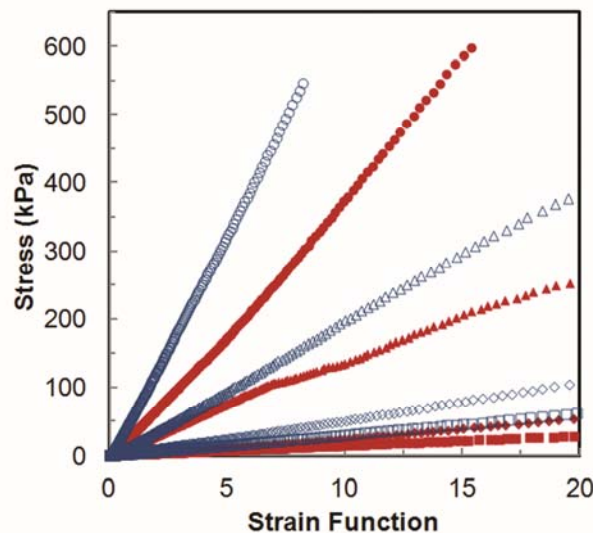


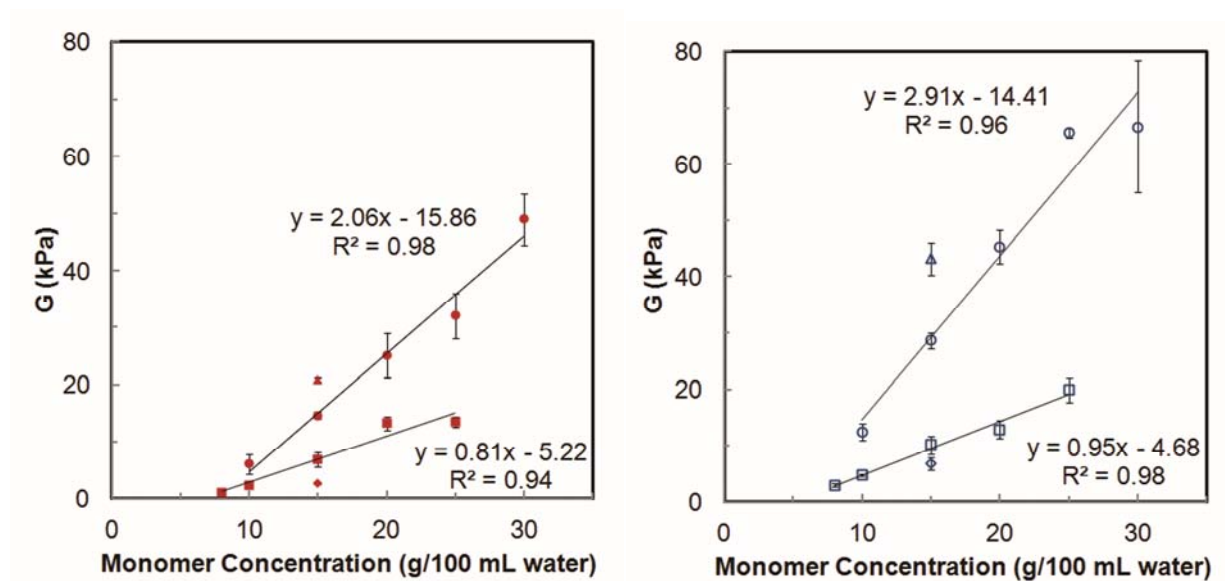
**Figure 9.5: Linearization of data in stress-strain function curves of PNVF and PAAM**

Representative stress versus strain function (from the neo-Hookean model, Eq. 4) curves taken from Figure 3 for PNVF (closed symbols) and PAAM (open symbols). The high degree of linearity is consistent with ideal elastic behavior. All of the formulations only use data up to a strain function of 10 or failure, whichever is lesser. Formulation in  $T \times C^*$ : (■)  $8 \times 0.46$ ; (◆)  $10 \times 0.46$ ; (▲)  $25 \times 0.46$ ; (●)  $25 \times 1.41$ .

In Figure 9.4 all of the curves had a similar shape, although all of the PNVF curves are slightly offset to the right of the PAAm curves as the result of their higher swelling for a given formulation. The linearization of the stress-strain data when plotted according to the neo-Hookean model of Equation 9.1, as shown in Figure 9.5, demonstrates that all gels behave as ideal elastomers. Tables 9.1 and 9.2 for PNVF and PAAm, respectively, compile the mechanical properties obtained from the compression tests: E, G, E/G, fracture properties and toughness. The stress-strain data used to calculate E were linear up to a strain of at least 10% but turned upward past this point. Using the neo-Hookean model to calculate G, all of the slopes were highly linear to a strain function of at least 10 (strain of 69%). E and G are directly related through the Poisson's ratio of E/G. For swollen gels, this ratio is typically slightly greater than 3 under compression and less than 3 upon extension.<sup>[202]</sup> However, almost all of the values for PNVF and PAAm were less than 3. E is very sensitive to slight defects in samples at small strains while G is not, and G uses much more of the stress-strain data, suggesting G is the more accurate parameter; therefore, G was used in further analysis of the gels. The toughness was determined as the area under the stress-strain curve up to failure (this measure of material toughness is also known as 'work to fracture').

The dependence of the shear modulus on the gel composition is given in Figures 6a and 6b for PNVF and PAAm, respectively. As the monomer concentrations and cross-linker concentrations were increased, G increased linearly ( $r^2 = 0.94-0.98$ ) for both PAAm and PNVF, with the slope depending upon cross-linker concentration as shown in Figures 9.6a and 9.6b. The slope increased by a factor of 2.5 from 0.81 to 2.06 as the cross-linker concentration increased from 0.46 to 1.41 mol/mol in PNVF. For PAAm, the slope increased by a factor of 3.1 from 0.95 to 2.91 as the cross-linker concentration increased over the same range. The magnitude of G is somewhat higher in PAAm than PNVF, as expected since the swelling degree of PAAm is less

than PNVF for the same formulation. However, when  $G$  is plotted against the polymer volume fraction,  $\phi_2$  ( $\phi_2 = 1/Q$ ), all of the data falls onto a single curve for each gel (shown in the Supplementary Information document S-9.3a and S-9.3b).



**Figures 9.6a and 9.6b:  $G$  of PAAM  $\sim 2\times$  PNVF but have similar trends**

The shear modulus of PNVF in Figure 9.6a (closed symbols) at a given formulation is about half that of PAAM in Figure 9.6b (open symbols) when plotted as a function of monomer and cross-linker concentration; however, the general trend that as monomer concentration increases the modulus increases is the same for both PNVF and PAAM. Most error bars are smaller than symbols. Cross-linker concentration,  $C^*$ : ( $\blacklozenge$ ) 0.23; ( $\blacksquare$ ) 0.46; ( $\bullet$ ) 1.41; ( $\blacktriangle$ ) 2.35.

Shear modulus, fracture strain and fracture stress are correlated with polymer volume fraction  $\phi_2$  in Figures 9.7 – 9.9. The data from Figures 9.6a and 9.6b fit well to the function  $G \propto \phi_2^n$ , with a single curve found for each gel type, independent of cross-linking ( $r^2 > 0.98$ ). As shown in Figure 9.7, the exponent is  $1.98 \pm 0.07$  for PNVF and  $2.51 \pm 0.12$  for PAAM. According to scaling theory for the modulus of a nonionic gel, the modulus is proportional to the volume fraction raised to an exponent of 2.25 in a good solvent, 3 in a theta solvent and  $\infty$  in a poor solvent.<sup>[31]</sup> The

PAAm results agree well with previously reported exponents of 2.55<sup>[13]</sup> and 2.25<sup>[47]</sup> for these gels, though a value as low as 1.88 has also been reported in a particular formulation range.<sup>[12]</sup>

A greater degree of uncertainty is associated with the fracture properties of these gels due to the sensitivity of the fracture to sample defects and the fact that some gels can be compressed to over 90% strain, where experimental artifacts may be introduced (under tension, many PAAm formulations have fracture strains over 100%).<sup>[13]</sup> Nonetheless, when fracture strain is plotted against polymer volume fraction, PAAm and PNVF follow nearly identical trends in which fracture strain decreases from about 100% to 65% strain as polymer volume fraction increases from 0.02 to 0.14 mol/mol, as shown in Figure 9.8. However, a small change in the fracture strain means a large change in the fracture stress, as shown in Figure 9.9, so no clear trend is observed in the fracture stresses. The fracture stresses above 600 kPa are seen at very high compressive strains (~90% or higher). Nevertheless, the data scatters at about 500 kPa for both gels independently of formulation or polymer volume fraction. The dependence of toughness (work to fracture) on composition mirrors Figure 9 because the toughness correlated closely with the fracture stress. The toughness values found for PAAm gels are of comparable magnitudes to previously reported values found under tension.<sup>[37]</sup>



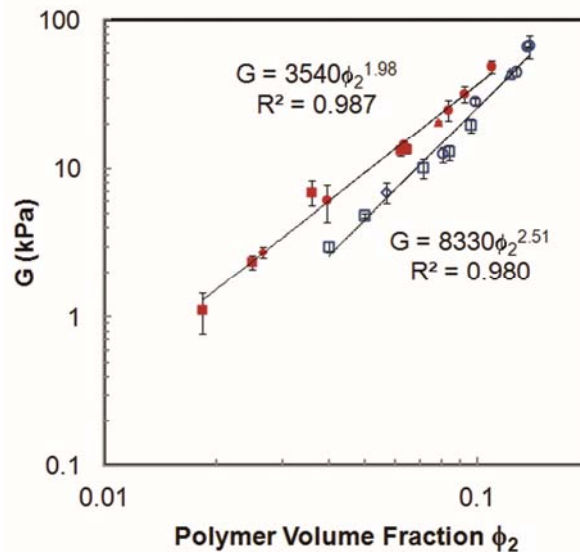


**Figure 9.7: G follows scaling theory, PNVF is more hydrophilic**

The shear moduli for all formulations of PNVF (closed symbols) and PAAm (open symbols) gels each fall onto a single line on a log-log plot against polymer volume fraction, with slopes consistent with predictions of scaling theory that for a good solvent:  $G \propto \phi_2^{9/4}$ . Cross-linker concentration,  $C^*$ : (◆) 0.23; (■) 0.46; (●) 1.41; (▲) 2.35.

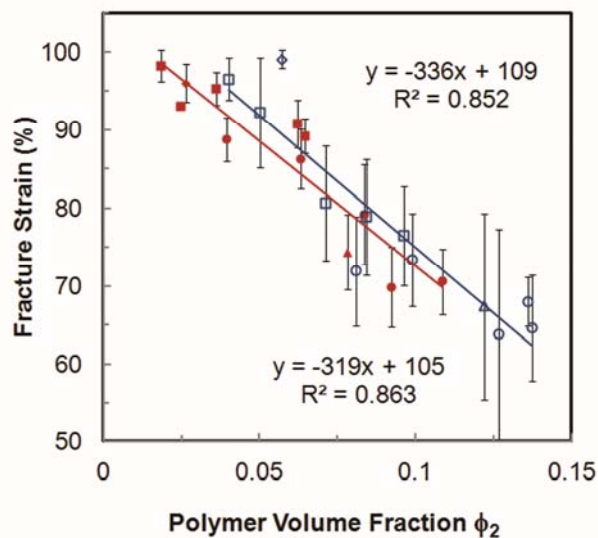


**Figure 9.8: Correlation of fracture strain with polymer volume fraction**

As the polymer volume fraction increases for PNVF (closed symbols) and PAAm (open symbols), the fracture strain decreases linearly by nearly the same function for each. Cross-linker concentration,  $C^*$ : (◆) 0.23; (■) 0.46; (●) 1.41; (▲) 2.35.

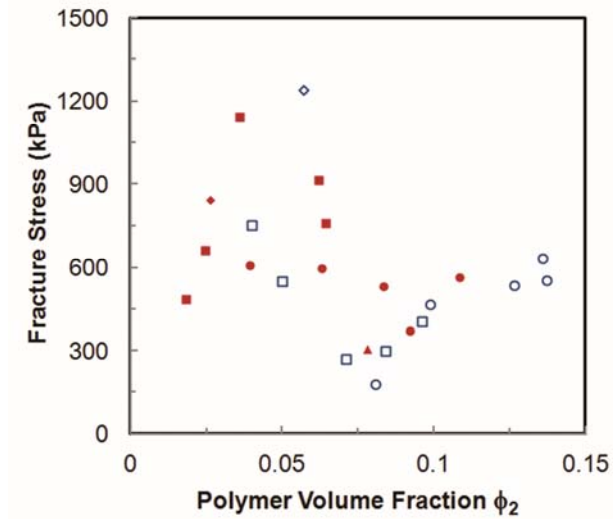


**Figure 9.9: Failure stress not dependent on polymer volume fraction**

Fracture stress is not strongly dependent upon polymer volume fraction for either PNVF (closed symbols) or PAAm (open symbols). The magnitudes are similar for both PNVF and PAAm. Error bars are not shown but are generally large; values above 600 kPa may be compromised by experimental artifacts due to high compressive strains. Cross-linker concentration,  $C^*$ : (◆) 0.23; (■) 0.46; (●) 1.41; (▲) 2.35.

### *Theoretical Parameters*

Using the swelling and mechanical data, other helpful properties for characterizing the networks were calculated, namely the molecular weight between cross-links,  $M_c$ , cross-link density,  $\rho_x$ , and the Flory-Huggins solubility parameter,  $\chi$ .  $M_c$  and  $\rho_x$  were calculated using the affine network theory and are listed in Tables 9.3 and 9.4 for PNVF and PAAm respectively. The  $M_c$  for PNVF and PAAm were in the range of 8,000-110,000 g/mol (4,000-55,000 g/mol for phantom model). For PAAm gels, the results are comparable to previously reported values of  $M_c$ .<sup>[13]</sup> The  $\chi$  values were calculated from the standard Flory-Rehner swelling theory described in Equation 9.7 using the measured polymer volume fraction,  $\phi_2$ , and cross-link density,  $\rho_x$ . Figure 9.10 shows that  $\chi$  values of PNVF and PAAm increase linearly with the polymer volume fraction, according to the functions  $\chi = (0.384 \pm 0.020)\phi_2 + (0.478 \pm 0.001)$  and  $\chi = (0.311 \pm 0.016)\phi_2 + (0.493 \pm 0.002)$ , respectively. The specific  $\chi$  values are listed in Tables 9.3 and 9.4 for PNVF and

PAAm, respectively. The values found using the phantom model listed in the Supplementary Tables S-9.1 and S-9.2 are quite similar. The function obtained for PAAm yields values that match well with the previously reported relationship  $\chi = 0.121\phi_2 + 0.491$  (determined in a similar fashion but using the phantom model; using the phantom model, our data yields  $\chi = 0.261\phi_2 + 0.491$ , as shown in the Supplementary Information Figure S-9.4).<sup>[12]</sup>

**Table 9.2: Calculated parameters for PNVF using the affine network model.**

T (g/mL)	C (g/g)	C*		Cross-link Density, $\rho_x$ (mol/cm <sup>3</sup> )	Theoretical Cross-link Density $\rho_t$ (mol/cm <sup>3</sup> )	Cross-linker Efficiency	$\chi$
		(mol/ mol)	$M_c$ (g/mol)				
8.0	1.37	0.46	1.10E+05	9.24E-06	5.70E-05	0.16	0.49
10.0	1.37	0.46	6.67E+04	1.52E-05	5.70E-05	0.27	0.49
10.0	4.08	1.41	3.00E+04	3.39E-05	1.73E-04	0.20	0.49
15.0	0.69	0.23	7.63E+04	1.33E-05	2.84E-05	0.47	0.48
15.0	1.37	0.46	3.36E+04	3.03E-05	5.70E-05	0.53	0.48
15.0	4.08	1.41	1.91E+04	5.33E-05	1.73E-04	0.31	0.50
15.0	6.75	2.37	1.44E+04	7.07E-05	2.91E-04	0.24	0.51
20.0	1.37	0.46	2.54E+04	4.01E-05	5.70E-05	0.70	0.50
20.0	4.08	1.41	1.48E+04	6.86E-05	1.73E-04	0.40	0.51
25.0	1.37	0.46	2.92E+04	3.48E-05	5.70E-05	0.61	0.50
25.0	4.08	1.41	1.39E+04	7.30E-05	1.73E-04	0.42	0.51
30.0	4.08	1.41	1.09E+04	9.36E-05	1.73E-04	0.54	0.52

**Table 9.3: Calculated parameters for PNVF using the affine network model.**

T (g/mL)	C (g/g)	C*		Cross-link		Theoretical	
		(mol/ mol)	M <sub>c</sub> (g/mol)	Density, ρ <sub>x</sub> (mol/cm <sup>3</sup> )	Density ρ <sub>t</sub> (mol/cm <sup>3</sup> )	Cross-linker Efficiency	χ
8.0	1.0	0.46	5.84E+04	1.92E-05	7.22E-05	0.27	0.50
10.0	1.0	0.46	4.49E+04	2.50E-05	7.22E-05	0.35	0.51
10.0	3.0	1.41	2.04E+04	5.49E-05	2.19E-04	0.25	0.52
15.0	0.5	0.23	4.35E+04	2.58E-05	3.60E-05	0.72	0.51
15.0	1.0	0.46	3.17E+04	3.53E-05	7.22E-05	0.49	0.51
15.0	3.0	1.41	1.25E+04	8.97E-05	2.19E-04	0.41	0.52
15.0	5.0	2.37	8.90E+03	1.26E-04	3.69E-04	0.34	0.53
20.0	1.0	0.46	3.18E+04	3.52E-05	7.22E-05	0.49	0.52
20.0	3.0	1.41	1.04E+04	1.08E-04	2.19E-04	0.49	0.53
25.0	1.0	0.46	2.52E+04	4.46E-05	7.22E-05	0.62	0.52
25.0	3.0	1.41	8.53E+03	1.31E-04	2.19E-04	0.60	0.53
30.0	3.0	1.41	9.52E+03	1.18E-04	2.19E-04	0.54	0.53

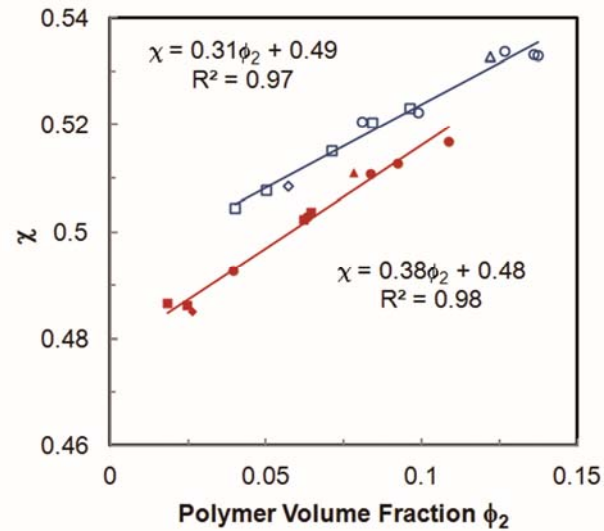


**Figure 9.10: Flory-Huggins parameter lower for PNVF, more hydrophilic**

Linear dependence of Flory-Huggins parameter (calculated using the affine model) as a function of polymer volume fraction for PNVF (closed symbols) and PAAm (open symbols). Cross-linker concentration, C\*: (♦) 0.23; (■) 0.46; (●) 1.41; (▲) 2.35.

## Discussion

Taken as a whole, the results show that PNVF is a slightly more hydrophilic polymer than PAAm. The greater hydrophilicity of PNVF results in gels that swell more than PAAm gels of the same formulation. Nonetheless, PNVF gels formed using NVEE as a cross-linker behave quite similarly to PAAm cross-linked with BIS, suggesting that PNVF gel formulations can be identified to match the performance of PAAm gels in a given application. In this section, we examine the data that lead to these conclusions.

The similarity in values and trends of cross-linking efficiency and of fracture properties indicate that NVEE cross-links NVF to form gels structurally comparable to PAAm cross-linked with BIS. Cross-linking efficiency essentially accounts for differences in swelling degree and normalizes the amount of elastically effective cross-links formed relative to the concentration of cross-linker in the synthesis formulation. Comparison of Tables 9.3 and 9.4 shows that the cross-linking efficiencies of similar formulations of PNVF and PAAm gels are similar, ranging from 0.16 to 0.70 in PNVF and 0.25 to 0.72 for PAAm. Of the 12 formulations studied, in 9 cases the efficiencies differ by 0.10 or less; generally PAAm is the higher value. The efficiency rises as the monomer concentration increases, especially in the range of 10 - 25% monomer, and tends to decline as the cross-linker concentration increases at constant monomer concentration (it is possible that at higher monomer concentrations than studied here, cross-linking efficiency could become higher for PNVF than PAAm due to cross-linking by chain transfer from the polymer, which has been observed upon homopolymerization of NVF at concentrations of 40 wt% NVF and higher<sup>[56]</sup>). Both Baselga *et al.* and Gehrke *et al.* have shown similar trends with polyacrylamide and poly(N-isopropylacrylamide), respectively.<sup>[13,44]</sup> Greater levels of intermolecular cross-linking are expected as monomer concentration increases and a greater

percentage of cross-linkers are expected to form structures that do not function as independent cross-link junctions at higher cross-linker concentrations, as shown by Baselga, *et al.*<sup>[12,13]</sup> We focus on the trends rather than the specific values of cross-linking efficiency because the specific values depend upon the elastic model chosen for calculating the cross-link density (the phantom model yields values twice as large, as given in Supplementary Table S-9.2).

Thus NVEE is shown to be an effective cross-linker for NVF, with cross-linking efficiencies only slightly lower than in the well-established BIS/AAM system. However, even for copolymerization of the BIS-AAM pair, the reactivity ratios are 3.36 and 0.57, respectively. This leads to preferential early consumption of BIS resulting in heterogeneity in the PAAM gels.<sup>[14,162]</sup> Our efforts to use BIS as a cross-linker for NVF yielded poor quality PNVF gels. This is likely due to the fact that to form good quality gels a tendency toward random copolymerization of the monomer and cross-linker is required so that they are consumed at comparable rates during copolymerization. However, Kathmann and McCormick have shown that NVF and AAM are strongly alternating in copolymerization reactions which would result in depletion of the dilute component (cross-linker) early in the reaction, with little available for cross-linking at later stages.<sup>[82]</sup> Alternating copolymerization of NVF and BIS is likely the result of the nitrogen adjacent to the propagating radical in NVF and NVEE in contrast to the carbonyl carbon in AAM and BIS (see Figure 9.1) which likely yields reactivity ratios significantly different from 1.<sup>[194]</sup> The same issue has been identified for the formation of PNVP and poly(vinyl acetamide) gels by copolymerization/cross-linking reactions and have been overcome by synthesizing cross-linkers with a nitrogen atom adjacent to the carbon with the propagating radical, similar to our design of NVEE to be an effective cross-linker for NVF.<sup>[3,4,194]</sup>

The similarity of the fracture properties of the two gels also suggests both similar molecular

structures and degrees of heterogeneity, as has been established for PAAm gels.<sup>[13,161,191]</sup> For both gels, the fracture strain decreases linearly with increasing polymer volume fraction, following essentially the same function within uncertainty limits. The fracture stresses of the gels are subject to a great degree of variability, but remain in the range of 500 kPa regardless of formulation. The observation of the linear trend of fracture strain with polymer volume fraction suggests existence of fundamental connection between these properties, but we are not aware of any theoretical work regarding such a correlation. The significance for this work is that for the same water content, PNVF fractures at the same strain as PAAm, an important consideration in applications.

The values calculated for the Flory-Huggins  $\chi$  parameters indicate that water is a slightly better solvent for PNVF than for PAAm; in other words, PNVF is slightly more hydrophilic than PAAm. In Flory-Huggins solution thermodynamics,  $\chi$  value of 0.5 represents a theta solvent, while  $\chi > 0.5$  represents a poor solvent and  $\chi < 0.5$  represents good solvent. For PAAm gels swollen in water, literature values for  $\chi$  range from 0.47-0.53 depending on temperature and the volume fraction, but  $\chi$  is commonly reported as 0.48 at 298 K with only a slight dependence on volume fraction.<sup>[8,26,90,121,129]</sup> The values of  $\chi$  as a function of composition for PAAm given in Figure 9.10 lie in a range comparable to these previously reported values. The values for PNVF run consistently lower, thus explaining why PNVF gels swell more than PAAm for the same formulations (and to a lesser extent, because of the slightly lower cross-linking efficiency of NVF/NVEE relative to AAm/BIS). The correlation of the  $\chi$ -parameter with volume fraction for PAAm matched the literature well, as noted in the Results section. The scaling law exponent for dependence of the shear modulus on the polymer volume fraction for PAAm gels also matched the literature well, with the lower value observed for PNVF gels relative to PAAm gels consistent with greater hydrophilicity.<sup>[44]</sup> While the use of gel swelling to calculate the  $\chi$  parameter of the

polymer assumes that  $\chi$  is independent of cross-linking, and while  $\chi$  may be expected to differ in the vicinity of the cross-link junctions, the validity of extracting  $\chi$  from the swelling of polymer networks is well-established.<sup>[141]</sup> We also found the choice of elastic model did not significantly affect the values of the  $\chi$  parameter (shown in Supplementary Information Figure S-9.4). Thus the function we have reported for the solubility parameter of PNVF can similarly be expected to be accurate for its solutions as well as its gels.

Neither gel swells significantly in acetone, but in acetone-water solutions, a higher concentration of acetone is required to induce the deswelling of PNVF gels than PNVF. Although the general behavior of the two gels in the mixed solvents is similar, the difference in the deswelling concentration range suggests that while the hydrogen-bonding capacities may be similar, they are not identical. Suwa *et al.* made a similar observation of an offset in phase separation behavior when solvent quality is systematically altered (by temperature, pressure and salt type and concentration) for polymers made from the isomeric monomers N-isopropylacrylamide and N-vinylisobutyramide. They related this to differences in hydration caused by swapping the location of the amide group on the side chain.<sup>[174]</sup>

PAAm gels are widely used as superabsorbents, chromatography media and in electrophoresis. The utility of PAAm in these applications depends upon on its swelling, moduli, fracture properties and permeability. Taken as a whole, these results indicate that PNVF could substitute for PAAm in a variety of applications with a small change in formulation to account for the slightly greater hydrophilicity of PNVF relative to PAAm. Similarity in network properties and hydrophilicity suggests that other properties, notably solute diffusivity and partition coefficients, should also be quite similar.<sup>[65,140]</sup> Thus we hypothesize that PNVF gels could substitute for PAAm in applications such as chromatography and gel electrophoresis. Key



advantages of NVF over AAm are that it is less toxic than AAm, reducing safety concerns during processing and with regard to residual monomer in products, a particular concern in medical and pharmaceutical applications.<sup>7-11</sup> Furthermore, NVF is liquid rather than a solid, which allows for easier processing. PNVF gels are also a convenient route to the production of the cationic gel poly(vinylamine) by simple hydrolysis. We have hydrolyzed these PNVF gels in 0.1 - 1 M NaOH at 60°C to create cationic gels based on PVAm, Such gels swell substantially in acidic solution and absorb negatively charged dyes from solution. This route to create a cationic network with a high charge density which may also have notable utility where amine functionality is desired<sup>[144,145]</sup>, as we have recently shown with siderophore-modified poly(allylamine gels) for iron chelation.<sup>[113,114]</sup>

## Conclusions

Poly(N-vinylformamide) hydrogels were synthesized using a novel cross-linker 2-(N-vinylformamido) ethyl ether, NVEE, by thermally-initiated free radical polymerization and the dependence of their thermodynamic and mechanical properties were determined as a function of composition. The cross-link efficiencies of NVF with NVEE were comparable to those of AAm with the conventional cross-linker N, N'-methylene bisacrylamide, generally increasing as the monomer concentration and the monomer to cross-linker ratio was increased. The swelling behavior was well-correlated with Flory-Rehner theory, and the  $\chi$  parameter was found to increase linearly with polymer volume fraction. The values of  $\chi$  were slightly less than those of PAAm, suggesting that PNVF is a slightly more hydrophilic polymer than PAAm. The dependence of the shear modulus on polymer volume fraction was also consistent with the finding that PNVF is more hydrophilic than PAAm. The fracture properties of the two gels were nearly identical, with the

fracture strain decreasing linearly with polymer volume fraction and fracture stresses around 500 kPa regardless of formulation.

For the same formulation, as a result of the greater hydrophilicity of the monomer, PNVF gel swells more than PAAm gel, and the shear modulus is lower. However, the results of this work can be used to modify a PNVF formulation to match the swelling of a given PAAm gel formulation. For the same swelling degree (polymer volume fraction), the mechanical properties should be identical. Thus PNVF hydrogels might function well in current PAAm applications where the benefits of reduced toxicity and a liquid rather than solid monomer are important. PNVF gels cross-linked with NVEE can also be hydrolyzed to form cationic gel networks with vinylamine side groups, which are readily functionalized.

## **Supplementary Information for Chapter 9: Synthesis and Characterization of Poly(N-Vinyl Formamide) Hydrogels – a Potential Alternative to Polyacrylamide Hydrogels**

This supplementary information provides further analysis of the data reported in Chapter 9. Included is normalized swelling data of PNVF and PAAm. Also, there is additional comparison of PNVF and PAAm by trends in Young's modulus with monomer concentration and cross-linker concentration and shear modulus with polymer volume fraction. Finally, the supplementary information contains calculated parameters for the phantom network model of PAAm and PNVF and the dependence Flory-Huggins parameter with polymer volume fraction obtained using this model. The materials and methods used are described in the main article.

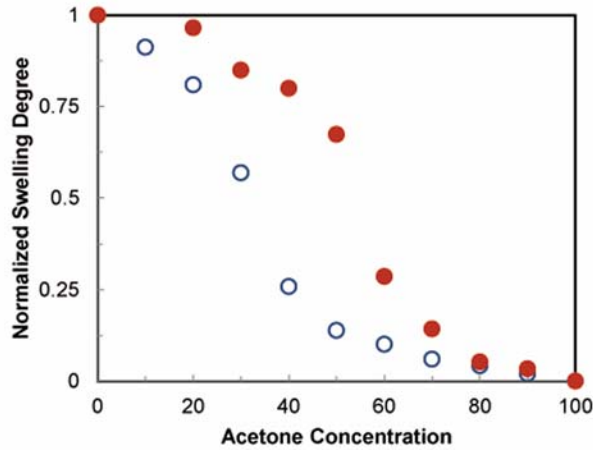
Swelling of PNVF and PAAm in acetone-water solutions are shown in Figure 9.3 of the main article, however by normalizing the swelling curves, as shown in Supplementary Figure S-9.1, it is clear that PNVF shrinks to about half its mass around in a 50:50 acetone:water mixture, while PAAm shrinks to about half its mass around in a 30:70 acetone:water mixture. Therefore, a higher concentration of acetone is required to induce deswelling of PNVF than PAAm.

To aid in comparison of PNVF to PAAm, the trends of the Young's modulus as a function of monomer and cross-linker concentration are shown in Supplementary Figures S-9.2a and S-9.2b to demonstrate their similar trends that as the monomer and cross-linker concentration are increased, Young's modulus,  $E$ , increased. It is also shown the  $E$  of PNVF is only about half that of PAAm.

In the main article, Figures 9.6a and 9.6b compare the shear modulus as a function of monomer and cross-linker concentration for PNVF and PAAm. To see the effects of polymer

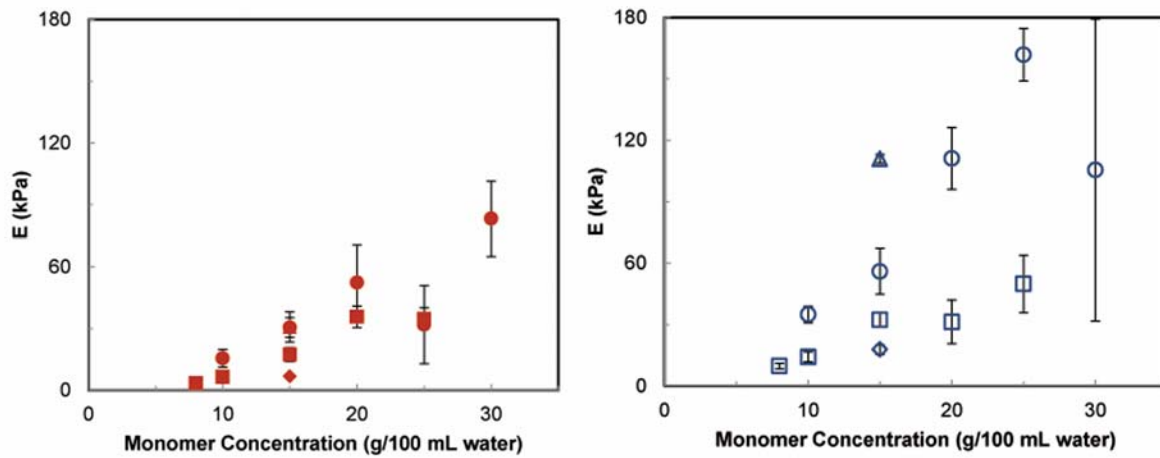
volume fraction, the shear modulus was plotted versus the polymer volume fraction and all of the data fall into a single curve. It is shown that the shear modulus increases as the volume fraction increases. It can also be seen that the trend seems to be unaffected by cross-linker concentration, monomer concentration or type of gel (PNVF and PAAm).

All of the hydrogel parameters for PNVF and PAAm presented in the main article were also calculated using the phantom model. These are listed in Supplementary Tables S-9.1 and S-9.2, respectively. As explained in the main article, the only quantitative difference between the classic phantom and affine models for rubber elasticity is that the cross-link densities predicted by the models differ by a factor of 2 due to the cross-linker functionality term in the phantom model.<sup>[33,38,179]</sup> Therefore, the cross-link densities listed in Supplementary Tables S-9.1 and S-9.2 are double that of Tables 9.3 and 9.4 in the main article. Of most interest is the Flory-Huggins solubility parameter ( $\chi$ ). Figure 9.10 shows the Flory-Huggins parameter as a function of the phantom model. It shows that the Flory-Huggins parameter as calculated using the phantom model yields values and a function of  $\chi$  with volume fraction quite similar to those found using the affine model. Hence we conclude that the  $\chi$  parameter is shown to be insensitive to the elastic models chosen for these gels.



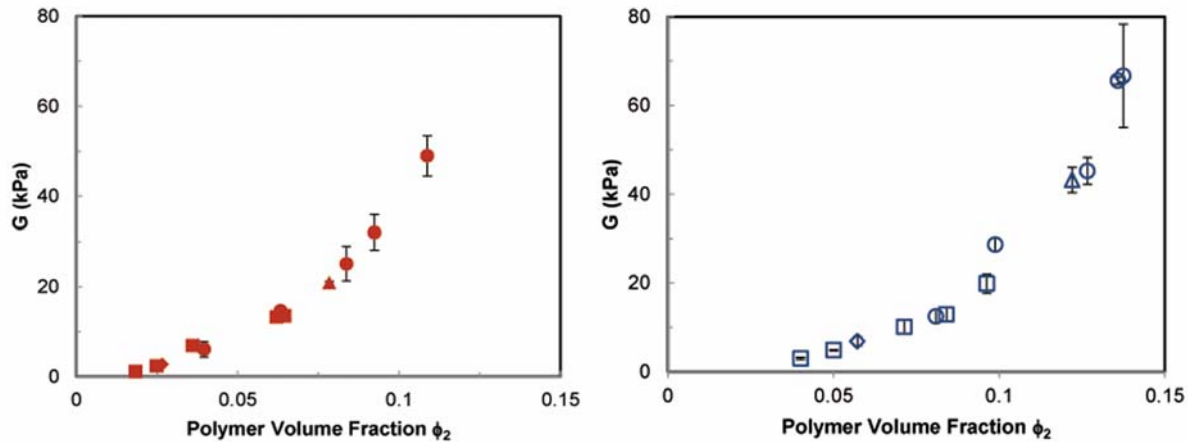
**Supplementary Figure S-9.1: Normalized swelling degree as a function of acetone concentration**

Swelling trends of PNVF and PAAm in acetone-water solutions for PNVF (closed symbols) and PAAm (open symbols). This shows that PAAm shrinks to half of its mass at a lower acetone concentration than PNVF. Swelling is normalized to show the transition. Formulation for both is 15 x 1.41 (T x C\*).



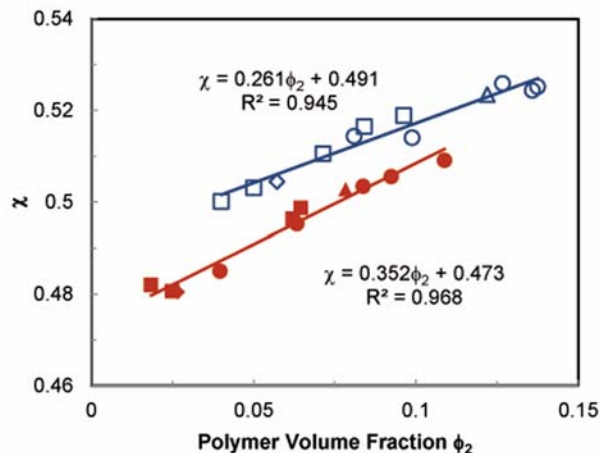
**Supplementary Figures S-9.2a and S-9.2b: E ~2x greater in PAAm than PNVF**

The Young's modulus E for PNVF (closed symbols) follows the same trends as PAAm (open symbols) with monomer and cross-linker concentration, but the values are only about half the PAAm values. Most error bars are smaller than symbols. Cross-linker concentration, C\*: (◆) 0.23; (■) 0.46; (●) 1.41; (▲) 2.35.



**Supplementary Figure S-9.3a and S-39.b: G falls on a single curve when plotted against the polymer volume fraction**

The data of Figure 9.6 fall onto a single curve when plotting shear modulus against polymer volume fraction for PNVF (closed symbols) and PAAm (open symbols). Most error bars are smaller than symbols. Cross-linker concentration,  $C^*$ : ( $\blacklozenge$ ) 0.23; ( $\blacksquare$ ) 0.46; ( $\bullet$ ) 1.41; ( $\blacktriangle$ ) 2.35



**Supplementary Figure S-9.4: Flory-Huggins parameter lower in PNVF, more hydrophilic in**

Linear dependence of Flory-Huggins parameter as a function of polymer volume fraction for PNVF (closed symbols) and PAAm (open symbols) using the phantom model. The trends are similar for both the phantom and the affine models (Figure 10 in the main paper). Cross-linker concentration,  $C^*$ : ( $\blacklozenge$ ) 0.23; ( $\blacksquare$ ) 0.46; ( $\bullet$ ) 1.41; ( $\blacktriangle$ ) 2.35.

**Supplementary Table S-9.1: Calculated parameters for PNVF gels using phantom network model.**

T (g/mL)	C (g/g)	C* (mol/mol)	M <sub>c</sub> (g/mol)	Cross-link Density, ρ <sub>x</sub> (mol/cm <sup>3</sup> )	Theoretical Cross-link Density, ρ <sub>t</sub> (mol/cm <sup>3</sup> )	Cross-linker Efficiency	χ
8.0	1.37	0.46	5.50E+04	1.85E-05	5.70E-05	0.32	0.48
10.0	1.37	0.46	3.33 E+04	3.05E-05	5.70E-05	0.53	0.48
10.0	4.08	1.41	1.50 E+04	6.79E-05	1.73E-04	0.39	0.49
15.0	0.69	0.23	3.82 E+04	2.66E-05	2.84E-05	0.94	0.48
15.0	1.37	0.46	1.68 E+04	6.06E-05	5.70E-05	1.06	0.47
15.0	4.08	1.41	9.54 E+03	1.07E-04	1.73E-04	0.62	0.50
15.0	6.75	2.37	7.19 E+03	1.41E-04	2.91E-04	0.49	0.50
20.0	1.37	0.46	1.27 E+04	8.02E-05	5.70E-05	1.41	0.50
20.0	4.08	1.41	7.41 E+03	1.37E-04	1.73E-04	0.79	0.50
25.0	1.37	0.46	1.46 E+04	6.95E-05	5.70E-05	1.22	0.50
25.0	4.08	1.41	6.97E+03	1.46E-04	1.73E-04	0.84	0.50
30.0	4.08	1.41	5.43 E+03	1.87E-04	1.73E-04	1.08	0.50

**Supplementary Table S-9.2: Calculated parameters for PAAM gels using phantom network model.**

T (g/mL)	C (g/g)	C* (mol/mol)	M <sub>c</sub> (g/mol)	Cross-link Density, ρ <sub>x</sub> (mol/cm <sup>3</sup> )	Theoretical Cross-link Density, ρ <sub>t</sub> (mol/cm <sup>3</sup> )	Cross-linker Efficiency	χ
8.0	1.0	0.46	2.92E+04	3.84E-05	7.22E-05	0.53	0.50
10.0	1.0	0.46	2.25E+04	4.99E-05	7.22E-05	0.69	0.50
10.0	3.0	1.41	1.02E+04	1.10E-04	2.19E-04	0.50	0.51
15.0	0.5	0.23	2.17E+04	5.16E-05	3.60E-05	1.43	0.50
15.0	1.0	0.46	1.59E+04	7.07E-05	7.22E-05	0.98	0.51
15.0	3.0	1.41	6.25E+03	1.79E-04	2.19E-04	0.82	0.51
15.0	5.0	2.37	4.45E+03	2.52E-04	3.69E-04	0.68	0.52
20.0	1.0	0.46	1.59E+04	7.05E-05	7.22E-05	0.98	0.52
20.0	3.0	1.41	5.20E+03	2.16E-04	2.19E-04	0.98	0.53
25.0	1.0	0.46	1.26E+04	8.92E-05	7.22E-05	1.24	0.52
25.0	3.0	1.41	4.27E+04	2.63E-04	2.19E-04	1.20	0.52
30.0	3.0	1.41	4.76E+04	2.36E-04	2.19E-04	1.08	0.53

## Chapter 10: High Charge Density Interpenetrating Hydrogels of Hydrolyzed Networks of Poly(N-Vinyl Formamide) and Polyacrylamide<sup>10</sup>

### Abstract

The primary goal of this work was to make tough hydrogels from high charge density IPNs of hydrolyzed networks of poly(N-vinylformamide) PNVF and polyacrylamide (PAAm). The hypothesis was that IPNs of PNVF and PAAm will have intimate molecular mixing of the two networks to help maximize charge-charge interactions of the networks after hydrolysis to polyvinylamine (PVAm) and polyacrylic acid (PAAc). Therefore, the same charge density of the two networks would lead to maximizing charge complexation. Earlier work on SN PAAm and SN PNVF show that they have similar  $\chi$  parameters and they also have similar structures being isomers of each other; suggesting IPNs will have minimal molecular phase separation. IPNs of both PNVF/PAAm and PAAm/PNVF were synthesized and were optically transparent, an indication of homogeneity at submicron length scales. Both IPNs were successfully hydrolyzed to PVAm/PAAc and PAAc/PVAm as indicated by a ~5-fold or greater decrease in swelling at intermediate pH values (3-6), consistent with the hypothesis of charge complexation. Finally, tough networks were achieved as shown in the mechanical tests with failure stresses (~14 MPa) comparable to the tough double-network hydrogels of MCS/PAAm.

---

<sup>10</sup>To be published as **Tiffany C. Suekama**, Cory J. Berkland, Stevin H. Gehrke



## Introduction

Hydrogels can be cross-linked by either irreversible chemical interactions (covalent bonds) or reversible physical interactions (van der Waals interactions, ionic interactions or dipole-dipole interactions such as hydrogen bonding).<sup>[136,156,183]</sup> Their ability to contain over 95% water content is a physical property that is desirable in many applications; in particular, hydrogels are being studied for use in the advancement of biomedical and pharmaceutical fields.<sup>[137]</sup> However, many hydrogels have poor mechanical properties. Double-networks have gained a lot of interest due to their superior mechanical properties, especially toughness. However, the accepted model for the improved toughness is from the energy dissipation mechanisms of the brittle first network breaking while the second holds the entire construct together. The problem with DNs are the sacrificial bonds from the first network are irreversibly damaged which is a limitation to applications such as tissue engineering where a continuous force may be applied. Therefore, the goal of this work was to create a high charge complexed network in which the interactions would provide reversible sacrificial bonds.

PNVF can be hydrolyzed to form PVAm. PVAm is a high density cationic hydrogel that can be readily functionalized and cannot be formed through direct methods. The PNVF hydrogels were previously created from cross-linking aqueous NVF solutions using a novel cross-linker, 2-(N-vinylformamido)ethylether (NVEE) and the thermally-activated initiator VAZO-44. We have found that for the same formulation of PNVF to PAAm, PNVF was slightly more hydrophilic, but the PNVF formulation can be modified to match the same swelling degree of PAAm gels, therefore having the same mechanical strength. Due to the monomers of PAAm and PNVF being isomers of each other and both forming neutral networks, intimate molecular mixing is hypothesized to occur. Upon hydrolysis, both networks can form high charge density networks. Thus, synthesis

PAAm/PNVF and PNVF/PAAm networks followed by hydrolysis was hypothesized to lead to collapse and improved failure properties due to the charge complexation when the charges are an equimolar ratio.

## Materials and Methods

### *Materials*

The reagents for PNVF and PAAm networks are as follows.<sup>[166]</sup> N-vinylformamide (NVF; Sigma-Aldrich: 98%) monomer was purified by distillation under vacuum at 80°C and stored at –10°C prior to polymerization. A novel cross-linker, 2-(N-vinylformamido) ethyl ether (NVEE; liquid of density of 1.3 g/mL), was synthesized and characterized by our previously reported procedure.<sup>19,20,26</sup> The monomer, acrylamide (AAm; Sigma-Aldrich: 99+ %) and the cross-linker, N,N'-methylenebisacrylamide (BIS; Sigma-Aldrich: 99+ %) are electrophoresis grade and were used as received. Hydrolysis was carried out using 0.1 M NaOH (Fisher Scientific). The initiator, 2,2'-Azobis[2-(2-imidazolin-2-yl)propane]dihydrochloride (VA-044; Wako Pure Chemical Industries, Ltd) was used as received. Various pH solutions were made by dilution of stock solutions of HCl (Fisher Scientific) and NaOH.

### *Synthesis of single-network hydrogels*

PNVF and PAAm were synthesized using the gel formulation notation,  $T \times C^*$ , as previously described in Chapter 9.<sup>[166]</sup> The procedure for synthesizing a single-network of PNVF or PAAm was similar to procedure in Chapter 9.<sup>[166]</sup> However, both PNVF and PAAm networks were synthesized using a thermal initiator VA-044. A solution is created by adding monomer, cross-linker and initiator to water. The solution was mixed, bubbled with nitrogen for 15 min to displace

dissolved oxygen, and then pipetted into molds consisting of two glass plates with a 2mm height silicon spacer. The molds were wrapped with Saran wrap and clamped with binder clips to eliminate evaporation. The free radical polymerization was carried out at 50°C in a preheated oven for 24 hrs. After the reaction was complete the molded SN of PNVF or PAAm resulted. Figure 10.1 shows a schematic of the types of hydrogels synthesized in this study and the treatments performed.

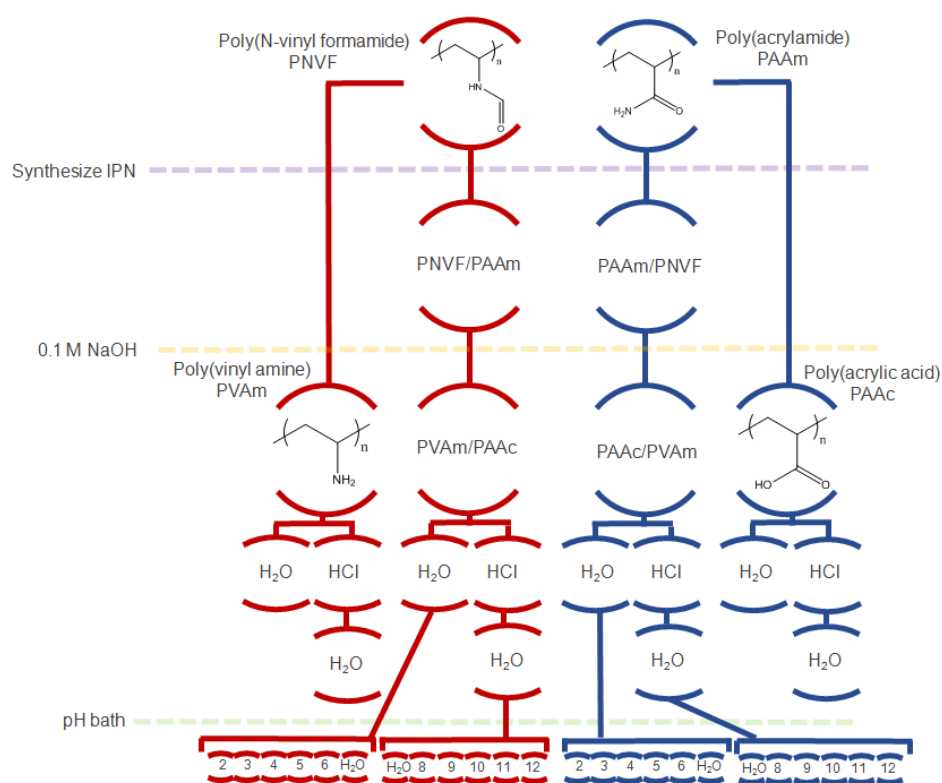


**Figure 10.1: Schematic of formulations and the treatments.**

Swelling and mechanical testing were done on all of these hydrogels.

### *Synthesis of IPN hydrogels*

To synthesize an IPN of PNVF/PAAm or PAAm/PNVF the first network was soaked in a solution of the second network for ~ 48 hours. Then the soaked gels are placed between two glass plates, wrapped with saran wrap and placed in a 50°C oven for 24 hrs. The resulting hydrogel is

an IPN of PNVF/PAAm or PAAm/PNVF. The IPNs were cut into cylindrical disks (~4 mm diameter and ~2 mm height) before hydrolysis.

### *Hydrolysis of hydrogels*

The hydrolysis conditions to achieve complete hydrolysis with mildest conditions (low NaOH, low temperature and shortest time) was determined from our group and prior research to be 0.1M NaOH at 60°C for 24 hours.<sup>[55,120,170]</sup> Hydrolysis and titration protocol is listed in Appendix 10. Cylindrical disks of PNVF, PAAm, PNVF/PAAm and PAAm/PNVF hydrogels were hydrolyzed by placing the gels in a container of 0.1 M NaOH and then placing in the oven at 60°C for 24 hours. The hydrolyzed gels were leached in water, changing the water multiple times to remove residual chemicals for 24 hours. Thus, leaving the carboxylic acid in the sodium salt form  $\text{RCOO}^-\text{Na}^+$  and the amines in the free base form  $\text{RNH}_2$ . Half of the hydrogels were placed in 0.1M HCl, changing the HCl solution multiple times, for 24 hours and then placed back in water (changing the water multiple times) to remove residual HCl, again for 24 hours. Thus, the carboxylic acid groups will be in the unionized state  $\text{RCOOH}$  and the amines are in the hydrochloride salt  $\text{RNH}_3^+\text{Cl}^-$ .

The hydrolyzed IPNs of PVAm/PAAc and PAAc/PVAm which were not treated with HCl were placed in pH baths of either a pH of 2, 3, 4, 5, 6 and the IPNs that were treated with HCl were placed in a pH bath of either a pH of 8, 9, 10, 11 or 12. The gels were soaked for 48 hours changing the pH bath multiple times. The pH of the solution of all of the baths was measured. In many occasions the pH was different from the original bath solution (even at equilibrium) because the gel acts as a buffer, therefore the final pHs of the solutions were taken by a pH probe. The reported data was correlated with these measured pHs.

### ***Swelling and mechanical tests***

The procedure for swelling and the mechanical analysis were followed as previously described in Chapter 10.<sup>[166]</sup>

The degrees of swelling,  $Q$  (g/g), are reported as the mass of the swollen gel over the mass of the desiccator-dried gel.<sup>[166]</sup>

Unconfined, uniaxial compression was performed using RSA III dynamic mechanical analyzer (TA Instruments) at a rate of 0.05 mm/s. The sample diameter was measured using a micrometer under a standard stereomicroscope ( $\sim 10\times$  magnification). The compression plates were protected by a nitrile layer which was lubricated with mineral oil. The nitrile layer protected the platens from harsh pH conditions but did not affect the mechanical test results. The stress-strain curves were evaluated to determine the mechanical properties.

### ***Equilibrium Swelling Degree and Mechanical Analysis***

The synthesis of both PAAm/PNVF and PNVF/PAAm hydrogels resulted in a swelling degree of 10. After hydrolysis of both of the IPNs equilibrium swelling degree increased from a swelling degree of 10 to  $\sim 20$ . After the IPNs were hydrolyzed to PVAm/PAAc and PAAc/PVAm they were subjected to different treatments outlined in Figure 10.1.

From the treatments, the equilibrium swelling degree of the IPNs of PVAm/PAAc (closed symbols) and PAAc/PVAm (open symbols) were plotted against the pH, Figure 10.2a. Immediately after hydrolysis the swelling degree was 18 for PAAc/PVAm and around 23 for PVAm/PAAc. Upon the hydrolyzed gels in water both of the gels continued to swell to an equilibrium swelling of 27 for PAAc/PVAm and 46 for PVAm/PAAc. When the IPNs were soaked in 0.1M HCl the gels collapsed. These gels were subjected to pH baths from a pH of 2 to a pH of 6. The gels remained collapsed but at a low pH the gel swells to 14 for PAAc/PVAm and 21 for

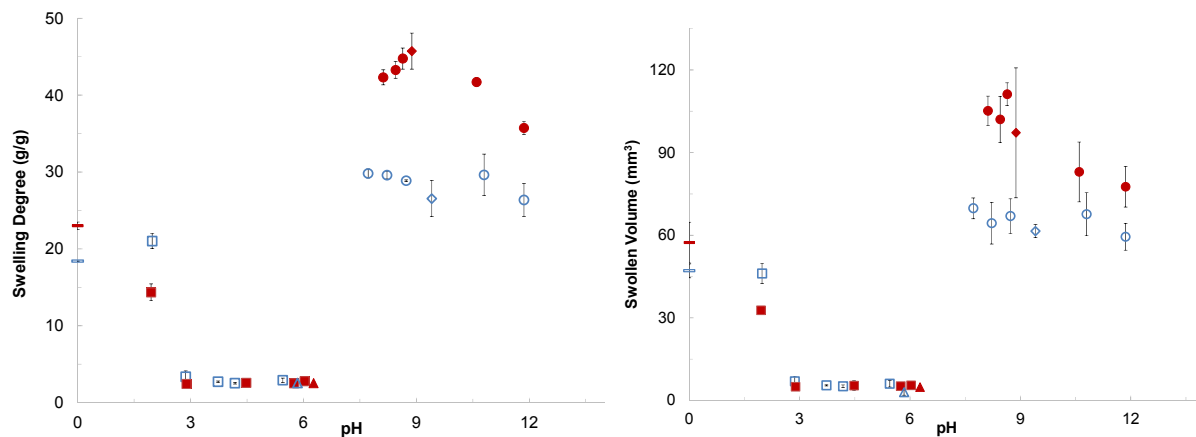
PVAm/PAAc. At higher pHs (8-18), the swelling degree is around 30 for PAAc/PVAm and around 40 for PVAm/PAAc. The PVAm/PAAc IPN shows a decrease in swelling degree at above a pH of 10. The trend that the PVAm/PAAc gel decrease with increasing pH becomes more obvious when the swollen volume is plotted against pHs from 8-10, Figure 10.2b. The other trends in the Figure 10.2a are consistent with Figure 10.2b. At higher pHs the swollen volume increases until a maximum is reached and then decreases.

## Results

The synthesis of both PAAm/PNVF and PNVF/PAAm hydrogels resulted in a swelling degree of 10. After hydrolysis of both of the IPNs equilibrium swelling degree increased from a swelling degree of 10 to ~20. After the IPNs were hydrolyzed to PVAm/PAAc and PAAc/PVAm they were subjected to different treatments outlined in Figure 10.1.

From the treatments, the equilibrium swelling degree of the IPNs of PVAm/PAAc (closed symbols) and PAAc/PVAm (open symbols) were plotted against the pH, Figure 10.2a. Immediately after hydrolysis the swelling degree was 18 for PAAc/PVAm and around 23 for PVAm/PAAc. Upon the hydrolyzed gels in water both of the gels continued to swell to an equilibrium swelling of 27 for PAAc/PVAm and 46 for PVAm/PAAc. When the IPNs were soaked in 0.1M HCl the gels collapsed. These gels were subjected to pH baths from a pH of 2 to a pH of 6. The gels remained collapsed but at a low pH the gel swells to 14 for PAAc/PVAm and 21 for PVAm/PAAc. At higher pHs (8-12), the swelling degree is around 30 for PAAc/PVAm and around 40 for PVAm/PAAc. The PVAm/PAAc IPN shows a decrease in swelling degree at above a pH of 10. The trend that the PVAm/PAAc gel decrease with increasing pH becomes more obvious when the swollen volume is plotted against pHs from 8-10, Figure 10.2b. The other trends in the

Figure 10.2a are consistent with Figure 10.2b. At higher pHs the swollen volume increases until a maximum is reached and then decreases.



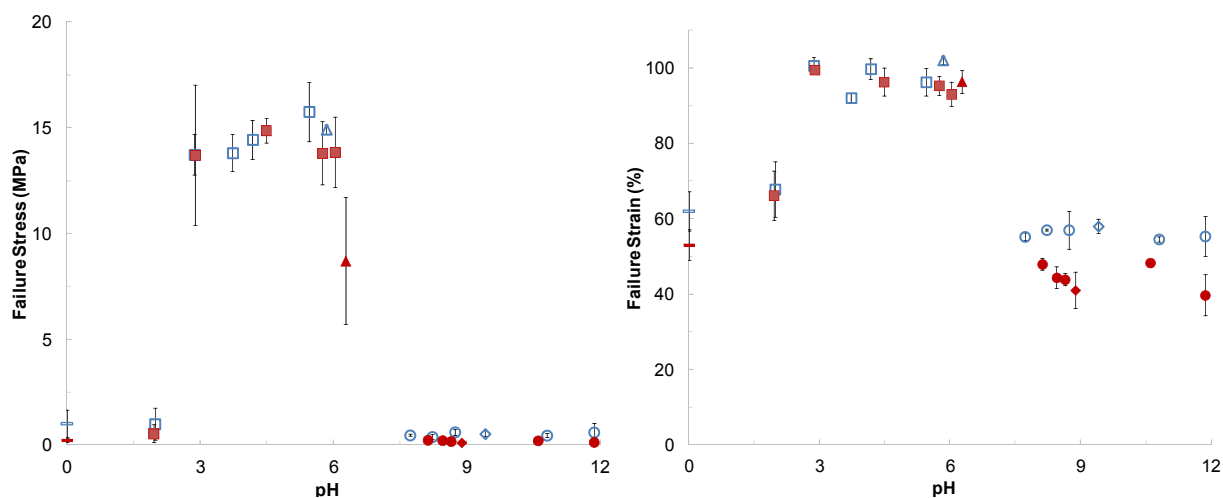
**Figures 10.2a and 10.2b: Decreased swelling degree at intermediate pHs indicate complexation**

Charge complexation is shown in the intermediate pHs as swelling in the IPNs. IPNs of PAAm/PNVF and PNVF/PAAm were hydrolyzed to PVAm/PAAc (closed symbols) and PAAc/PVAm (open symbols). After hydrolysis: (—) not treated, right after hydrolysis; (◆) treated with water; (▲) treated with 0.1M HCl and then water; (■) treated with 0.1M HCl, water and then pH (varied from 2-6); (●) treated with water and then pH (varied from 8-12).

Both sets of IPNs had improved failure stress and failure strain, at the intermediate pHs, Figures 10.3a and 10.3b. The failure strains, Figure 10.3b, at the intermediate pHs (3-7) were all around 100% and a few of the gels did not break. The failure stresses are around 14 MPa, Figure 10.3a.

The PVAm/PAAm IPN treated with 0.1M HCl and then water has a failure stress which is a bit lower than 14MPa. On a closer inspection, of the stress-strain data of this PVAm/PAAm IPN, the general curve follows the PAAc/PVAm gel analogous treatment but prematurely failed leading to large deviations in failure stress and large error even though the point fits in the failure strain. This could be due to the gel being close to a transition region and the gel not being completely

homogeneously complexed leading to defects in the gel. Additionally, when the charge complexation is not as strong (at high and low pH) the PAAc/PVAm hydrogels typically fail at higher stresses and strains than the PVAm/PAAc hydrogels. This work is comparable to double-network hydrogels which have failure stresses around 6 MPa and a swelling degree around 8 under compression, data in Chapter 6.



**Figures 10.3a and 10.3b: Charge complexed IPNs show large improvements in failure stress (10.3a) and failure strain (10.3b)**

At intermediate pHs the failure properties are improved in comparison to the uncomplexed state. IPNs of PAAm/PNVF and PNVF/PAAm were hydrolyzed to PVAm/PAAc (closed symbols) and PAAc/PVAm (open symbols). After hydrolysis: (—) not treated, right after hydrolysis; (◆) treated with water; (▲) treated with 0.1M HCl and then water; (■) treated with 0.1M HCl, water and then pH (varied from 2-6); (●) treated with water and then pH (varied from 8-12).

Figure 10.4 depicts that the toughness of the IPNs follow the general trends from the failure stress and failure strain data in Figures 10.3a and 10.3b. At the intermediate pHs the toughnesses of both the IPN gels are greatly improved to the uncomplexed state. The PAAc/PVAm IPN has a higher toughness than the corresponding PVAm/PAAc in all of the conditions; this trend becomes



clear at intermediate pHs of the toughness, although the toughness is not greater in PAAc/PVAm IPNs in comparison to PVAm/PAAc hydrogels in the intermediate pHs.

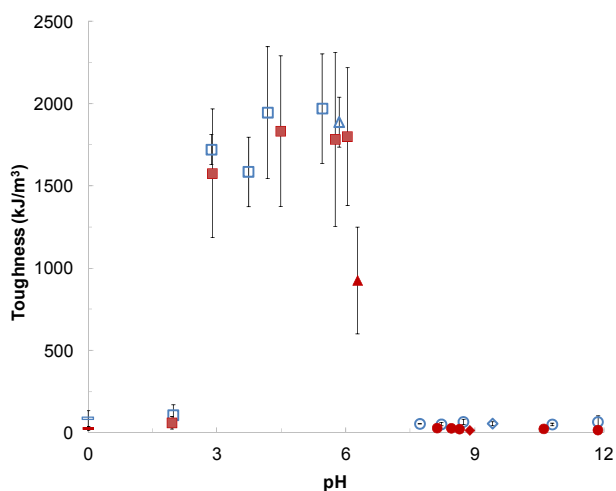


**Figure 10.4: Toughness improved at intermediate pHs**

Toughness of the at the intermediate pHs are much greater than at uncomplexed state. IPNs of PAAm/PNVF and PNVF/PAAm were hydrolyzed to PVAm/PAAc (closed symbols) and PAAc/PVAm (open symbols). After hydrolysis: (—) not treated, right after hydrolysis; (◆) treated with water; (▲) treated with 0.1M HCl and then water; (■) treated with 0.1M HCl, water and then pH (varied from 2-6); (●) treated with water and then pH (varied from 8-12).

Investigating the failure properties (failure stress and failure strain) of the IPNs as a function of swelling and the polymer volume fraction are shown in Figures 5-8. When plotting the failure strain versus the equilibrium swelling degree, the failure strain decreases linearly with increasing swelling Figure 10.5. Also, when plotting the failure strain versus the polymer volume fraction, Figure 10.8a and 8b, as the failure strain is increased there is an increase in the polymer volume fraction at low polymer volume fraction and at higher polymer volume fractions there is no trend due to being the extent of compression, 100% strain. Figures 10.6a, 10.6b and 10.6c show the failure stress as a function of the equilibrium swelling degree and Figures 10.7a and 10.7b show the failure stress as a function of polymer volume fraction. Figure 10.6b is a close up of the lower

swelling in Figure 10.6a and show that the swelling degree does not affect the failure stress, also observed in Figure 10.7a. Figure 10.6c is a close up of the higher swelling degrees in Figure 6a and show a loose correlation of an increase in swelling leads to a decrease in failure stress, also observed in Figure 10.7b.

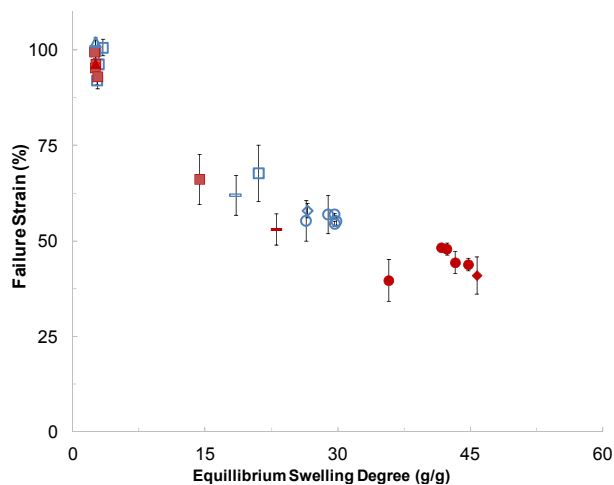
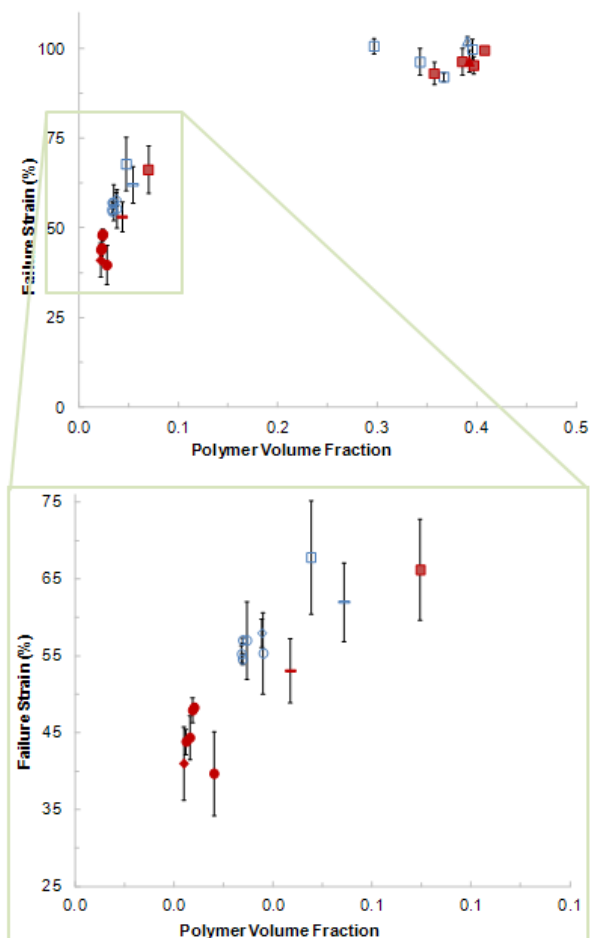


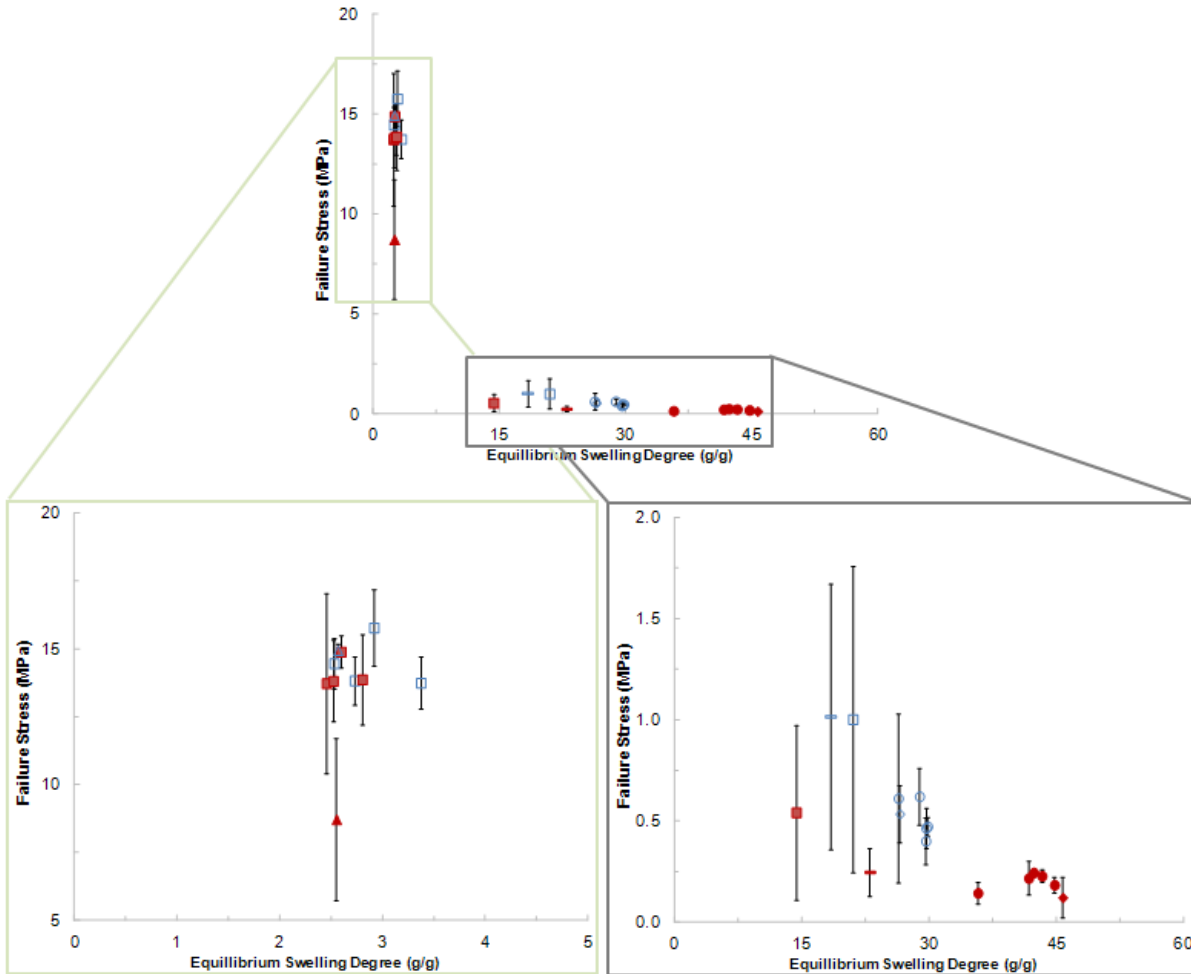
**Figure 10.5: Failure strain decreases with increasing equilibrium swelling**

IPNs of PAAm/PNVF and PNVF/PAAm were hydrolyzed to PVAm/PAAc (closed symbols) and PAAc/PVAm (open symbols). After hydrolysis: (—) not treated, right after hydrolysis; (◆) treated with water; (▲) treated with 0.1M HCl and then water; (■) treated with 0.1M HCl, water and then pH (varied from 2-6); (●) treated with water and then pH (varied from 8-12).



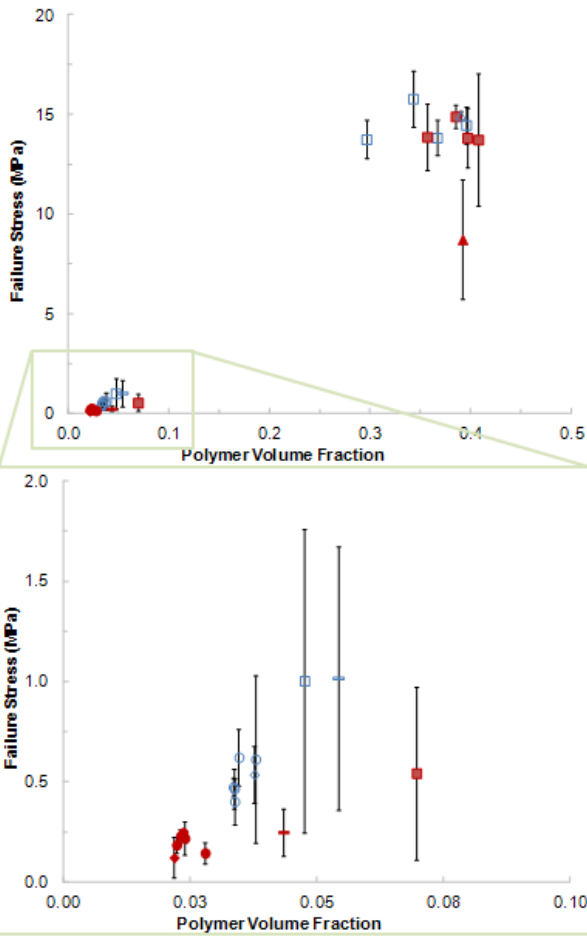
**Figures 10.8a and 10.8b: Failure strain increases with increasing polymer volume fraction at low polymer volume fraction**

At higher polymer volume fractions there is no trend this is possibly from the limit of compression. IPNs of PAAm/PNVF and PNVF/PAAm were hydrolyzed to PVAm/PAAc (closed symbols) and PAAc/PVAm (open symbols). After hydrolysis: (—) not treated, right after hydrolysis; (◆) treated with water; (▲) treated with 0.1M HCl and then water; (■) treated with 0.1M HCl, water and then pH (varied from 2-6); (●) treated with water and then pH (varied from 8-12).



**Figures 10.6a, 10.6b and 10.6c: Failure stress decreasing at high swelling degrees and no obvious trends at lower swelling**

IPNs of PAAm/PNVF and PNVF/PAAm were hydrolyzed to PVAm/PAAc (closed symbols) and PAAc/PVAm (open symbols). After hydrolysis: (—) not treated, right after hydrolysis; (◆) treated with water; (▲) treated with 0.1M HCl and then water; (■) treated with 0.1M HCl, water and then pH (varied from 2-6); (●) treated with water and then pH (varied from 8-12).



**Figures 10.7a and 10.7b: Failure stress slightly increasing at small polymer volume fractions**

IPNs of PAAm/PNVF and PNVF/PAAm were hydrolyzed to PVAm/PAAc (closed symbols) and PAAc/PVAm (open symbols). After hydrolysis: (—) not treated, right after hydrolysis; (◆) treated with water; (▲) treated with 0.1M HCl and then water; (■) treated with 0.1M HCl, water and then pH (varied from 2-6); (●) treated with water and then pH (varied from 8-12).

## Conclusions

This work has demonstrated the synthesis of neutral IPN networks of PAAm/PNVF or PNVF/PAAm. These IPN hydrogels produced optically transparent gels, an indication of homogeneity at submicron length scales. Thus, the two networks were hypothesized to have intimate molecular mixing to help maximize charge-charge interactions after the networks were hydrolyzed. The two IPNs were successfully hydrolyzed to PAAc/PVAm and PVAm/PAAc hydrogels. Both IPNs showed deswelling of ~5 fold at intermediate pHs (3-6) indicating charge complexation. Further, the failure properties were 15 times greater in the collapsed state in comparison to right after hydrolysis. The IPNs in the collapsed state were showing toughness values on the order of ~1500 kJ/m<sup>3</sup>. Further work is needed to uncouple the effects of swelling to the mechanical properties, however, these gels had superior mechanical properties which were comparable to DNs of MCS/PAAm.

## Chapter 11: An Introduction to a New Technique for Visualizing Hydrogel Networks: dSTORM Microscopy<sup>11</sup>

### Abstract

The aim of this work was to develop non-invasive imaging technique to visualize the individual polymer networks strands of hydrated hydrogels, a long term aspiration to many scientists. Through the development of super resolution techniques such as direct stochastic optical reconstruction microscopy (dSTORM), imaging on the nanoscale (~20nm) has become possible. To the best of our knowledge, dSTORM imaging has never been applied to hydrogels. Thus, this work successfully fluorescently tags both a poly(acrylic acid)(PAAc) and tetra-polyethylene glycol (tetra-PEG) hydrogel network and then imaged the hydrogel network using dSTORM. Results revealed pores around 200-400 nm in diameter in the PAAc hydrogel. This work is an introduction to applying dSTORM imaging technique to visualize the network structure of hydrogels to hopefully be applicable to many different hydrogels.

---

<sup>11</sup> Initial data was possible with the help of the University of Melbourne: Angus Johnston and Benjamin Hibbs as well as the University of Tokyo: Shinji Kondo, Takamasa Sakai, and Ung-il Chung

## Introduction

In recent years, imaging subdiffraction levels have become possible through the development of super resolution techniques.<sup>[71,176,200]</sup> Tradition light microscopy has a spatial resolution limit of ~250nm and using super-resolution florescence microscopy imaging techniques researchers have been able to image down to ~20nm.<sup>[112,136]</sup> Super resolution microscopy is most commonly applied to biology, such as imaging biological structures, and to our knowledge has never been applied to gels. One of the techniques, direct stochastic optical reconstruction microscopy (dSTORM), images a single-molecule, fluorophore.<sup>[183,200]</sup> This technique works by activating, by an oxidizing and reducing buffer, and localizing a single-molecule fluorescent probe and then imaging these switchable fluorophores to resolve sub-diffraction-limited spatial features. These fluorophores are photoswitching which they are excited.<sup>[63,183]</sup> The fluorophores are tracked and reconstructed to find the position of the single-molecule.<sup>[63,183]</sup>

The goals of the project are two-fold. (1) To develop a new technique to image the network structure of hydrogels in the hydrated state. (2) To apply the technique to answer important questions about the network structure of hydrogels. First of all, imaging hydrated hydrogels under dSTORM would be a new technique in the field. Visualizing the hydrogels network would lead to pertinent information about the network structure. An important aspect to the network structure is the rate of diffusion of bioactive molecules such as cells, small molecules such as drugs and proteins and other solutes.<sup>[139]</sup> Another aspect is the relationship between the structure and the mechanical properties of hydrogels. Imaging the network structure on the nanoscale in hydrated hydrogels is important for many applications such as drug delivery and tissue engineering. Thus, being able to visualize hydrogel networks in their natural state is an aspiration of many scientists.



This work intended to contrast heterogeneous, free radical polymerized (FR) hydrogels with the tetra-PEG hydrogels which are believed to have homogeneous networks, with the hypothesis that the difference in the networks structure will be observable using dSTORM. In FR polymerizations the growth and termination of the polymers are quick which leads to a varied number of chain lengths (high polydispersity) and heterogeneous structures. At the University of Tokyo Dr. Sakai and Dr. Chung work on the homogeneous structure of tetra-polyethylene glycol (PEG).<sup>[91,92,109]</sup> Tetra-PEG hydrogels form homogeneous networks and have a reduction number of defects and improved mechanical properties.<sup>[86,106,142,179]</sup> The objective of this work was to look at the differences between a polyacrylamide hydrogel (heterogeneous network and common hydrogel) and a tetra-PEG hydrogel (with a homogeneous network) under dSTORM microscopy. Thus, collaboration was established between three groups (the University of Kansas, the University of Melbourne and the University of Tokyo). The members at the University of Kansas developed the idea of imaging hydrogels using dSTORM. These members worked with the University of Melbourne to attach the fluorophores and develop methods for imaging hydrogels using dSTORM, and worked with the University of Tokyo to have tetra-PEG samples shipped to be analyzed.

## **Materials and Methods**

### ***Synthesis of heterogeneous network (PAAm) and samples of heterogeneous networks (tetra-PEG)***

The polyacrylamide hydrogels (PAAm; Life Technologies, SDS-PAGE NuPAGE® Bis-Tris Precast Gels) were hydrolyzed to polyacrylic acid (PAAc) by placing the PAAm gels in vial with

0.1M NaOH solution and then placing the vial in a 60°C oil bath for 24 hours. The procedure for hydrolysis was previously determined from previous research and can be found in hydrolysis and titration protocol is listed in Appendix 10. After hydrolysis the gels were rinsed in DI water and water was exchanged several times over a few days. The PAAc gels were fluorescently dyed by a coupling reaction of the carboxylic acid groups on the polyacrylic acid and Alexa fluor 647 cadaverine dye (alexa 647) with 4-(4,6-Dimethoxy-1,3,5-triazin-2-yl)-4-methylm orpholinium chloride (DMTMM).<sup>[29]</sup> The labeling density is as follows: 10µL of alexa 647 (1mg/mL concentration) in 200µL DI water and 100µL DMTMM (10mg/mL concentration).

The University of Tokyo group sent samples of tetra-PEG gels: Sample 1: 10K Tetra-PEG gels (10 kg/mol Tetra-PEG-NH<sub>2</sub> + 10 kg/mol Tetra-PEG OSu), volume fraction in the as-prepared state = 0.081; Sample 2: 20K Tetra-PEG gels (20 kg/mol Tetra-PEG-NH<sub>2</sub> + 20 kg/mol Tetra-PEG OSu), volume fraction in the as-prepared state = 0.081; Sample 3: 40K Tetra-PEG gels (40 kg/mol Tetra-PEG-NH<sub>2</sub> + 40 kg/mol Tetra-PEG OSu), volume fraction in the as-prepared state = 0.081. The tetra-PEG samples were fluorescently dyed by a coupling reaction of the amine groups on the tetra-PEG and the amine-reactive Alexa Fluor 647 carboxylic acid, succinimidyl ester dye. The labeling density is as follows for the 20K tetra-PEG 0.2 µL of alexa 647 (1mg/mL concentration) in 200µL DI water and for 10K tetra-PEG 0.04 µL of alexa 647 (1mg/mL concentration) in 200µL DI water.

For the coupling reaction a thin, to minimize diffusion time, hydrogel sample was added to a vial with the dye and water (DMTMM for PAAc gels). The vial was covered with foil and placed on a shaker for 24 hours. The gel was leached many times over 24 hours of any unreacted chemicals. The resulting gel has an extremely light blue tinted color from the fluorescently dye.

## Imaging

The dSTORM images were acquired on a Nikon – N –Storm (N-STORM) system using an objective CFI Apo TIRF 100x 1.49 oil and an EM-CCD Camera iXon DU897 (Andor). The software used to was NIS-Elements Ar. Figure 11.1 is a schematic of how the gels were prepared for imaging. The gels were sliced with a razor blade as thin as possible and placed on a cleaned cover slide (cleaned with 1M NaOH, sonicated for 30 min and then rinsed with DI water). A small cover slip was added to the top of the gel and then a silicon rubber mold was used to hold in the buffer solution. The buffer was added so the gel was fully submerged. Following the imaging buffering protocol in the N-storm manual, the buffer consisted of 70  $\mu$ L of a 1 M MEA (cystaemine) Glox and 620  $\mu$ L of buffer B (50 mM tris-HCl pH 8 with 10 mM NaCl and 10% glucose). Another cover slide was added to the top to enclose the buffer/solution to prevent evaporation.

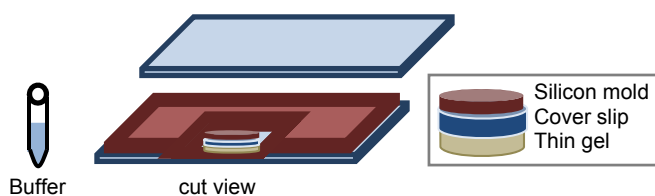


**Figure 11.1: Schematic of the layered view of the prepared gel for imaging.**

## Results and Discussion

The first goal of this work was to successfully image a hydrogel using dSTORM but in order to image it was necessary to get adequate labeling density of both a PAAc and a tetra-PEG hydrogel with alexa 647 fluorophore through two different reactions that both resulted in peptide bonds. The preferred labeling densities for all of the gels were previously described in the methods

section. Once the gels were labeled they prepared for imaging. As previously described the gels were thinly cut. This was important to be able to get clear images. A cover slip and silicon mold was placed on top of the gel to hold it in place when the buffer was added. The enclosed system was imaged using dSTORM. To the best of our knowledge, this is the first hydrogel to be imaged using dSTORM technique.

Secondly, this work aimed to visualize the network structure and to show differences between heterogeneous structure formed from FR techniques such as PAAc and homogeneous networks such as tetra-PEG hydrogels. An example of a 2-D image produced from dSTORM is shown in Figure 11.2. From Figure 11.2, at this point there is speculation that pores of a dimension of 200-400 nm are visible. Although, more work on developing adequate analysis and processing techniques is needed to interpret and best display the results.

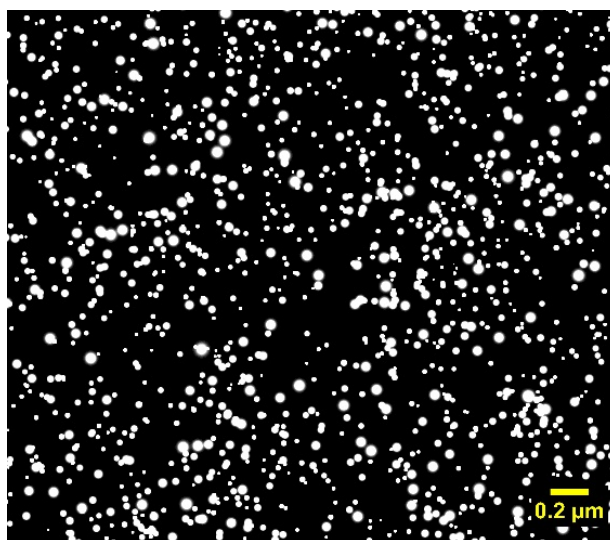


**Figure 11.2: Image of a PAAc hydrogels through dSTORM.**

Further analysis is needed to provide statistical evidence of pores around 200-400 nm.

## Conclusions and Future Directions

This work introduces a new technique to visualize hydrogel networks in the hydrated state. This work shows it is possible to use super resolution microscopy for single-molecule imaging down to nanoscale (~20nm) resolution which helps to gain an understanding of the network. Further advances in processing techniques is needed to extract relevant information about the network structure, but developing methods for imaging hydrogels has hopefully open up doors to new ways of imaging hydrogels. Potential future areas of using dSTORM imaging on hydrogel networks in the hydrated state: (1) Visualize the cracks in the network live as the crack propagates; therefore, being able to study the failure mechanisms in hydrogel networks. Also, dSTORM producing multi-color images by using multiple fluorophore probes which activate at different wavelengths<sup>[183]</sup> <sup>[15,185]</sup>, opening up the possibility for studying (2) the interactions of multi-component hydrogel networks such as interpenetrating networks or (3) the interactions of the extracellular matrix (ECM) of cells with the hydrogel networks or cellular development investigating tissue formation and function or (4) diffusion and transport of molecules through the hydrogel network via kinetic studies or tracking single-molecules such as drugs or proteins as they diffuse through the network.

## Chapter 12: Conclusion and Recommendations for Future Work

This dissertation advances the knowledge on the properties and mechanisms of multi-component hydrogel systems by correlating swelling, mechanical properties (toughness, failure properties, modulus, tearing energy), calculated properties ( $\chi$ , cross-link density, molecular weight between cross-links) and images (pore size). Specifically, three types of interpenetrating network (IPN)s were investigated: semi-IPNs of agarose/poly(ethylene glycol) (PEGDA), double-network (DN)s of methacrylated chondroitin sulfate (MCS)/polyacrylamide (PAAm) and MCS/poly(*N, N*-dimethyl acrylamide) (PDMAAm) and IPNs with charge complexation by hydrolyzing PAAm/poly(*N*-vinyl formamide) (PNVF) and PNVF/PAAm networks. The basic science of the complexities of the network interactions in multi-component hydrogels were explored to create networks which are tough and can withstand continual loading. These hydrogels help to overcome some of the limitations of hydrogels in potential fields such as tissue engineering, drug delivery and separations. Figure 12.1 wraps up the progression of the aims throughout this dissertation.

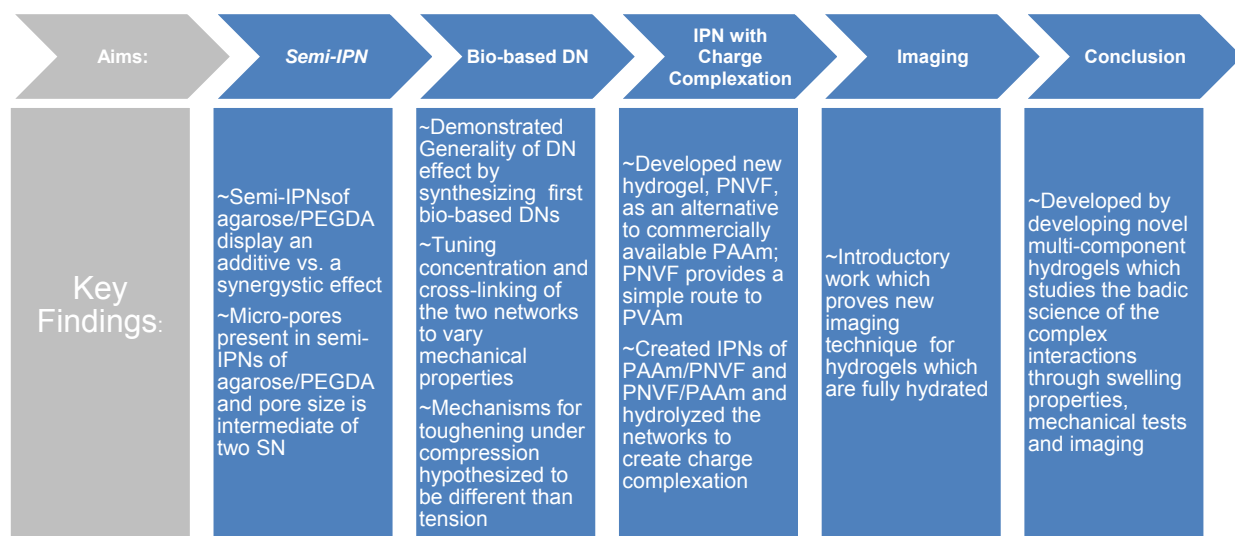


**Figure 12.1: Progression of aims throughout the dissertation**

The semi-IPNs and their SN counterparts behaved as ideal elastomers. PEGDA is the dominant network in the semi-IPN; this is shown by the semi-IPNs of agarose/PEGDA and the SNs of PEGDA falling on the same line in log-log plot of shear modulus against the polymer volume fraction. The slopes are consistent with predictions of scaling theory for a good solvent. Imaging using atomic force microscopy (AFM) and scanning electron microscopy (SEM) revealed large micro-porous (up to 20  $\mu\text{m}$ ) SN agarose networks. The pore sizes of the semi-IPNs of 5 wt% agarose / 10 or 20% PEGDA were intermediate to the two SNs. The pores decreased in size with increasing PEGDA content from 1-4  $\mu\text{m}$  pores. Overall, the semi-IPNs of agarose/PEGDA displayed more of an additive effect, sum of two single-networks (SN), than a synergistic effect in both the mechanical properties (modulus, failure properties, and toughness). The need for mechanical properties which are orders of magnitude greater led to work on DNs which were known for their superior mechanical properties, especially toughness.

The MCS/PAAm DN developed in this work was the first demonstration of a tough and ductile biopolymer-based hydrogel with a distinct yielding phenomenon. To the best of our knowledge, when the MCS/PAAm DNs were synthesized they were the only other DN hydrogels (besides the original poly(2-acrylamido-2-methylpropanesulfonic acid) (PAMPS)/ PAAm) which showed two of the three characteristic regions: preyielding and yielding regions, with significantly improved mechanical properties. Creating DN of MCS/PAAm was significant because it confirmed the generality of the DN effect: high toughness, substantial yielding region, and significant improvement in mechanical properties compared to the SNs. DNs show non-ideality even at low strains indicating a synergistic effect. Furthermore, the DN of MCS/PAAm exhibited a failure stress more than 20 times greater than the single-network (SN) of either MCS or PAAm and exhibited yielding stresses over 1500 kPa. DN of MCS/PDMAAm was synthesized, removing

the hypothesis of specific chemical interaction between PAMPS and PAAm or hydrogen bonding being the reason for superior mechanical properties. The DN of MCS/PDMAAm showed a comparable stress-strain curve and thus, mechanical properties to MCS/PAAm. The MCS/PAAm DN formulations were manipulated by adjusting the concentration and cross-linking of the two networks to achieve mechanical properties (failure stress, failure strain, Young's modulus, and yielding behavior) over a broad range (more than 5 times in most cases). Furthermore, a wide range of mechanical properties were achieved in these DNs of MCS/PAAm with limited changes in the swelling degrees, emphasizing the changes in mechanical properties were not from the water content. Improved failure properties and toughness were shown under tension as well as compression.

The most accepted model for the enhanced mechanical properties is from the energy dissipation from the covalent bonds of the first network breaking irreversibly. To test the mechanisms for the bonds breaking, repeated loading of MCS/PAAm were completed under compression. The repeated loading cycles showed no permanent damage under up to 15% strain after 12 compression cycles. Up to 45% strain, the cycle 1 or cycles 1 and 2 were significant difference from cycles 3-12 but after the initial loading cycles there was no further damage in cycles 7-12, which suggests that that fracturing the first network does not lead to significant reduction in mechanical properties (failure properties and toughness). Nevertheless, a system which uses non-covalent bonds as reversible sacrificial bonds for toughening was the hypothesis for exploring IPNs with high density charge complexation.

The goals were to create an IPN with two networks which are as close to identical as possible and then to hydrolyze these two networks to form opposite charges but matching high charge densities. Since PAAm and PNVF were isomers of each other and both undergo hydrolysis at same



conditions and form opposite and matching high charge density networks. The first step was synthesizing a new hydrogel, PNVF. Then, the PNVF was hydrolyzing to determine if the properties suitable for creating a charge complexed IPN. SN PNVF gels are significant because they provide a simple route to poly(vinylamine) (PVAm), high density cationic network, and are an alternative to commercially important PAAm. PNVF had values of  $\chi$  which were slightly less than those of PAAm, suggesting that PNVF is a slightly more hydrophilic polymer than PAAm but can be formulated to be the same as PAAm. PNVF and PAAm had similar trends in swelling E, G and failure properties.

IPNs of PNVF/PAAm and PNVF/PAAm were synthesized and hypothesized to have intimate molecular mixing of the two networks (monomers are isomers of each other and polymers have similar interaction with water) to help minimize molecular phase separation. The networks were hydrolyzed to PVAm/ poly(acrylic acid) (PAAc) and PAAc/PVAm. Charge complexation was shown in the IPNs as the deswelling of the gels at intermediate pHs. Also these charge complexed IPNs of PAAc/PVAm and PVAm/PAAc showed failure stress and toughness in the complexed state at intermediate pHs ~15 times greater than the PAAc/PVAm and PVAm/PAAc right after hydrolysis. Although the mechanical properties were in the same magnitude to the DNs, more work is needed to decouple the water content from the mechanical properties.

In creating multi-component networks, a need to visualize the individual polymer strands in order to better understand the molecular level interactions arose. Common techniques such as AFM and SEM have downfalls to imaging in the swollen state; therefore, introductory work on applying a super resolution microscopy technique, dSTORM to hydrogels was developed. A fluorescent tag was attached to both PAAc and tetra-polyethylene glycol (tetra-PEG) hydrogels and the gels were successfully imaged proving the potential of using dSTORM to image hydrogels.

Overall, this dissertation works on understanding multi-component, IPN hydrogels and to develop better understanding and correlations for the relationships between the composition, water content, microstructure network properties, and mechanical properties. This is important for advancing basic science of hydrogels in order to better engineer materials for potential applications in fields such as tissue engineering, drug delivery, and separations.

### **Recommendations for Future Work**

This section describes several ideas in which I feel worthwhile in pursuing for future research. This section is organized by some of the bigger picture areas: continuation of research described in this dissertation, fracture mechanisms in hydrogels, multi-component hydrogels and controlling the microstructure of hydrogels through controlled radical polymerizations. There are some smaller project ideas listed in the Appendix for Chapter 12.

The first section has research which would be a continuation of the research on PNVF hydrogels in Chapter 9. From the synthesis of PNVF we have learned the synthesis of this hydrogel was not as straightforward as we originally imagined. We had to synthesize a novel cross-linker which was difficult to purify. Therefore, I have started initial work on creating PNVF hydrogels with a commercially available cross-linker. We have preliminary data but we still need a complete study.

The second section is on developing a systematic way to study fracturing mechanisms in hydrogels. On a macroscale, when testing the bulk mechanical properties of hydrogels the hydrogels had specific fracturing patterns. I have noted some observations but a more systematic study is needed. On a micro or nanoscale, simultaneous fracturing while imaging hydrated

samples is the way to go. At KU we have the capability to start this research with the new environmental scanning electron microscopy (ESEM) machine.

The third is developing different multi-component hydrogels. There several of these multi-component hydrogels which I feel would be exciting to pursue. The first is using graphene particles as a platform for creating multiple cross-links. Besides being an extremely strong material, graphene has conductivity properties worth studying in hydrogels. Next, is using electrospun fibers embedded in a hydrogel matrix. Again, the fibers would provide a platform for creating multiple cross-links Also, multi-component hydrogels of nano gels in a macrogel can be would help to provide movable cross-links.

The last avenue is controlling the microstructure of hydrogels through controlled radical polymerizations. Having homogeneous networks is hypothesized to decrease premature failure and improve the failure properties.

## **Continuation of Current Projects**

### ***PNVF using commercially available cross-linker 1,3-Divinylimidazolidin-2-one BVU\****

\* Acknowledgement to Andrea Brown and Justin Smith undergraduate students who helped with preliminary data

As shown in Chapter 9 PNVF has similar network structures to commercially relevant PAAm hydrogels. However, the biggest problem with synthesizing PNVF hydrogels is the difficulty finding a cross-linking agent. Thus, we synthesized a novel cross-linker (NVEE, from Dr. Cory Berkland's lab). Although the synthesis was not extremely complicated, the purification process was rather elaborate and difficult to achieve a product with a high purity. In order for

PNVF to be a viable replacement for PAAm there is a need for a better cross-linker (easily created with high purity or commercially available). Therefore we searched for commercially available cross-linkers. Chapter 9 describes how the reactivity ratios of the monomer and cross-linker (co-polymerization) are important in understanding if the system is undergoing alternating co-polymerization, if one monomer is more reactive towards propagating species, or if random co-polymerization is occurring. Figure 12.2 is a schematic which depicts that the co-polymerization of NVF and NVEE is random, therefore leading to the formation of a hydrogel. To achieve random copolymerization it is important that molecules do not prefer to react to a specific molecule thus we hypothesize that the more similar the chemical structures the more random, especially the chemicals closest to the propagating radical. Therefore we looked for cross-linkers with a nitrogen attached to the carbon with the propagating radical. We acquired 1,3-Divinylimidazolidin-2-one (BVU) from BASF. BASF donated some cross-linker to our group. The structure is shown in Figure 12.3 and has nitrogen groups situated next to the propagating radical.

**Random Copolymerization Yields Gels**

**- Reactivity Ratios**

$$r_1 = \frac{k_{11}}{k_{12}} \quad r_2 = \frac{k_{22}}{k_{21}}$$

$r_1 = 0$   
 $r_2 = 0$

alternating copolymerization

$r_1 > 1$  and  $r_2 < 1$   
or

$r_1 < 1$  and  $r_2 > 1$

one monomer is more reactive towards propagating species

$r_1 = r_2 = 1$

random copolymerization

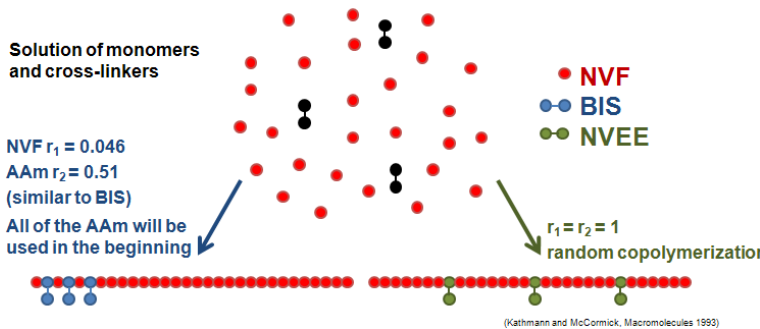
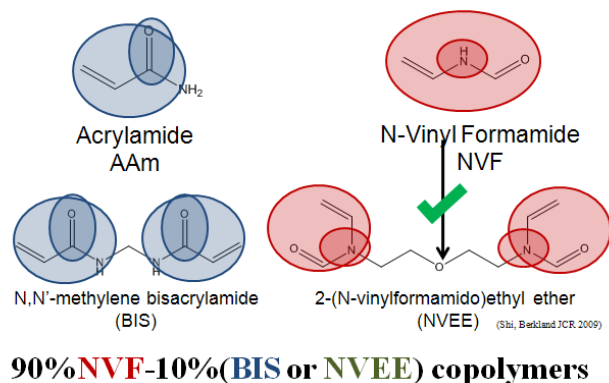
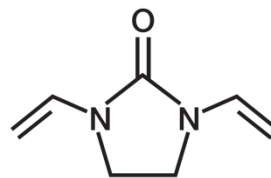


Figure 12.2: Random copolymerization of monomers and crosslinkers is needed to yield good gels.



**Figure 12.3: Structure of 1,3-Divinylimidazolidin-2-one (BVU) from BASF**

Our initial attempts to make PNVF hydrogels with BVU as the cross-linking agent were successful in creating a gel but overall the swelling degree was higher using the BVU as the cross-linker, Figure 12.4. The reactivity ratios may be closer to random=1 using NVEE. However, it also may be steric hindrance.

We also made formulations with significantly higher concentrations of monomer (40 x 1.41 and 60 x 1.41). We hypothesized there would be auto-polymerization from previous publication.<sup>[36]</sup> However, tried the same monomer concentrations with no cross-linker (40 x 0 and 60 x 0) and to our knowledge auto-polymerization was not evident (solution did not change or become viscous).

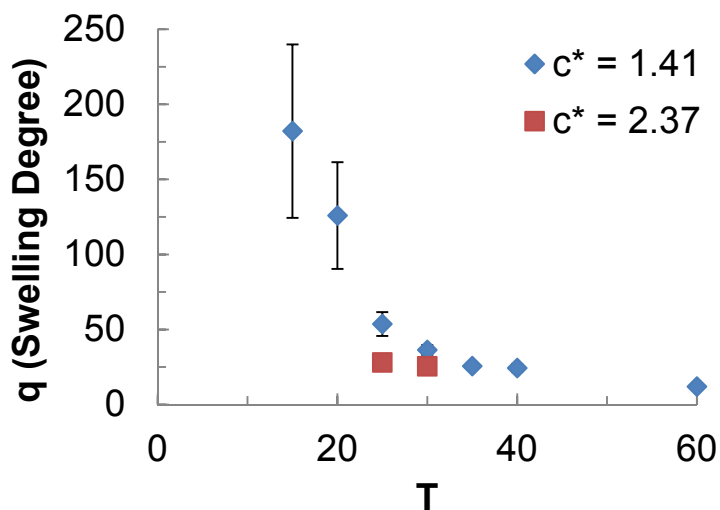


**Figure 12.4: Swelling data for PNVF hydrogels with BVU cross-linker**

### ***Conjugating small molecules or peptides to PNVF\****

\*Acknowledgement to Dr. Cory Berkland and Joshua Sestack for the advice for this avenue of research on PNVF

Another potential project is conjugating small molecules or peptides to PNVF. While studying PNVF, Dr. Berkland suggested conjugating small molecules directly to PNVF. To test if this project would be viable we can add aminooxy-benzene or aminooxy-phenol to a vial with either PAAm or PNVF gels in an acetate buffer (pH 5.5) at 40 degrees C for 24 hrs. Rinse the gels in water to remove unreacted compounds. The gels visually should be slightly colored (yellow) and less swollen. Can use FTIR or NMR to test if the reaction proceeded. The compound can be released by placing in a pH bath, rinsing and then testing using FTIR or NMR.

### **Studying Fracturing Mechanisms in Hydrogels**

#### ***Macro-scale investigating of network structure through fracturing mechanisms***

The suggestion of systematic macro-scale investigation of fracturing mechanisms is not a “fleshed-out” idea. However, after testing many hydrogel samples there seems to be differences in the way hydrogels are fracturing. Some preliminary work has been done a bit to try to see trends and to note differences. Though no systematic studies correlating the way hydrogels fracture with the properties or micro- and nano-scale structures have been completed.

Some of the different observations seen included splitting vs crushing. Also, different patterns on how the gels fractured under compression were noted. For example, the gels split in half vertically and horizontally, split in thirds, have a cylindrical center in which does not crack, have one large piece and several small pieces, and sometimes there are many small pieces. Other observations include an audible cracking noise or pieces flying from the machine.

***Investigating network structure and fracturing mechanisms using environmental SEM (ESEM)\****

\*Acknowledgement to Dr. David Moore and the MAI lab at KU for preliminary work on ESEM of hydrogels.

This project will advance understanding of fracture mechanics in hydrogels by exploring the micro- and nanoscale structure and also fracturing mechanics. Fracturing in hydrogels is not well-studied and there is not a clear connection between the microstructure of the hydrogel network and the fracture properties. Understanding fracture mechanics of hydrogels is particularly important to biomedical, tissue engineering and pharmaceutical fields. The overall idea of the research is to study the structures of the hydrogel network to be able to create optimal hydrogel networks.

Imaging capabilities are expanding. As a result, this project has the opportunity to visualize the hydrogels in the fully hydrated state, as well as in combination with applied force, on the micro- and even the nanoscale. At KU we have the capability to do environmental scanning electron microscopy (ESEM) Versa 3-D (ESEM option and focused ion beam). ESEM is optimal because we would like to see the hydrogels in the fully swollen state. The ESEM uses a low vacuum therefore hydrated samples may be imaged.<sup>[25],51,52</sup> The system is temperature and humidity controlled<sup>[108]</sup> and coating is not needed.<sup>[25,108]</sup> ESEM will be used at 2 °C and 5 torr (6.7 mbar).<sup>[150,151]</sup> Figure 12.5 shows preliminary results of 5% agarose hydrogels under ESEM. ESEM seems to be promising in investigating the network structure of hydrogels in the swollen state. Figure 12.5 shows evidence of holes or pores in the bulk hydrogel networks.

For further studies, a tensometer can be added into the ESEM chamber to perform fracturing tests while obtaining images.<sup>[150,151]</sup> Imaging can occur at different stages: before force is added, during force application, and after the force is released looking at structural changes and fracturing

patterns. Also, liquids can be introduced into the ESEM chamber,<sup>[108]</sup> to induce localized degradation in order to direct fracturing or to see changes in network structure with interactions of molecules. ESEM has been done on hydrogels by several scientists. Rizzieri uses ESEM to study gelatin while also taking stress-strain data in tension.<sup>[150]</sup> They show “folds” at 20% stain and then relaxation of the folds after fracture.<sup>[150]</sup>

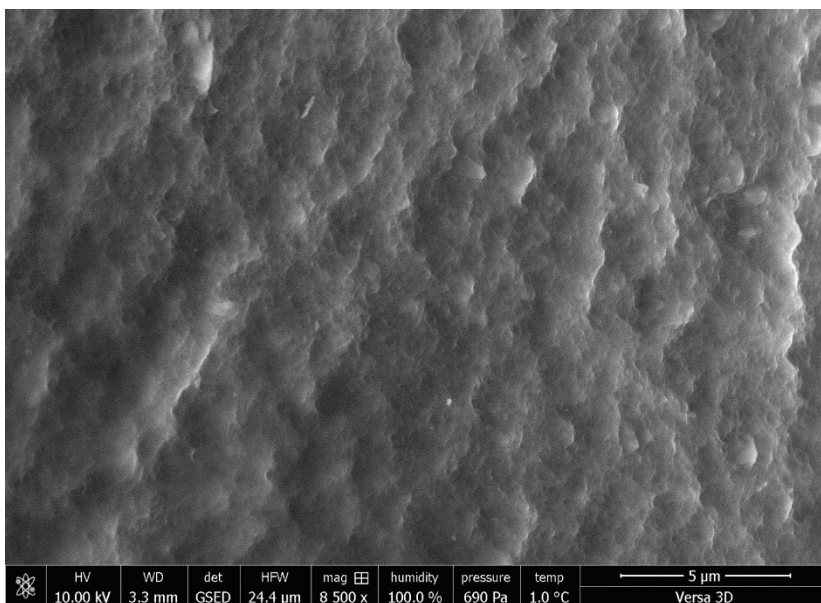


**Figure 12.5: 5% Agarose hydrogel imaged using ESEM.**

## Multi-component Hydrogels

### *Graphene hydrogels as a method of improving strength\**

\*Acknowledgement to Dr. Shenqiang Ren who helped in synthesizing graphene particles for preliminary studies.

The idea of this proposed future direction for research is to use graphene in a multicomponent hydrogel to produce high strength and other properties such as conductivity. In 2010, Andre Geim and Konstantin Novoselov from the University of Manchester, were awarded the Nobel Prize winners in Physics for their work with graphene. Graphene is a two-dimensional mono-layer of



carbon atoms in a honeycomb lattice.<sup>[208]</sup> Graphene has been studied since the 40's but lately had gained a lot of attention for having great electronic, conductivity, optical and mechanical properties. Currently graphene has become a highly studied material in a variety of fields including materials, medical, electronics, energy and water.<sup>[138,170]</sup> One of the down sides of using graphene is the difficulty of large-scale production but graphene oxide (GO), the oxidized form of graphene, is a potential intermediate route for producing large amounts of graphene. Graphene oxide (GO) has been shown to be reversibly oxidized and reduced through stimulus.<sup>[173]</sup> Graphene has been described as the strongest material and extremely thin. The Young's modulus of these materials was found to be 1.0 TPa<sup>[96]</sup> with a strain of 20%<sup>[5]</sup>.

To create these graphene oxide hydrogels the two ways I would propose to go about this are (1) to create graphene oxide hydrogels through a hydrothermal reduction of graphene oxide to form graphene oxide hydrogels<sup>[201]</sup> and then creating an IPN with PNVF, followed by hydrolysis of PNVF to form PVAm. The charge complexation and mechanical properties can be studied. (2) Another avenue is using GO as nanoparticles or multi-functional cross-linkers (similar to nanoclays). Several researchers have used PAAm<sup>[24,105]</sup>, poly(acryloyl-6-aminocaproic acid) (PAACA)<sup>[23]</sup>, polyvinyl alcohol<sup>[45]</sup> with GO but this area is still a promising future area for growth and development.

### ***Electrospinning mats for reinforced hydrogel matrices\****

\*Acknowledgement to Dr. Michael Detamore and Lindsey Ott who helped with the preliminary studies especially electrospinning

Electrospinning is a techniques are frequently used to create porous scaffolds for use in tissue engineering and also are used in controlled drug delivery, separations and catalysis.<sup>[110]</sup>

Electrospinning can create variable nanofibers and fibers with diameters near 100 nm. Figure 12.6 shows a SEM image of an electrospun 4 wt. % polyvinyl alcohol (PVA) solution. The solution was electrospun at a flow rate of 0.5 mL/hr, voltage of 10.2 kV and current of 2  $\mu$ A (taken from my senior design project with Dr. Matt Kipper at Colorado State University and with other students Jacqueline Acres, Kiel Brennan and Daniel Hemphill).

The aim of this research idea is to add strength by reinforcing the hydrogels with electrospun mats. Figure 12.7 shows a schematic of the idea of a brittle and ductile single network. By electrospinning fibers these networks are created to be thicker. Depending on the materials used fibers with pores can be created. Therefore, the second networks can essentially go through the pores in the first networks creating more entangled cross-linking joints. Further, if the electrospun fibers essentially non-porous or have very small pores then polymers may be functionalized (or have functionalized groups on them) to cross-linking sites on networks of these fibers.

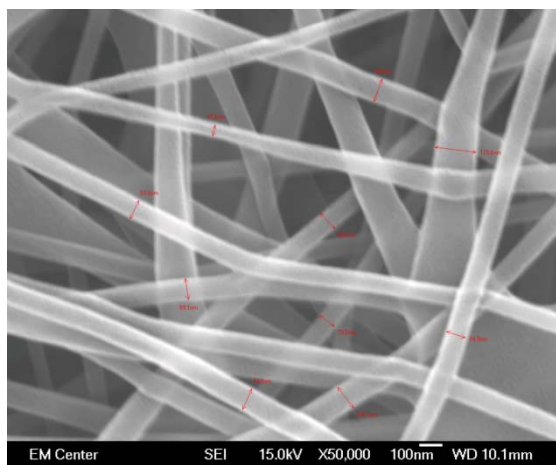


**Figure 12.6: Electrospun fibers of PVA shown in SEM.**

This SEM image shows an average diameter of 95nm diameters fibers created from a polyvinyl alcohol solution of 4wt% at a flow rate of 0.5 mL/hr, voltage of 10.2 kV and current of 2  $\mu$ A These images were taken from my senior design project with Dr. Matt Kipper at Colorado State University and with other students Jacqueline Acres, Kiel Brennan and Daniel Hemphill.

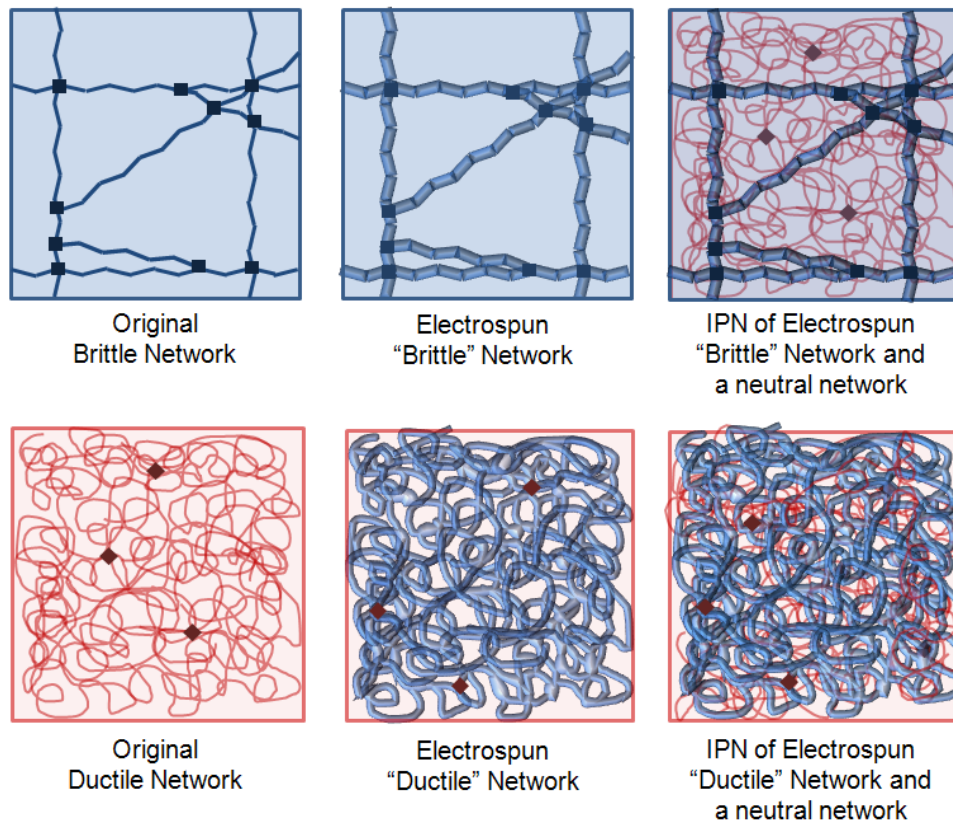


**Figure 12.7: Scheme of electrospun fibers in networks.**

Prof. Jason Burdick’s group at university of Pennsylvania has electrospun mHA fibers in an aqueous solution and has cross-linked them using UV.<sup>[88]</sup> Preliminary studies to create mHA using Dr. Burdick’s procedures have been explored but more work is needed to successfully electrospin solutions of mHA.<sup>[67]</sup>

Some final words on using electrospinning as a technique for creating multi-component systems for strength are that at CSU our senior design group (Dr. Matt Kipper, Jacqueline Acres, Kiel Brennan and Daniel Hemphill) found some interesting results when we were electrospinning, viscosity of the material is not sufficiently large thus forming ionized droplets. A few of the SEM images are shown in Figure 12.8. Rather than the fibers we found other formations such as beads, globs and spheres. By systematically forming these structures we may be able to create unique combinations of designed structures at a microscale.

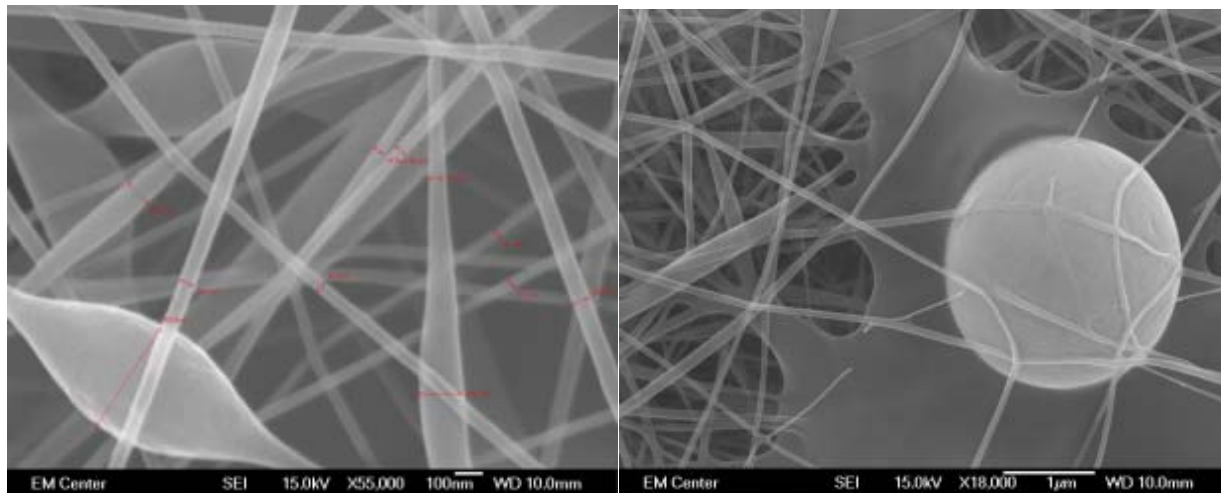


**Figure 12.8: SEM of unique structures formed by electrospaying.**

The left shows the beading in the fibers and the right shows a ball that has formed under a glob. These images were taken from my senior design project with Dr. Matt Kipper at Colorado State University and with other students Jacqueline Acres, Kiel Brennan and Daniel Hemphill.

***Methacrylated hyaluronic acid (mHA) nanogels in macrogel\****

\*Acknowledgement to Dr. Cory Berkland, Dr. Michael Detamore, Huili Guan and Chuda *Chittasupho* and Emily Beck for help with synthesis of nanogels for preliminary testing.

The hypothesis for creating a multi-component system using microgels embedded in a macrogel was to improve the fracture strain by having movable cross-links similar to slide ring gels.<sup>[75]</sup> However, having a small microgels (around 100nm) imbedded into a macrogel would allow for a cross-linker with a high functionality (multi-functional cross-linker). Hu *et al.* has published on this idea.<sup>[68-70]</sup> However microgel/macrogel concept still has many avenues to be explored. Using Chapter 10 conclusion, nanoparticles of PAAm or PNVF can be embedded in a matrix and then hydrolyzed for charge complexation, Appendix for Chapter 12 has the procedures for making PAAm or PNVF nanogels. Though, synthesizing nanoparticles from PAAm or PNVF

leaves a surfactant which is difficult to remove. Therefore, nanogels have been synthesized from methacrylated hyaluronic acid (mHA) and MCS.<sup>[35]</sup> For a detailed procedure refer to reference.<sup>[156]</sup>

## Controlling Microstructure of Hydrogels through Controlled Radical Polymerizations

### *Hydrogels with controlled microstructure using nitroxide-mediated polymerization (NMP)*

There are many researchers working on controlled radical polymerizations (NMP, atom transfer radical polymerization (ATRP), and radical addition fragmentation chain transfer (RAFT)). To our knowledge, is not much work on using controlled radical polymerized on hydrogels but it is believed to have promise.<sup>[43,155]</sup> However, the benefit of controlling network properties has been a growing area in hydrogels. For example tetra-PEG hydrogels form homogeneous networks and have a reduction number of defects and improved mechanical properties.<sup>[86,106,142,179]</sup> Figure 12.9 shows a schematic of potential networks structures achievable using controlled radical polymerizations. Homogeneous networks have better control of the transportation of small molecules through the networks and provide enhanced mechanical properties.

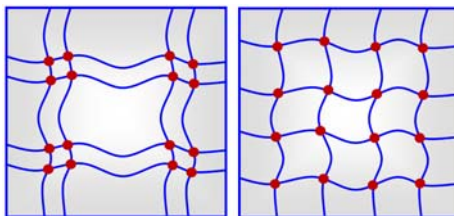


**Figure 12.9: Schematic of heterogeneous (left) and homogeneous (right) network structures.**

Creating hydrogels with a specific controlled microstructure using a controller radical technique, nitroxide-mediated polymerization (NMP), was derived from the work on poly N-vinyl

formamide (PNVF). The monomer N-vinyl formamide (NVF) was distilled to remove impurities and inhibitors. However, polymerization was tested without first distilling. The product resulted in a tougher hydrogel. 4-Hydroxy-2,2,6,6 tetramethylpiperidine 1-oxyl (TEMPO) was added to the NVF as a stabilizer and upon further investigation TEMPO works a molecule in NMP reactions.<sup>[98,165]</sup> Therefore, a more systematic study using TEMPO using materials/methods below is suggested:

### Materials and Methods

For the synthesis of PAAm, the reagents include: the monomer, acrylamide (AAm); the cross-linker, N,N'-methylenebisacrylamide (MBAA); the initiator, 2,2'-Azobis[2-(2-imidazolin-2-yl)propane]dihydrochloride (VA-044); the counter ion 4-Hydroxy-2,2,6,6 tetramethylpiperidine 1-oxyl (TEMPO) or N-tert-butyl-N-[1-diethylphosphono-(2,2-dimethylpropyl) nitroxide] (SG1). Deionized ultra-filtered (DIUF) water will be used for all of the synthesis solutions.

An example of a 15 x 3 (*T* x *C*, gel electrophoresis notation) PAAm synthesis is as follows: AAm (0.582 g), MBAA (0.018 g) and a constant molar ratio of TEMPO/VA-44 of 1.8, based upon Grassel *et al.*<sup>[52]</sup>, was added to 4 mL of DIUF water in a 5 mL pressure safe glass vial. The solution will be mixed, bubbled with nitrogen for 15 min, and then quickly capped. The free radical polymerization will be carried out at in an oil bath at 120°C for 24 hrs.

## References

- [1] Abraham, G. A., De Queiroz, A. A. and Román, J. S., *Biomaterials* **22**, 1971-1985 (2001).
- [2] Ajiro, H., Takemoto, Y., Asoh, T. and Akashi, M., *Polymer* **50**, 3503-3507 (2009).
- [3] Ajiro, H., Watanabe, J. and Akashi, M., *Chemistry Letters* **36**, 1134-1135 (2007).
- [4] Akashi, M., Saihata, S., Yashima, E., Sugita, S. and Marumo, K., *Journal of Polymer Science Part A: Polymer Chemistry* **31**, 1153-1160 (1993).
- [5] Alfrey, T., Morawetz, H., Fitzgerald, E. B. and Fuoss, R. M., *Journal of the American Chemical Society* **72**, 1864-1864 (1950).
- [6] Alonso, J. L. and Goldmann, W. H., *Life Sciences* **72**, 2553-2560 (2003).
- [7] Am Ende, M. T. and Peppas, N. A., *Journal of Controlled Release* **48**, 47-56 (1997).
- [8] Amsden, B., *Macromolecules* **32**, 874-879 (1999).
- [9] Andersen, F. A., *International journal of toxicology* **24**, 21-50 (2005).
- [10] Annabi, N., Nichol, J. W., Zhong, X., Ji, C., Koshy, S., Khademhosseini, A. and Dehghani, F., *Tissue Engineering Part B: Reviews* **16**, 371-383 (2010).
- [11] Azuma, C., Yasuda, K., Tanabe, Y., Taniguro, H., Kanaya, F., Nakayama, A., Chen, Y. M., Gong, J. P. and Osada, Y., *Journal of Biomedical Materials Research Part A* **81A**, 373-380 (2007).
- [12] Baselga, J., Hernandezfuentes, I., Masegosa, R. M. and Llorente, M. A., *Polymer Journal* **21**, 467-474 (1989).
- [13] Baselga, J., Hernandezfuentes, I., Pierola, I. F. and Llorente, M. A., *Macromolecules* **20**, 3060-3065 (1987).
- [14] Baselga, J., Llorente, M. A., Nieto, J. L., Hernandez-Fuentes, I. and Pierola, I. F., *European Polymer Journal* **24**, 161-165 (1988).
- [15] Bates, M., Huang, B., Dempsey, G. T. and Zhuang, X., *Science* **317**, 1749-1753 (2007).
- [16] Boonyongmaneerat, Y. and Dunand, D. C., *Acta Materialia* **57**, 1373-1384 (2009).
- [17] Calvert, P., *Advanced Materials* **21**, 743-756 (2009).
- [18] Calvet, D., Wong, J. Y. and Giasson, S., *Macromolecules* **37**, 7762-7771 (2004).
- [19] Chen, Q., Zhu, L., Zhao, C., Wang, Q. and Zheng, J., *Advanced Materials* **25**, 4171-4176 (2013).
- [20] Christensen, L. H., *Dermatologic Surgery* **35**, 1612-1619 (2009).
- [21] Colby, R. H., *Rheologica Acta* **49**, 425-442 (2010).
- [22] Colby, R. H. and Rubinstein, M., *Macromolecules* **23**, 2753-2757 (1990).

- [23] Cong, H.-P., Wang, P. and Yu, S.-H., *Chemistry of Materials* **25**, 3357-3362 (2013).
- [24] Cong, H. P., Wang, P. and Yu, S. H., *Small* (2013).
- [25] Crockett, R., Roos, S., Rossbach, P., Dora, C., Born, W. and Troxler, H., *Tribology Letters* **19**, 311-317 (2005).
- [26] Day, J. C. and Robb, I. D., *Polymer* **22**, 1530-1533 (1981).
- [27] Dejongh, J., Nordin-Andersson, M., Ploeger, B. A. and Forsby, A., *Toxicology and Applied Pharmacology* **158**, 261-268 (1999).
- [28] Dekosky, B. J., Dormer, N. H., Ingavle, G. C., Roatch, C. H., Lomakin, J., Detamore, M. S. and Gehrke, S. H., *Tissue Engineering Part C - Methods* **16** (2010).
- [29] Dempsey, G. T., Vaughan, J. C., Chen, K. H., Bates, M. and Zhuang, X., *Nature methods* **8**, 1027-1036 (2011).
- [30] Dillon, G. P., Yu, X., Sridharan, A., Ranieri, J. P. and Bellamkonda, R. V., *Journal of Biomaterials Science, Polymer Edition* **9**, 1049-1069 (1998).
- [31] Dubrovskii, S. A. and Rakova, G. V., *Macromolecules* **30**, 7478-7486 (1997).
- [32] Erman, B. and Flory, P. J., *Macromolecules* **15**, 806-811 (1982).
- [33] Erman, B. and Mark, J., *Structures and Properties of Rubberlike Networks*, Oxford University Press, New York, 1997.
- [34] Erman, B. and Mark, J. E., *Annual Review of Physical Chemistry* **40**, 351-374 (1989).
- [35] Fakhari, A., 2012, vol. 73, p. 2012.
- [36] Feng, X. H., Pelton, R. and Leduc, M., *Industrial & Engineering Chemistry Research* **45**, 6665-6671 (2006).
- [37] Ferruzzi, G. G., Pan, N. and Casey, W. H., *Soil science* **165**, 778-792 (2000).
- [38] Flory, P. J., *Principles of Polymer Chemistry*, Cornell University Press, 1953.
- [39] Flory, P. J., *Journal of Chemical Physics* **66**, 5720-5729 (1977).
- [40] Flory, P. J. and Rehner, J., *The Journal of Chemical Physics* **11**, 512 (1943).
- [41] Fried, J. R., *Polymer Science and Technology*, Pentice-Hall PTR, USA, 1995.
- [42] Friedman, M., *Journal of Agricultural and Food Chemistry* **51**, 4504-4526 (2003).
- [43] Gao, H. F. and Matyjaszewski, K., *Progress in Polymer Science* **34**, 317-350 (2009).
- [44] Gehrke, S., Palasis, M. and Akhtar, M., *Polymer International* **29**, 29-36 (1992).
- [45] Gehrke, S. H., in *Transport in Pharmaceutical Sciences*, eds. Amidon, G. L., Lee, P. I. and Topp, E. M., Marcel Dekker, New York, NY, 2000, pp. 473-546.



- [46] Gehrke, S. H., *Synthesis, Equilibrium Swelling, Kinetics, Permeability and Applications of Environmentally Responsive Gels.*, Springer, Berlin Heidelberg, 1993.
- [47] Geissler, E., Hecht, A.-M., Fhorkay and Zrinyi, M., *Macromolecules* **21**, 2594-2599 (1988).
- [48] Gong, J., Iwasaki, Y., Osada, Y., Kurihara, K. and Hamai, Y., *The Journal of Physical Chemistry B* **103**, 6001-6006 (1999).
- [49] Gong, J. and Osada, Y., in *High Solid Dispersions* Springer, 2010, pp. 203-246.
- [50] Gong, J. P., *Soft Matter* **6**, 2583-2590 (2010).
- [51] Gong, J. P., Katsuyama, Y., Kurokawa, T. and Osada, Y., *Advanced Materials* **15**, 1155-1158 (2003).
- [52] Grassl, B., Clisson, G., Khoukh, A. and Billon, L., *European Polymer Journal* **44**, 50-58 (2008).
- [53] Greensmith, H. W., *Journal of Applied Polymer Science* **3**, 183-193 (1960).
- [54] Greensmith, H. W. and Thomas, A., *Journal of polymer Science* **18**, 189-200 (1955).
- [55] Gu, L., Zhu, S. and Hrymak, A. N., *Journal of Applied Polymer Science* **86**, 3412-3419 (2002).
- [56] Gu, L. M., Zhu, S. P., Hrymak, A. N. and Pelton, R. H., *Macromolecular Rapid Communications* **22**, 212-214 (2001).
- [57] Guenet, J.-M., *Polymer-Solvent Molecular Compounds*, Access Online via Elsevier, 2010.
- [58] Hagiwara, Y., Putra, A., Kakugo, A., Furukawa, H. and Gong, J. P., *Cellulose* **17**, 93-101 (2010).
- [59] Hao, J. and Weiss, R., *Polymer* **85**, 2174-2182 (2013).
- [60] Hao, J. and Weiss, R., *Macromolecules* **44**, 9390-9398 (2011).
- [61] Haque, M. A., Kurokawa, T. and Gong, J. P., *Polymer* **53**, 1805-1822 (2012).
- [62] Haque, M. A., Kurokawa, T., Kamita, G. and Gong, J. P., *Macromolecules* **44**, 8916-8924 (2011).
- [63] Heilemann, M., Van De Linde, S., Schüttpelz, M., Kasper, R., Seefeldt, B., Mukherjee, A., Tinnefeld, P. and Sauer, M., *Angewandte Chemie International Edition* **47**, 6172-6176 (2008).
- [64] Henderson, K. J., Zhou, T. C., Otim, K. J. and Shull, K. R., *Macromolecules* **43**, 6193-6201 (2010).
- [65] Hill, R. G. and Labok, S. A., *Journal of Materials Science* **26**, 67-74 (1991).
- [66] Hoffman, A. S., *Advanced Drug Delivery Reviews* **64**, 18-23 (2012).
- [67] Horkay, F., Tasaki, I. and Basser, P. J., *Biomacromolecules* **1**, 84-90 (2000).
- [68] Hu, J., Hiwatashi, K., Kurokawa, T., Liang, S. M., Wu, Z. L. and Gong, J. P., *Macromolecules* **44**, 7775-7781 (2011).
- [69] Hu, J., Kurokawa, T., Hiwatashi, K., Nakajima, T., Wu, Z. L., Liang, S. M. and Gong, J. P., *Macromolecules* **45**, 5218-5228 (2012).

- [70] Hu, J., Kurokawa, T., Nakajima, T., Sun, T. L., Suekama, T., Wu, Z. L., Liang, S. M. and Gong, J. P., *Macromolecules* **45**, 9445-9451 (2012).
- [71] Huang, B., Babcock, H. and Zhuang, X., *Cell* **143**, 1047-1058 (2010).
- [72] Ilavsky, M., *Polymer* **22**, 1687-1691 (1981).
- [73] Ingavle, G., Dormer, N., Gehrke, S. and Detamore, M., *Journal of Materials Science: Materials in Medicine*, 1-14 (2012).
- [74] Ingavle, G. C., Frei, A. W., Gehrke, S. H. and Detamore, M. S., *Tissue Engineering Part A* **19**, 1349-1359 (2013).
- [75] Ito, K., *Polymer Journal* **39**, 489-499 (2007).
- [76] Jang, S. S., Goddard, W. A. and Kalani, M. Y. S., *The Journal of Physical Chemistry B* **111**, 1729-1737 (2007).
- [77] Jensen, G., *Cryo-Em Part A: Sample Preparation and Data Collection*, Academic Press, 2010.
- [78] Jin, S., Bian, F., Liu, M., Chen, S. and Liu, H., *Polymer International* **58**, 142-148 (2009).
- [79] Junk, M. J. N., Berger, R. D. and Jonas, U., *Langmuir* **26**, 7262-7269 (2010).
- [80] Kabra, B. G., Gehrke, S. H. and Spontak, R. J., *Macromolecules* **31**, 2166-2173 (1998).
- [81] Kang, H.-W., Tabata, Y. and Ikada, Y., *Biomaterials* **20**, 1339-1344 (1999).
- [82] Kathmann, E. E. L. and McCormick, C. L., *Macromolecules* **26**, 5249-5252 (1993).
- [83] Kato, N. and Gehrke, S. H., *Reflexive Polymers and Hydrogels: Understanding and Designing Fast Responsive Polymeric Systems*, 189 (2004).
- [84] Kawauchi, Y., Tanaka, Y., Furukawa, H., Kurokawa, T., Nakajima, T., Osada, Y. and Gong, J. P. in Brittle, Ductile, Paste-Like Behaviors and Distinct Necking of Double Network Gels with Enhanced Heterogeneity, (**184**, 2009) pp. 012016.
- [85] Kelmanovich, S. G., Parke-Houben, R. and Frank, C. W., *Soft Matter* **8**, 8137-8148 (2012).
- [86] Khanlari, A., Detamore, M. S. and Gehrke, S. H., *Macromolecules* **46**, 9609-9617 (2013).
- [87] Khondee, S., Yakovleva, T. and Berklund, C., *Journal of Applied Polymer Science* **118**, 1921-1932 (2010).
- [88] Kim, I. L., Khetan, S., Baker, B. M., Chen, C. S. and Burdick, J. A., *Biomaterials* **34**, 5571-5580 (2013).
- [89] Kim, S. H., Opdahl, A., Marmo, C. and Somorjai, G. A., *Biomaterials* **23**, 1657-1666 (2002).
- [90] Kizilay, M. Y. and Okay, O., *Macromolecules* **36**, 6856-6862 (2003).
- [91] Kondo, S., Chung, U.-I. and Sakai, T., *Polymer Journal* (2013).
- [92] Kondo, S., Sakurai, H., Chung, U.-I. and Sakai, T., *Macromolecules* **46**, 7027-7033 (2013).
- [93] Kroner, M., Dupuis, J. and Winter, M., *Journal fur praktische chemie* **342**, 115-131 (2000).

- [94] Krsko, P. and Libera, M., *Materials Today* **8**, 36-44 (2005).
- [95] Krueger, S., Andrews, A. P. and Nossal, R., *Biophysical chemistry* **53**, 85-94 (1994).
- [96] Lee, C., Wei, X., Kysar, J. W. and Hone, J., *Science* **321**, 385-388 (2008).
- [97] Lee, K. Y. and Mooney, D. J., *Chemical reviews* **101**, 1869-1880 (2001).
- [98] Li, D. and Brittain, W. J., *Macromolecules* **31**, 3852-3855 (1998).
- [99] Li, Q., Wang, D.-A. and Elisseeff, J. H., *Macromolecules* **36**, 2556-2562 (2003).
- [100] Li, Q., Williams, C. G., Sun, D. N., Wang, J., Leong, K. and Elisseeff, J. H., *Journal of Biomedical Materials Research* **68**, 28-33 (2004).
- [101] Liang, S., Wu, Z. L., Hu, J., Kurokawa, T., Yu, Q. M. and Gong, J. P., *Macromolecules* **44**, 3016-3020 (2011).
- [102] Liang, S., Yu, Q. M., Yin, H., Wu, Z. L., Kurokawa, T. and Gong, J. P., *Chemical Communications*, 7518-7520 (2009).
- [103] Lin, C.-C. and Anseth, K. S., *Pharmaceutical Research* **26**, 631-643 (2009).
- [104] Liu, J., Hilderink, J., Groothuis, T. A., Otto, C., Blitterswijk, C. A. and Boer, J., *Journal of tissue engineering and regenerative medicine* (2013).
- [105] Liu, R., Liang, S., Tang, X.-Z., Yan, D., Li, X. and Yu, Z.-Z., *Journal of Materials Chemistry* **22**, 14160-14167 (2012).
- [106] Lomakin, J., Huber, P. A., Eichler, C., Arakane, Y., Kramer, K. J., Beeman, R. W., Kanost, M. R. and Gehrke, S. H., *Biomacromolecules* **12**, 321-335 (2010).
- [107] Lutolf, M. and Hubbell, J., *Nature biotechnology* **23**, 47-55 (2005).
- [108] Manero, J., Gil, F., Padros, E. and Planell, J., *Microscopy research and technique* **61**, 469-480 (2003).
- [109] Matsunaga, T., Sakai, T., Akagi, Y., Chung, U.-I. and Shibayama, M., *Macromolecules* **42**, 1344-1351 (2009).
- [110] Matthew T Hunley, T. E. L., *Polymer International* **57**, 385-389 (2008).
- [111] Mcauley, K., *Journal of Physics: Conference Series* **3**, 29 (2004).
- [112] Moerner, W., *Journal of Microscopy* **246**, 213-220 (2012).
- [113] Mohammadi, Z., Cole, A. and Berkland, C., *The Journal of Physical Chemistry C* **113**, 7652-7658 (2009).
- [114] Mohammadi, Z., Xie, S. X., Golub, A. L., Gehrke, S. H. and Berkland, C., *Journal of Applied Polymer Science* **121**, 1384-1392 (2011).
- [115] Mow, V. C., Ratcliffe, A. and Robin Poole, A., *Biomaterials* **13**, 67-97 (1992).
- [116] Myung, D., Koh, W., Ko, J., Hu, Y., Carrasco, M., Noolandi, J., Ta, C. N. and Frank, C. W., *Polymer* **48**,

- 5376-5387 (2007).
- [117] Myung, D., Koh, W., Ko, J., Noolandi, J., Carrasco, M., Smith, A., Frank, C. and Ta, C., *Investigative Ophthalmology and Visual Science* **46**, 5003 (2005).
- [118] Myung, D., Waters, D., Wiseman, M., Duhamel, P. E., Noolandi, J., Ta, C. N. and Frank, C. W., *Polymers for advanced technologies* **19**, 647-657 (2008).
- [119] Na, Y. H., Tanaka, Y., Kawauchi, Y., Furukawa, H., Sumiyoshi, T., Gong, J. P. and Osada, Y., *Macromolecules* **39**, 4641-4645 (2006).
- [120] Nagase, K. and Sakaguchi, K., *Journal of Polymer Science Part A: General Papers* **3**, 2475-2482 (1965).
- [121] Naghash, H. J. and Okay, O., *Journal of Applied Polymer Science* **60**, 971-979 (1996).
- [122] Nakajima, T., Furukawa, H., Tanaka, Y., Kurokawa, T. and Gong, J. P., *Journal of Polymer Science Part B: Polymer Physics* **49**, 1246-1254 (2011).
- [123] Nakajima, T., Furukawa, H., Tanaka, Y., Kurokawa, T., Osada, Y. and Gong, J. P., *Macromolecules* **42**, 2184-2189 (2009).
- [124] Nakajima, T., Sato, H., Zhao, Y., Kawahara, S., Kurokawa, T., Sugahara, K. and Gong, J. P., *Advanced Functional Materials* **22**, 4426-4432 (2012).
- [125] Nakayama, A., Kakugo, A., Gong, J. P., Osada, Y., Takai, M., Erata, T. and Kawano, S., *Advanced Functional Materials* **14**, 1124-1128 (2004).
- [126] Nemir, S., Hayenga, H. N. and West, J. L., *Biotechnology and Bioengineering* **105**, 636-644 (2010).
- [127] Normand, V., Lootens, D. L., Amici, E., Plucknett, K. P. and Aymard, P., *Biomacromolecules* **1**, 730-738 (2000).
- [128] Oliveira, E. D., Hirsch, S. G., Spontak, R. J. and Gehrke, S. H., *Macromolecules* **36**, 6189-6201 (2003).
- [129] Orwoll, R. and Arnold, P., *Physical Properties of Polymers Handbook*, 233-257 (2007).
- [130] Park, S., Costa, K. D. and Ateshian, G. A., *J Biomech* **37**, 1679-1687 (2004).
- [131] Patel, S. K., Rodriguez, F. and Cohen, C., *Polymer* **30**, 2198-2203 (1989).
- [132] Patras, G., Qiao, G. G. and Solomon, D. H., *Macromolecules* **34**, 6396-6401 (2001).
- [133] Patterson, J., Martino, M. M. and Hubbell, J. A., *Materials Today* **13**, 14-22 (2010).
- [134] Pelton, R. and Hoare, T., *Microgels and Their Synthesis: An Introduction*, Wiley-VCH, 2011, pp. 1-32.
- [135] Peppas, N., *Hydrogels in Medicine and Pharmacy*, CRC Press Boca Raton, FL, 1987.
- [136] Peppas, N., Bures, P., Leobandung, W. and Ichikawa, H., *European Journal of Pharmaceutics and Biopharmaceutics* **50**, 27-46 (2000).
- [137] Peppas, N. A., in *Biomaterials Science: An Introduction to Materials in Medicine*, Elsevier, Academic, Toronto, 2 edn., 1996, ch. 2.5, p. 100.

- [138] Peppas, N. A., Bures, P., Leobandung, W. and Ichikawa, H., *European Journal of Pharmaceutics and Biopharmaceutics* **50**, 27-46 (2000).
- [139] Peppas, N. A., Hilt, J. Z., Khademhosseini, A. and Langer, R., *Advanced Materials* **18**, 1345-1360 (2006).
- [140] Peppas, N. A. and Kim, B., *Journal of Drug Delivery Science and Technology* **16**, 11-18 (2006).
- [141] Peppas, N. A. and Merrill, E. W., *Journal of Applied Polymer Science* **21**, 1763-1770 (1977).
- [142] Pernodet, N., Maaloum, M. and Tinland, B., *Electrophoresis* **18**, 55-58 (1997).
- [143] Pines, E. and Prins, W., *Macromolecules* **6**, 888-895 (1973).
- [144] Pinschmidt, R. K., *Journal of Polymer Science Part A: Polymer Chemistry* **48**, 2257-2283 (2010).
- [145] Pinschmidt, R. K., Renz, W. L., Carroll, W. E., Yacoub, K., Drescher, J., Nordquist, A. F. and Chen, N., *Journal of Macromolecular Science Part a-Pure and Applied Chemistry* **A34**, 1885-1905 (1997).
- [146] Pittolo, M. and Burford, R., *Journal of Materials Science* **19**, 3330-3336 (1984).
- [147] Pook, L. P. and Sharples, J. K., *International Journal of Fracture* **15**, R223-R226 (1979).
- [148] Rennerfeldt, D. A., Renth, A. N., Talata, Z., Gehrke, S. H. and Detamore, M. S., *Biomaterials* **34**, 8241-8257 (2013).
- [149] Rill, R. L., Van Winkle, D. H. and Locke, B. R., *Analytical chemistry* **70**, 2433-2438 (1998).
- [150] Rizzieri, R., Baker, F. and Donald, A., *Review of scientific instruments* **74**, 4423-4428 (2003).
- [151] Rizzieri, R., Baker, F. S. and Donald, A. M., *Polymer* **44**, 5927-5935 (2003).
- [152] Rosen, S. L., *Fundamental Principles of Polymeric Materials*, Wiley New York, 1993.
- [153] Rouquerol, J., Avnir, D., Fairbridge, C., Everett, D., Haynes, J., Pernicone, N., Ramsay, J., Sing, K. and Unger, K., *Pure and Applied Chemistry* **66**, 1739-1758 (1994).
- [154] Sanabria-Delong, N., Crosby, A. J. and Tew, G. N., *Biomacromolecules* **9**, 2784-2791 (2008).
- [155] Sanson, N. and Rieger, J., *Polymer Chemistry* **1**, 965-977 (2010).
- [156] Seliktar, D., *Science* **336**, 1124-1128 (2012).
- [157] Shi, L. J. and Berkland, C., *Macromolecules* **40**, 4635-4643 (2007).
- [158] Shi, L. J. and Berkland, C., *Advanced Materials* **18**, 2315-2319 (2006).
- [159] Shi, L. J., Khondee, S., Linz, T. H. and Berkland, C., *Macromolecules* **41**, 6546-6554 (2008).
- [160] Shin, H., Olsen, B. D. and Khademhosseini, A., *Biomaterials* **33**, 3143-3152 (2012).
- [161] Silberberg, A., *Acs Symposium Series* **480**, 146-158 (1992).
- [162] Smith, M. H., Herman, E. S. and Lyon, L. A., *Journal of Physical Chemistry B* **115**, 3761-3764 (2011).

- [163] Stach, M., Lacik, I., Kasak, P., Chorvat, D., Jr., Saunders, A. J., Santanakrishnan, S. and Hutchinson, R. A., *Macromolecular Chemistry and Physics* **211**, 580-593 (2010).
- [164] Stevens, L., Calvert, P. and Wallace, G. G., *Soft Matter* **9**, 3009-3012 (2013).
- [165] Studer, A. and Schulte, T., *The Chemical Record* **5**, 27-35 (2005).
- [166] Suekama, T. C., Aziz, V., Mohammadi, Z., Berkland, C. and Gehrke, S. H., *Journal of Polymer Science Part A: Polymer Chemistry* **51**, 435-445 (2013).
- [167] Suekama, T. C., Hu, J., Kurokawa, T., Gong, J. P. and Gehrke, S. H., *ACS Macro Letters* **2**, 137-140 (2013).
- [168] Suekama, T. C., Hu, J., Kurokawa, T., Gong, J. P. and Gehrke, S. H., *Macromolecular Symposia* **329**, 9-18 (2013).
- [169] Suekama, T. C., Khanlari, A. and Gehrke, S. H., *Manuscript in preparation*
- [170] Suekama, T. C., Khanlari, A. and Gehrke, S. H., *MRS Proceedings* **1622**, mrsf13-1622-e1607-1603 (2014).
- [171] Suekama, T. C., Rennerfeldt, D., Khanlari, A. and Gehrke, S. H., *Manuscript in preparation*
- [172] Sun, J. Y., Zhao, X., Illeperuma, W. R. K., Chaudhuri, O., Oh, K. H., Mooney, D. J., Vlassak, J. J. and Suo, Z., *Nature* **489**, 133-136 (2012).
- [173] Sun, T. L., Kurokawa, T., Kuroda, S., Ihsan, A. B., Akasaki, T., Sato, K., Haque, M. A., Nakajima, T. and Gong, J. P., *Nature materials* **12**, 932-937 (2013).
- [174] Suwa, K., Yamamoto, K., Akashi, M., Takano, K., Tanaka, N. and Kunugi, S., *Colloid and Polymer Science* **276**, 529-533 (1998).
- [175] Takemoto, Y., Ajiro, H., Asoh, T. and Akashi, M., *Chemistry of Materials* **22**, 2923-2929 (2010).
- [176] Testa, I., Wurm, C. A., Medda, R., Rothermel, E., Von Middendorf, C., Fölling, J., Jakobs, S., Schönle, A., Hell, S. W. and Eggeling, C., *Biophysical Journal* **99**, 2686-2694 (2010).
- [177] Thaiboonrod, S., Cellesi, F., Ulijn, R. V. and Saunders, B. R., *Langmuir* **28**, 5227-5236 (2012).
- [178] Tompa, H., *Polymer Solutions*, Butterworths Scientific Publications, 1956.
- [179] Treloar, L., *The Physics of Rubber Elasticity, 3rd Edn.* Clarendon, Oxford University Press, USA, 2005.
- [180] Tutas, M., Saglam, M., Yüksel, M. and Güler, Ç., *Thermochimica Acta* **111**, 121-126 (1987).
- [181] Van Dijk, M., Van Nostrum, C. F., Hennink, W. E., Rijkers, D. T. S. and Liskamp, R. M. J., *Biomacromolecules* **11**, 1608-1614 (2010).
- [182] Van Dyke, J. D. and Kasperski, K. L., *Journal of Polymer Science Part A: Polymer Chemistry* **31**, 1807-1823 (1993).
- [183] Van Vlierberghe, S., Dubruel, P. and Schacht, E., *Biomacromolecules* **12**, 1387-1408 (2011).
- [184] Vats, K. and Benoit, D. S., *Tissue Engineering Part B: Reviews* **19**, 455-469 (2013).
- [185] Vaughan, J. C., Jia, S. and Zhuang, X., *Nature methods* (2012).

- [186] Vincent, J. F. V., *Structural Biomaterials*, Princeton Univ Pr, Princeton 1990, p. 244.
- [187] Wang, X., Wang, H. and Brown, H. R., *Soft Matter* **7**, 211-219 (2011).
- [188] Waters, D. J., Engberg, K., Parke-Houben, R., Hartmann, L., Ta, C. N., Toney, M. F. and Frank, C. W., *Macromolecules* **43**, 6861-6870 (2010).
- [189] Waters, D. J., Engberg, K., Parke-Houben, R., Ta, C. N., Jackson, A. J., Toney, M. F. and Frank, C. W., *Macromolecules* **44**, 5776-5787 (2011).
- [190] Webber, R. E., Creton, C., Brown, H. R. and Gong, J. P., *Macromolecules* **40**, 2919-2927 (2007).
- [191] Weiss, N. and Silberberg, A., *British Polymer Journal* **9**, 144-150 (1977).
- [192] Weng, L., Gouldstone, A., Wu, Y. and Chen, W., *Biomaterials* **29**, 2153-2163 (2008).
- [193] West, J. L. and Hubbell, J. A., *Macromolecules* **32**, 241-244 (1998).
- [194] White, L., Jönson, S., Hoyle, C. and Mathias, L., *Polymer* **40**, 6597-6605 (1999).
- [195] Wu, Z. L., Sawada, D., Kurokawa, T., Kakugo, A., Yang, W., Furukawa, H. and Gong, J. P., *Macromolecules* **44**, 3542-3547 (2011).
- [196] Xin, H., Saricilar, S. Z., Brown, H. R., Whitten, P. G. and Spinks, G. M., *Macromolecules* **46**, 6613-6620 (2013).
- [197] Xiong, J.-Y., Narayanan, J., Liu, X.-Y., Chong, T. K., Chen, S. B. and Chung, T.-S., *The Journal of Physical Chemistry B* **109**, 5638-5643 (2005).
- [198] Xu, J. J. and Pelton, R., *Journal of Colloid and Interface Science* **276**, 113-117 (2004).
- [199] Xu, J. J., Timmons, A. B. and Pelton, R., *Colloid and Polymer Science* **282**, 256-263 (2004).
- [200] Xu, K., Babcock, H. P. and Zhuang, X., *Nat Meth* **9**, 185-188 (2012).
- [201] Xu, Y., Sheng, K., Li, C. and Shi, G., *Acs Nano* **4**, 4324-4330 (2010).
- [202] Xue, W., Huglin, M. B. and Jones, T. G. J., *European Polymer Journal* **41**, 239-248 (2005).
- [203] Yamamoto, K., Serizawa, T., Muraoka, Y. and Akashi, M., *Macromolecules* **34**, 8014-8020 (2001).
- [204] Yang, W., Furukawa, H. and Gong, J. P., *Advanced Materials* **20**, 4499-4503 (2008).
- [205] Yin, H., Akasaki, T., Sun, T. L., Nakajima, T., Kurokawa, T., Nonoyama, T., Taira, T., Saruwatari, Y. and Gong, J. P., *J. Mater. Chem. B* **1**, 3658-3693 (2013).
- [206] You, H. X. and Yu, L., *Methods in cell science* **21**, 1-17 (1999).
- [207] Yu, Q. M., Tanaka, Y., Furukawa, H., Kurokawa, T. and Gong, J. P., *Macromolecules* **42**, 3852-3855 (2009).
- [208] Zurick, K. M. and Bernards, M., *Journal of Applied Polymer Science* **131** (2014).

## Appendix for Chapter 2

### Conversion: X (%)

This section explains how to calculate % conversion of single-network hydrogel samples by mass. Conversion is useful especially if the monomers and or cross-linkers do not fully react (reaction is not complete).

To calculate conversion:

1.  $m_{\text{mold}}$ , mold mass: mass of sample directly in the as prepared state
2.  $m_{\text{dry}}$ , dry mass: mass of the completely dried sample after leaching unreacted chemicals
3. initial mass of the monomer
4. initial mass of the crosslinker
5. initial water

$$X (\%) = \frac{\text{mass in the gel}}{\text{mass in the reaction solution}} \cdot 100 = \frac{m_{\text{dry}}}{m_{\text{synthesis}}} \cdot 100 = \frac{m_{\text{dry}}}{\frac{T}{1+T} \cdot m_{\text{mold}}} \cdot 100$$

$$T = \frac{\text{mass of monomer} + \text{mass of crosslinker}}{100 \text{ mL of water}} = \frac{m_{\text{monomer}} + m_{\text{XL}}}{W}$$

Formulas to double check conversion equation:

$$\frac{T}{1+T} = \frac{\frac{T}{T}}{\frac{1}{T} + \frac{T}{T}} = \frac{1}{\frac{1}{T} + 1} = \frac{1}{\frac{W}{m_{\text{monomer}} + m_{\text{XL}}} + 1} = \frac{1}{\frac{W + m_{\text{monomer}} + m_{\text{XL}}}{m_{\text{monomer}} + m_{\text{XL}}}} = \frac{m_{\text{monomer}} + m_{\text{XL}}}{W + m_{\text{monomer}} + m_{\text{XL}}}$$

$$m_{\text{mold}} = W + m_{\text{monomer}} + m_{\text{XL}}$$

$$X (\%) = \frac{m_{\text{dry}}}{\frac{T}{1+T} \cdot m_{\text{mold}}} \cdot 100 = \frac{m_{\text{dry}}}{\frac{m_{\text{monomer}} + m_{\text{XL}}}{W + m_{\text{monomer}} + m_{\text{XL}}} \cdot m_{\text{mold}}} \cdot 100$$

$$= \frac{m_{\text{monomer}} + m_{\text{XL}}}{W + m_{\text{monomer}} + m_{\text{XL}}} \cdot \frac{(W + m_{\text{monomer}} + m_{\text{XL}})}{m_{\text{dry}}} \cdot 100$$

$$= \frac{m_{\text{monomer}} + m_{\text{XL}}}{m_{\text{dry}}} \cdot (W + m_{\text{monomer}} + m_{\text{XL}})$$

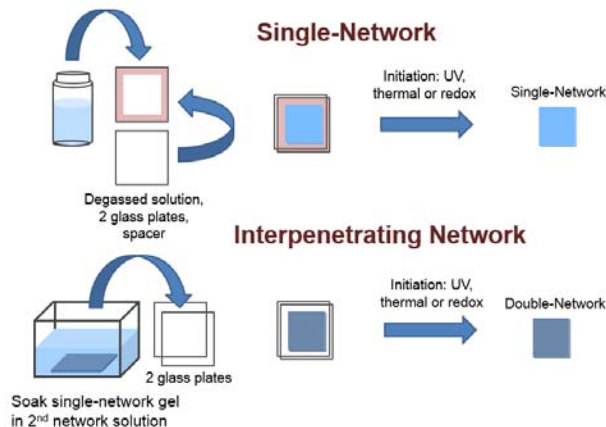
$$= \frac{m_{\text{mold}}(m_{\text{monomer}} + m_{\text{XL}} - W \text{ portion})}{m_{\text{dry}}} \cdot 100$$



## *Synthesis*

All of the hydrogels were synthesized using a free radical polymerization technique. The specific details for the individual techniques are listed in each chapter. A schematic of the synthesis typical methods is shown in Appendix Figure A-2.1. For most of the hydrogels synthesized in this work the monomer (or polymer), cross-linker agent (in some cases), initiator (UV, thermal or redox agents) and solvent (water) were mixed together. Then the solutions were typically degassed to reduce oxygen inhibition by either bubbling nitrogen or vacuuming for 15-30 min. Further, a glovebox is helpful in keeping out the oxygen during synthesis. The degassed solution is pipetted on a glass plate with a spacer. A second glass plate is carefully placed on top. The glass plates are held together with binder clips. The apparatus is subjected to initiation. For UV initiation the type of glass is important since the UV may not penetrate it. The resulting gel is a single network in the as prepared state. For most IPNs the single network gels were soaked to equilibrium in solution of monomer (or polymer), cross-linker agent (in some cases already attached to the polymer), initiator (UV, thermal or redox agents) and solvent (water). Then, the solution was placed between two glass plates with a silicon mold and was initiated. The resulting gel is an IPN in the as prepared state. All of the swelling and mechanical tests were completed in the equilibrium swollen state which is achieved after soaking the as prepared gel in water.

Ultrathin film gels have potential applications in tissue engineering, biomedical and biosensing fields. Ultrathin film hydrogels have comparable mechanical properties to bulk hydrogels and although they are more difficult to synthesize and characterize, they have the benefits of using less material and the ease of visualizing fracturing and necking. The synthesis methods and characterization of ultrathin film hydrogels can be found in Appendix 4, 5 and 6.



**Appendix Figure A-2.1: Typical single-network and IPN hydrogel synthesis methods.**

UV initiation at 312-nm wavelength for 30 min was the most common initiation method used in this work. Some of the hydrogels were initiated by thermal initiators or through redox reactions.

***The formulations:***

The monomer, cross-linker or initiator concentrations in this work are commonly presented as a weight (w/w) percentage, weight/volume (w/v) percentage or as the conventional gel formulation notation,  $T \times C$ .<sup>27,28</sup>  $T$  represents the total mass of monomer and cross-linker over the volume of water in which it was dissolved (w/v) as a percentage:

$$T = \frac{\text{total mass (monomer + cross-linker) (g)}}{\text{volume of water (ml)}} \times 100 \quad (\text{A-2.1})$$

$C$  represents the ratio of the mass of cross-linker by the total mass of monomer and cross-linker (w/w) as a percentage:

$$C = \frac{\text{mass of cross-linker}}{\text{mass of monomer + cross-linker}} \times 100 \quad (\text{A-2.2})$$

However, to directly compare formulations using cross-linkers with different molecular weights, a mole fraction is used in place of  $C$  and is defined here as  $C^*$ :

$$C^* = \frac{\text{moles of cross-linker}}{\text{moles of monomer + cross-linker}} \times 100 \quad (\text{A-2.3})$$

## ***Swelling***

If the conversion of mass, X, is not 100% a conversion factor is applied:

$$\phi_p = \phi'_p X \quad (\text{A-2.4})$$

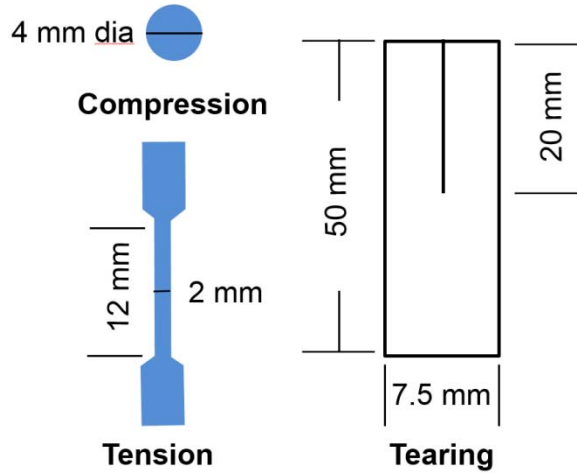
$$X = \frac{\text{mass in the gel}}{\text{mass in the reaction solution}} = \frac{m_{\text{dry}}}{m_{\text{synthesis}}} = \frac{m_{\text{dry}}}{\frac{T}{1+T} m_{\text{mold}}} \quad (\text{A-2.5})$$

## ***Mechanical Testing***

The hydrogels were cut out of larger sheets into specific shapes for mechanical testing. Schematic of shapes and typical dimensions are in Appendix Figure A-2.2. Typical shapes were cylinder-shaped (typically 4 mm diameter) for compression\*, dogbone-shaped(standardized JIS-K6251-7; length 35mm, width 2 mm, gauge length 12 mm) for tension and trouser-shaped (standardized JIS-K6252 ½; length 50mm, width 7.5 mm, initial notch 20mm) for tearing.

### ***Biopsy samples for cylindrical compression***

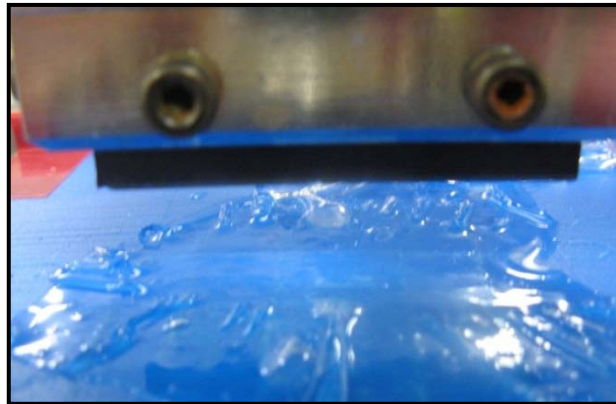
Some interesting observations that were noted are that in many of the “softer” samples the gel was not perfectly cylindrical. It was more like a slight cone shape, where the top had a bigger diameter than the bottom. So to help this cylinder could be cut in half so the cone effect is less notable. Also, bigger biopsy punches can be used for the gels. The “4” was the best; it is big enough that the gels will cut out and small enough that the gels will typically fail. Also there could be a lot of discrepancy in measuring the diameter of the gel. It is very easy for the diameter to vary  $\pm 0.3\text{-}0.5$  mm using a caliper. This was fixed this by using a microscope to measure the diameter.



**Appendix Figure A-2.2: Typical hydrogel shapes**

Compression was 4 mm diameter cylinders

Using a gel cutting device helps to reduce crack initiation that leads to premature failure, Appendix Figure A-2.3: SDAP-100N Dumbbell Co, Ltd. Appendix Figure A-2.4 shows dogbone-shaped hydrogels cut from gel cutting device.



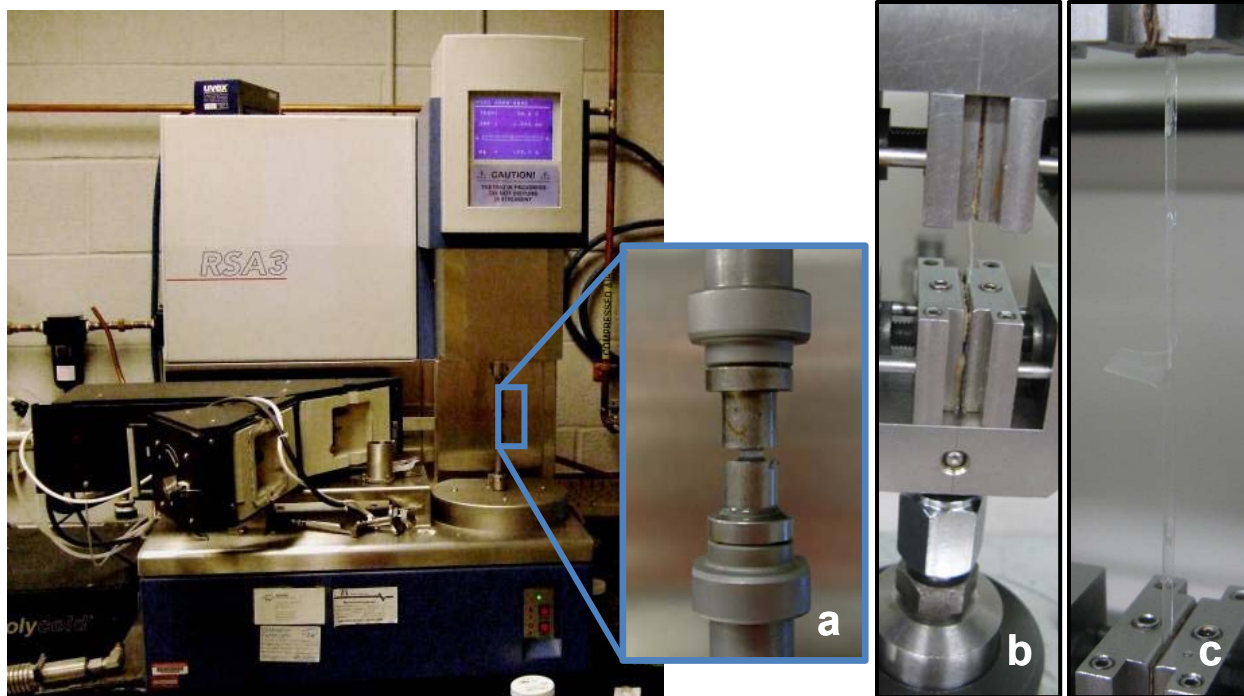
**Appendix Figure A-2.3: Gel cutting device, SDAP-100N Dumbbell Co, Ltd**

This gel cutting device helps to reduce irregularities introduced from cutting the gels which were hypothesized to be introducing premature cracks.



**Appendix Figure A-2.4: Cut dogbone gels**

For mechanical testing a TA RSAIII dynamic mechanical analyzer (DMA) was used for all compression tests and a tensilon machine RTC-1150A, Orientic Co was used for all tension and tearing tests. Appendix Figure A-2.5a, A-2.5b and A-2.5c show mechanical testing setups. Each of the formulations are tested between 3-8 trails. All of the hydrogels were lubricated with mineral oil to minimize both gel adhesion to the plate and evaporation of water from the gel during testing. Compression tests were completed at a constant velocity of 0.05 mm/s which was determined to be a rate where stress-strain curves are strain-rate independent. The sample diameter was measured using calipers, and the height was measured by the RSA III. Tension and tearing tests were completed at a constant velocity of 100 mm/min. The sample thicknesses were measured using either a caliper (if bulk gels) or a phase contrast optical microscope (ultrathin film gels shown in Appendix 4, 5 and 6). Tearing tests were completed in mode III: out-of-plane shear. Sand paper and kimwipes wrapped around the ends of the gels helped with gripping.



**Appendix Figures A-2.5a, A-2.5b and A-2.5c**

Dynamic mechanical analyzer (DMA) TA instruments RSA3 was used for all compression (Ia) tests. Tensilon machine RTC-1150A, Orientic Co was used for all tension (Ib) and tearing (Ib) tests.

## Imaging

The visualization of the microstructure of the hydrogel is of interest to scientists. By understanding the structure more mechanically tough hydrogels can be engineered. In this work the hydrogels have been imaged by scanning electron microscopy (SEM), atomic force microscopy (AFM) and direct stochastic optical reconstruction microscopy (dSTORM).

### ***Scanning electron microscopy (SEM)***

The fully swollen hydrogels were submerged into liquid ethane cooled with liquid nitrogen for quick freezing. Once frozen, the samples were lyophilized. The dry hydrogels were sputter coated with Au (10 mAmps for 2 min. 200 Å thickness) and imaged by using a Leo 1550 field emission SEM.

### ***Atomic force microscopy (AFM)***

AFM was performed on a Veeco BioScope (Digital Instruments, Inc) with a Veeco Dimension XYZ head, Nanoscope 3D controller and Nanoscope software V613r1. Veeco DNP1 tips were used for convectional topographic surface mapping. The samples were tested in the fully hydrated state, submerged in water.

### ***Direct stochastic optical reconstruction microscopy (dSTORM).***

The dSTORM images were acquired on a Nikon – N –Storm system using an objective CFI Apo TIRF 100x 1.49 oil and an EM-CCD Camera iXon DU897 (Andor) shown in Appendix Figure A-2.7.. The software used to was NIS-Elements Ar. The gels were sliced very thinly and placed on a cleaned cover slide (cleaned with 1M NaOH, sonicated for 30 min and then rinsed with DI water). A small cover slip was added to the top of the gel and then a silicon rubber mold was used to hold in the buffer solution. The buffer was added so the gel was fully submerged. The buffer consisted of 70  $\mu$ L of a 1 M MEA (cysteamine) Glox and 620  $\mu$ L of buffer B (50 mM tris-HCl pH 8 with 10 mM NaCl and 10% glucose). Another cover slide was added to the top to enclose the buffer/solution to prevent evaporation.



**Appendix Figure A-2.7: Nikon – N –Storm system for dSTORM imaging.**

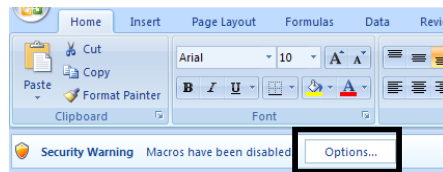


## How to use Excel DMATEMPLATE

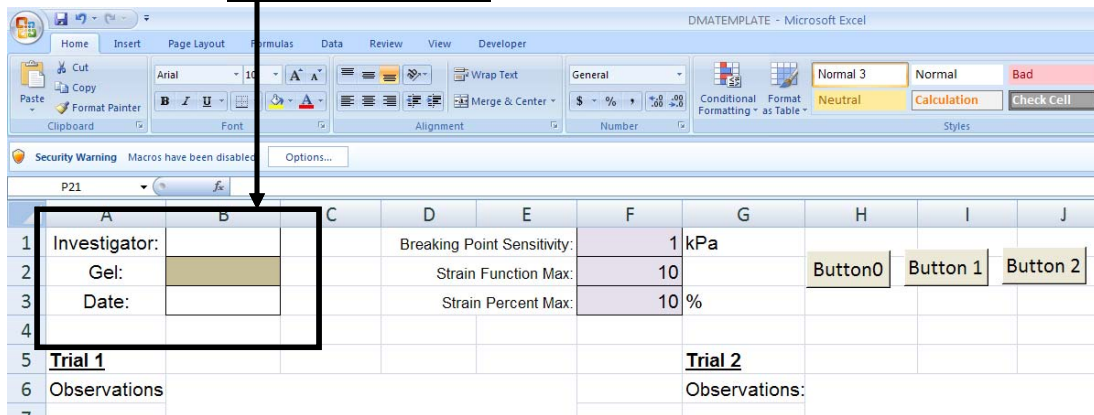
In running many, upon many, upon many (1000's of gels) under compression and starting off analyzing the samples by hand (not 1000!), a need for a program which will analyze the samples quickly was absolutely needed. Therefore, with the expertise of Tony Livengood, the DMATEMPLATE was developed to process raw data to create stress-strain curves and tabulate mechanical properties.

Instructions for using the DMATEMPLATE in excel for calculating values from DMA:

Remember to enable the macros and always have your raw data saved somewhere else. "Edit undo" cannot be done on a macro!



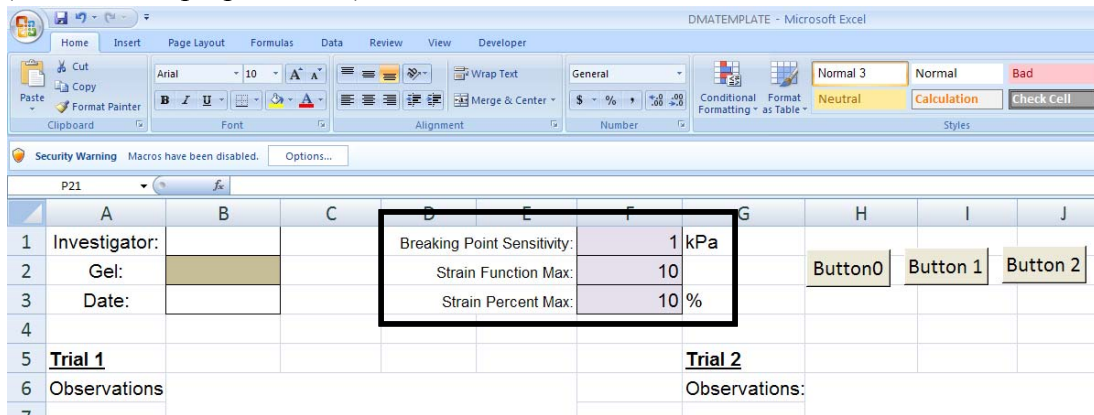
1. Fill out Cells for Name, Date, and Gel.



2. Hit **Button0**, it will enter what is located in the "Gel:" cell into the tab name.
3. Enter the data for the stress in (Pa) and strain (%) into the respective columns of each trial. Make sure to fill out the trials consecutively. (For example, do not fill trials 1, 3 and 4. Use trials 1, 2, and 3.)

9	Breaking Point, Row:				Breaking Point, Row:				Breaking Point, Row:						
10	stress v. strain fcn				stress v. strain fcn				stress v. strain fcn						
11	m=	b=			m=	b=			m=	b=					
12	SEm=	SEb=			SEm=	SEb=			SEm=	SEb=					
13	R^2=	SEy=			R^2=	SEy=			R^2=	SEy=					
14	F=	DOF=			F=	DOF=			F=	DOF=					
15	SSReg=	SSResid=			SSReg=	SSResid=			SSReg=	SSResid=					
16															
17	Strain Fcn Max, Row:	G			Strain Fcn Max, Row:				Strain Fcn Max, Row:						
18	stress v. strain fcn				stress v. strain fcn				stress v. strain fcn						
19	m=	b=			m=	b=			m=	b=					
20	SEm=	SEb=			SEm=	SEb=			SEm=	SEb=					
21	R^2=	SEy=			R^2=	SEy=			R^2=	SEy=					
22	F=	DOF=			F=	DOF=			F=	DOF=					
23	SSReg=	SSResid=			SSReg=	SSResid=			SSReg=	SSResid=					
24															
25	Strain % Max, Row:	E			Strain % Max, Row:				Strain % Max, Row:						
26	stress v. strain fraction				stress v. strain fraction				stress v. strain fraction						
27	m=	b=			m=	b=			m=	b=					
28	SEm=	SEb=			SEm=	SEb=			SEm=	SEb=					
29	R^2=	SEy=			R^2=	SEy=			R^2=	SEy=					
30	F=	DOF=			F=	DOF=			F=	DOF=					
31	SSReg=	SSResid=			SSReg=	SSResid=			SSReg=	SSResid=					
32															
33	Stress (Pa)	Stress(kPa)	Strain (%)	Strain(%)	Strain Fcn	Stress (Pa)	Stress(kPa)	Strain (%)	Strain(%)	Strain Fcn	Stress (Pa)	Stress(kPa)	Strain (%)	Strain(%)	Strain Fcn
34															
35															
36															
37															
38															
39															

- Fill out cells for Breaking Point Sensitivity, Strain Function Max, and Strain Percent Max (these are the purple boxes,) or use standard values.

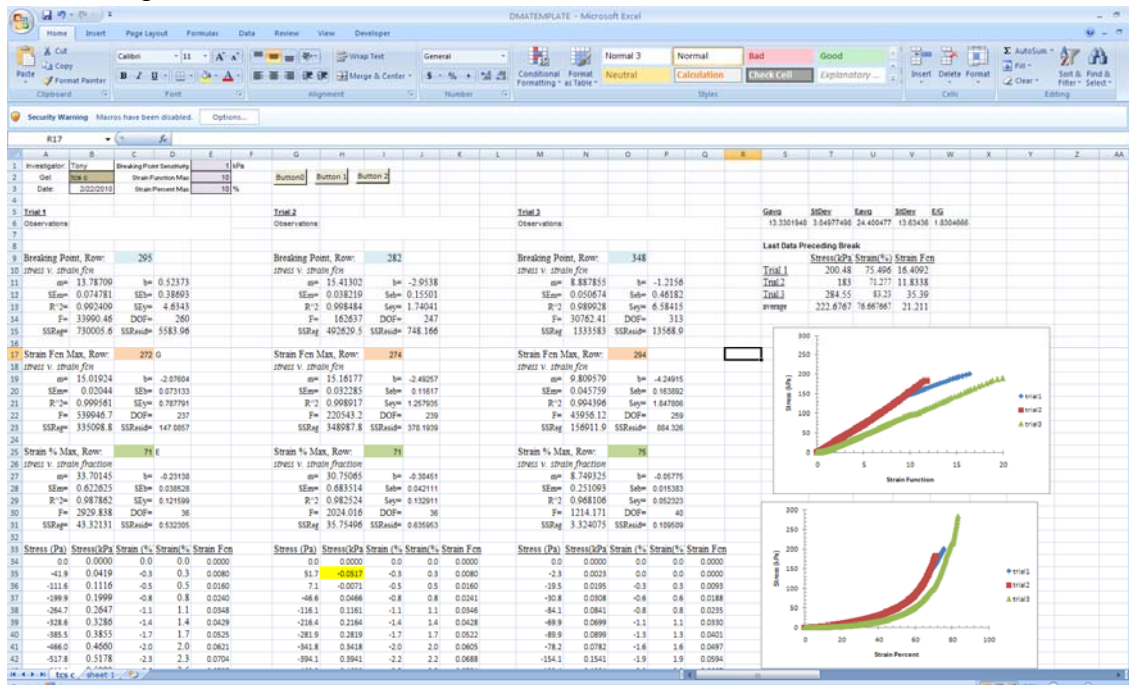


To find the break point manually, we look for a large drop in value in the stress (kPa) column. The computer will do the same thing, and the sensitivity defines how large that drop must be.

- Hit **Button 1**, it will find the row address for the break point, the strain function max, and the strain % max, and it will place the row address in the blue, peach and green cells respectively.

Breaking Point, Row:	
10	stress v. strain fcn
11	m=
12	SEm=
13	R^2=
14	F=
15	SSReg=
16	SSResid=
Strain Fcn Max, Row:	G
18	stress v. strain fcn
19	m=
20	SEm=
21	R^2=
22	F=
23	SSReg=
24	SSResid=
Strain % Max, Row:	E
25	stress v. strain fraction
26	

- Check the break point row addresses. If they do not make sense, CHANGE them. It will make a difference for the next button. The same goes for the strain fcn max and strain % max row addresses.
- Hit **Button 2**. It will evaluate the linest function for Stress(kpa) vs. strain function for the top two, and stress vs. strain fraction for the bottom one. The linest function will be evaluated from the first data point until the breakpoint, the Strain Function Max, and Strain % Max, respectively.
- Button 2** will also give G, E, and E/G calculated by the slopes of the stress vs. strain function, and stress vs. strain fraction. The value given is an average of however many trials were entered. Also, data will be given for the last line of data before the gel broke (breaking point).
- Charts are given. They will appear on top of each other, so be sure to move the one on top, to see the next one.



## Appendix for Chapters 4, 5 and 6

### Synthesizing Ultrathin Film Hydrogels

The T x C or wt.% were the commonly used notation within this Chapter and other double-network chapters, but the leader in the field Jian Ping Gong's group used a formulation explained below (monomer concentration-crosslinker concentration (mol%)-initiator concentration (mol%)). To compare with their work a detailed explanation of their formulation is listed.

**The formulation:** (\_\_\_-\_\_\_-\_\_\_) *monomer concentration (M) -crosslinker concentration (mol%)-initiator concentration (mol%)*

$$\begin{aligned} \text{Monomer concentration (M)} &= \frac{\text{mass of monomer}}{\text{MW of monomer} * \text{Final solution volume}} \\ \text{Crosslinker concentration (mol \%)} &= \frac{(100 \%) * \text{mass of crosslinker}}{\text{Monomer concentration (M)} * \text{MW of crosslinker} * \text{Final solution volume}} \\ \text{Initiator concentration (mol \%)} &= \frac{(100 \%) * \text{mass of initiator}}{\text{Monomer concentration (M)} * \text{MW of initiator} * \text{Final solution volume}} \end{aligned}$$

Example of how to calculate out how much materials used:

Formulation (2-0.02-0.01) with a final volume of 30 mL for AAm, BisAAm, Irgacure

$$\begin{aligned} \text{Amount of AAm (g)} &= 2 \left( \text{monomer concentration} \frac{\text{mol}}{\text{L}} \right) * (30 * 10^{-3}) \text{ (solution volume L)} \\ &* 71.04 \left( \text{MW of AAm} \frac{\text{g}}{\text{mol}} \right) \\ &= 4.26 \text{ g AAm} \end{aligned}$$

$$\begin{aligned} \text{Amount of BisAAm (g)} &= \frac{0.02 \text{ (crosslinker concentration mol\%)}}{100 \text{ (\%)}} * 2 \left( \text{monomer concentration} \frac{\text{mol}}{\text{L}} \right) \\ &* (30 * 10^{-3}) \text{ (solution volume L)} * 154.17 \left( \text{MW of BisAAm} \frac{\text{g}}{\text{mol}} \right) \\ &= 0.00185 \text{ g BisAAm} \end{aligned}$$

$$\begin{aligned} \text{Amount of Irgacure (g)} &= \frac{0.01 \text{ (initiator concentration mol\%)}}{100 \text{ (\%)}} * 2 \left( \text{monomer concentration} \frac{\text{mol}}{\text{L}} \right) \\ &* (30 * 10^{-3}) \text{ (solution volume L)} * 224 \left( \text{MW of Irgacure} \frac{\text{g}}{\text{mol}} \right) \\ &= 0.001344 \text{ g Irgacure} \end{aligned}$$

### *Polymerization of PAAm:*

<u>Chemicals</u>	<u>Purchase From and Details</u>	<u>Role</u>
Acrylamide	Fisher Scientific: 99+ % Electrophoresis Grade AC164851000	Monomer
AAm(Japan)	Junsei Chemical Co. Ltd. recrystallized from chloroform	
MCS		Monomer
BisAcrylamide	Fisher Scientific: 99+ % Electrophoresis Grade AC164790250	Crosslinker
MBAA(Japan)	Tokyo Kasei Co., Ltd. recrystallized from ethanol	
Water	Fisher Scientific: Deionized ultra-filtered water (DIUF) W2-20	Solvent
TEMED	Sigma-Aldrich: Electrophoresis Grade T9281-25ML	Accelerator
APS	Sigma-Aldrich: Electrophoresis Grade A3678-25G	Initiator
Irgacure 2595 (Japan)		Initiator

Because the MCS and PAAm gels synthesized were ultrathin, they were synthesized in a 0.1 M NaCl solution to help handle the brittle nature of the gel.

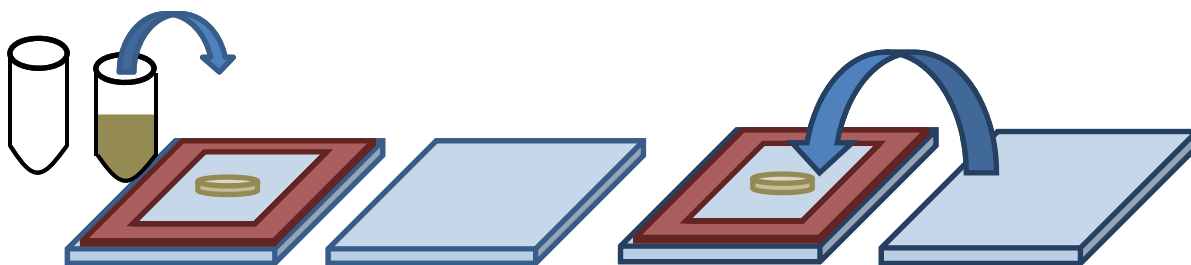
### Equipment

10x10 cm glass plates  
100 micrometer plastic spacer  
Plastic tube for mixing  
Glovebox  
4 metal clips

### ***Synthesis Protocol for film DN gels MCS network:***

We acknowledge Prof. Gong's lab, especially Jian Hu for helping teach procedures for film DN gels.

1. Remove chemicals from the fridge and allow them to equilibrate to room temperature. If the chemicals are not allowed to warm before opening, water will condense in the container.
2. Measure out the MCS (PEGDA if used) and put it into the plastic tube. Be careful for static electricity.
3. Add water to the tube and mix until homogenous
4. Put a plastic wrap on the tube and poke holes in the plastic.
5. Put this tube in the vacuum oven and slowly vacuum out all of the air. Bubbles will form in the tube so be careful not to bump the solution.
6. Degassing takes about 30 min. Wait until no more bubbles form and all of the solution is degassed.
7. Put glass slides, spacer, 4 clips and solution in the glovebox.
8. In the glovebox assemble the one glass plate with the spacer and pour the solution in the middle.
9. Slowly drop the second glass plate on top (bubbles will form in not done slowly).
10. Put on the clips on all four sides.
11. Polymerization from the top 10 cm away
12. Do not flip the sample and polymerize using the 312 nm wavelength bulbs.
13. Polymerize for 30 min
14. After polymerization carefully open the glass plates. (open the plates slowly or the gel will break)
15. Cut off the dry edges and peel off the gel (slowly)
16. Put the gel in a AAm, BisAAM and Irgacure solution for 30 min
17. After place the gel on a glass plate and pipette a bit of solution on the gel.
18. Add a second plate and wrap with plastic wrap.
19. Place in the glovebox
20. Polymerize for 30 min
21. After polymerization carefully open the glass plates. (open the plates slowly or the gel will break)



The gels might have a light tint but are fairly clear. They also might have some large bubbles, try to avoid using these pieces for tests.

### Swelling Tests:

The volume degree of swelling (Q) / mass degree of swelling (q): can vary from 1.2 to over 1000  
The equilibrium water content (EWC) can vary from 20% to over 95%

$$Q = \frac{\text{volume of swollen hydrogel}}{\text{volume of dry polymer}} \quad (\text{A-4.1})$$

$$q = \frac{\text{mass of swollen gel}}{\text{mass of dry polymer}} \quad (\text{A-4.2})$$

$$\text{EWC} = \frac{\text{mass of water absorbed by gel}}{\text{mass of swollen gel}} 100 \% \quad (\text{A-4.3})$$

The polymer volume fraction is the inverse of the volume degree of swelling:


$$\Phi'_p = \frac{1}{Q} \quad (\text{A-4.4})$$

If the conversion of mass, X, is not 100% a conversion factor is applied:

$$\Phi_p = \Phi'_p X \quad (\text{A-4.5})$$

$$X = \frac{\text{mass in the gel}}{\text{mass in the reaction solution}} = \frac{m_{\text{dry}}}{m_{\text{synthesis}}} = \frac{m_{\text{dry}}}{\frac{T}{1+T} m_{\text{mold}}} \quad (\text{A-4.6})$$

### Swelling Protocol:

1. Pre weigh a glass jar with sea sand about 3/4ths full and record the weight.
2. Cut a small piece of the mold gel on glass plate usually a thin rectangle.
3. Tare the scale and then place the mold gel on the scale, record the weight
4. Swell the mold gel in water for a couple of days/hours (depending on size). 24 hours is usually sufficient.
5. Exchange the water for fresh DI water at least 3 times and preferably every couple of hours in the beginning and once right before taking the swollen gel measurements.
6. Place gel on a spatula and dab the spatula with a kimwipe making sure not to touch the gel: This is important to not have excess water, yet not to absorb the water from the interior of the gel. Another technique is to place the gel on your glove and move it around slightly to remove the excess water, however sometimes the gel will flake off.
7. Weigh the swollen gel
8. Put in the jar with the sea sand. 
9. Shake the jar not making sure not to lose any of the sand.
10. Put the jar with the gel and sea sand in an oven at 120 degrees C. for 2 hrs.
11. The gel physically looks smaller and shriveled. It may be flat, discolored, misshaped, etc.
12. Weigh the dry gel, sand and jar

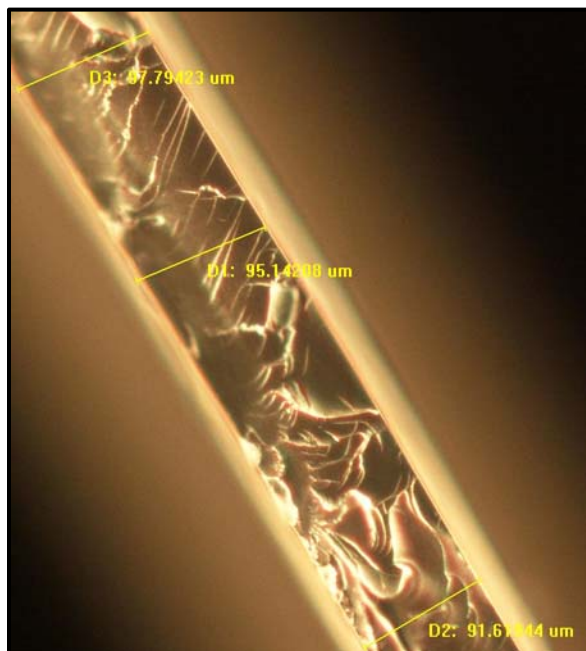


For each sample steps 1-10 are done 3+ times to take an average of the results

From the tests there are 4 weights: The weigh boat, the mold gel, the swollen gel and the dry gel. It is advised to do steps 6-7, 3+ times to insure that results are consistent. When a consistent number is measured this is used as the recorded weight. The variations in the technique and measurements can throw off the results.

### *Gel Thickness*

Because the gels are ultrathin and the accuracy of the thickness is very important in the mechanical tests we measured the thicknesses of the hydrogels using a phase contrast optical microscope (Olympus CKX41). Using Image Pro Plus 6.0 to analyze gel images we averaged the thickness and took the average number over 4+ gel samples. The figure below shows an example of the gel ultrathin hydrogels achieved.





## Appendix for Chapter 9

### Synthesis of NVEE

We acknowledge Dr. Berkland's lab, especially Zahra Mohammadi, Joshua Sestack and Vara Aziz for helping teach procedures for synthesis and purification of NVEE as follows:

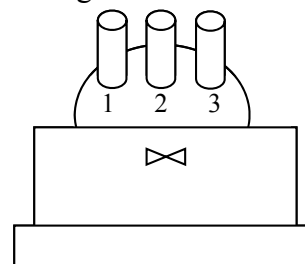
<u>Chemicals</u>	<u>Purchase From and Details</u>	<u>Role</u>
NVF	Sigma-Aldrich: Vacuum distilled, stored at -10°C 447331-(21 g)	base unit
	Potassium tert-butoxide (35.44 g)	Base
	Dicyclohexyl-18-crown-6 (3 g)	Enhancer
THF	Anhydrous THF (280 mL total)	Solvent
	Bis(2-bromthyl)ether (27.8 g or 22.787ml) 1.22 g/ml	Connector
	Nitrogen or argon	Gas

### Equipment

3 port flask = 3-neck round bottom flask  
2 glass stoppers  
1 rubber stopper  
Glass recrystallization dish  
Glass stir bar  
small venting needle  
nitrogen or argon needle  
nitrogen or argon needle  
small addition funnel  
Ice

### ***Synthesis Protocol for NVEE:***

1. Wash all of the items used for the synthesis of NVEE and put them in the heated vacuum for 12 hours remove all of the water:
  - a. 3 port glass round bottom flask
  - b. 2 glass stoppers
  - c. Glass stir bar
  - d. Small addition funnel
2. Take the items out of the oven and let them reach room temperature
3. Take out the chemicals: let it reach room temperature if it was in the fridge or freezer
  - a. potassium tert-butoxide (35.44 g)
  - b. anhydrous THF (280 mL total)
  - c. dicyclohexyl-18-crown-6 (3 g)
  - d. distilled N-vinylformamide (21 g or 20.71ml) 1.014g/ml
4. Put the glass stir bar in the 3-neck round bottom flask
5. Set-up similar to shown on right in the hood
  - a. Use a glass recrystallization dish for the ice that will be added later



- b. Make sure the stir plate is as close to the stir bar as possible or the solution will not be able to stir well enough
          - i. Add a big enough stir bar in the beginning or use a long stir rod (this will go into port 2 and will be sealed)
6. Measure out the potassium tert-butoxide
  - a. put it in the 3-neck round bottom flask
7. In port (neck) 1,2 put a glass stopper
8. Put a rubber stopper in port 3
9. Flush the flask with nitrogen or argon by attaching a needle (that is attached to the nitrogen or argon line) in the rubber stopper with another small venting needle
10. Add the anhydrous THF (280 mL total) to the inert 3-neck round bottom flask
11. Stir the mixture using the stir bar
12. Make sure the nitrogen or argon is still going in port 3: take off the glass stopper from port 1 and add the dicyclohexyl-18-crown-6 (3 g), keep stirring
13. Add the distilled N-vinylformamide (21 g or 20.71ml) 1.014g/ml
14. Remove the small venting needle
15. Remove the nitrogen or argon needle
16. Mixture stirred vigorously at room temperature for 45 min
  - a. The mixture tends to turn a light yellowish color but remains clear
  - b. After about 45 min the mixture suddenly turns viscous and has a torn up paper appearance.
  - c. Make sure it is still stirring
  - d. While this is going the Bis(2-bromthyl)ether (27.8 g or 22.787ml) can be prepared in a small addition funnel with a glass stopper on the top
17. Cool in an ice bath
18. Get slurry stirring
  - a. Make sure the mixture breaks up
  - b. This takes a while sometimes over an hour so keep an eye for it
19. Flush the flask with nitrogen or argon by attaching a needle back to the rubber stopper in port 3 (that is attached to the nitrogen or argon line) in the rubber stopper with another small venting needle
20. Put the small addition funnel with the bis(2-bromthyl)ether (27.8 g or 22.787ml) 1.22 g/ml in port 2
21. Add the bis(2-bromthyl)ether dropwise while stirring
  - a. This process takes ~30 min to 1 hr
22. Once complete take out the addition funnel and recap with the glass stopper
23. Remove the small venting needle
24. Remove the nitrogen or argon needle
25. The mixture was stirred at room temperature for 72 hrs
  - a. Make sure the solution is stirring before wrapping it in foil to leave to react
    - i. The foil helps to keep out light

## Purification of NVEE

### Chemicals

NVEE + impurities from synthesis  
Chloroform  
Distilled water  
brine: Saturated solution of sodium chloride  
anhydrous sodium sulfate  
ethyl acetate  
hexane  
Silica beads

### Role

NVEE  
Purification extraction  
Separation  
  
Remove water  
column chromatography  
column chromatography  
column chromatography

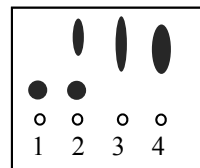
### Equipment

Apparatus for vacuum filtration  
Filter paper  
Rotavap and setup: glass round bottom flasks  
Ice, dry ice (preferable) or liquid nitrogen for trap  
separatory funnel  
beakers  
flasks  
column chromatography (large diameter column)  
TLC plates  
TLC glass container  
capillary tube

### ***Purification Protocol for NVEE:***

1. Clean all of the equipment needed for purification the day before so it can dry in the oven and eliminate the chance of impurities
2. After reacting the potassium bromide salt was removed by filtration
  - a. I have used a light vacuum filtration with a large funnel and filter paper
  - b. I have also used gravity filtration (it takes a while so be patient, but I think it is very effective)
3. Sometimes I need to do this filtration 2-3 times
4. Collect the liquid and throw away the salts
5. Then the reaction mixture was concentrated under vacuum in the rotavap
  - a. honey like consistency is formed.
6. Then, diluted with 300 mL of water.
7. Set up a separatory funnel
  - a. Add the water, NVEE mixture
8. The crude product was obtained by extraction with chloroform five times (50 mL × 5)
  - a. The chloroform is collected, which is the lower part.
  - b. However do not throw anything away until completed
9. The combined organic layers were washed twice with brine and dried over 3 full teaspoons of anhydrous sodium sulfate.
  - a. What is the brine: Saturated solution of sodium chloride that is made in the lab

10. This is capped and put into the refrigerator overnight
11. The resulting product was recovered after concentration in a vacuum distillation column.
  - a. Collect filter and transfer to a small round bottom flask
  - b. Then rotavap until a black tea or honey consistency, about 4-6 hours. Put into a oven vacuum overnight. This is the crude material.
12. Purification by chromatography on silica (ethyl acetate:hexane 7:3 vol/vol)
13. Mix silica beads and let swell in the 7:3 mixture and then pack the column 2/3 full
  - a. Tap silica beads to help with uniformity
14. Add sea sand to the top of the column
15. Add the 7:3 mixture to the middle of the sea sand layer
16. Add the sample to the top to completely layer the top then add the 7:3 mixture to the top of the sample.
  - a. Do this slowly not to disturb the column
17. Making sure never to run out of the 7:3 mixture on the top
18. Collect on the bottom in vials approx. 50-60 vials
  - a. It takes awhile to start collecting
19. TLC is performed on the samples. Put on the sample with a capillary tube one from each vial.
  - a. Determine which vials have just the pure product and which have contaminants
  - b. Usually vials 15-end have the pure product. Use the good old xL to compare.
20. Put into 7:3 mixture in glass jar that is for TLC. Just a bit.
21. On the right is what is typically seen
  - a. 1 pure product with just one spot
  - b. 2 has pure product and an impurity
  - c. 3 has an impurity
  - d. 4 has an impurity
22. The vials with the pure product were rotavaped
23. The vials with some product were combined and rotavaped and then placed on the column again and steps 12-22 were repeated



***Purification assay of NVEE:***

1. HPLC with a C18 column was used.
2. Samples delivered at a flow rate of 1mL/min.
3. The mobile phase consisted of acetonitrile/water (0.1%TFA) and was programmed as follow, 0% acetonitrile between 0 to 3 minutes, a linear increase to 10% at 8 minutes, a linear increase to 13.8% between 8 to 27 minutes and then linear increase to 70% between 27 to 29 minutes, a hold at 70% acetonitrile for 2 minutes and then return to 0% acetonitrile at 33 minutes. The UV absorbance wavelength was 220 "
4. Gives two peaks. Collect those peaks for mass spec to find out the product peak.
5. Collect the peaks manually (analytical column and not the prep) because it is more accurate since the flow rate is slow.

\*1H and Carbon NMR can also be performed to compared to the pure product

## Polymerization of PAAm

<u>Chemicals</u>	<u>Purchase From and Details</u>	<u>Role</u>
Acrylamide	Fisher Scientific: 99+ % Electrophoresis Grade AC164851000	Monomer
BisAcrylamide	Fisher Scientific: 99+ % Electrophoresis Grade AC164790250	Crosslinker
Water	Fisher Scientific: Deionized ultra-filtered water (DIUF) W2-20	Solvent
TEMED	Sigma-Aldrich: Electrophoresis Grade T9281-25ML	Accelerator
APS	Sigma-Aldrich: Electrophoresis Grade A3678-25G	Initiator

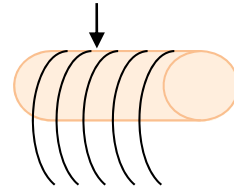
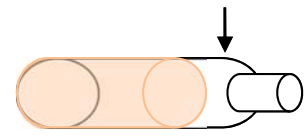
### Equipment

Weigh boats  
4mL glass vial  
Pipette  
Nitrogen gas  
Coffee straw  
Brown paper towels  
Beakers  
Hammer  
Vial for storage

### ***Synthesis Protocol for PAAm:***

1. Remove chemicals from the fridge and allow them to equilibrate to room temperature or water will condense in the container.
2. Measure out the acrylamide and bisacrylamide in separate weighboats. Be careful for static electricity. Using a metal weighboat might help to lessen these effects.
3. By pipette, add ~1.5mL of water to both of the weighboats of acrylamide and bisacrylamide.
4. Pipette up and down the water and chemical mixture until dissolved. Add this solution to the 4mL glass vial. A bit more water may be needed, but make sure not to exceed 4 mL total.
5. Add the TEMED to the 4mL glass vial.
6. Add remaining water (so that the total amt of water is 4mL)
7. Vortex the solution
8. Make a 1 M APS solution by dissolving 0.22818g of APS in 1mL of water in a separate container of a weighboat.
9. Bubble the solution in the 4mL glass vial with nitrogen gas by using a coffee straw attached to the pipette tip that is on the end of the hose attached to the nitrogen tank. The coffee straw helps so the solution does not bubble over. The bubbles should be a steady stream but not violently bubbling. Bubble for about 14 min, if at any time the solution is not being bubbled then start the time over. (Should be 14 min of continuous bubbling.)
10. Add the correct amount of APS to the 4mL glass vial while still bubbling.
11. Bubble for another 30 seconds (should be just enough time to put down the APS solution and pick up the vial lid.
12. Quickly withdraw the nitrogen (coffee straw) and put on the lid. Do not allow oxygen to the vial. Oxygen will inhibit the reaction.

13. Leave for 24 hours which allows the reaction to complete by placing the vial in a place where it will not be moved for the duration of the reaction.
14. Prepare an area for breaking the vials. Get 2 large beakers full of water, brown paper towels and a hammer.
15. Take off the lid to the glass vial and wrap in 1-2 paper towels.
16. Hit the lid side with the hammer between the neck and the gel. (as figure to the right)
17. Unwrap the gel and peel off the large glass pieces.
18. Dip the gel in the first beaker of water.
19. Dip the gel in the second beaker of water to get the remaining shards of glass off.
20. Pat with a paper towel to get water off of the gel
21. Cut into slices: The bottom two are used for the DMA, the third slice from the bottom is used for swelling tests. The rest of the gels can be saved incase need for future tests.



The gels might have a light tint but are fairly clear. They also might have some large bubbles. However for the most part it is clear and not bubbles are present.

## Polymerization of PNVF

<u>Chemicals</u>	<u>Purchase From and Details</u>	<u>Role</u>
NVF	Sigma-Aldrich: Vacuum distilled, stored at -10°C 447331-500ML	Monomer
NVEE	Berkland's Lab: 2-(N-vinylformamido) ethyl ether	Crosslinker
Water	Fisher Scientific: Deionized ultra-filtered water (DIUF) W2-20	Solvent
VA-044	Wako Pure Chemical Industries, Ltd: CAS 27776-21-2 50g	Initiator

### Equipment

Weigh boat  
4mL glass vial  
Pipette  
Nitrogen gas  
Coffee straw  
Large Crystallization dish for water bath  
Heat plate/source  
Brown paper towels  
Beakers  
Hammer  
Vial for storage

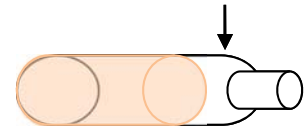
### ***Synthesis Protocol for PNVF:***

1. Remove chemicals from the fridge and allow them to equilibrate to room temperature or water will condense in the container.
2. Start the water bath by using a large crystallization dish and setting the temperature to 50°C on a heating plate. Place a stir bar to help make a uniform heating system.
3. Measure out the VA-044 in a weigh boat. Be careful for static electricity. Using a metal weigh boat might help to lessen these effects
4. Push the distilled clear NVF solution through a syringe and filter
5. By pipette, add 3mL of the water, the distilled NVF and the NVEE to the 4mL glass vial.
6. Pipette up and down the water with the pipette tip to get out all of the residual chemicals in the tip.
7. Add the VA-44 to 1 mL of water and then add to the 4mL glass vial.
8. Vortex the solution
9. Bubble the solution in the 4mL glass vial with nitrogen gas by using a coffee straw attached to the pipette tip that is on the end of the hose attached to the nitrogen tank. The coffee straw helps so the solution does not bubble over. The bubbles should be a steady stream but not violently bubbling. Bubble for about 15 min, if at any time the solution is not being bubbled then start the time over. (Should be 15 min of continuous bubbling.).
10. Quickly withdraw the nitrogen (coffee straw) and put on the lid. Do not allow oxygen to the vial. Oxygen will inhibit the reaction.
11. Make sure the cap is securely fastened and placed in the 50°C heated water bath. Try not to place directly on the heat place surface.
12. Leave for 24 hours which allows the reaction to complete. Make sure to fill the water bath as needed. Fill before leaving overnight.

13. Prepare an area for breaking the vials. Get 2 large beakers full of water, brown paper towels and a hammer.

14. Take off the lid to the glass vial and wrap in 1-2 paper towels.

15. Hit the lid side with the hammer between the neck and the gel.  
(as figure to the right)



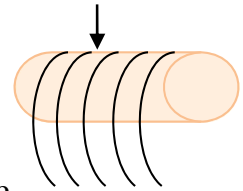
16. Unwrap the gel and peel off the large glass pieces.

17. Dip the gel in the first beaker of water.

18. Dip the gel in the second beaker of water to get the remaining shards of glass off.

19. Pat with a paper towel to get water off of the gel

20. Cut into slices: The bottom two are used for the DMA, the third slice from the bottom is used for swelling tests. The rest of the gels can be saved incase need for future tests.



The gels might have a light tint but are fairly clear. They also might have some large bubbles. However for the mist part it is clear and not bubbles are present.



## Appendix for Chapter 10

### Hydrolysis of PAAm and PNVF

We acknowledge Brad Strathman for help in developing protocols for hydrolysis.

<u>Chemicals</u>	<u>Role</u>	<u>Equipment</u>	
PAAm gels	Test Samples	Biopsy	Weigh Boats
PNVF gels	Test Samples	4 ml glass vials	25 ml glass vials
NaOH	Base	Pipette	Beakers
HCl	Acid	Balance	Oven
NaCl	Salt	Thermometer	
Water	Solvent		

#### *Hydrolysis Protocol for PAAm and PNVF:*

1. Prepare a NaOH solution of desired molarity (0.001, 0.01, 0.1 or 1) by weighing an appropriate amount of NaOH and combining with an appropriate amount of water.
2. Preheat the NaOH solution in the oven. By using a thermometer, check the solution temperature until the desired temperature is achieved.
3. Soak 3 samples cut with a biopsy in NaOH at desired temperature, time, and molarity.
4. If PAAm gel samples are used, record the masses of the gel samples under NaOH Weight after removing the samples from the NaOH solution.
5. After being removed from the NaOH solution, place gels in filtered water for 24 hrs.
6. Exchange the water for fresh filtered water at least 3 times and preferably every couple of hours in the beginning and once right before taking the water weight gel measurements.
7. Place the gel on a spatula and dab the spatula with a kimwipe, making sure not to touch the gel. This is important not to have excess water, yet not to absorb the water from the interior of the gel. Another technique is to place the gel on your glove and move it around slightly to remove the excess water, however sometimes the gel will flake off.
8. Record the masses of the gel samples under Water Weight.
9. For PAAm gel samples: After swelling in water for 24 hours and obtaining the Water Weights, place the gel samples in 0.1 M NaCl solution for 24 hours.
10. For PAAm gel samples: After soaking in the salt solution for 24 hours, record the masses of the gel samples under Salt Weight. Rinse the gel samples with filtered water.
11. For PNVF gel samples: After swelling in water for 24 hours and obtaining the Water Weights, place the gel samples in an acid solution made from water and drops of 1.0 M HCl. (After the trial run of various pH's was done, a pH of 3.0 was desired)
12. For PNVF gel samples: Allow the gel samples to swell in the acid solution for 24 hours. After this swelling, record the masses of the gel samples under Acid Weight.
13. For PNVF gel samples: Place the samples in water for 24 hours; record the masses of the gels, this is the swollen weight. Soak the samples in 0.1 M NaCl solution for 24 hours; record the masses of the gels this is the salt weight. Rinse the gels with filtered water.
14. Pre-weigh a weigh boat and record the weight.
15. Put the gel samples in desiccators for at least 24 hours.

16. The gel physically looks smaller and shriveled. It may be flat, discolored, misshaped, etc.
17. Weigh the dry gel, if possible, on a torn weigh boat or subtract the weigh boat's mass.

### Titration of PAAM and PNVF

<u>Chemicals</u>	<u>Role</u>	<u>Equipment</u>	
PAAM gels	Test Samples	pH Probe	100 ml Buret
PNVF gels	Test Samples	Stir Plate	Stirring Rod
NaOH	Base	Beakers	Spatula
HCl	Acid	Parafilm	Scissors
Water	Solvent	25 ml glass vials	

#### *Titration Protocol for PAAM and PNVF:*

1. Prepare a 1 M NaOH solution for the PNVF gels and a 0.1 M NaOH solution for the PAAM gels.
2. Preheat the two NaOH solutions to 60°C in the oven.
3. Take 10 samples of 15 x 3 PNVF and 10 samples of 15 x 3 PAAM that have been cut with a biopsy and place the samples into the respective NaOH solution.
4. Allow the samples to undergo hydrolysis for 2 hours.
5. Place the samples in individual vials filled with water.
6. Allow the samples to soak for 24 hours
7. For PNVF gels: After swelling in water for 24 hours, soak the samples in a solution of HCl and water with a pH of 3 for 24 hours.
8. For PNVF gels: To have the gels change into their hydrogen form, soak the gels in 0.01 M NaOH solution for 2 hours. This solution was made by combining 10 ml 0.1 N NaOH with 90 ml of water.
9. For PAAM gels: After swelling in water for 24 hours, dry the samples for 24 hours.
10. For PAAM gels: After drying, soak the samples in 0.01 M HCl for 2 hours. This solution was made by combining 10 ml 0.1 N HCl with 90 ml of water.
11. Dry all the samples for 24 hours.
12. After doing calculations assuming 100% hydrolysis, the PNVF and PAAM gels were each divided into 2 batches. 0.01 M HCl seemed an appropriate titrant for PNVF, and 0.01 M NaOH seemed an appropriate titrant for PAAM. The titrants were made by combining 10 ml of the respective 0.1 N base or acid with 90 ml of water.
13. To prepare for titration, a batch of either PNVF or PAAM was allowed to swell in 50 ml of water in a beaker to soften the gels.
14. Using a spatula, the gels were broken into pieces.
15. A stirring rod was added, and the beaker was placed on a Stir Plate set to 600 rpm for 10 minutes to further crush the gels.
16. The Stir Plate was reduced to 150 rpm.
17. The pH probe was calibrated before each batch.
18. Parafilm was placed over the beaker to prevent carbon dioxide exposure.
19. The initial pH of the gel solution was recorded.
20. Waiting 30 minutes between each addition of titrant, the pH was further recorded until either the PAAM batches turned dominantly basic or the PNVF batches turned dominantly acidic.

## Appendix for Chapter 12

### PAAm Nanoparticles

We acknowledge Dr. Berkland's lab, especially Huili Guam and Chuda Chittasupho for teaching the procedures for making PAAm and PNVF particles as well as providing nanoparticles.

#### Solution A: oil phase

1. Span 83 (Sorbitan sequeioleate)	5 g
2. PHS (polyoxyethylene sorbitol helaoleate)	2.8 g
3. kerosene	20 g

#### Solution B: water phase

1. AAm	9.9 g
2. BisAAm Cross linker (XL)	0.1 g
3. Water (DI)	10 g
4. VAZO-52 (initiator)	20 mg

Set temperature of the oil bath to 55 °C. The knob on the heat plat should be set to around 135 °C in order to heat the oil bath to 55 °C.

A: vial 1 should be a 50 ml centrifuge tube. Add all of the oil phase components. Mix vigorously.

B: vial 2 should be a 150 ml glass beaker. Add all of the water phase chemicals to the beaker and stir. Use the sonicator to further dissolve the chemicals.

Set up reaction vessel. A round bottom flask with a stir bar. Then get a rubber stopper and the metal ring to hold the rubber stopper on.

Add VAZO-52 to the round bottom flask.

Using the sonicator wash with pure Kerosene for 5 min.

Sonicate B and pipette A slowly, add drop by drop

Sonicate for 5-10 min

Add solution to reaction vessel.

Add stopper

Add purge needles

Bubble nitrogen for 15 min

Place in the oil bath for 4 hrs.

Take off the heat bath and add to 2 centrifuge tubes equally.

Put into centrifuge at these conditions: RPM 15000, time 45 min temp 4 degrees C

When done remove the liquid and there is a gel on the bottom (a small round spot).

Add a small amount of acetone to rinse and pour out liquid.

Rinse with acetone at least 3 times.

To remove the excess acetone add Sample in a tube and put it in the -80 degrees C freezer for 2 hrs. and then in the lyophilizer for 2 days.

## PNVF Nanoparticles

We acknowledge Dr. Berkland's lab, especially Huili Guam and Chuda Chittasupho for teaching the procedures for making PAAm and PNVF particles as well as providing nanoparticles.

### Solution A:

1. Span 80 (Sorbitan monooleate)	4.1 g
2. Tween 80	3 g
3. VAZO-52 (initiator)	30 mg
4. Hexane	100 ml

### Solution B:

1. NVF	350 $\mu$ l
2. Nondegradable Cross linker (X-L)	50 $\mu$ l
3. PBS or Water (DI)	165 $\mu$ l
4. VAZO-52 (initiator)	20 mg

Set up reaction vessel. The vessel is a 3 necks (14/20), has water around walls to maintain temperature. The vessel is found in the bottom drawer. The vessel has two black tubes for the water to flow in and out and can be connected together at the ends of the tubing.

Add a stir bar to the vessel and get three rubber stoppers. Put vessel on a stir plate.

Set temperature of the circulating water bath to 50 degrees C. Make sure the water bath is filled with water.

Add VAZO-52 to 2 vials.

A: vial 1 should be around 125 ml add 30 mg of VAZO-52

Add approx. 50 ml of hexane to VAZO-52 and let dissolve.

Then add the Span 80 and Tween 80.

Wash Span 80 and Tween 80 with remaining hexane (to dissolve it) and then add to vial.

B: vial 2 should be small add 20 mg of VAZO-52

Add NVF to VAZO-52 and let dissolve.

Then add Nondegradable Cross linker (X-L)

Then add water

Using the sonicator wash with pure hexanes for 5 min.

Sonicate A and pipette B slowly, add drop by drop

Sonicate for 5 min

Add solution to reaction vessel.

Add stoppers

Add purge needles

Bubble nitrogen for 15 min

Hook system up to heat bath set at 50 degrees C.

Let the reaction run for 24 hours. The solution should turn be cloudy (these are the particles).

Take off the heat bath and add to 4 centrifuge tubes equally.

Put into centrifuge at these conditions: RPM 15000, time 45 min temp 4 degrees C

When done remove the liquid and there is a gel on the bottom (a small round spot).

Add a small amount of hexane to rinse and pour out liquid.

Add 10 ml of DI water to each tube.

Mix the tubes with a vortex

Add tubes to a sonicator.

After 1 hour vortex the tubes and place back in sonicator for a total of 4 hours or leave in the sonicator overnight. (make sure the sonicator is filled with water)

Make sure the gel is mixed with the water.

Put into centrifuge at these conditions: RPM 15000, time 30 min temp 4 degrees C

Remove tubes and take out water being careful not to lose the pellet.

Add 10 ml of DI water.

Mix the tubes with a vortex

Put in the sonicator for 1 hr.

To remove the excess hexane add all 4 of the solutions in the tubes to a 50ml round bottom flask with a glass attachment. Vacuum the flask out for 10 min. It should bubble. Keep removing the hose and putting it back on the attachment.

Then pour the solution into a dialysis bag. The dialysis bag should be the 10 kDa in the fridge. Cut off a piece and clip the end with the orange clip. Add solution to the bag and then clip the top.

Place dialysis bag into a 4000 ml beaker filled with DI water. Add stir bar to the beaker and stir the dialysis bag so that the bag is vertical.

Change the water after 2 hrs and then every 4 hrs 5 times.

Sample is ready in the liquid state. To dry, put the sample in a tube and put it in the -80 degrees C freezer for 2 hrs. and then in the lyophilizer for 2 days.